Sayyed Ahmad Alavian

Modeling CO_2 Injection in Fractured Reservoirs Using Single Matrix Block Systems

Thesis for the degree of Philosophiae Doctor

Trondheim, October 2011

Norwegian University of Science and Technology

Faculty of Engineering Science and Technology

Department of Petroleum Engineering

and Applied Geophysics

NTNU – Trondheim
Norwegian University of
Science and Technology

To my Hometown

Abstract

In this thesis, CO_2 injection in matrix/fracture systems has been studied using a finely-gridded compositional simulator representing a single matrix block. Three laboratory experiments were modeled to investigate whether CO_2 injection in a fracture-matrix system could be simulated using commercial simulators that include basic fluid flow physics, phase behavior, and molecular diffusion.

The first experiment was performed by Karimaie (2007) using an equilibrium, saturated gas-oil fluid system (C_1-n-C_7) at 220 bar and 85 ^{o}C. Because no recovery was expected from non-equilibrium thermodynamic mass transfer, reported recovery stemmed only from Darcy displacement driven by gravity and capillary forces. When the oil production stopped from the equilibrium gas displacement, a second injection period with pure CO_2 followed.

The numerical modeling was conducted using a compositional reservoir simulator (SENSOR) without diffusion. The 2-dimensional r-z model used fine grids for the core matrix and surrounding fracture. Automated history matching was used to determine parameters which were not accurately known (fracture permeability, fracture and matrix porosity, and separator conditions), using surface volumetric oil production rates reported experimentally. The final model match was relatively unique with a high degree of confidence in final model parameters. The oil recovery improved significantly with CO_2 injection.

Our model indicated that the recovery mechanism in the Karimaie experiment was dominated, for both equilibrium gas and CO_2 injection, by top-to-bottom Darcy displacement caused by low conductivity in the artificial fracture; little impact of capillary-gravity displacement was found. Changes in CO_2 injection rate had a significant impact on recovery performance. This experiment was also modeled using ECL300, with the same production performance as SENSOR for the set of history-match parameters determined without diffusion. When molecular diffusion was used in ECL300, results were nearly identical with those found without diffusion.

Two other experiments were performed by Darvish (2007) at a higher temperature and pressure (130 ^{o}C and 300 bara) using a similar chalk and live reservoir oil. A similar modeling approach to that described above was also used for these experiments. In both experiments, the matching process based on reported oil production data gave a high degree of confidence in the model. The reported experimental mass fractions of produced-stream components were also matched well.

Our modeling study indicates that gravity drainage affects the displacement process, but that mass transfer – including vaporization, condensation and molecular diffusion – also impact the recovery performance of CO_2 injection in the Darvish experiments. The CO_2 injection rate and initial water saturation were investigated by comparing the two Darvish experiments.

Our studies from all of the Karimaie and Darvish experiments show a strong influence of the surface separator temperature on surface oil production, and this is an important consideration in designing and interpreting laboratory production data consistently.

Once the laboratory recovery mechanisms had been successfully modeled, predictive numerical simulation studies were conducted on field-scale matrix/fractured systems, albeit mostly for single matrix blocks surrounded by a fracture. The effects of several key parameters on recovery production performance were studied in detail for field-scale systems: matrix permeability, matrix block size, matrix-matrix capillary continuity (stacked blocks), and the use of mixtures containing CO_2 and hydrocarbon gas.

The field-scale results were affected by gridding, so grid was refined to the degree necessary to achieve a more-or-less converged solution – i.e. recovery production performance didn't change with further refinement.

We studied the effect of molecular diffusion on oil recovery by CO_2 injection in laboratory experiments and field-scale systems. Because the fluid systems considered had complex phase behavior and a wide range of conditions from strongly immiscible to near-miscible, the diffusion driving potential used was *total component potential* including chemical and gravity effects; concentration-driven diffusion did not represent the more-complex non-equilibrium CO_2 injection processes observed in the laboratory tests.

A key result of this study was that diffusion can have an important effect on oil recovery, and that this effect varies with matrix block size and CO_2 injection rate. We have shown that diffusion has a dominant effect on the recovery mechanism in experimental tests, except at very low rates of CO_2 injection (and equilibrium hydrocarbon gas injection). For the field-scale matrix/fracture systems, diffusion can have a significant effect on the rate of recovery, with the effect becoming noticeable for low reservoir pressures and/or matrix block sizes less than ~40 ft.

Acknowledgements

I would like to especially thank my supervisor and close friend Professor Curtis H. Whitson for guiding me thought this work. The thesis would not have been possible without his advice, valuable discussion and support.

Special thanks to Dr. Hassan Karimaie and Dr. Gholam Reza Darvish who made their experimental data available to me, and provided helpful discussions during my modeling of their experiments.

All colleagues and staff at the Department of Petroleum Engineering and Applied Geophysics at NTNU are greatly acknowledged for their cooperation and for creating a very good working environment. For this I would like to thank Marit Valle Raaness, Tone Sanne, Madelein Wold, Ann Lisa Brekken, Turid Halvorsen, Solveig Johnsen and Turid Oline Uvsløkk.

I acknowledge the financial support from Shell and PERA.

Thanks to PERA staff engineers: Dr. Kameshwar Singh, Dr. Mohammad Faizul Hoda, Snjezana Sunjerga and Sissel Ø. Martinsen and also Dr. Øivind Fevang and Dr. Knut G. Uleberg (now at Statoil) for providing software and helping me during the thesis. I enjoyed and benefited a lot from working with them.

Sincere thanks to Arif Kuntadi and Mohmmad Ghasemi for introducing me to Ruby programing.

I wish to express my deepest gratitude to my mother for all support, encouragement and inspiration throughout my life. I am also indebted to my wife and my son for understanding, patience and support during the work of this thesis.

Finally, I would also like to thank all my family members and close friends for support and encouragement.

Sayyed Ahmad Alavian

List of Papers

Throughout this PhD work, five papers were written by the author of this thesis, together with co-author. Two papers are published in a reviewed journal, Two papers are under review for publishing and also presented in SPE conference. One paper will be presented at an upcoming SPE conference. The papers are included at the end of the thesis.

1. Alavian, S.A., and Whitson C.H. 2010. CO_2 EOR Potential in Naturally-Fractured Haft Kel Field, Iran. SPE Reservoir Evaluation and Engineering: 720-729. SPE-139528-PA.
2. Alavian, S.A., and Whitson C.H. 2011. Numerical Modeling CO_2 Injection in a Fractured Chalk Experiment. Journal of Petroleum Science and Engineering, Volume 77, Issue 2, May 2011, Pages 172-182.
3. Alavian, S.A., and Whitson C.H. 2010. Scale Dependence of Diffusion in Naturally Fractured Reservoirs for CO_2 Injection. Paper SPE 129666 presented at the 2010 SPE Improved Oil Recovery Symposium, Tulsa, Oklahoma, USA, 24–28 April.

   (The paper is under review for publication in the Journal of Petroleum Science and Engineering)
4. Alavian, S.A., and Whitson C.H. 2010. Modeling CO_2 Injection Including Diffusion in a Fractured-Chalk Experiment. Paper SPE 135339 presented at the 2010 Annual Technical Conference and Exhibition, Florence, Italy, 19–22 September.

   (The paper is under review for publication in the Journal of Petroleum Science and Engineering)

5. Alavian, S.A., and Whitson C.H. 2011. Modeling CO_2 Injection Including Diffusion in a Fractured-Chalk Experiment with Initial Water Saturation. Will be presented at Carbon Management Technology Conference to be held 7-9 February 2012 in Orlando, Florida.

Table of Contents

Chapter 3 Modeling CO_2 Injection in Karimaie Fractured Chalk Experiment 19

Appendix A: Simulator Input Data Sets

Appendix B: Papers

List of Tables

List of Figures

Nomenclature

B_o = oil formation volume factor, L^3/L^3,
c = molar concentration, n/L^3
D_i = diffusion coefficient of component *i*, L^2/t, cm^2/s
D_i^a = activity-corrected diffusion coefficient of component *i*, L^2/t, cm^2/s
D_i^T = thermal diffusion coefficient of component *i*, L^2/t, cm^2/s
D_g = gas diffusion coefficient, L^2/t, cm^2/s
D_o = oil diffusion coefficient, L^2/t, cm^2/s
F = formation resistivity
f_i = fugacity of component *i*, m/Lt^2
G = gravity acceleration
h = height, L
h_0 = reference height, L
J_i = molar flux of component *i* per unit area
k_r = relative permeability
M_i = component *i* molecular weight, m/n
M_g = gas molecular weight, m/n
M_o = oil molecular weight, m/n
m = cementation factor in porous media
m_k = current mass of component *i* in place, m, kg
m_{ki} = initial mass of component *i* in place, m, kg
m_{op} = produced oil mass at surface condition, m, kg
m_{oi} = initial oil mass in place at experiment condition, m
N = number of grid cells
Nx = number of grid cells in x-direction
Ny = number of grid cells in y-direction
Nz = number of grid cells in z-direction
n_k = current moles of component *i* in place
n_{ki} = initial moles of component *i* in place
p = pressure, m/Lt^2, bara
P_C = capillary pressure, m/Lt^2, bara or psia
$P_{C,lab}$ = measured capillary pressure, m/Lt^2, bara or psia
P_{cgo} = drainage gas-oil capillary pressure, m/Lt^2, bara or psia
P_{cwoi} = imbibition water-oil capillary pressure, m/Lt^2, bara or psia
Pi = parachor of component *i*
R = gas constant
RF = oil recovery factor
RF_{comp} = mole based component recovery factor

RF_{mole} = mole based oil recovery factor
RF_{mass} = mass based oil recovery factor
RF_{so} = saturation based oil recovery factor
RF_{surf} = oil recovery factor based on produced oil mass at surface condition
s = components volume shift
S_g = gas saturation
S_{gc} = critical gas saturation
S_o = oil saturation
S_{oi} = initial oil saturation
S_{org} = residual oil saturation to gas
S_{orw} = residual oil saturation to water
S_{wc} = connate water saturation
T = temperature, T
T_{ci} = critical temperature of component i, T
V_{oi} = initial oil volume in place, L^3, m^3
v_{ci} = critical molar volume of component i,L^3/n
x_i = oil mole fraction of component i
y_i = gas mole fraction of component i
Z_i = critical compressibility factor
ε/κ = Lennard-Jones 12-6 potential parameter
μ_i = chemical potential of component i
μ_{i0} = reference chemical potential of component i
ρ_g = gas density, m/L^3, kg/m^3
ρ_M = molar density, n/L^3
ρ_{Mpc} = pseudo-critical molar density, n/L^3
ρ_{pr} = pseudo-reduced molar density
ρ_o = oil density, m/L^3, kg/m^3
σ = characteristic length
σ_{go} = gas-oil interfacial tension, m/t^2, mN/m
σ_{lab} = reference gas-oil interfacial tension, m/t^2, mN/m
τ = tortuosity
ϕ = porosity
Ω_{ij} = low-pressure diffusion coefficient correlation parameter

SI Metric Conversion Factors

bbl x 1.589 873 E – 01 = m^3
D x 9.869 23 E – 13 = m^2
dyne/cm x 1.000 000 E + 00 = mN/m
ft x 3.048* E – 01 = m
ft^3 x 2.831 685 E – 01 = m^3
°F (oF+459.67)/1.8 E – 01 = K
in x 2.54* E – 02 = m
in^2 x 6. 4516* E – 04 = m

lbm/ft^3 x 2.831 685 E – 02 = m
psi x 6.894 757 E + 03 = Pa
°R °R/1.8 E – 01 = K

*Conversion factor is exact.

Chapter 1

Introduction

1.1 Background

CO_2 injection has recently been shown to provide significant enhanced oil recovery from naturally fractured reservoirs[1]. Li *et al.* (2000) performed CO_2 injection at 1750 psig on artificially-fractured cores after water flooding in a dead-oil system. Gravity drainage was suggested to be the dominant recovery mechanism in these tests, with significant tertiary oil recovery after water flooding. The authors observed that the recovery of initial oil at the start of the CO_2 injection declined as the rock permeability decreased and the initial water saturation increased. Darvish *et al.* (2006) performed CO_2 injection experiments on an outcrop chalk core that was surrounded by an artificial fracture, at reservoir conditions where the core was initially saturated with live oil. These authors reported that gas produced at an early stage was enriched with methane. During later stages, the amount of intermediate components increased in the production stream, and that heavier components were recovered toward the end of the experiment. This result was also reported by Moortgat, Firoozabadi and Farshi (2010) in a paper that presented simulation studies of the Darvish *et al.* (2006) experiments.

Trivedi and Babadagli (2008) investigated the injection flow rate effect on first contact miscible displacement in a matrix/fracture system that used heptane

---

[1] Holm and Josendal (1974), among many others, have studied CO_2 injections in unfractured rock.

(C_7) as the injectant displacing kerosene or mineral oil at atmospheric conditions. These authors reported that higher solvent injection rates yielded higher rates of oil production during the early stages of the experiment, whereas lower injection rates resulted in greater ultimate oil recovery.

Er, Babadagli and Zhenghe (2010) investigated micro-scale matrix/fracture interactions during CO_2 injection in a synthetic fractured system. The authors used a glass bead model with normal decane ($n\text{-}C_{10}$) as the oil and CO_2 as the injectant. They concluded that for immiscible CO_2 displacement, the amount of oil trapped in the matrix was reduced with increasing injection rates. They also observed that for miscible CO_2 conditions, oil was recovered faster with increasing injection rate.

Morel *et al.* (1993) and Le Romancer *et al.* (1994a) studied the effects of diffusion on a C_1-C_5 oil mixture by injecting methane (C_1), nitrogen (N_2) and CO_2 into an outcrop core. Hua, Whitson and Yuanchang (1991) simulated Morel's experiments with a model that combined an analytical calculation for the fracture and a numerical model for the core. These authors showed that the correction of the capillary pressure curve for the changes in interfacial tension was due to diffusion-driven compositional variation. Recently, Jamili, Willhite and Green (2010) simulated both of these previous experiments using a (self-built, non-commercial) numerical model. These authors reported that diffusion was the main mass transfer mechanism between the matrix and fracture during nitrogen (N_2) injection. In other CO_2 experiments conducted by Le Romancer, diffusion and convection were both shown to be important.

Asghari and Torabi (2008) performed CO_2 gravity drainage experiments with a synthetic dead oil ($n\text{-}C_{10}$), above and below the CO_2 MMP. These authors were not able to match their laboratory experiments using a simulation model.

Hoteit and Firoozabadi (2009) studied diffusion in fractured media for gas injection and recycling schemes, using a (self-built, non-commercial) numerical model. They reported that diffusion improved the amount of oil recovery and delayed gas breakthrough. In their modeling study, these authors did not consider matrix gas-oil capillary pressure.

Le Romancer, Defives and Fernandes (1994b) performed 1-D experiments on a chalk core that was saturated with a methane-pentane (C_1-C_5) mixture in the presence of different levels of water saturation, using two different injection gases (N_2 and C_1). They concluded that the effect of water saturation on recovery strongly depended on the nature of the diffusing gas. In their methane injection experiments, the oil was produced into a fracture faster for higher water saturations. In their nitrogen (N_2) injection experiments, the methane rate of production was proportional to the hydrocarbon mass initially present, whereas the rate of pentane production remained unchanged.

1.2 Thesis Outline

The present thesis contains two main sections: a) a modeling study of experimental tests performed at NTNU by H. Karimaie (Chapter 3) and G.R. Darvish (Chapters 4 and 5); and b) a detailed study of CO_2 injection recovery mechanisms in field-scale matrix/fracture systems (Chapters 6 and 7).

The mechanism of small-scale, laboratory CO_2 injection was investigated by modeling lab experiments, assessing the ability of commercial numerical simulators to model physical phenomena contributing to oil recovery by CO_2 injection.

Once it was established that physics-based numerical models could model accurately the laboratory tests, without unphysical parameters or empirical pseudo-physics (e.g. relative permeability model adjustments), these models were extended to field-scale matrix/fracture systems to quantify recovery performance affected by capillary-gravity effects, non-equilibrium thermodynamics and diffusion-controlled mass transfer – and which mechanisms controlled recovery under different assumptions of matrix-fracture geometry and injection rate.

Nomenclature is provided at the beginning of the thesis. Conclusions, recommendations for further work and references are provided at the end of each chapter. Consequently, chapters can be read separately, and more-or-less independently. Samples of input data sets are given in Appendix A.

1.3 References

Asghari, K and Torabi, F. 2008. Effect of Miscible and Immiscible CO_2 Flooding on Gravity Drainage: Experiment and Simulation Results., Paper SPE 110587 presented at the 2008 SPE/DOE Improved Oil Recovery Symposium, Tulsa, Oklahoma, U.S.A., 19-23April.

Chang, Y., and Coats B.K and Nolen, J.S. 1998. A Compositional Model for CO_2 Floods Including CO_2 Solubility in Water. SPE Reservoir Evaluation and Engineering, **1**(2): 155-160. SPE-35164-PA.

Darvish, G.R., Lindeberg, E., Holt, T., Utne, S.A. and Kleppe, J. 2006. Reservoir Conditions Laboratory Experiments of CO_2 Injection into Fractured Cores. Paper SPE 99650 presented at the 2006 SPE Europec/EAEG Annual Technical Conference and Exhibition, Vienna, Austria, 12-15 June.

Er, V., Babadagli, T and Zhenghe X. 2010. Pore-Scale Investigation of the Matrix-Fracture Interaction during CO_2 Injection in Naturally Fractured Oil Reservoir. Energy Fuels 2010, **24**: 1421-1430.

Holm, L.W. and Josendal, V.A. 1974. Mechanism of Oil Displacement by Carbon Dioxide. Journal of Petroleum Technology **26**(12): 1427-1438.

Hoteit, H. and Firoozabadi, A. 2006. Numerical Modeling of Diffusion in Fractured Media for Gas Injection and Recycling Schemes. Paper SPE 103292 presented at the 2006 SPE Annual Technical Conference and Exhibition, San Antonio, Texas, U.S.A., 24-27 September.

Hua, H. Whitson, C.H., and Yuanchang, Q. 1991. A Study of Recovery Mechanisms in a Nitrogen Diffusion Experiment. Presented at the 9th European IOR Symposium, Stavanger, Norway, May.

Jamili, A. and Willhite, G.P and Green, D.W. 2006. Modeling Gas-Phase Mass Transfer Between Fracture and Matrix in Naturally Fractured Reservoirs. Paper SPE 132622 presented at the SPE Western Regional Meeting, Anaheim, California, U.S.A., May.

Le Romancer, J.F., Defives, D., Kalaydjian, F. and Fernandes, G. 1994a. Influence of the Diffusion Gas on the Mechanism of Oil Recovery by Gas Diffusion in Fractured Reservoir. Presented at the IEA Collaborative Project on Enhanced Oil Recovery Workshop and Symposium, Bergen, Norway, August.

Le Romancer, J.F., Defives, D. and Fernandes, G. 1994b. Mechanism of Oil Recovery by Gas Diffusion in Fractured reservoir in Presence of Water. Presented at the SPE/DOE Ninth Symposium on Improved Oil Recovery, Tulsa, USA, April.

Li, H., Putra, E., Schechter, D.S. and Grigg, R.B. 2000. Experimental Investigation of CO_2 Gravity Drainage in a Fractured System. Paper SPE 64510 presented at the SPE Asia Pacific Oil and Gas Conference and Exhibition, Brisbane, Australia, 16-18October.

Moortgat, J., Firoozabadi, A. and Farshi M.M., 2009. A New Approach to Compositional Modeling of CO_2 Injection in fractured Media Compared to Experimental Data. Paper SPE 124918 presented at the 2009 SPE Annual Technical Conference and Exhibition, New Orleans, Louisiana, U.S.A., 4-7 October.

Morel, D.D., Bourbiaux B., Latil, M., and Thiebot B. 1990. Diffusion Effect in Gas Flooded Light Oil Fractured Reservoir. Paper SPE 20516 presented at the 65th SPE Annual Technical Conference and Exhibition, New Orleans, Louisiana, U.S.A., September.

Trivedi, J. and Babadagli, T. 2008. Efficiency of Diffusion Controlled Miscible Displacement in Fractured Porous Media. Transport in Porous Media, **71**(3): 379-394.

Chapter 2

Fundamentals and Calculations

2.1 Introduction

This chapter presents some fundamental concepts and calculations used in the research – e.g., diffusion coefficient estimation and relative permeability modeling.

2.2 Diffusion

Diffusion plays an important role in some of the experiments that are modeled in the next sections. Fick presented the equation for molecular diffusion in 1885 and stated that the flux of a substance diffusing through a unit area of cross section is proportional to the concentration gradient that is measured perpendicular to the cross section:

$$J_i = -cD_i \frac{\partial x_i}{\partial d} \quad \text{.......} (2.1)$$

However, diffusion in a hydrocarbon fluid is also affected by factors other than the concentration gradient. Therefore, it is more appropriate to use a diffusion flux that is driven by the total potential given by chemical, gravity, and thermal forces (Bird, Stewart and Lightfoot 1960):

$$J_i = -cD_i^a x_i \frac{1}{RT}\frac{\partial}{\partial d}\left[\mu_i - M_i G(h-h_0) + M_i D_i^T \ln(T)\right] \quad (2.2)$$

where $\mu_i = \mu_{i0} + RT\ln(f_i)$ .... (2.3)

If gravity and the thermal diffusion term in Eq. (2.2) are omitted, Eq. (2.2) can written as:

$$J_i = -cD_i^a x_i \frac{\partial}{\partial d}(\ln f_i)_{T,P} \quad (2.4)$$

Using the chain rule, Eq. (2.4) can be rewritten as:

$$J_i = -cD_i^a \frac{\partial(\ln f_i)}{\partial \ln(x_i)}\frac{\partial xi}{\partial d} \quad (2.5)$$

Comparing Eq. (2.1) and Eq. (2.5), the activity-corrected diffusion coefficient D_i^a (Reid, Prausnitz and Poling 1987) is given by:

$$D_i^a = \frac{D_i}{\partial \ln(f_i)/\partial \ln(x_i)} \quad (2.6)$$

2.2.1 Diffusion Coefficient

Several diffusion correlation coefficients are given in the literature (Poling, Prausnitz and O'Conell. 2004 and Riazi 2005). We used the following equations to calculate the oil and gas diffusion coefficients. Sigmund (1976a) proposed correlations for high pressure and temperature that are widely used in petroleum engineering:

$$\frac{\rho_M D_{ij}}{\rho_M^o D_{ij}^o} = 0.99589 + 0.096016\rho_{pr} + 0.22035\rho_{pr}^2 + 0.032874\rho_{pr}^3 \quad (2.7)$$

To avoid a negative D_{ij} for $\rho_{pr}>3.7$ and to allow for a better prediction of the measured liquid diffusion coefficients, da Silva and Belery (1989) recommended the following extrapolation for $\rho_{pr}>3.0$:

$$\frac{\rho_M D_{ij}}{\rho_M^o D_{ij}^o} = 0.18839\exp(1-\rho_{pr}) \quad (2.8)$$

where pseudo-reduced molar density (ρ_{pr}) is calculated from:

$$\rho_{pr} = \frac{\rho_M}{\rho_{Mpc}} \quad \text{..}(2.9)$$

and pseudo-critical molar density (Reid, Prausnitz and Poling 1987) is obtained from:

$$\rho_{Mpc} = \frac{\sum_{i=1}^{n} z_i v_{ci}^{2/3}}{\sum_{i=1}^{n} z_i v_{ci}^{5/3}} \quad \text{..}(2.10)$$

The low-pressure binary diffusion coefficient ($D^o{}_{ij}$) can be calculated using Chapman-Enskog theory (Hirschfelder, Curtiss and Bird 1954; Bird, Stewart and Lightfoot 1960; Neufield, Janzen and Aziz 1972; Reid, Prausnitz and Poling 1987):

$$D^o_{ij} = 0.001883 \frac{T^{3/2}\left[(1/M_i)+(1/M_j)\right]^{0.5}}{p^o \sigma_{ij}^2 \Omega_{ij}} \quad \text{..............................}(2.11a)$$

where

$$\Omega_{ij} = \frac{1.06036}{T_{ij}^{0.1561}} + \frac{0.193}{\exp(0.47635 T_{ij})} + \frac{1.03587}{\exp(1.52996 T_{ij})} + \frac{1.76474}{\exp(3.89411 T_{ij})} \quad .(2.11b)$$

$$T_{ij} = \frac{T}{(\varepsilon/k)_{ij}} \quad ,\text{..}(2.11c)$$

$$(\varepsilon/k)_{ij} = \left[(\varepsilon/k)_i (\varepsilon/k)_j\right]^{1/2} \quad ,\text{..}(2.11d)$$

$$(\varepsilon/k)_i = 65.3 T_{ci} Z_{ci}^{18/5} \quad ,\text{..}(2.11e)$$

$$\sigma_{ij} = 0.5(\sigma_i + \sigma_j) \quad ,\text{..}(2.11f)$$

and $\sigma_i = 0.1866 \dfrac{v_{ci}^{1/3}}{Z_{ci}^{6/5}}$,..(2.11g)

with the diffusion coefficient, $D^o{}_{ij}$,in cm^2/s; molecular weight, M, in gr/gmol; temperature, T, in K; pressure, p, in bar; characteristic length,σ, in Å; Lennard-Jones 12-6 potential parameter, ε/k, in K; critical volume v_c in cm^3/gmol and critical compressibility factor Z_c.

We used the idea-gas law, $\rho^o{}_M = p^o/RT$, to determine the low-pressure density-diffusivity product (Bird, Stewart and Lightfoot 1960; Sigmund 1976a; Whitson and Brule 2000):

$$\rho^o_M D^o_{ij} = (2.2648 \times 10^{-5}) \frac{T^{1/2}\left[(1/M_i) + (1/M_j)\right]^{0.5}}{\sigma^2_{ij}\Omega_{ij}} \quad \text{................................} (2.11a)$$

2.2.2 The Diffusion Coefficient in a Multicomponent System

The diffusion coefficient for each component in a multicomponent system is calculated using Wilke's equation (Wilke 1950):

$$D_{im} = \frac{1 - z_i}{\sum\limits_{\substack{j=1 \\ j \neq i}}^{N} (z_i / D_{ij})} \quad \text{...} (2.12)$$

Eq. (2.12) is based on the Stefen-Maxwell diffusion equations and is simply a weighted harmonic mean. Sigmund (1976b) reported that Eq. (2.12), which was developed for gas mixtures, may be used also for liquid mixtures.

2.2.3 Diffusion Coefficient in Porous Media

The diffusion path of the components in a porous media deviates from a straight line because of the presence of solid particles. Consequently, the diffusion coefficient of a component must be corrected for the tortuosity, τ. The following equation has been suggested in the literature (Petersen 1958, van Brakel and Heertjes 1974, Ullman and Aller 1982) for correcting the diffusion coefficient for tortuosity in porous media:

$$D_{i,eff} = \frac{D_i}{\tau^2} \quad \text{...} (2.13)$$

where $D_{i.eff}$ is the effective diffusion coefficient in a porous media, and D_i is the diffusion coefficient in the absence of a porous media.

Shen and Chen (2007) reviewed the impact of tortuosity on the diffusion coefficient. Empirically, tortuosity is related to the porosity (ϕ) and the formation resistivity (F) as follows:

$$\tau^2 = (F\phi)^n \quad \text{...} (2.14)$$

Substituting Archie's law, F=a/ϕ^m (Archie 1942), into Eq.(2.14) gives tortuosity in terms of porosity (Lerman 1979, Ullman and Aller 1982 and Nelson and Simmons 1995):

$$\tau^2 = (a\phi^{1-m})^n \qquad (2.15)$$

Substituting Eq. (2.15) with $n = a = 1$ into Eq. (2.13) gives:

$$D_{i,eff} = D_i \phi^{m-1} \qquad (2.16)$$

where m is the cementation factor in the porous media. In the present study, m is equal to 2.

In this work, any pressure and composition dependency of the diffusion coefficients are not considered.

2.3 Relative Permeability and Capillary Pressure Curve

In the next chapters, we use the following equations to calculate the relative permeability and capillary pressure in all numerical simulation (SENSOR Manual 2009):

$$k_{rw} = k_{rwro}[(S_w - S_{wc})/(1 - S_{orw} - S_{wc})]^{nw} \qquad (2.17)$$

$$k_{row} = k_{rocw}[(1 - S_{orw} - S_w)/(1 - S_{orw} - S_{wc})]^{now} \qquad (2.18)$$

$$k_{rog} = k_{rocw}[(1 - S_{org} - S_{wc} - S_g)/(1 - S_{org} - S_{wc})]^{nog} \qquad (2.19)$$

$$k_{rg} = k_{rgro}[(S_g - S_{gc})/(1 - S_{org} - S_{wc} - S_{gc})]^{ng} \qquad (2.20)$$

$$P_{cwoi} = b_1 + b_2[1 - (S_w - S_{wc})/(1 - S_{wc})]^{b_3} - b_4[(S_w - S_{wc})/(1 - S_{wc})]^{b_5} \qquad (2.21)$$

$$P_{cgo} = c_1 + c_2[(S_g)/(1 - S_{wc})]^{c_3} \qquad (2.22)$$

where S_{wc} is the connate water saturation; S_{orw} is the residual oil saturation to water; S_{org} is the residual oil saturation to gas; S_{gc} is the critical gas saturation; k_{rwro} is the relative permeability of water at S_w=1-S_{orw} and S_g=0; k_{rgro} is the relative permeability of gas at S_w=S_{wc} and S_g=S_{org}; k_{rocw} is the relative permeability of oil at S_w=S_{wc} and S_g=0; n_w, n_{ow}, n_g and n_{og} are the exponents of the relative permeability; P_{cwoi} is the imbibition water-oil capillary pressure; and P_{cgo} is the gas-oil capillary pressure.

2.3.1 Three Phase Relative Permeability

Because mobile oil, gas and water exist in the modeling, three-phase oil relative permeabilities are needed. Extended Stone's first method (Stone 1970 and Fayers 1973), in which the minimum or residual oil saturation is treated as a function of S_g, was used:

$$S_{om} = S_{org}S_{gn} + S_{orw}(1 - S_{gn}) \quad \text{.......} (2.23a)$$

$$S_{gn} = \frac{S_g}{1 - S_{wc} - S_{org}} \quad \text{.......} (2.23b)$$

where S_{om} is the minimum oil saturation, S_{org} is the residual oil saturation to gas, S_{orw} is the residual oil saturation to water and S_{wc} is the connate water saturation.

2.3.2 Capillary Pressure Scaling with IFT

The capillary pressure is scaled with the interfacial tension (IFT) according to:

$$P_{cgo} = \left(\frac{\sigma}{\sigma_{ref}}\right)P_{cgo,lab} \quad \text{.......} (2.24)$$

where $P_{cgo,lab}$ is the original capillary pressure input in the model, σ_{ref} is the reference IFT and σ is the IFT calculated using an equation developed by Weinaug and Katz (1943):

$$\sigma_{go} = \left[\sum P_i\left(x_i\frac{\rho_o}{M_o} - y_i\frac{\rho_g}{M_g}\right)\right]^4 \quad \text{.......} (2.25)$$

2.4 Minimum Miscibility Conditions

The minimum conditions at which the resulting mixture of two fluids mixed together at any proportion is homogeneous in compositions and is identical in intensive properties.

Because the reservoir temperature is usually assumed to be constant in reservoir engineering, the minimum miscibility conditions refer to either the minimum miscibility pressure (MMP), when the compositions of the two fluids are fixed, or the minimum miscibility enrichment (MME), when the oil composition and the reservoir pressure are specified. No fluid interface between the two fluids exists when these fluids are fully miscible and their IFT becomes zero. In the absence of any dispersion, if the reservoir oil is fully miscible with an injection gas at the minimum miscibility conditions, the residual oil saturation behind the injection gas front is essentially zero, and the microscopic oil recovery is expected ~100%.

The process of achieving miscibility at the minimum miscibility conditions can vary depending on the compositions of the displacing and displaced fluids and on the reservoir temperature. Fluids may become miscible upon first contact, which is called first-contact miscibility. Most fluids are not first-contact miscible but can achieve miscibility during continuous contact by interphase mass transfer. These fluids are termed multi-contact miscible, much more common in hydrocarbon reservoirs. Several multi-contact miscible mechanisms have been proposed and summerized in the literature (Stalkup 1983; Zick 1986; Whitson and Brule 2000) based on the compositions of the two fluids, the pressure and temperature: vaporizing gas drive (VGD), condensing gas drive (CGD) and condensing/vaporizing gas drive (C/V).

2.4.1 MMP calculation

Several methods for determining the MMP are available in the literature, such as the slimtube experiment (Orr *et al.* 1982), the single-cell, forward- and backward-contact algorithms (Stalkup 1982), the multi-cell algorithm (Cook *et al.* 1969a and 1969b), the slimtube-type compositional numerical simulations (Zick 1986), a proprietary multi-cell algorithm (Zick 1986), and analytical methods that are based on the method of characteristics (Johns and Orr 1996 and Wang and Orr 1998). A rising bubble apparatus (Novosad and Costain 1988) has also been suggested as an alternative to the slimtube experiment

If it is designed, conducted, and interpreted properly, the slimtube experiment is considered to define a “true thermodynamic” MMP. This method is usually expensive and time-consuming. Alternatively, 1D slimtube-type simulations can be used to evaluate the MMP_{1D}. For any method a properly tuned equation of state (EOS) model is required, capable of modeling the important phase behavior, such as forward and/or backward-contact experiments, swelling tests and MMP experiments. In the present study, the MMP values were calculated by a the *PhazeComp* PVT program or by a 1D numerical simulation that requires elimination of numerical dispersion (Høier 1997).

2.5 Numerical Gridding

One needs to continue refining the grid size in each dimension until the performance no longer changes and has appeared a "converged" solution. The first sensitivity that should be performed in a numerical study is the grid-sensitivity analysis. However, this analysis may not be possible when the laboratory experiments are simulated because the numerical effect should be eliminated or reduced to a minimum in the model results. Therefore, the simulation should start with the fine grid model, and then the grid sensitivity should be assessed at the end of simulation to determine how this sensitivity can affect the model results. We present the investigation of the numerical grid effect in Chapters 5 and 6.

2.6 References

Bird, R.B., Stewart, W.E. and Lightfoot, E.N., 1960. Transport Phenomena. John Wiley & Sons Inc, New York.

Coats Engineering, 2009. SENSOR Manual, www.coatsengineering.com, October.

Cook, A. B., Johnson, F. S., Spencer, G. B., Bayazeed, A.F. and Walker, C. J., 1969a. Effects of Pressure, Temperature, and Type of Oil on Vaporization of Oil During Gas Cycling, RI 7278, USBM(1969).

Cook, A. B., Johnson, F. S., Spencer, G. B., Bayazeed, A.F. and Walker, C. J., 1969b. Realistic K Values of C_{7+} Hydrocarbons for Calculating Oil Vaporization During Gas Cycling at High Pressures. JPT **21**(7):901-915.

da Silva, F.V and Belery, P., 1989. Molecular Diffusion in Naturally Featured Reservoirs: a Decisive Recovery Mechanism., Paper SPE 19672 presented at the 64th SPE Annual Technical Conference and Exhibition, San Antonio, Texas, U.S.A., 8-11 October.

Fayers F.J. 1973. Extension of Three-Phase Relative Permeability and Residual Oil Data. Journal of Canadian Petroleum Technology, **251**:419-425

Hirschfelder, J.O., Curtiss C.F. and Bird R.B., 1954. Molecular Theory of Gas and Liquids, Wilye, New York.

Høier, L. 1997. Miscibility Variation in Compositionally Grading Petroleum Reservoir. PhD Dissertation, NTNU, Trondheim, Norway.

Johns, R.T. and Orr, F.M., Jr.,1996. Miscible Gas Displacements of Multicomponent Oils. SPEJ **1**(1):39-50.

Lerman, A., 1979. Geochemical Processes: Water and Sediment Environments. Wiley, New York.

Neufeld, P.D., Janzen, A.R. and Aziz R.A., 1972. Empirical Equations to Calculate 16 of the Transport Collision Integrals Ω(l, s)* for the Lennard- Jones (12–6) Potential. Journal of Chemical Physics, 57(3), DOI: 10.1063/1.1678363.

Nelson, J.S., Simmons, E.C., 1995. Diffusion of Methane and Ethane through The Reservoir Cap Rock: Implications for The Timing and Duration of Catagenesis. AAPG Bulletin 79, 1064–1074.

Novosad, Z. and Costain, T.G., 1988. New Interpretation of Recovery Mechanisms in Enriched Gas Drives. Journal of Canadian Petroleum Technology. March-April, **21**(2): 54-60.

Orr. F.M.J., Silva, M.K., Lien, C.L. and Pelletier, M.T., 1982. Laboratory Experiments to Evaluate Field Prospects for CO_2 Flooding. JPT **34**(4):888-898.

Petersen, E.E., 1958. Diffusion in a pore of varying cross section. American Institute of Chemical Engineers Journal **4**:343–345.

Poling, B.E., Prausnitz, J.M. and O'Connell, J.P., 2004. The Properties of Gases and Liquids. Fifth Edition, McGraw-Hill, New York.

Reid, R.C., Prausnitz, J.M. and Poling, B.E., 1987. The Properties of Gases and Liquids. Fourth Edition, McGraw-Hill, New York.

Riazi, M.R. 2005. Characterization and Properties of Petroleum Fractions. First Edition, ASTM, Philadelphia.

Sigmund, P.M., 1976a. Prediction of Molecular Diffusion at Reservior Condition. Part I - Measurment and Prediction of Binary Dense Gas Diffusion Coefficients. Journal of Canadian Petroleum Technology, Apr-Jun, **15**(2). DOI: 10.2118/76-02-05

Sigmund, P.M., 1976b. Prediction of Molecular Diffusion At Reservoir Conditions. Part II - Estimating the Effects Of Molecular Diffusion And Convective Mixing In Multicomponent Systems. Journal of Canadian Petroleum Technology, Jul-Sept, **15**(3). DOI: 10.2118/76-03-07.

Stalkup, F.I. Jr. 1982: Status of Miscible Displacement. paper SPE 9992 presented at the 1982 SPE International Petroleum Exhibition and Symposium, Beijing, China.

Stalkup, F.I. Jr. 1983. Miscible Displacement. Henry L. Doherty Monograph Series, SPE, Richardson, Texas, USA, 8.

Stone, H.L., 1970. Probability Model for Estimating Three-Phase Relative Permeability. J. Pet. Tech. 249:214-218, Trans. AIME 249.

Ullman, W.J., Aller, R.C., 1982. Diffusion Coefficients in Near Shore Marine Sediments. Limnology Oceanography **27**: 552–556.

van Brakel, J., Heertjes, P.M., 1974. Analysis of Diffusion in Macroporous Media in Terms of a Porosity, a Tortuosity and a Constrictivity Factor. International Journal of Heat and Mass Transfer **17**: 1093–1103.

Wang, Y. and Orr, F.M., Jr., 1998. Calculation of Minimum Miscibility Pressure. paper SPE 39683 presented at the 1998 SPE/DOE Improved Oil Recovery Symposium, Tulsa, April 19-22.

Weinaug C.F. and Katz D.L. 1943. Surface Tension of Methane-Propane Mixtures. Ind. & Eng. Chem. **35**(2): 239–246.

Whitson, C.H. and Brule M.R., 2000. Phase Behavior. Monograph Vol. **20**, Richardson, TX.

Wilke, C.R., 1950. Diffusion Properties of Multicomponent Gases. Chemical Engineering Progress, **46**(2): 95-104.

Zick, A.A., 1986: "A Combined Condensing/Vaporizing Mechanism in the Displacement of Oil by Enriched Gases," paper SPE 15493 presented at the 1986 SPE Annual Technical Conference and Exhibition, New Orleans, Oct. 5-8.

Zick Technologies: MMPz Manual, www.zicktech.com.

Zick Technologies: ***PhazeComp***, www.zicktech.com.

Chapter 3

Modeling CO_2 Injection in Karimaie Fractured Chalk Experiment

3.1 Introduction

Karimaie (2007) performed equilibrium gas injection followed by CO_2 injection in a series of experiments on chalk and carbonate cores at reservoir conditions, where the cores were initially saturated with live synthetic oil. This chapter presents a numerical modeling study of CO_2 injection in a chalk core based on experimental data, as reported by Karimaie (2007). The experiment consisted of a vertically-oriented 19.6 cm long chalk outcrop core initially saturated with reservoir synthetic oil consisting of C_1 and n-C_7 at a temperature of 85 ^oC and pressure of 220 bar. After saturating the core with the oil mixture by displacement, a small "fracture" volume surrounding the core was created by heating the solid Wood's metal that originally filled the volume between the core and core holder.

Gas injection was conducted initially using an equilibrium C_1-n-C_7 gas at 220 bar. This gas should have had no recovery by thermodynamic mass transfer, only from immiscible Darcy-controlled displacement driven by pressure gradients and gravity-capillary forces. Once oil production ceased in this first displacement, a second period with pure CO_2 gas injection followed.

Our numerical modeling was conducted with a compositional reservoir simulator. The 2-dimensional r-z model used fine grids for the core matrix and the surrounding fracture.

In a fractured system, matrix permeability controls the rate of recovery. The pressure gradients along fractures are negligible for high permeability fractures where most injected gas flows through the fracture space and the main production mechanism from the matrix is gravity drainage. That means the ratio between the matrix and fracture permeability determines whether viscous displacement (Darcy flow by pressure gradients) governs the displacement, or not. Therefore, fracture permeability should be sufficiently high in an experiment to eliminate viscous displacement in the core. Uncertainty analysis and sources of experimental error had to be studied to understand and simulate the Karimaie experiment.

3.2 Rock and Fluid Properties

Chalk core from Faxe area outcrop in Denmark was used in the Karimaie experiment, with similar rock properties to North Sea chalk. The core had a cylindrical shape with a length of 19.6 cm and 3.8 cm in diameter. Core porosity and permeability were reported as 44% and 5 md, respectively (Karimaie 2007; Karimaie and Torsæter 2009).

Relative permeabilities were not reported by Karimaie (2007) and Karimaie and Torsæter (2009). The capillary pressure curve presented (Karimaie 2007) was water-oil drainage capillary pressure of Ekofisk chalk core measured by Talukdar (2002). In our modeling study, we used instead a C_1-n-C_5 capillary pressure data set from Faxe outcrop chalk core measured by Christoffersen (1992). The water-oil capillary pressure curve was measured with a centrifuge, while the C_1-n-C_5 capillary curve was measured by a high-pressure, porous-plate method. Porosity and permeability of the core used to interpret the water-oil P_{cow} curve was 31% (anomonously low for outcrop chalk) and 1.94 m d, respectively. Porosity and permeability of the core used to obtain C_1-n-C_5 P_{cgo} curve were 46.5% and 5 md, respectively. Reference IFT of the water-oil system was not reported, whereas

C_1-n-C_5 was reported and equal to 1.5 mN/m. Reference IFT was used to scale capillary pressure. We found it more appropriate to use the C_1-n-C_5 capillary pressure.

Reported compositions were not measured. 33% of C_1 with 67% of n-C_7 mass fraction were mixed and then flashed at P=220 bar and T= 85 °C. The liquid phase was used as live oil for the experiment and gas injected as equilibrium gas. Karimaie simulated the above process in a PVT simulator to calculate reported EOS oil and gas compositions. Using his reported equation of state (EOS) we were not able to reproduce his reported oil and gas compositions (**Table 3.1**).

Table 3.1 – Comparison of Reported Oil and Gas Compositions by Karimaie (2007) and Recalculated Compositions Using His Reported EOS.

Component	Calculated compositions from reported EOS		Reported compositions	
	x_i	y_i	x_i	y_i
C_1	0.6885	0.9197	0.7034	0.8825
nC_7	0.3115	0.0803	0.2966	0.1175

Given this finding, the reported oil and gas compositions and EOS were not used in our study. Bubble point pressure, oil density and interfacial tension (IFT) were measured by the SINTEF PVT lab. *PhazeComp* PVT software using the SRK EOS was used to determine the laboratory oil composition with a 220 bar saturation pressure at 85 °C. The resulting oil composition consisted of 68.44 and 31.56 mole percent of C_1 and n-C_7, respectively. Deviation of calculated oil density (0.413 g/cm^3) at 220 bar was about 1.6 % which is in the range of laboratory measurement error. The EOS together with parachor method was tuned to match measured IFT at 220 bar (0.15 mN/m). EOS parameters used in this study are given in **Tables 3.2** and **3.3**.

Table 3.2 – EOS Properties for The SRK Characterization

Component	MW	Tc, K	Pc, bara	Zc	Vshift	ω	Parachor
CO_2	44.01	304.12	73.74	0.2743	0.2175	0.225	80.00
C_1	16.04	190.56	45.99	0.2862	-0.0025	0.011	64.23
n-C_7	100.20	540.20	27.40	0.2611	0.1435	0.350	281.33

Table 3.3 – SRK Binary Interaction Parameters

	CO2	C1	n-C7
CO_2	0.00000	0.12000	0.15000
C_1	0.12000	0.00000	0.01574
n-C_7	0.15000	0.01574	0.00000

3.3 Experimental Procedure

This section describes an experiment originally designed to study gravity drainage in a fracture-matrix system by injecting equilibrium gas followed by CO_2. The experimental procedure is described by Karimaie (2007), Karimaie and Torsæter (2009) and personal communication with Karimaie. Uncertainties and possible sources of lab error are discussed in the next section.

A dried cylindrical chalk core was placed in a steel core holder. The core holder inner length and diameter were 20 cm and 4.2 cm respectively. The core diameter was 3.8 cm and had 19.6 cm length. The fracture was represented by a 2 mm space between core and core holder. Core porosity was reported as 44%, and absolute permeability measured with n-heptane (n-C_7) at room temperature was ~ 5 md (Karimaie 2007; Karimaie and Torsæter 2009).

Due to large permeability contrast between the core and the surrounding space (artificial fracture), it was complicated to saturate the core with live oil. Oil would flow through the high permeable space leaving the core only partially saturated with live oil. Therefore, the space between the core and the core holder wall was initially filled with Wood's metal. The metal melting point is 70 ^oC; the experiment was conducted at 85 ^oC. Prior to saturating the core, the Wood's metal was melted and poured into the space between the core and core holder. The fracture was sealed with the metal and had zero permeability after cooling the system.

The core was evacuated and saturated with dead n-C_7. The dead n-C_7 oil was injected at several injection rates to determine absolute permeability. The system was then pressurized and live oil was injected into the core at a rate of 0.1 cm^3/min. During injection, the pressure was kept above 220 bar (saturation pressure) and three pore volumes of live oil were injected. Then the system was heated to 85 ^oC at a constant pressure and Wood's metal was removed from the annular space by injecting live oil. Oil was injected from the top and the melted Wood's metal drained from the bottom of the core holder. Fracture porosity was not measured after the metal was removed from the system. Total core+fracture permeability was not measured after removal of the Wood's metal.

Oil in the fracture was replaced by equilibrium gas. Reported gas injection rate at the beginning of displacement was 5 cm^3/min and was later reduced to 0.1 cm^3/min. The time at which the rate was changed was not reported. The experiment continued with equilibrium gas injection until no more oil was produced. After 4.2 days of equilibrium gas injection, CO_2 injection was started and lasted for 2.2 days.

With respect to measured surface oil production, Karimaie and Torsaeter (2009) state "The standard volumes of liquid and gas obtained were measured after passing two step condensers at a constant temperature of 5^{o}C (41^{o}F) and -4^{o}C (24.8^{o}F), respectively, to condense any heavy hydrocarbons that may have been carried along with it."

3.4 Uncertainties and error sources

Core porosity defines the fluid in place, but had no direct impact on the fluid displacement process. Core diameter varied between 3.8 and 3.7 cm along the core height. Core diameter variation caused uncertainty in core and fracture pore volume, justifying our use of core (matrix) and fracture porosity as uncertainties used as regression parameters.

Ideally, the study of gravity drainage requires that viscous displacement in the core be eliminated or minimized. Unfortunately, it was observed in the Karamaie experiments that some Wood's metal remained in the space between the core and core holder. Reported fracture porosity was 93%, and fracture permeability may have been reduced. Porosity reduction of the fracture will affect fracture pore volume. Fracture permeability reduction could affect the recovery mechanism, changing from gravity-dominant to viscous-dominant for gas injection.

Another uncertainty is surface separation efficiency in the lab tests, and the correct modeling of the separation process. It was reported that the produced stream was passed through a two-step condenser 5°C (41°F) and -4°C (24.8°F). But according to direct discussion with Karamaie and observation of the laboratory system, the stream was passed through coiled pipe in an ice-fresh-water bath (condenser) and then flashed to a measuring cylinder at atmospheric pressure. The measuring cylinder was placed in and ice-brine bath. Stream temperature might not reach 5 °C (41 °F) after passing through the condenser. The whole stream was not passed through a -4 °C (24.8 °F) condenser, only the flashed liquid was cooled. According to these observations, temperature of the gas-oil separation was not known with any accuracy, and it is difficult to model accurately.

3.5 Model Description

The matrix block and fractures were initially filled with oil. The fractures were assumed to have negligible capillary pressure. The matrix and the fracture dimensions were the same as core and fracture in the experiment. A two-dimensional radial gridded model was used, where the matrix block was surrounded by two horizontal fractures at the top and bottom and one vertical fracture. Fine gridding was needed for CO_2 gas injection to reduce numerical dispersion and achieve better results. Ten and 51 grid cells were used in radial and vertical directions, respectively.

The *SENSOR* and *Eclipse 300* simulators with implicit solution method were used for simulation models. *Eclipse 300* was used to examine diffusion effects on the production behavior. A 3-component SRK EOS was used. The EOS properties of the components are summarized in Table 3.2 and the binary interaction parameters are given in Table 3.3. SENSOR and Eclipse 300 models gave the same results without diffusion.

An analytical capillary pressure and relative permeability formulation were used as described in section 2.3. C_1- n-C_5 capillary pressure measured by Christoffersen (1992) at similar core was taken as core capillary pressure in the model. This capillary pressure was scaled with IFT according to the Eq. (2.24) where reference interfacial tension (IFT) is 1.5 mN/m. There was no capillary pressure in the fracture. *Eclipse 300* had the same formulation for scaling capillary pressure and calculating IFT.

The *Pipe-It/Streamz* software was used to calculate cumulative oil and gas production from reservoir simulation results. One separator was defined to simulate produced stream in the experiment. Atmospheric pressure was considered as separator pressure same as the experiment. As mentioned above separator temperature was not measured during the experiment, thus, it was used as a regression parameter.

3.6 Matching Experimental Data

3.6.1 Fracture Permeability

In our work, measured cumulative oil production from the outset of injection (**Table 3.4**) was history-matched. Karimaie (2007) and Karimaie and Torsæter (2009) report recovery factors based on the assumption that injected gas replaces only oil in the space between the core and core holder at early times, and that no oil was produced from the core during that time. That means the oil production before 0.083 day (about 2 hours) amounting to 24 cc in Table 3.4 (compared with 90.5 cc total production during entire test) was neglected in their oil recovery calculation. Their assumption of zero flow resistance in the fracture was shown to be suspect, if not wrong, based on our analysis. Together with some uncertainty in core porosity (i.e. initial oil in place in the core), we decided not to use the Karimaie-reported oil recovery factors in history matching, but instead to match reported surface oil volumes produced from the outset of injection.

To illustrate the impact of fracture flow resistance on oil recovery from the core in the Karimaie experiments, we setup two comparison models where the matrix block is filled initially with oil, and the fracture was initialized with equilibrium injection gas. This condition corresponds to the Karimaie *assumption* at the end of the 0.083 days when all the oil had been removed from the fracture and gas had yet to enter the core.

Table 3.4 – Measured Cumulative Oil and Gas Production

Time days	Cumulative Oil Production cm^3	Cumulative Gas Production L	Time days	Cumulative Oil Production cm^3	Cumulative Gas Production L
0.000	0.0	0.00	2.339	68.0	65.96
0.010	6.0	0.05	2.397	68.0	67.03
0.016	8.0	0.10	2.470	70.0	68.49
0.020	10.0	0.89	2.523	70.0	69.87
0.027	12.0	3.27	2.589	71.0	70.95
0.037	14.0	5.34	3.084	76.0	85.39
0.044	16.0	9.20	3.318	76.0	90.59
0.051	18.0	12.68	3.350	76.0	91.00
0.057	20.0	15.87	3.517	78.0	96.75
0.066	22.0	17.10	4.130	82.0	116.83
0.083	24.0	18.05	**4.233***	83.0	117.87
0.182	27.0	18.78	4.264	83.0	122.43
0.191	28.0	18.87	4.277	84.0	123.38
0.244	28.0	19.33	4.291	84.0	124.09
0.368	32.0	21.46	4.391	85.0	133.47
0.757	40.0	30.01	4.410	86.0	138.29
0.908	46.0	38.37	4.437	87.0	140.20
1.128	46.0	38.89	4.462	88.0	145.10
1.141	46.0	39.06	4.483	88.0	145.68
1.208	52.0	44.38	4.606	88.0	147.12
1.254	52.0	44.81	4.639	88.0	150.54
1.280	52.0	45.22	4.668	88.0	151.11
1.313	60.0	54.67	5.154	90.0	166.10
1.462	60.0	56.03	5.187	90.0	166.32
1.487	61.0	56.61	5.458	90.0	169.08
1.506	62.0	56.89	5.500	90.0	172.01
2.037	64.0	59.50	5.520	90.0	172.17
2.085	64.0	60.12	6.129	90.5	191.71
2.108	65.0	60.50	6.229	90.5	197.84
2.116	65.0	60.90	6.379	90.5	202.16
2.320	68.0	65.42			

*CO_2 injection start

The fractures had zero capillary pressure and high permeability (100 D) to ensure that flow resistance in the fracture was negligible and that oil recovery from the core was controlled by capillary-gravity drainage. Core porosity and separator temperature were set to 44% and 5 ^oC (41 ^oF), respectively, in both models. One model used a capillary pressure curve, where gas drainage was expected only if the core height was greater than the capillary entry height (2.7 cm). In the other model we assumed zero capillary pressure in the core, to provide an extreme (albeit unphysical) case of oil drainage from the core.

Our first model used a chalk capillary pressure curve, the shape of which dictates the rate of oil recovery from the core as gravity and capillary forces balance. Clearly, there exists some uncertainty in the capillary pressure curve and its scaling with IFT (constant for the equilibrium gas injection test). **Fig. 3.1** shows predicted oil production compared with the reported oil recovery by Karimaie using oil production data after 0.083 days. Predictions are significantly lower than reported.

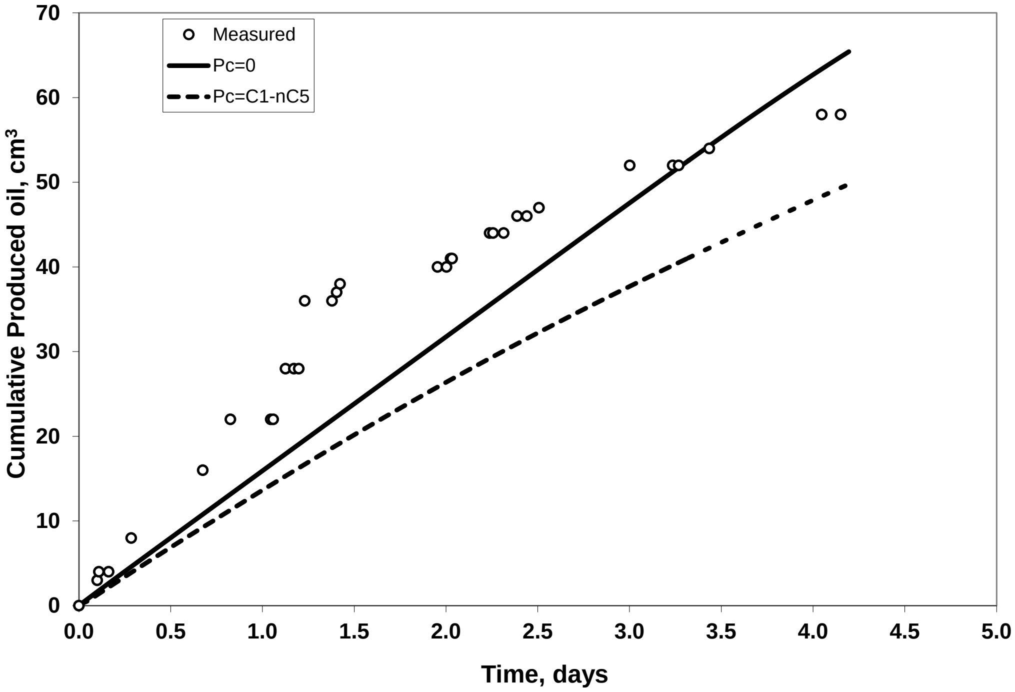

Figure 3.1 – Measured oil production without considering early produced oil and simulation result of assuming gravity-drainage mechanism.

As an extreme treatment of core capillary pressure, we used zero capillary pressure in a second model. The only driving force of recovery is now gravity. Fig. 3.1 shows that even in the absence of capillary pressure in the core, predicted oil recovery was lower than reported recoveries up to 3 days, and had a very different production rate profile than reported.

Our conclusion, as shown in the final model history match of the Karimaie data, was that the oil production from the core starts immediately after gas was injected, and that the core and fracture jointly produce oil over a period significantly longer than 0.083 days. The fracture resistance was found to be significant, and not justifying the assumption of an infinite conductivity fracture.

3.6.2 Equilibrium Gas Injection Rate

It was reported that equilibrium gas was injected at high rate (5 cm^3/min) from the top and then decreased to 0.1 cm^3/min after 0.083 days. **Fig. 3.2** clearly shows a rate change at 0.015 days. However, using 5 cm^3/min injection rate in the model

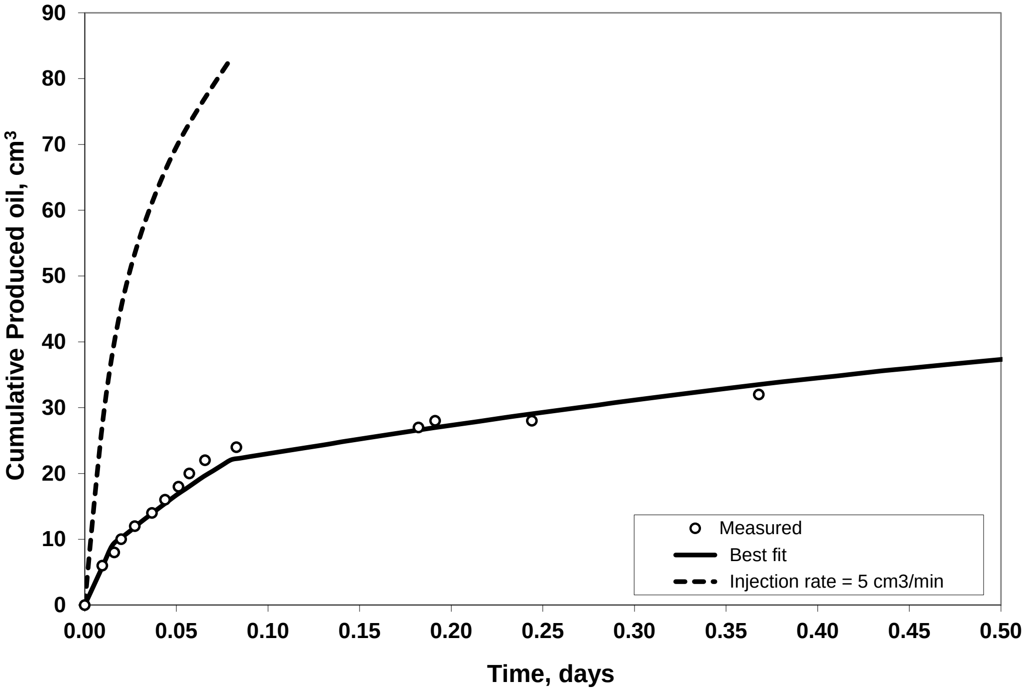

Figure 3.2 – Early measured oil production of the experiment and simulation results of 5 cm^3/min injection rate and best fit.

during the time period up to 0.083 days leads to significantly higher oil production than reported experimentally. Our final model used the following injection rates: 1 cm^3/min (0<t<0.015 days=22 min), 0.386 cm^3/min (0.0150<t<0.083 days=120 min), and 0.1 cm^3/min (t>0.083 days); this is to be compared with reported injection rates: 5 cm^3/min (0<t<0.083 days), and 0.1 cm^3/min (t>0.083 days).

3.6.3 CO_2 Injection Rates

Cumulative gas production was matched reasonably well during equilibrium gas injection, as illustrated in **Fig. 3.3**. There was a rapid increase in gas production when CO_2 injection started. This could be caused by: (a) increasing gas injection rate, (b) change in effective surface temperature and/or (c) decreasing gas formation volume factors. CO_2 was injected from the top, and gas produced from the bottom of core holder. It was expected that equilibrium gas would be produced early during CO_2 injection. On the other hand, Fig. 3.3

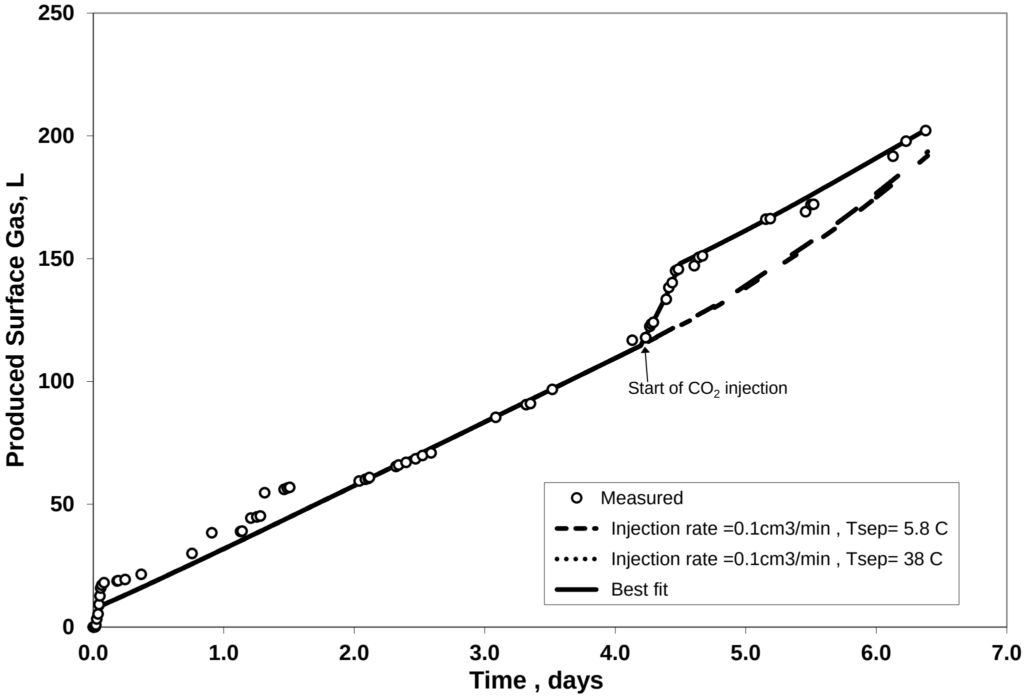

Figure 3.3 – Measured gas production with matched simulation result and results of 0.1 cm^3/min injection rate.

indicates that increasing temperature alone could not justify this change of gas production profile. Karimaie does not report an injection rate increase when CO_2 injection starts, but according to gas production behavior in Fig. 3.3 and later communication with Karimaie, the injection rate was in fact increased at about 4 days. By trial and error we found that CO_2 injection rate was increased from 0.1 cm^3/min to 0.364 cm^3/min at 4.2 days, and then reduced to 0.07 cm^3/min at 4.5 days, this CO_2 injection rate profile giving a consistent match to produced gas rate. The final injection rate profile during the entire experiment is shown in **Fig. 3.4**.

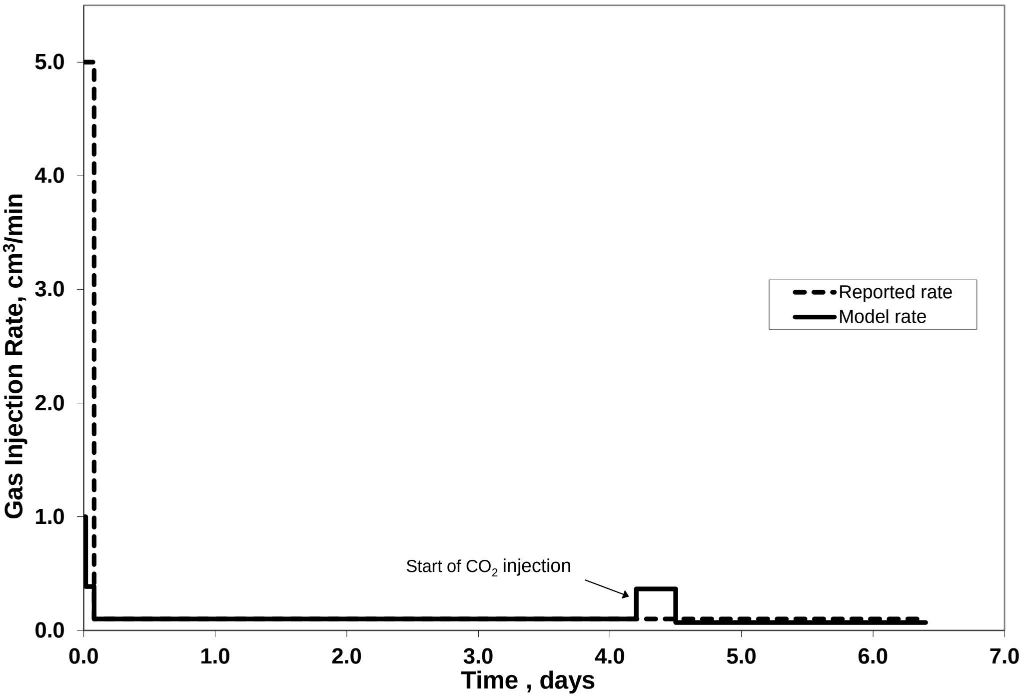

Figure 3.4 – Reported and model gas injection rate profile during the experiment.

3.6.4 Surface Separation

The produced mixture from the core holder was separated with a simple process, namely a flash to atmospheric pressure and temperature controlled by a pre-separation ice-water bath. The effective surface process temperature is assumed to vary with the injection rate, and particularly CO_2 injection because CO_2 has lower thermal conductivity than equilibrium gas. We found that the assumed separator temperature had a pronounced effect on volume produced, and the surface temperature model used for CO_2 injection was 30 °C (86 °F) in the period 4.2<t<4.5 days, and 26.7 °C (80 °F) for t>4.5 days.

3.6.5 Regression Parameters

A number of laboratory parameters were considered as uncertain to the extent that their value could be adjusted as part of the history matching process. These include: (a) fracture permeability, (b) core residual oil saturation, (c) core porosity, (d) fracture porosity, and (e) separator temperature. Core relative permeability was also considered uncertain, but instead of using an IFT-dependent relative permeability model, we simply considered two cases – mild curvature with exponents $n_g=n_{og}= 2$ in Eqs. (2.19) and (2.20), and low-IFT/near-miscible straight-line curves ($n_g=n_{og} = 1$). Automated regression was run to obtain a best fit of the measured cumulative oil produced by adjusting the five parameters above (a)-(e). Initial values, lower and upper limits of the regression parameters are given in **Table 3.5**. Because the experiment was conducted at a low IFT (0.15 mN/m) for equilibrium gas injection, and even lower for CO_2 injection, we used two sets of oil-gas relative permeabilities using saturation exponents of 2 and 1 both models giving a reasonable match of lab data (**Fig. 3.5**). Best-fit parameters for core and fracture porosities determined with straight-line relative permeabilities were more consistent with values reported by the lab. IFT decreased during CO_2 injection from 0.15 to 0.0001 mN/m at the displacement front, and therefore the n=1 relative permeability model was considered the most appropriate to simulate the

Table 3.5 – Regression Variables

	Final		Initial value	Lower limit	Upper limit
Relative permeability	n=1	n=2			
Residual oil saturation (%)	5.1	5.8	10.0	5.0	20.0
Fracture permeability (md)	26.3	20.4	30.0	10.0	100.0
Core porosity (%)	44.5	48.0	44.0	44.0	48.0
Fracture porosity (%)	93.6	89.1	90.0	85.0	100.0
Separator temperature of equilibrium gas injection (°C)	5.8	7.0	5.0	-4.0	15.6

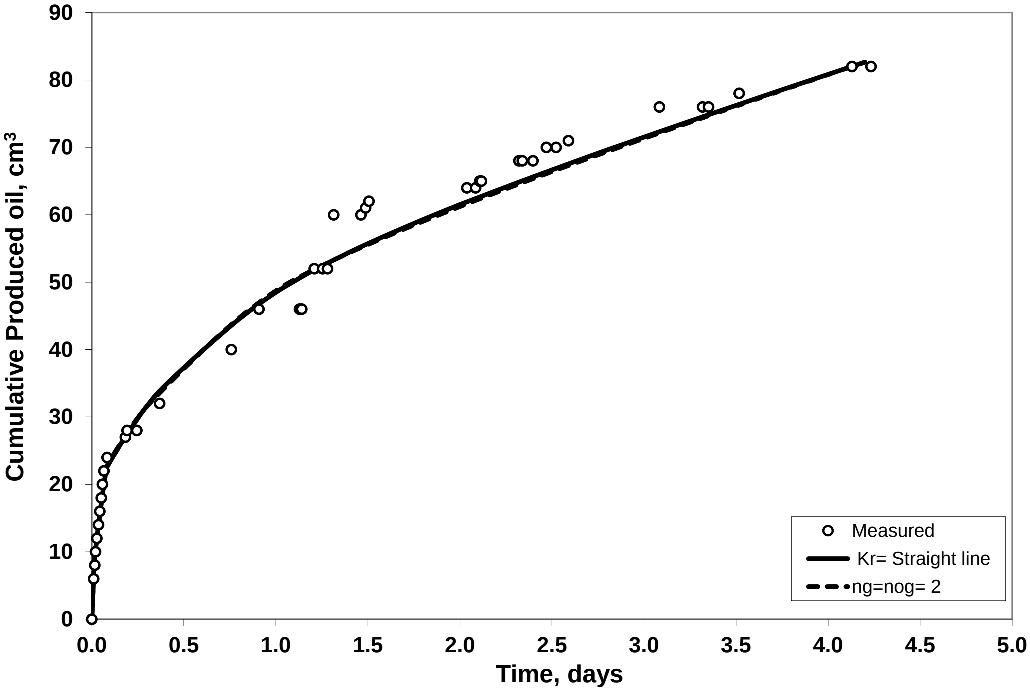

Figure 3.5 – Measured oil production with matched simulation results of equilibrium gas injection period.

CO_2 injection period. **Fig. 3.6** shows measured cumulative oil production and simulation results.

3.7 Recovery Mechanism

Reported oil recovery factor was not reliable because (a) it was based on the invalid assumption that only fracture oil, located in the space between the core and core holder, is produced at early times, and (b) initial oil in place used to calculate reported recovery factors was found to be erroneous. In this study, the model oil recovery factor is calculated from oil saturations and is used to study the oil recovery mechanism.

Viscous/gravity ($R_{v/g}$) dimensionless ratios was used to understand the importance of the various recovery mechanisms during production (Wylie and Mohanty 1999; Stalkup 1983; Løvoll et al. 2005):

$$R_{v/g} = \frac{\Delta P_{visc}}{\Delta P_{grav}} = \frac{u\mu_o}{kg\Delta\rho_{og}} \quad \text{...}(3.1)$$

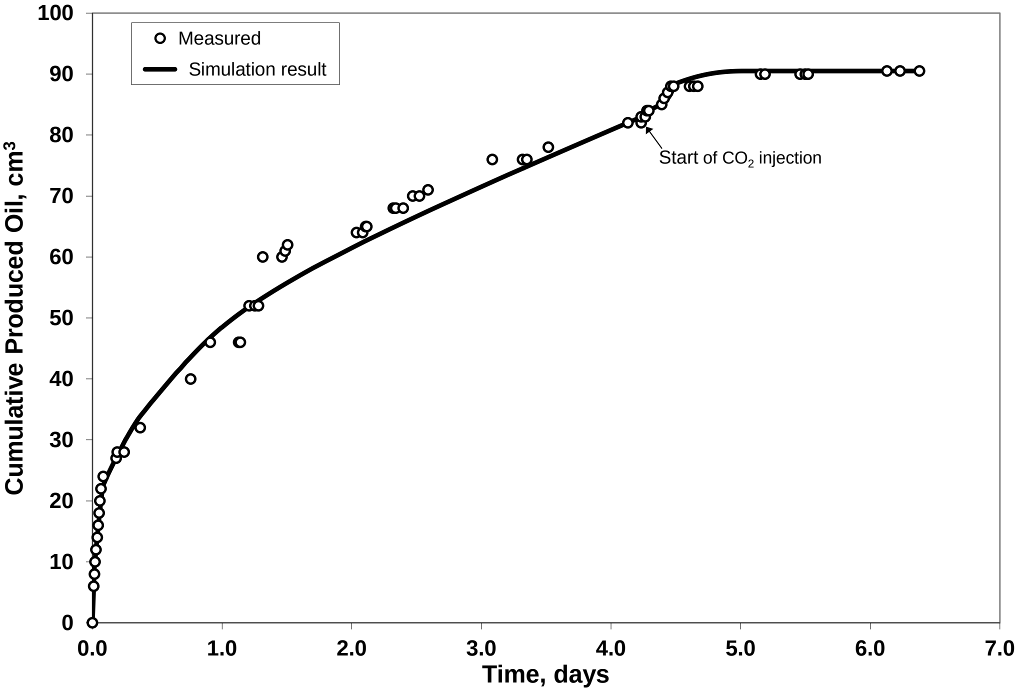

Figure 3.6 – Measured oil production with matched simulation result of equilibrium gas injection and CO_2 injection periods.

where u is linear Darcy velocity in z-direction, μ_o is oil viscosity, k is matrix-block permeability, $\Delta\rho_{og}$ is oil and gas density difference and g is gravity-acceleration constant.

This experiment was conducted to study low interfacial tension gravity drainage in fractured porous media. However, as mentioned above, fracture permeability was not sufficiently large to study fracture-matrix gravity drainage. One characteristic of gravity drainage with equilibrium-gas injection is that oil below the capillary threshold height is not recovered. As shown in **Figs. 3.7-3.10** the displacement front from our history-matched model does not stop above the capillary threshold height (2.7 cm), and hence gravity drainage alone could not be the recovery mechanism. We found that viscous displacement was dominant during equilibrium-gas injection, as verified from a frontal viscous/gravity ratio $R_{v/g}$ of 5.5 calculated at the fifth hour of the experiment.

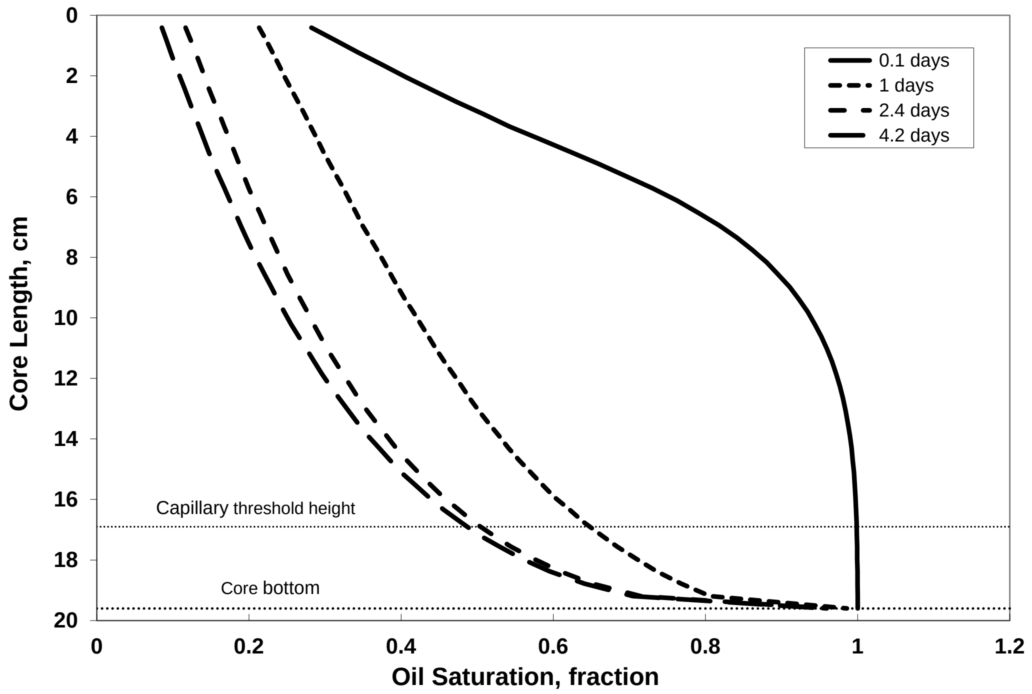

Figure 3.7 – Core oil saturation profile during equilibrium gas injection period from numerical model with linear core relative permeability.

More oil was produced after injecting CO_2, as shown in Fig. 3.6. At the end of the experiment no oil production was observed while still injecting CO_2. The model shows that 100% oil recovery was achieved after somewhat more than one PV CO_2 injected. As seen in **Fig. 3.11**, CO_2 is first-contact miscible with the equilibrium oil and first-contact miscible after reaching 30 mol-% CO_2 content when contacting an equilibrium oil-gas mixture having approximately 60% gas saturation initially. A 100% recovery after about 1 PV CO_2 injected is expected given the thermodynamic miscibility conditions and an efficient top-down, gravity-stable core displacement.

Diffusion was another mechanism that could play a role in production during CO_2 injection period. We examined the effect of diffusion by running the model with and without diffusion transport. As describe in section 2.2, diffusion coefficients were calculated from the extended Sigumnd correlation (da Silva and Belery 1989), given in **Table 3.6**. As illustrated in **Fig. 3.12** average oil saturation of the core was identical for runs with and without diffusion.

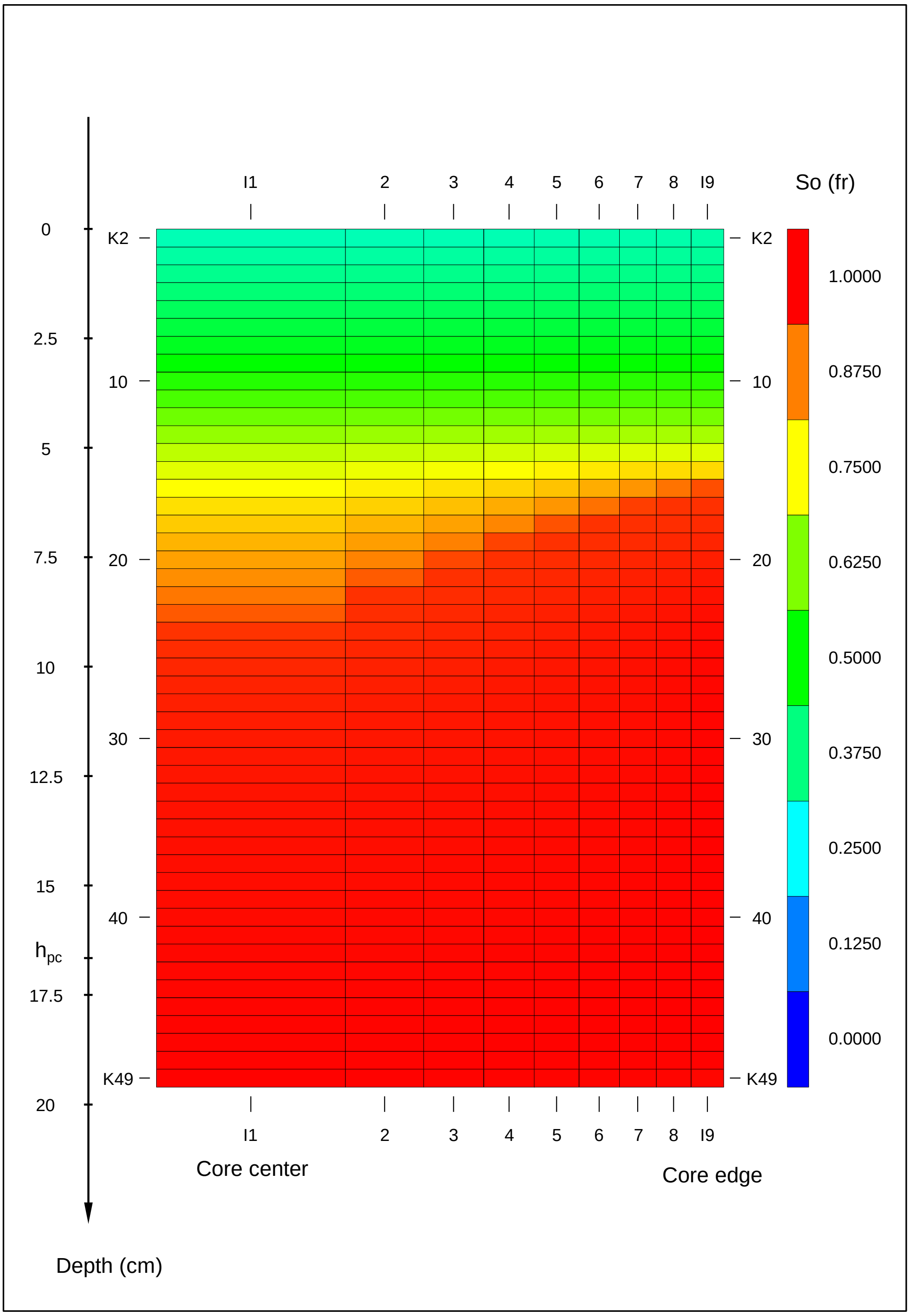

Figure 3.8 – Oil saturation map of core after 2.4 hours for matched model with linear core relative permeability (at about 18% oil recovery).

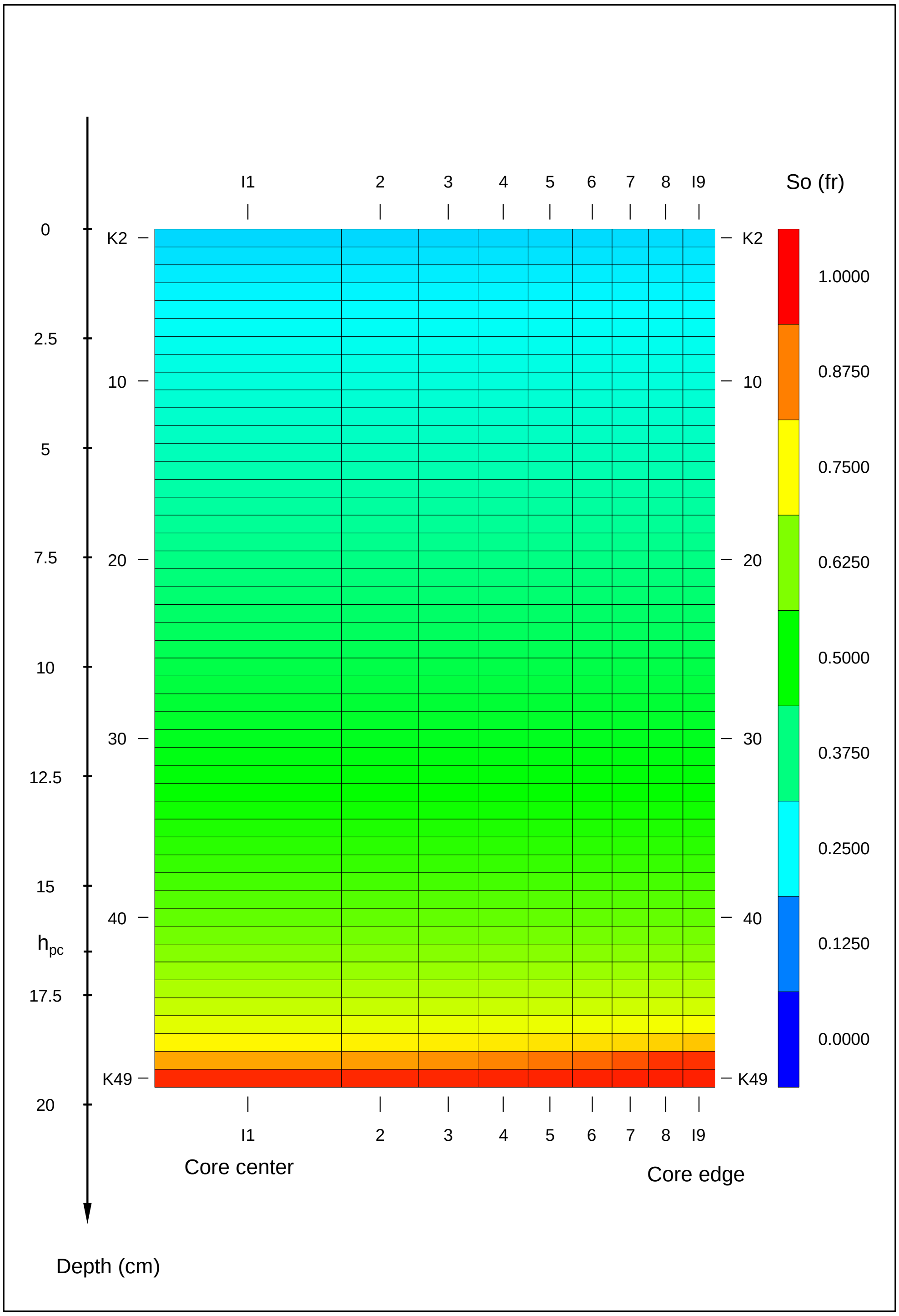

Figure 3.9 – Oil saturation map of core after 1 day for matched model with linear core relative permeability (at about 54% oil recovery).

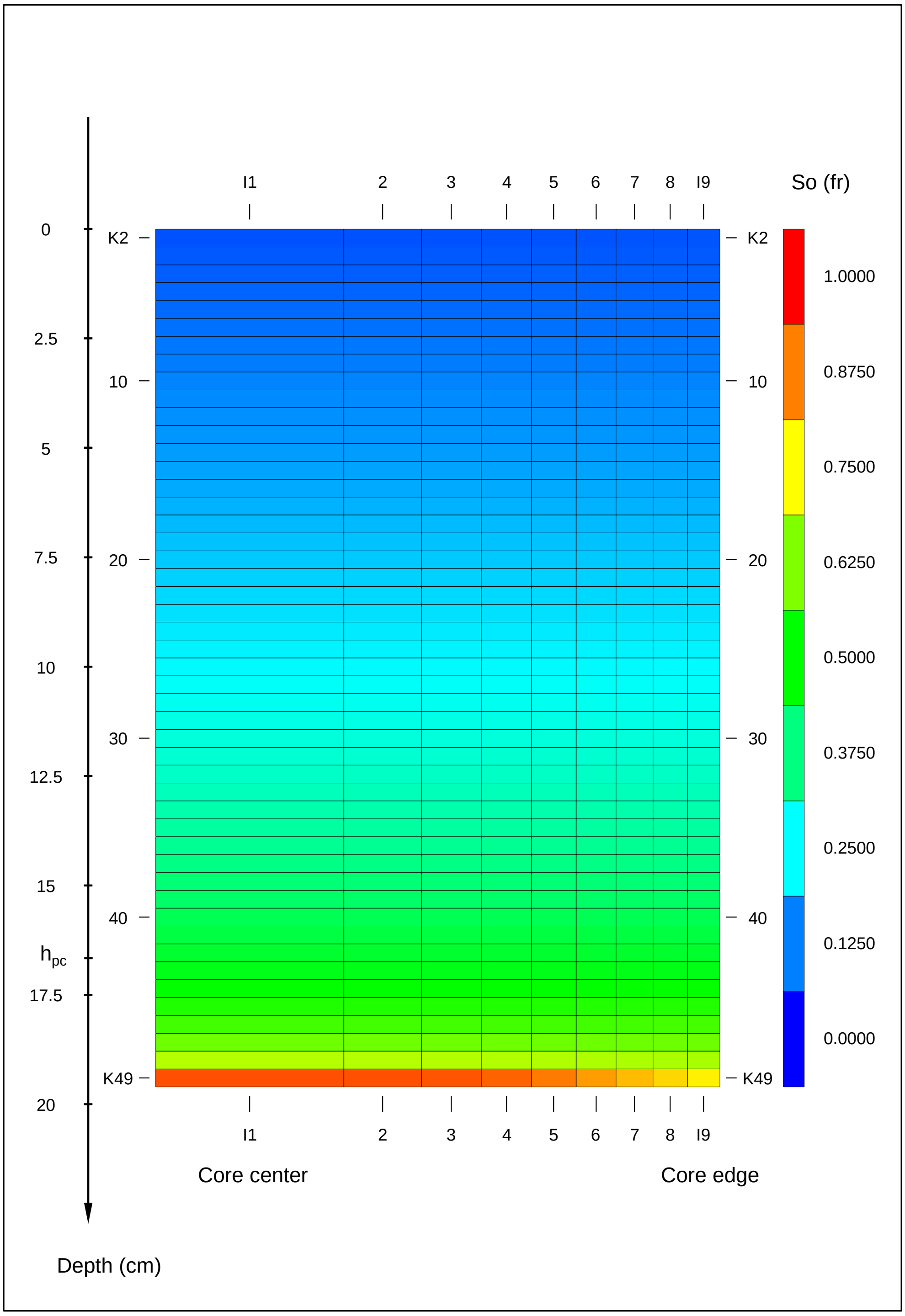

Figure 3.10 – Oil saturation map of core after 4.2 day for matched model with linear core relative permeability (at about 70% oil recovery).

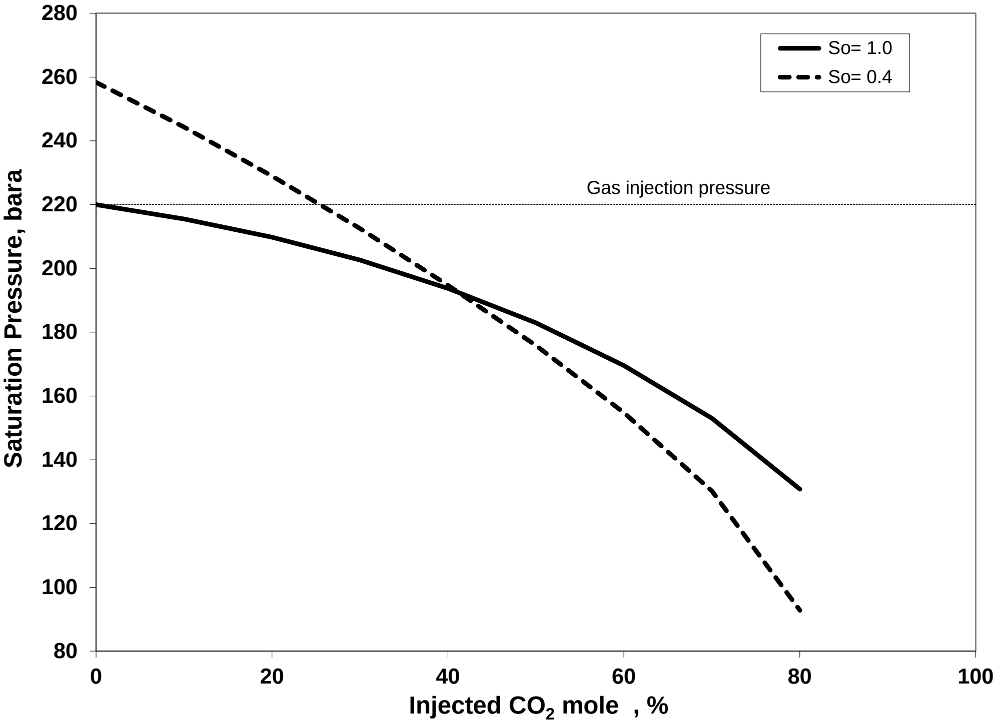

Figure 3.11 – Saturation pressure versus injected CO_2 mole percent calculated by swelling test for 1 and 0.4 oil saturation.

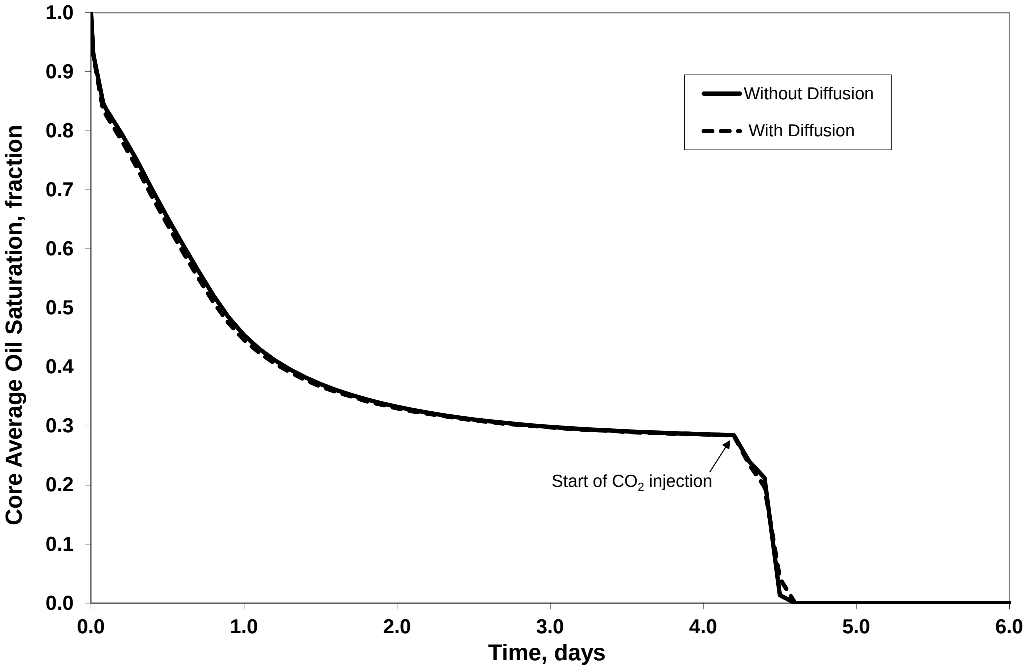

Figure 3.12 – Profile of average oil saturation in the core during equilibrium gas and CO_2 injection period with and without diffusion.

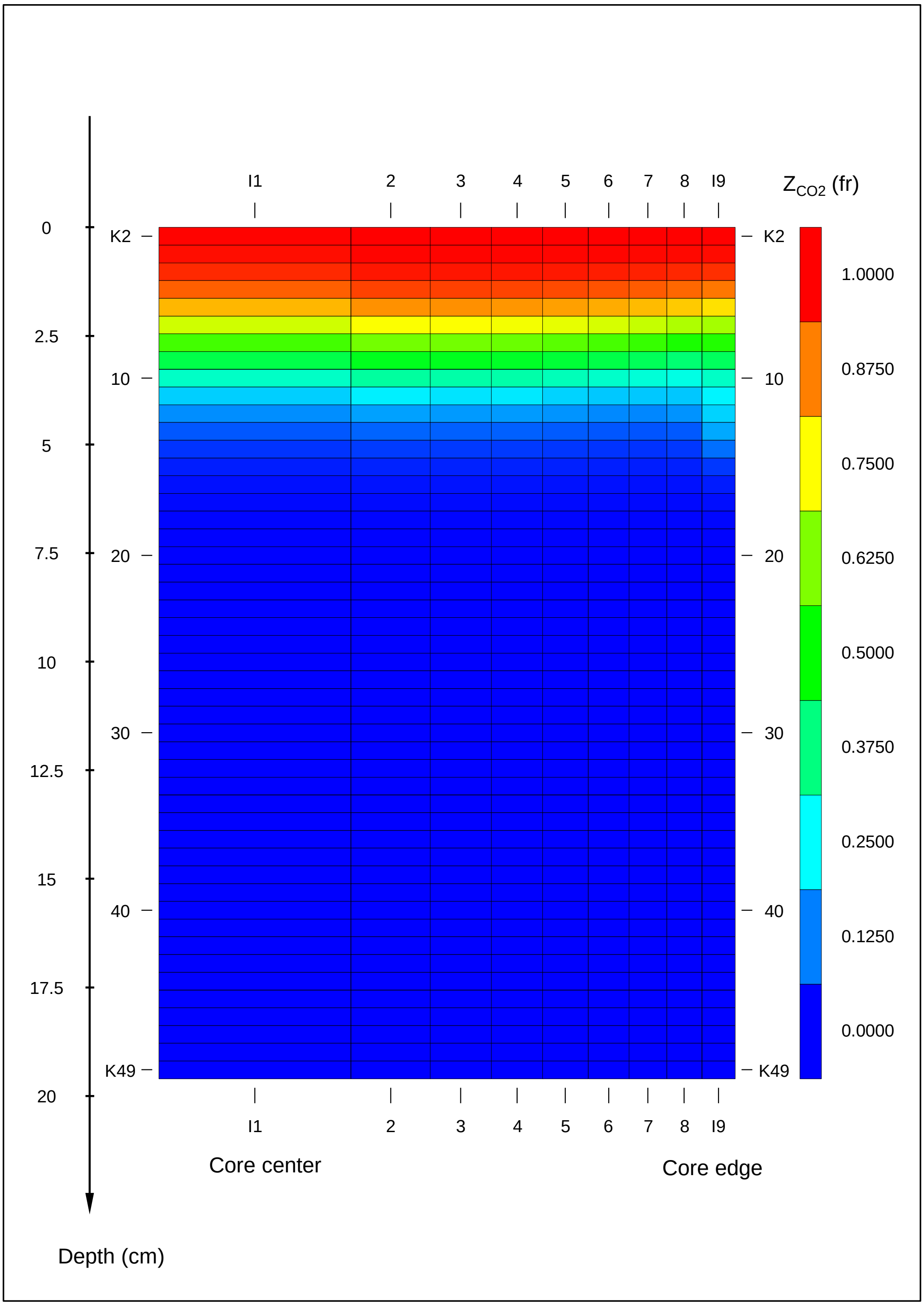

Figure 3.13 – CO_2 mole fraction map of core after 4.25 days for matched model without diffusion effect.

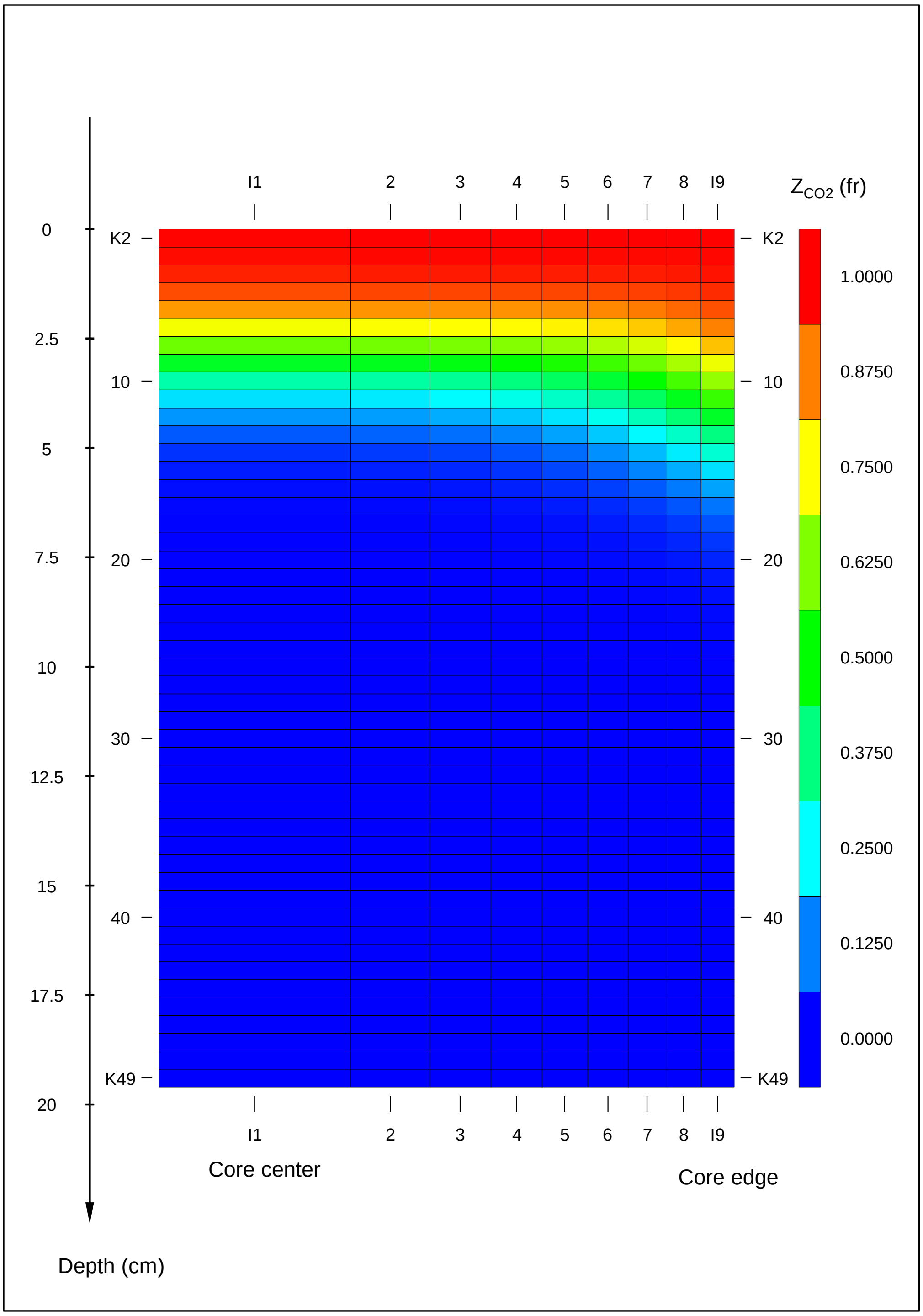

Figure 3.14 – CO_2 mole fraction map of core after 4.25 days for matched model with diffusion effect.

Comparison of CO_2 map at 4.25 days (102 hours) for diffusion and non-diffusion cases revealed small differences, as shown in **Figs. 3.13** and **3.14**. Our results agree with Hoteit and Firoozabadi (2006) who show that diffusion has minor effect in viscous-dominated displacements.

Table 3.6 – Diffusion Coefficients for Oil and Gas Phase

Component	D_o (cm^2/s)	D_g (cm^2/s)	D_g / D_o
C_1	1.04E-05	3.43E-05	3.3
n-C_7	1.04E-05	3.43E-05	3.3
CO_2	1.27E-05	6.45E-05	5.1

Near-miscible and viscous displacements were the main two production mechanisms during CO_2 injection. Pressure gradient caused CO_2 to enter into the core and the core oil was displaced miscibly by CO_2. Model oil saturation profile and gas mole fractions indicate that that an oil bank builds ahead of the miscible front (where Sg→0), as illustrated in **Figs. 3.15** and **3.16**. Note that the oil carrying capacity of gas ahead of and behind the front increases with time.

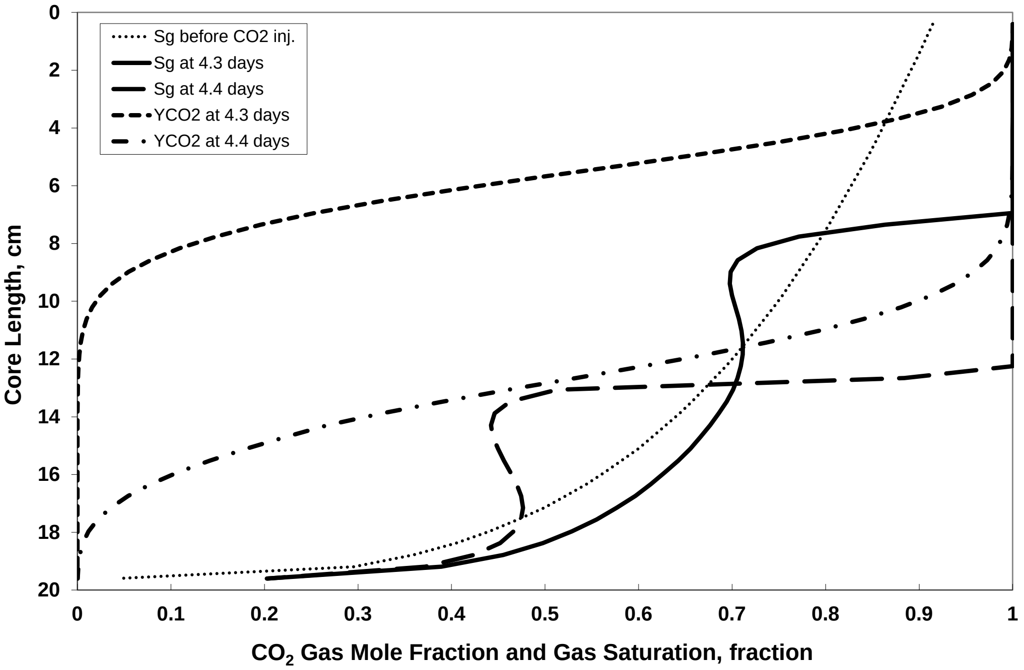

Figure 3.15 – Profile of CO_2 gas mole fraction and gas saturation in the core during CO_2 injection period.

Because oil was produced from both the matrix and the fracture at early times, it is difficult to calculate matrix recovery factor based on produced oil. Therefore matrix oil recovery was calculated from total average oil saturation S_o in the core using the following relation:

$$RF = (1 - \frac{S_o}{S_{oini}}) \quad \text{.......................................} (3.2)$$

For model results at a given time, the calculated oil recovery from Eq. (3.2) is slightly higher than oil recovery calculated based on production. The difference stems mainly from the oil carried in solution in the gas behind the displacement front, this oil being produced (by surface condensation) only after the enriched CO_2-rich gas reaches the end of the core and is produced. Calculated oil recovery is shown in **Fig. 3.17**. About 70% of the initial oil in place in the core was recovered by equilibrium gas injection and all residual oil was produced by CO_2 injection at the end of the experiment.

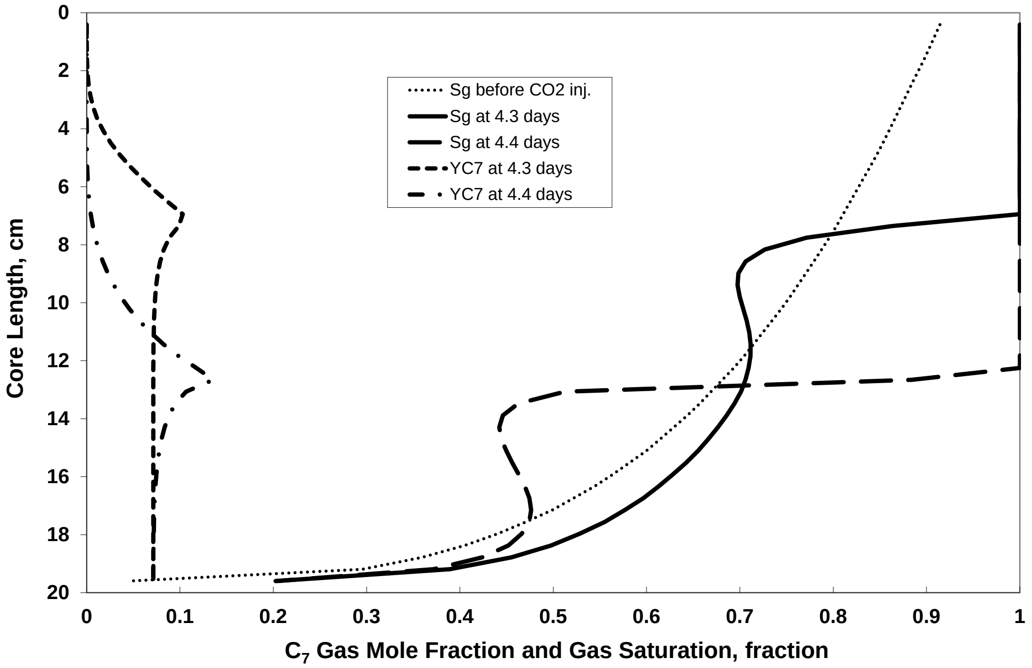

Figure 3.16 – Profile of n-C_7 gas mole fraction and gas saturation in the core during CO_2 injection period.

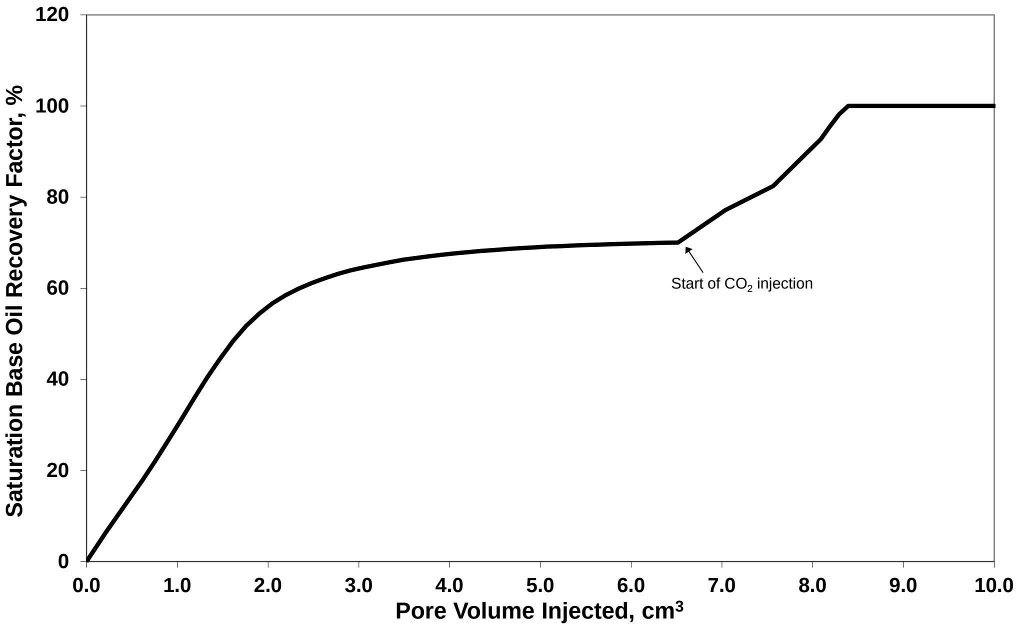

Figure 3.17 – Calculated oil recovery factor based on core oil saturation.

3.8 Designing Fractured Reservoir Experiments using CO_2

We recommend the following experimental design procedures when performing CO_2 injection experiments for fractured reservoirs:

1. Fracture (core-annulus) permeability should be measured after the core is initialized with oil. A rule-of-thumb for fracture conductivity is that total core+fracture pressure drop is small compared the pressure drop when flow occurs only through the core.
2. Continuous measurement of separator temperature and pressure.
3. Oil and gas produced mass and volume should be reported, together with periodic surface oil densities.
4. Periodic measurement of produced surface gas and surface oil stream assumptions.
5. Oil and gas compositions initially saturating the core should be determined experimentally.
6. Additional PVT experiment like a swelling test that includes bubblepoint, near-critical, and dewpoint mixtures should be conducted for tuning the EOS model.

7. Determine relevant (drainage and/or imbibition) capillary pressure and relative permeability of core used in the experiment.

3.9 Conclusions

Based on analysis of experimental results and a history-matched numerical model which describes accurately all key laboratory performance data; we make the following conclusion, which are specific to this particular experimental study:

1. Viscous displacement is significant and gravity-capillary drainage is not significant in the Karimaie experiments due to low “fracture” (core-annulus) permeability.
2. The laboratory data history matched include cumulative oil and gas produced during displacements with equilibrium gas and CO_2 injection.
3. During the CO_2 injection period, near-first-contact miscible displacement is the dominant production mechanism.
4. Separator conditions play an important role in measuring and modeling oil production for high-pressure, high-temperature CO_2 injection experiments – mainly because reservoir gas contains significant oil in solution which is produced by condensation at surface conditions.
5. Diffusion has no impact on the CO_2 injection recovery mechanism because of the dominant viscous-force displacement.

3.10 Reference

Christoffersen, K. 1992. High-Pressure Experiments with Application to Naturally Fractured Chalk Reservoirs. PhD Dissertation, NTNU, Trondheim, Norway.

Coats Engineering: ***SENSOR***, www.coatsengineering.com.

Hoteit, H. and Firoozabadi, A. 2006. Numerical Modeling of Diffusion in Fractured Media for Gas Injection and Recycling Schemes. Paper SPE 103292 presented at the 2006 SPE Annual Technical Conference and Exhibition, San Antonio, Texas, U.S.A., 24-27 September.

Karimaie, H. 2007. Aspects of Water and Gas Injection in Fractured Reservoir. PhD Dissertation, NTNU, Trondheim, Norway.

Karimaie, H. and Torsæter, O. 2009. Low IFT Gas-Oil Gravity Drainage in Fractured Carbonate Porous Media. Journal of Petroleum Science and Engineering.

Løvoll, G., Meheust, Y., Måløy, K. L., Aker, E., and Schmittbuhl, J. 2005. Competition of gravity, capillary and viscous forces during drainage in a two-dimensional porous medium, a pore scale study. Energy 30 (6): 861–872. doi:10.1016/j.energy.2004.03.100.

Petrostreamz AS: ***Pipe-It/Streamz***, www.petrostreamz.com.

Talukdar, S. 2002. Ekofisk Chalk: core measurements, stochastic reconstruction, network modeling and simulation. PhD Dissertation, NTNU, Trondheim, Norway.

Schlumberger: ***ECLIPSE 300*** Reservoir Engineering Software. 2009. www.slb.com.

Stalkup, F.I. Jr. 1983. Miscible Displacement. Henry L. Doherty Monograph Series, SPE, Richardson, Texas, USA, 8.

Wylie, P.L. and Mohanty, K.K. 1999. Effect of Wettability on Oil Recovery by Near-Miscible Gas Injection. SPE Res Eval & Eng 2 (6): 558–564. SPE-59476-PA. doi: 10.2118/59476-PA.

Zick Technologies: ***PhazeComp***, www.zicktech.com.

Chapter 4

Modeling CO_2 Injection in Darvish Fractured Chalk Experiment (Sw=0%)

4.1 Introduction

This chapter presents a modeling study of a CO_2 injection in a chalk core based on the laboratory data that were reported by Darvish *et al.* (2006). The experiment consisted of a vertically-oriented, 60-cm-long chalk outcrop core that was initially saturated with live reservoir oil at 130 ^{o}C and 300 bar. After saturating the core with the oil mixture by displacement, a small fracture volume surrounding the core was created by heating the solid Wood's metal that originally filled the volume between the core and core holder. CO_2 was then injected for 22 days. The experiment was performed at a pressure above the minimum miscibility pressure (MMP), as defined by a traditional 1D multi-contact displacement process (MMP_{1D}).

Darvish *et al.* (2006) was not able to match the experimental data to the numerical compositional model. This lack of a match may have resulted from the use of an improper equation of state (EOS) or incorrect input data in their models. Moortgat, Firoozabadi and Farshi (2009) modeled the experiment using the combined discontinuous Galerkin, mixed-hybrid, finite-element and discrete-fracture techniques. Our modeling study was conducted using a compositional reservoir simulator. The 2D, r-z model used a fine grid for the core and surrounding fracture.

4.2 Rock and Fluid Properties

A chalk core from the Faxe area outcrop in Denmark was used in this experiment; it has rock properties that are similar to those of North Sea chalk. The core had a cylindrical shape with a length of 59.6 cm and a diameter of 4.6 cm. The core porosity and permeability have been reported as 44.4% and 4 md, respectively (Darvish *et al.* 2006; Darvish 2007).

Relative permeabilities and capillary pressures for the core were not measured. We used the C_1-n-C_5 capillary pressure of a Faxe outcrop chalk core, as measured by Christoffersen (1992). The linear and Corey-type relative permeabilities (Eqs. (2.19) and (2.20)) were used for modeling the experiment. The gas and oil exponents for the Corey-type relative permeabilities were 2.4 and 3.8, respectively, with unit end points.

The reservoir fluid was flashed to standard conditions (T= 15.5 ^{o}C, P= 1 bar), and the flashed oil and gas compositions were measured using the techniques in Darvish 2007. These fluids were used to determine the reservoir fluid composition at a bubble point pressure of 242 bar and a temperature of 130 ^{o}C by combining it with the measured gas/oil ratio (GOR) of 133.2 Sm^3/Sm^3. The EOS model had 39 components, including the non-hydrocarbons N_2 and CO_2, the hydrocarbon components C_1, C_2, C_3, i-C_4, n-C_4, i-C_5, n-C_5, and C_6 and the single-carbon number (SCN) components C_7, C_8, …, C_{33} and C_{34} with a C_{35+} residue. The EOS was reduced to thirteen components with five heavy pseudo-components. The lumped components were chosen to be the same as the pseudo-components that were reported by Darvish in 2007 because the reported oil-produced mass fractions were to be compared with the numerical model results. The Peng-Robinson (1979) equation of state (PR-EOS) with a volume shift was used. The PR-EOS was tuned to match the measured constant composition expansion (CCE), the differential liberation expansion (DLE) and the CO_2 swelling test experiments. The comparisons of the measured and calculated properties are shown in **Figs. 4.1 – 4.5**. The Lohrenz-Bray-Clark (LBC) compositional viscosity correlation is usually adequate for gas viscosity

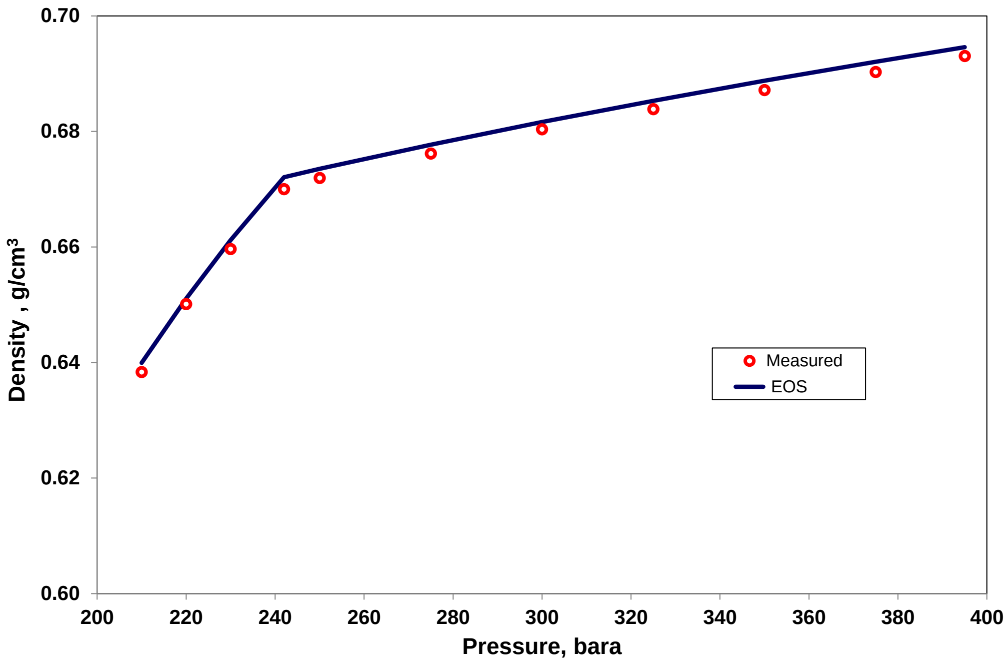

Figure 4.1 – Measured and calculated total (gas + oil) density at 130 °C.

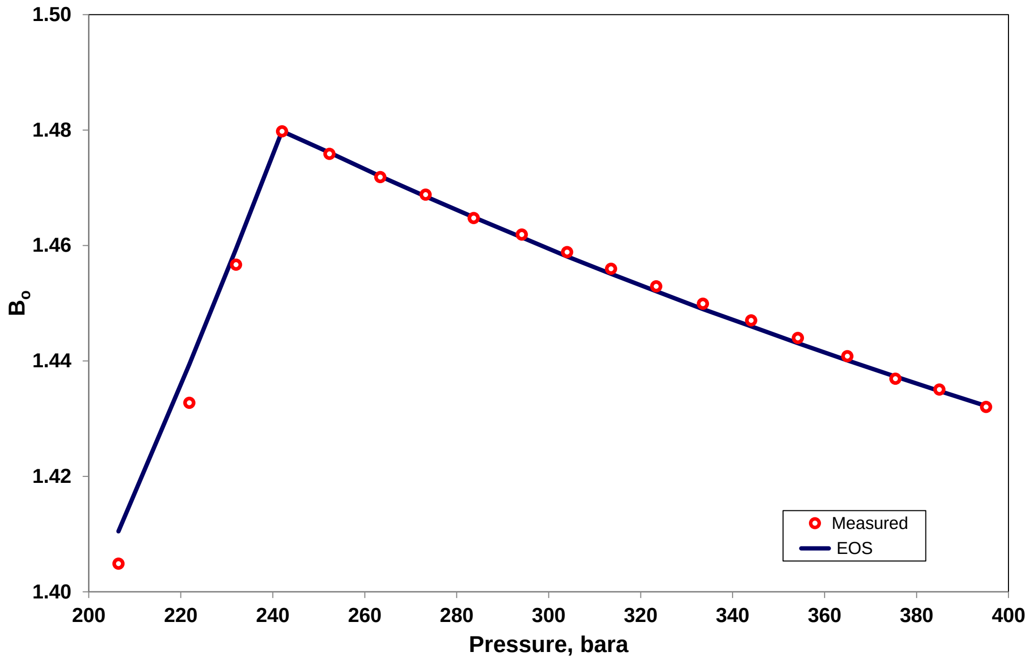

Figure 4.2 – Measured and calculated differential oil volume factor at 130 °C.

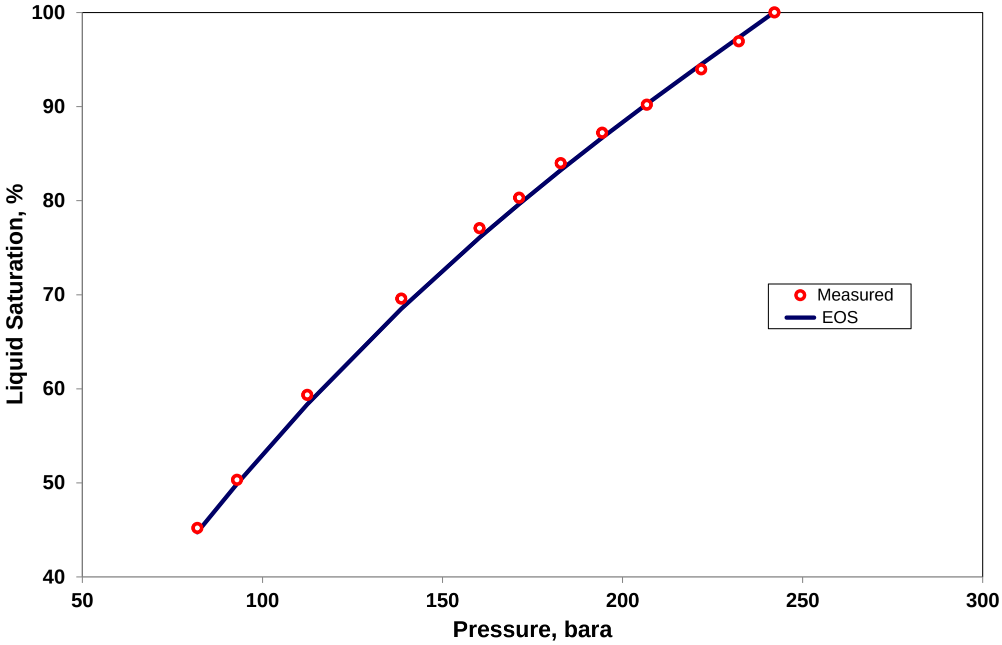

Figure 4.3 – Measured and calculated liquid saturation at 130 ^oC.

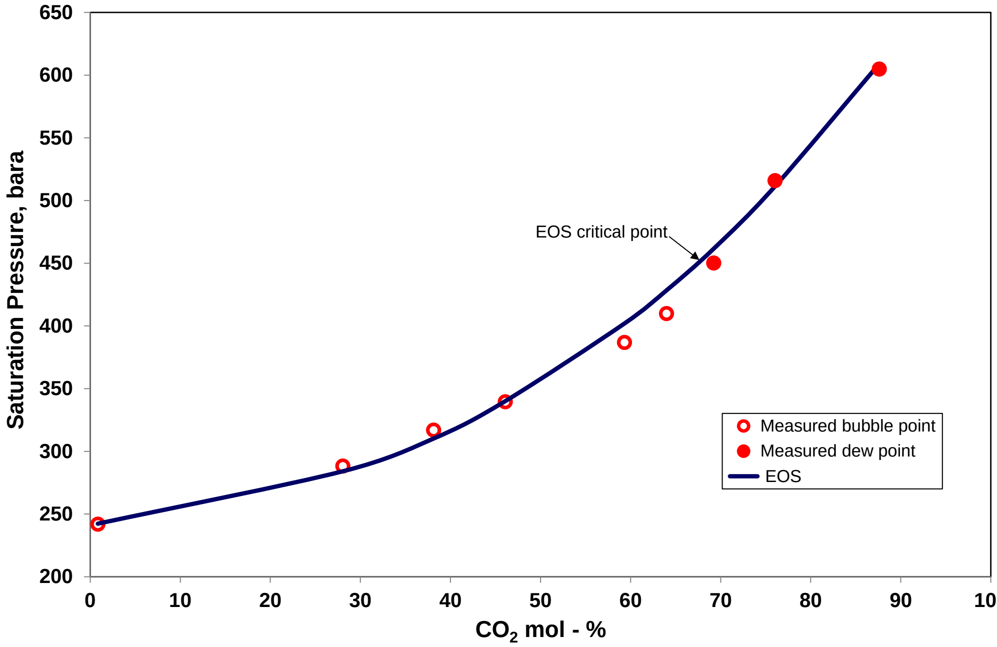

Figure 4.4 – Measured and calculated saturation pressure versus CO_2 mole injected at 130 ^oC from CO_2 swelling test.

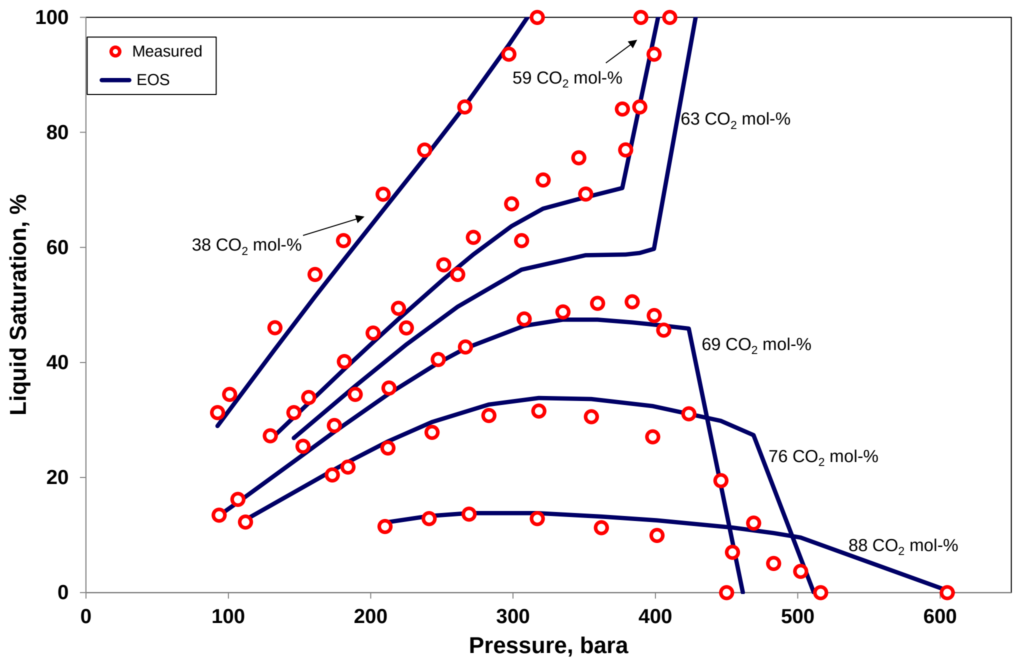

Figure 4.5 – Measured and calculated liquid saturation for different CO_2 mol-% mixtures from CO_2 swelling test.

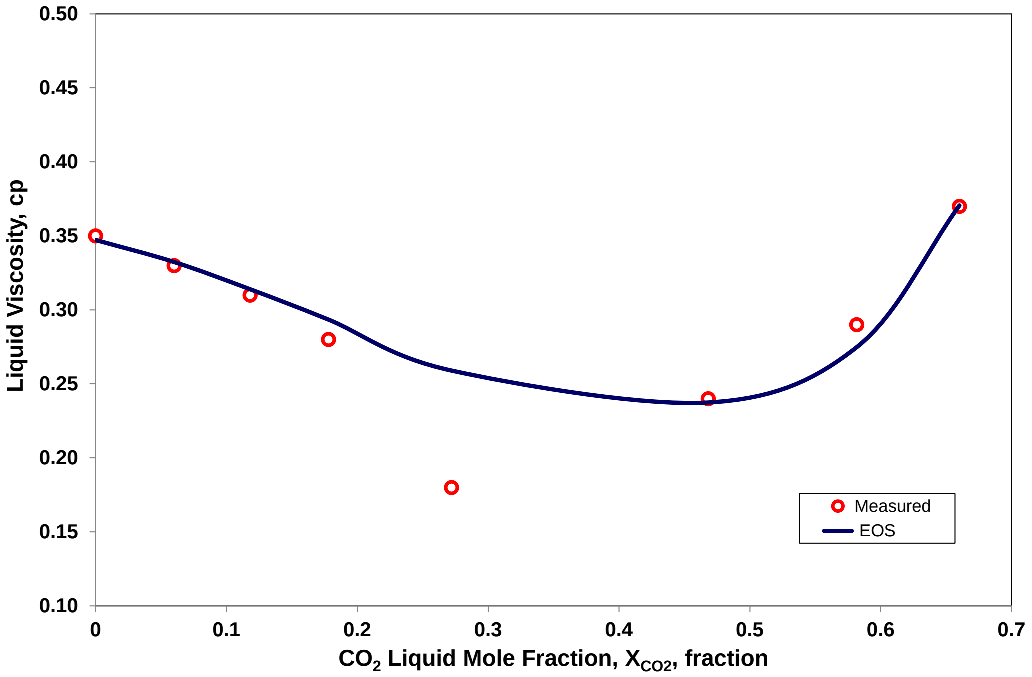

Figure 4.6 – Measured and calculated saturated oil viscosity versus CO_2 liquid mole fraction at 130 °C.

predictions, but this correlation is not usually predictive for oil viscosity. The critical Z_c's for the C_6 and heavier components were modified to force fit the LBC correlation to the measured oil viscosities at the different CO_2 mole fractions (**Fig. 4.6**). The 13 components PR-EOS/LBC parameters that were used in the present study are given in **Tables 4.1 - 4.3**.

Table 4.1 – Fluid Properties for the 13-Component Peng-Robinson Characterization

Component	MW	Tc, K	Pc, bar	ω	s	Tb, K	Zc	Parachor
N2	28.01	126.20	33.98	0.0370	-0.1676	77.25	0.2918	59.1
CO2	44.01	304.12	73.74	0.2250	-0.0057	184.88	0.2928	80.0
C1	16.04	190.56	45.99	0.0110	-0.1500	111.56	0.2862	71.0
C2	30.07	305.32	48.72	0.0990	-0.0628	184.43	0.2792	111.0
C3	44.10	369.83	42.48	0.1520	-0.0638	230.93	0.2763	151.0
C4	58.12	416.49	37.18	0.1930	-0.0580	267.06	0.2779	189.9
C5	72.15	465.10	33.76	0.2405	-0.0427	305.28	0.2703	229.2
C6	84.14	511.14	32.20	0.2598	-0.0027	338.81	0.2995	236.9
C7-C9	110.40	577.75	27.91	0.3262	0.0269	394.65	0.2797	300.0
C10-C15	167.32	682.95	20.72	0.4918	0.0909	495.49	0.2567	436.6
C16-C22	244.90	782.17	15.27	0.7082	0.1494	601.17	0.2402	622.8
C23-C34	347.73	874.10	11.56	0.9713	0.1890	705.51	0.2327	869.6
C35+	578.83	1024.78	10.21	1.4054	0.0726	859.68	0.2216	1424.2

Table 4.2 – Binary Interaction Coefficients for the 13-Component Peng-Robinson Characterization

	N2	CO2	C1	C2	C3	C4	C5	C6	C7-C9	C10-C15	C16-C22	C23-C34	C35+
N2	-												
CO2	0.0000	-											
C1	0.0250	0.2100	-										
C2	0.0100	0.2600	0.0000	-									
C3	0.0900	0.2500	0.0000	0.0000	-								
C4	0.0950	0.2349	0.0000	0.0000	0.0000	-							
C5	0.1051	0.2300	0.0000	0.0000	0.0000	0.0000	-						
C6	0.1100	0.2300	0.0000	0.0000	0.0000	0.0000	0.0000	-					
C7-C9	0.1100	0.1056	-0.0446	0.0000	0.0000	0.0000	0.0000	0.0000	-				
C10-C15	0.1100	0.0965	-0.0676	0.0000	0.0000	0.0000	0.0000	0.0000	0.0000	-			
C16-C22	0.1100	0.0870	-0.0896	0.0000	0.0000	0.0000	0.0000	0.0000	0.0000	0.0000	-		
C23-C34	0.1100	0.0784	-0.1079	0.0000	0.0000	0.0000	0.0000	0.0000	0.0000	0.0000	0.0000	-	
C35+	0.1100	0.0685	0.1949	0.0000	0.0000	0.0000	0.0000	0.0000	0.0000	0.0000	0.0000	0.0000	-

Table 4.3 – Fluid Composition and K-Value at Saturation Pressure (242 bara) an 130 °C

Component	Z_i	X_i	Y_i	K-Value
N2	0.0012	0.0012	0.0034	2.79E+00
CO2	0.0084	0.0084	0.0105	1.24E+00
C1	0.4473	0.4473	0.8026	1.79E+00
C2	0.0766	0.0766	0.0840	1.10E+00
C3	0.0426	0.0426	0.0340	7.98E-01
C4	0.0318	0.0318	0.0197	6.18E-01
C5	0.0220	0.0220	0.0100	4.57E-01
C6	0.0211	0.0211	0.0071	3.34E-01
C7-C9	0.0799	0.0799	0.0176	2.20E-01
C10-C15	0.0988	0.0988	0.0089	8.98E-02
C16-C22	0.0654	0.0654	0.0019	2.93E-02
C23-C34	0.0540	0.0540	0.0004	6.76E-03
C35+	0.0510	0.0510	0.0000	4.50E-06
MW	106.613	106.613	23.940	
Z-Factor	1.15E+00	1.15E+00	9.11E-01	
Density (kg/m^3)	672.16	672.16	189.87	

4.3 Experimental Procedure

This section describes an experiment that was performed to study CO_2 injection in fractured reservoir. The experimental procedure that is described was based on Darvish (2007), Darvish *et al.* (2006) and personal communications with Darvish.

A dried cylindrical chalk core was placed in a steel core holder. The core holder inner diameter was 5.0 cm. The core diameter was 4.6 cm, and the length was 59.6 cm. The fracture was represented by a 2 mm space between the core and the core holder. The core porosity and absolute permeability were reported as 44.4% and 4 md, respectively (Darvish 2007; Darvish *et al.* 2006).

Due to the large permeability contrast between the core and the surrounding space (the artificial fracture), the process of initially saturating the core with live oil was complicated. The oil would flow through the highly-permeable space, leaving the core partially saturated with live oil. Therefore, the space between the core and the core holder wall was initially filled with Wood's metal. The metal's melting point is 70 °C, and the experiment was performed at 130 °C. The metal was melted and poured into the space between the core and core holder. The fracture sealed with the metal and had zero permeability after the system was cooled.

The core was evacuated and pressurized to 300 bar with 85% toluene and 15 % Exxsol. The Toluene-Exxsol mixture had a higher density than the experimental fluid, and therefore, this mixture was injected from the top of the core with stable gravity displacement. Two pore volumes of live oil were injected at a constant pressure (300 bar) and temperature (40 ^{o}C). The system was heated to 130 ^{o}C at a constant pressure (300 bar), and the Wood's metal was removed from the annular space by injecting the oil. The oil was injected from the top and the metal drained from the bottom of the core holder. The fracture porosity and permeability were not measured after the metal was removed from the system, but the pressure difference was measured between the top and the bottom of the core holder, which was used in this work to determine the fracture permeability for the model.

The oil in the fracture was replaced by CO_2. The injection rate during the first 30 min of the experiment was 5.6 cm^3/min and was then reduced to 0.1 cm^3/min. The CO_2 gas injection was continued for 22 days. The fluid that was produced was diverted to a separator at ambient conditions. The mass of the separated oil was measured continually, and the component mass fractions were measured periodically gas chromatography.

4.4 Model Description

The matrix block (core) was initially filled with oil, and the fractures were initially filled with CO_2. The fractures were assumed to have negligible capillary pressure. The matrix and the fracture dimensions were the same as those of the core and the fracture in the experiment. A two-dimensional radial grid was used in which the matrix block was surrounded by two horizontal fractures (at the top and bottom) and one vertical fracture. A fine grid was required to reduce numerical dispersion in the CO_2 gas injection. 10 and 51 grid cells were used in the radial and vertical directions, respectively, to simulate the experiment.

The *ECLIPSE 300* simulator with an implicit solution method was used for all of the simulations. A 13-component PR-EOS was used. The EOS properties of the components are summarized in Table 4.1, and the binary interaction parameters are given in Table 4.2.

Linear and Corey-type relative permeabilities were used to model the experiment. The gas and oil exponents for the Corey-type relative permeabilities were 2.4 and 3.8, respectively, with unit end points. The C_1-n-C_5 capillary pressures that were measured by Christoffersen (1992) at a similar core were used as the core capillary pressures in the model. These capillary pressures were scaled with IFT according to Eq. (2.24), in which the reference interfacial tension (IFT) was 1.5 mN/m. There was no capillary pressure in the fracture.

The *Pipe-it/Streamz* software was used to calculate the cumulative mass of the oil that was produced from the reservoir simulation results. One separator was defined to simulate the produced stream in the experiment. The separator pressure was atmospheric, as it was in the experiment. As mentioned above, the separator temperature was not measured during the experiment.

The oil and gas effective diffusion coefficients are given in Table 4.4. The gas diffusion coefficients were determined from the equilibrium gas at the bubble point pressure. More details of the diffusion coefficients calculation are given in section (2.2).

4.5 Matching The Experimental Data

In this section, we try to match the measured experimental data. As was mentioned above, the cumulative mass of the separator oil was measured and matched. The oil recovery that were reported in Darvish (2007) and Darvish *et al.* (2006) were based on the mass produced and were not mentioned in the above references. In their study, Moortgat, Firoozabadi and Farshi (2009) considered that to be the volumetric oil recovery. A fracture permeability of 80 md was needed to obtain the pressure difference that was measured in the experiment. As shown in **Fig. 4.7**, the measured pressure difference was slightly higher than the calculated pressure difference because we accounted for the pressure drop in the

Table 4.4 – Gas and Oil Diffusion Coefficients and Initial Oil Composition

Component	z_i mole fr.	D_{ig} cm^2/s	D_{io} cm^2/s
N2	0.0012	5.15E-05	2.92E-06
CO2	0.0084	3.20E-04	7.26E-06
C1	0.4473	2.70E-04	7.72E-06
C2	0.0766	2.62E-04	7.09E-06
C3	0.0426	2.46E-04	5.84E-06
C4	0.0318	2.09E-04	4.91E-06
C5	0.0220	1.81E-04	4.25E-06
C6	0.0211	1.64E-04	3.83E-06
C7-C9	0.0799	1.42E-04	3.25E-06
C10-C15	0.0988	1.05E-04	2.55E-06
C16-C22	0.0654	7.66E-05	2.01E-06
C23-C34	0.0540	5.72E-05	1.52E-06
C35+	0.0510	4.30E-05	1.33E-06

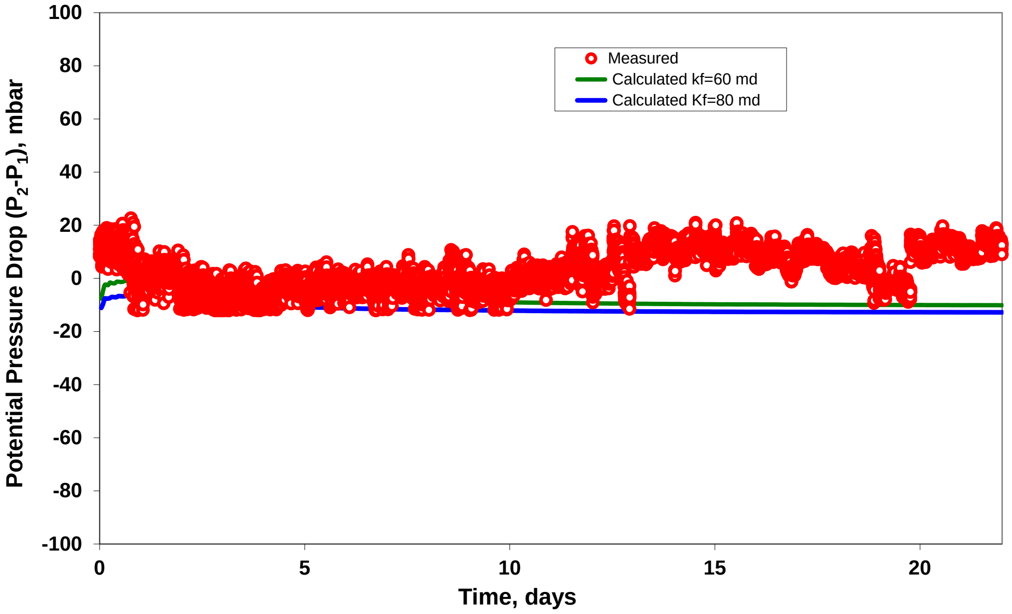

Figure 4.7 – Measured and calculated saturated oil viscosity versus CO_2 liquid mole fraction at 130 ^oC.

inlet and outlet tubes, which were where the measurement instruments for the experiment were set. No condenser or cooler was present in the outlet stream, and consequently, the separator temperature was set to 30 ^{o}C, which was slightly higher than the ambient temperature when accounting for the high temperature (130 ^{o}C) of the outlet fluid.

The other parameters in the numerical model were defined as reported values in the experiment. The two models were run with two sets of relative core permeabilities, as described in the previous section. The results of the models were similar, as illustrated in **Fig. 4.8**. The mass transfer mechanism was more pronounced than the viscous displacement in the present experiment, as will be discussed in the next section. We selected the model with linear core relative permeability for use in the remainder of the study.

Reported heavy-component mass fractions in the experiment were compared with the numerical model results. All of the calculated mass fractions from the model followed the same trend as the measured values, as shown in **Fig. 4.9**. If the C_{10} and heaver components are lumped together, then numerical model

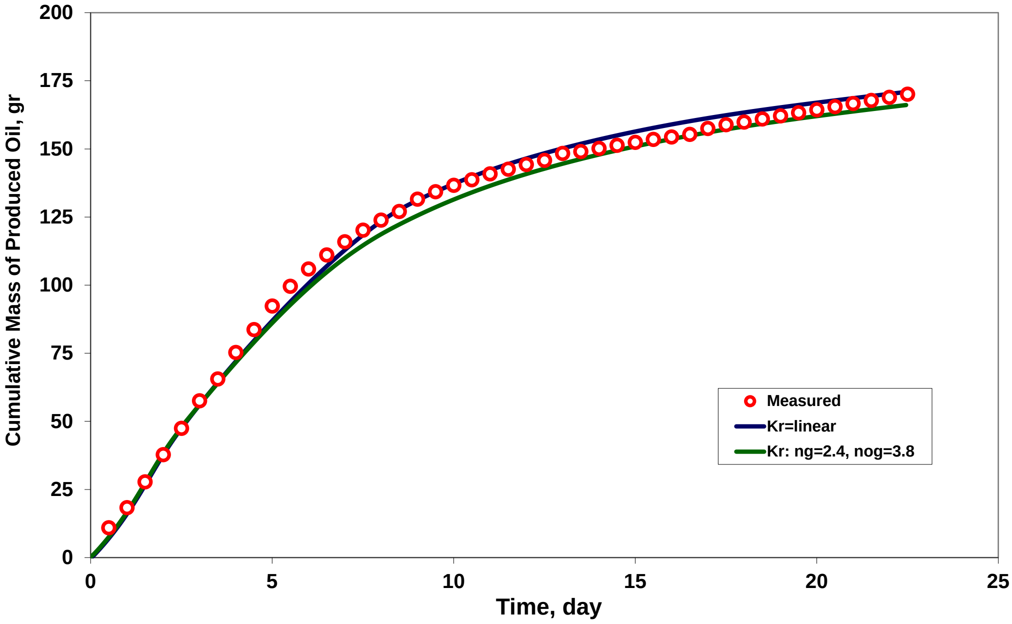

Figure 4.8 – Measured produced oil mass with matched simulation results for two set of core relative permeability with 80 md fracture permeability at 30 ^{o}C separator temperature.

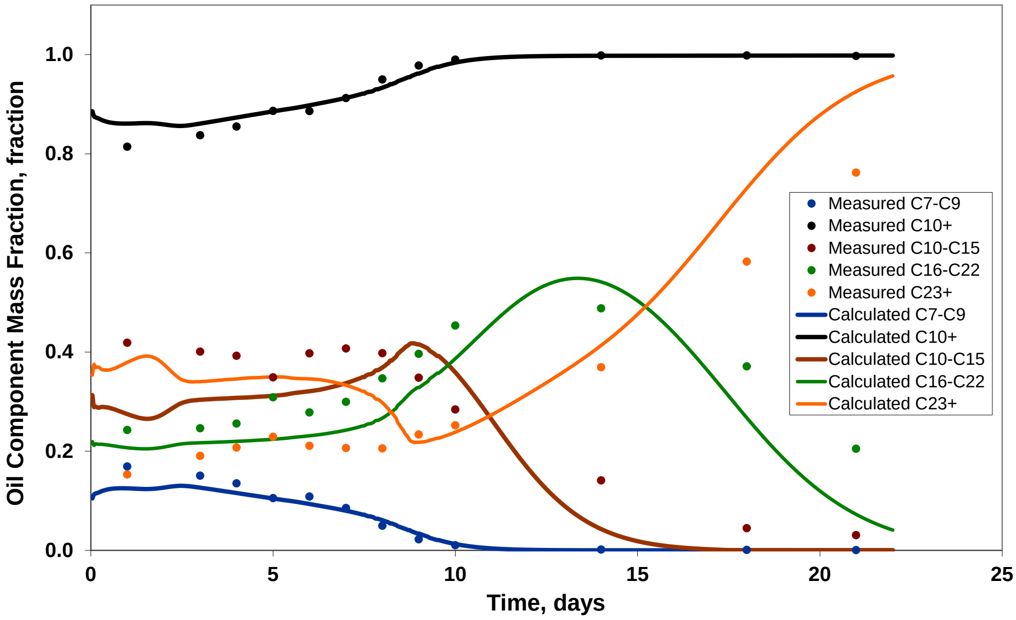

Figure 4.9 – Measured and calculated heavy components mass fraction of produced oil at separator condition.

results and the experimental data are even closer, as shown in Fig. 4.9. This result might indicate that the grouping of the C_{10+} components was performed slightly differently in the laboratory than in the EOS calculations. The calculated molecular weights of the stock tank oil produced in the laboratory have the same trend as the molecular weights in the numerical model (**Fig. 4.10**).

4.6 Recovery Mechanism

Darvish (2007) converted the initial volume (V_{oi}) in the core to an equivalent mass under laboratory separator conditions ($m_{oi} = V_{oi}\rho_o/B_o$), and the recovery was calculated using:

$$RF_{surf} = \frac{m_{op}}{m_{oi}} = \frac{m_{op}}{V_{oi}\left(\frac{\rho_o}{B_o}\right)} \quad \text{..........} (4.1)$$

The composition of oil that was produced varied during the experiment (Fig. 4.9); as a result, the oil density (ρ_o) values and the oil formation volume factor (B_o) were not constant. Darvish (2007) used a constant oil density and oil

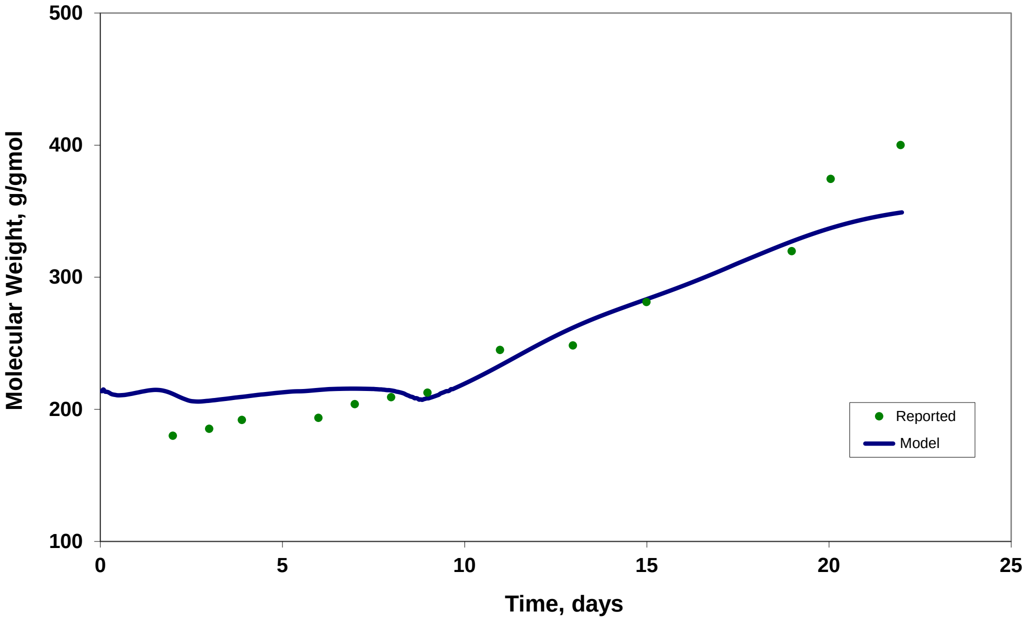

Figure 4.10 – Reported and calculated molecular weight of produced oil at separator condition.

formation volume factor in his calculations. Therefore, in the present study, we did not use the recovery factor calculated by Darvish (2007).

Fig. 4.11 shows CO_2 condensation in the oil phase at the experimental pressure and temperature. Consequently, the oil saturation should be corrected as follows:

$$RF_{so} = 1 - \frac{S_o(1 - x_{CO2} + x_{CO2i})}{S_{oi}} \quad \text{.......................................} (4.2)$$

where S_{oi} and S_o are the initial and current oil saturations in the core, respectively, and x_{CO2i} and x_{CO2} are the initial and current CO_2 mole fractions in the liquid phase, respectively. The component and the total molar oil recoveries based on the component moles are given by

$$RF_{comp} = 1 - \frac{n_k}{n_{ki}} \quad \text{.......................................} (4.3)$$

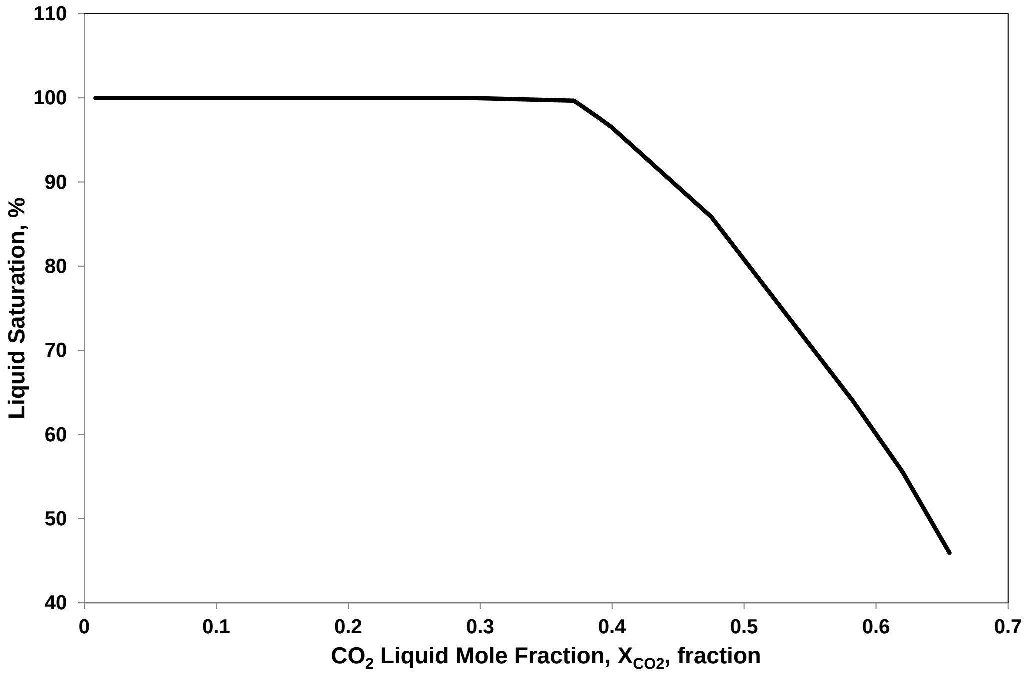

Figure 4.11 – Calculated liquid saturation versus CO$_2$ liquid mole fraction from constant pressure (300 bara) and temperature (130 °C) swelling test.

$$RF_{mole} = 1 - \frac{\sum\limits_{\substack{k=N2 \\ k \neq CO2}}^{C35+} n_k}{\sum\limits_{\substack{k=N2 \\ k \neq CO2}}^{C35+} n_{ki}} \quad \text{..........} (4.4)$$

where n_{ki} and n_k are the initial and current moles of component *k*. The total oil recovery was based on the component mass, as calculated by:

$$RF_{mass} = 1 - \frac{\sum\limits_{\substack{k=N2 \\ k \neq CO2}}^{C35+} m_k}{\sum\limits_{\substack{k=N2 \\ k \neq CO2}}^{C35+} m_{ki}} \quad \text{..........} (4.5)$$

where m_{ki} and m_k are the initial and current masses of component *k*.

The oil recoveries that were calculated using the above equations are shown in **Fig. 4.12**. The oil saturation and mole-based recoveries were similar and gave similar ultimate recoveries (at 22 days) of approximately 95%. The mass-based recovery led to a lower recovery (76%) because the heavy components were recovered more slowly than the light and medium components, as shown in **Figs. 4.13** and **4.14**. For consistency, the mole-based oil recovery is considered to be the oil recovery factor from this point forward.

The numerical models were performed using two sets of core relative permeabilities. The mole-based recovery factors for these two models were similar and overlapped each other (**Fig. 4.15**). A model using 5 D fracture permeability was evaluated to understand the effects of actual fracture permeability reduction on the experimental result. As seen in Fig. 4.15, oil recovery was close to the 80 md cases, which indicates that the viscous force had a minor impact on the recovery mechanism. One additional model, in which the diffusion option was turned off, was constructed to observe the effects of diffusion on the experiment. The oil recovery was slower, and the ultimate oil recovery (at 22 days) was reduced to 76 %.

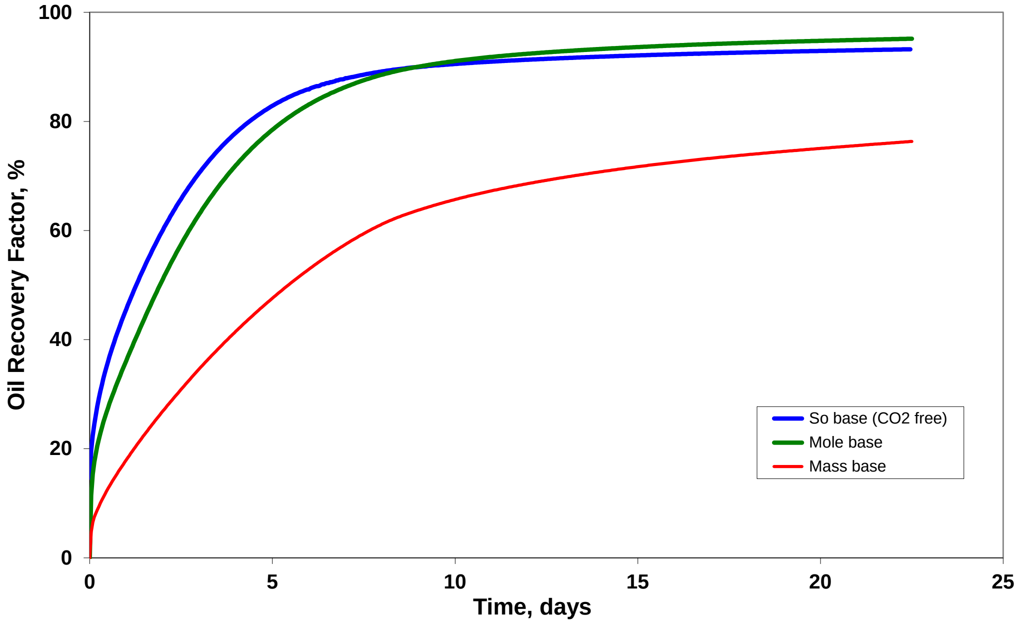

Figure 4.12 – Calculated oil recovery factor based on mole, mass and oil saturation from matched model with linear core relative permeability.

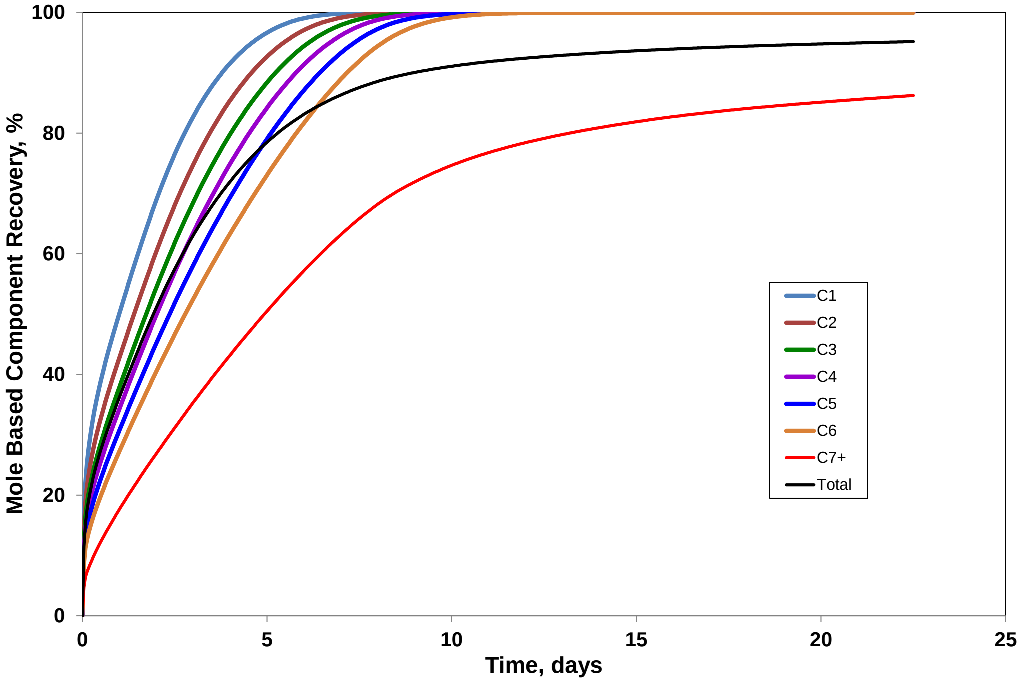

Figure 4.13 – Calculated mole based oil recovery of light and intermediate components from matched model with linear core relative permeability.

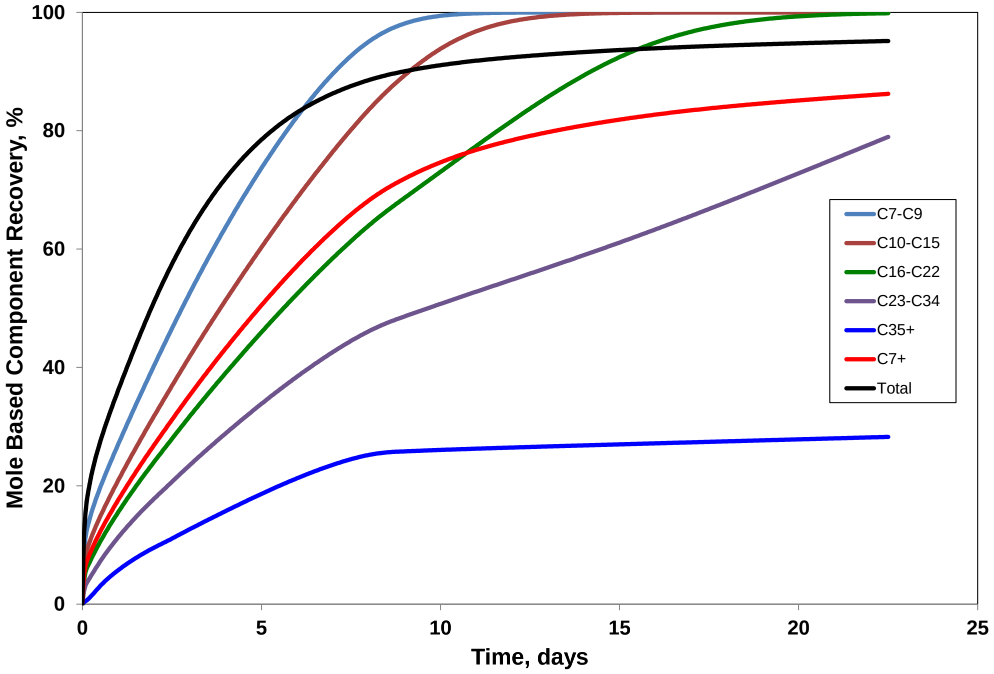

Figure 4.14 – Calculated mole based oil recovery of heavy components from matched model with linear core relative permeability.

Figs. 4.13 and 4.14 show that lighter components were produced first, which indicates that CO_2 preferentially vaporizes the light and intermediate components. These components are transported out of the matrix block by molecular diffusion, as fresh CO_2 enters the fracture (annular space) and the area behind the front of the displacement. During the early production period, a front develops from the fracture inwards caused by CO_2 entry through gravity and mass transfer as shown in **Fig. 4.16**. After the light components were vaporized (5 days), the gravity-drainage process appeared to be more pronounced, with less lateral displacement compared to the early period of the experiment (**Fig. 4.17**).

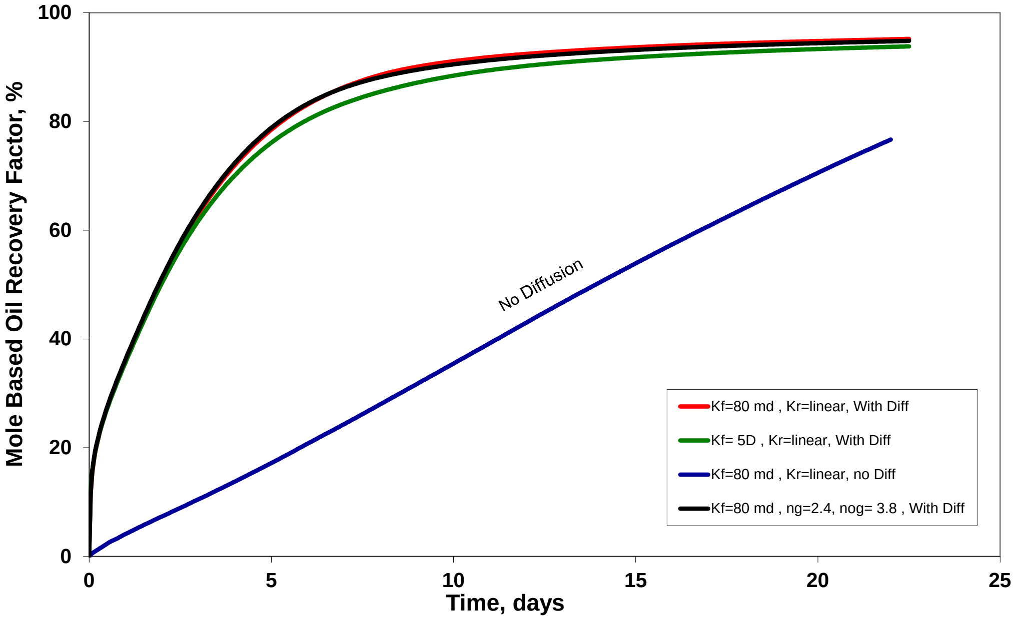

Figure 4.15 – Mole based oil recovery results from numerical sensitivity models at 30 °C separator temperature.

4.7 Conclusions

The following conclusions were determined after analyzing the experiment and the numerical studies.

1. The measured production data from the experiment were matched with a commercial compositional, finite-difference simulator model.
2. Mass transfer (vaporization, condensation and molecular diffusion) was the dominant production mechanism during the early stages of the

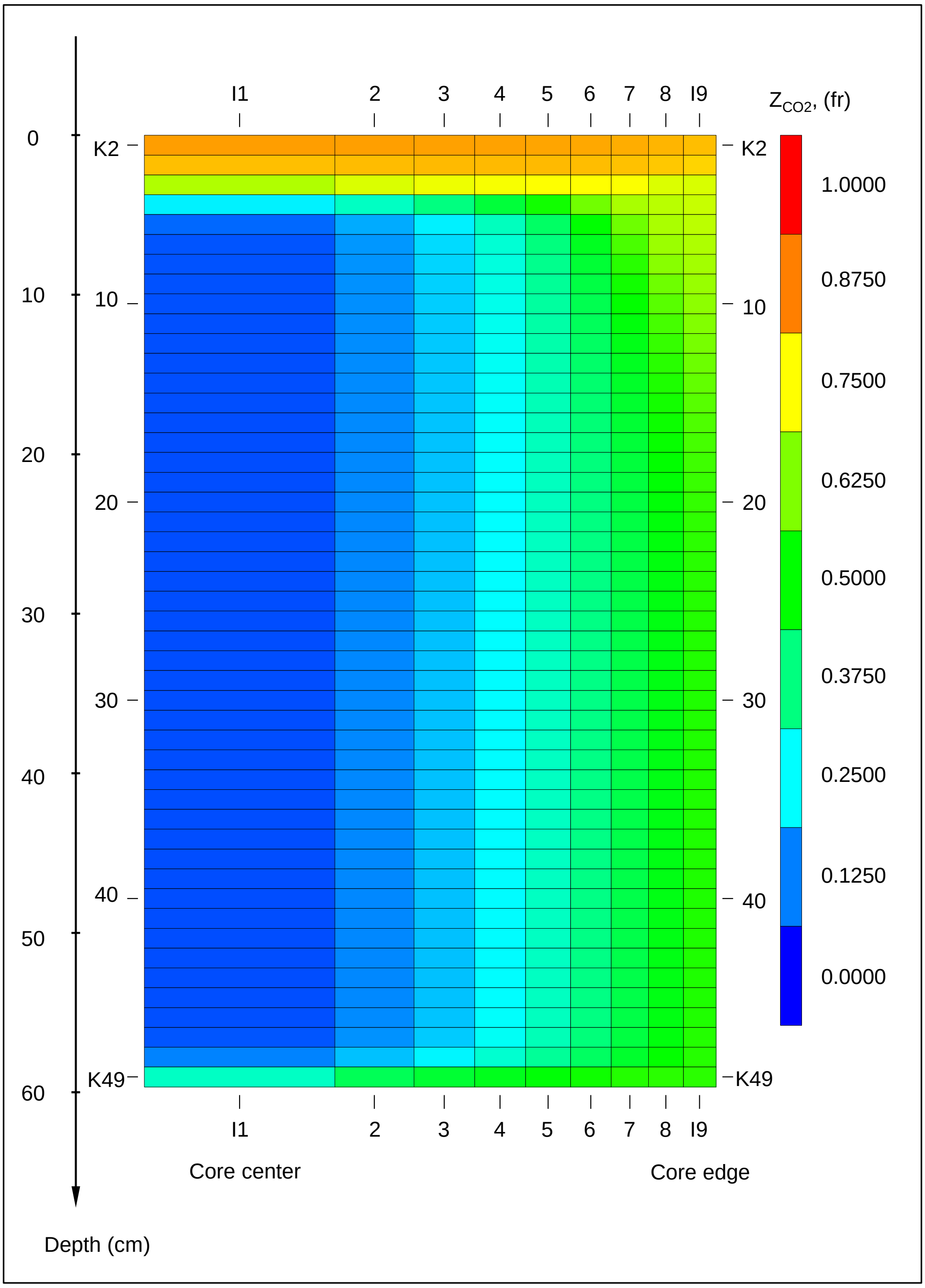

Figure 4.16 – CO_2 mole fraction profile of core after 12 hours for matched model with linear core relative permeability (at about 36% oil recovery).

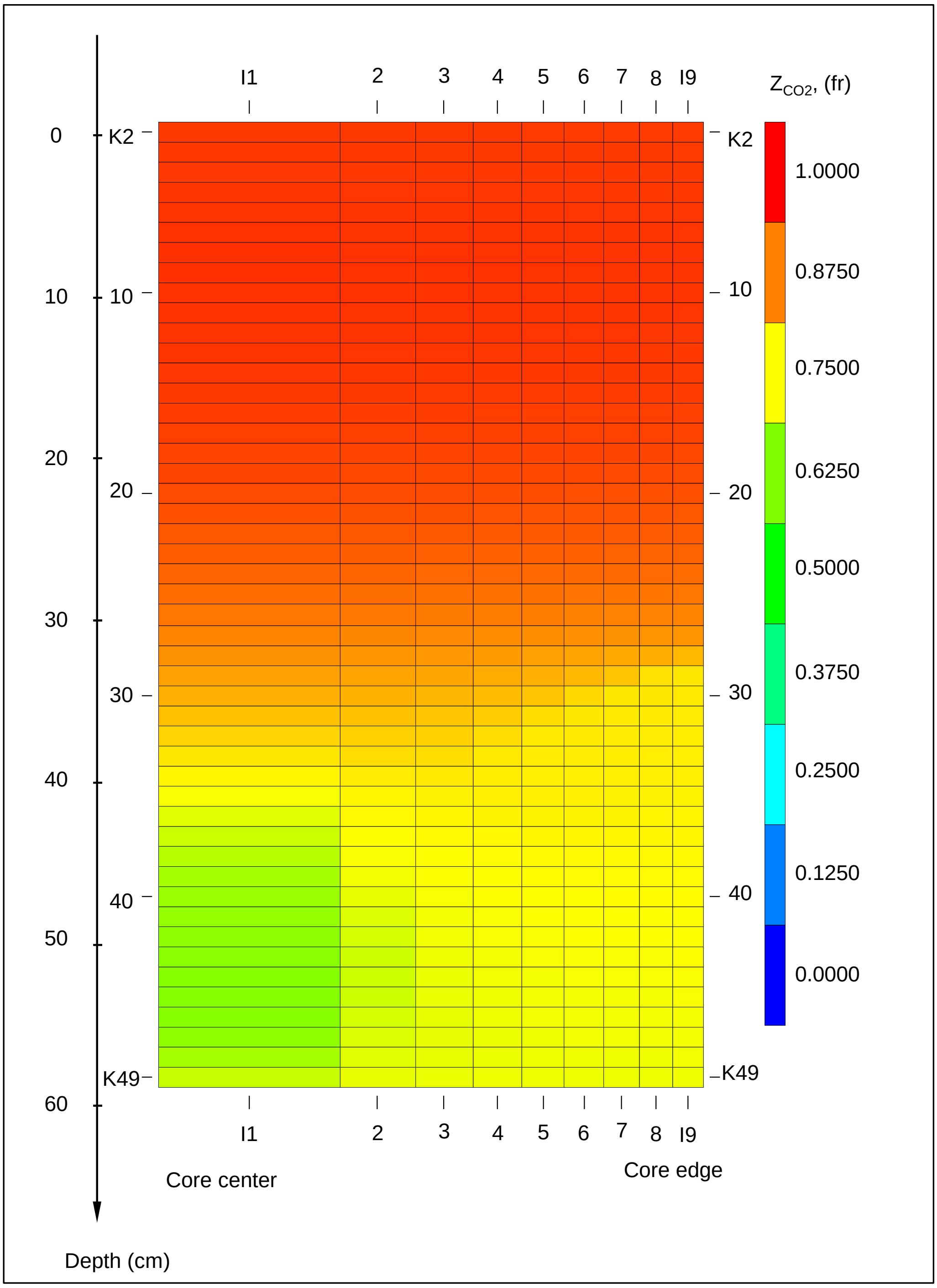

Figure 4.17 – CO_2 mole fraction profile of core after 5 days for matched model with linear core relative permeability (at about 79% oil recovery).

experiment, in which the gravity drainage became more pronounced after the light components were recovered.

3. The fractured permeability level that resulted from the remaining sealing material after core initialization did not affect the experiment results.
4. The high recoveries that were observed did not appear to be related to the pressure exceeding the minimum miscibility pressure.

4.8 Reference

Christoffersen, K. 1992. High-Pressure Experiments with Application to Naturally Fractured Chalk Reservoirs. PhD Dissertation, NTNU, Trondheim, Norway.

Darvish, G.R. 2007. Physical Effects Controlling Mass Transfer in Matrix Fracture system During CO_2 Injection in to Chalk Fractured Reservoir. PhD Dissertation, NTNU, Trondheim, Norway.

Darvish, G.R., Lindeberg, E., Holt, T., Utne, S.A. and Kleppe, J. 2006. Reservoir Conditions Laboratory Experiments of CO_2 Injection into Fractured Cores. Paper SPE 99650 presented at the 2006 SPE Europec/EAEG Annual Technical Conference and Exhibition, Vienna, Austria, 12-15 June.

Moortgat, J., Firoozabadi, A. and Farshi M.M., 2009. A New Approach to Compositional Modeling of CO_2 Injection in fractured Media Compared to Experimental Data. Paper SPE 124918 presented at the 2009 SPE Annual Technical Conference and Exhibition, New Orleans, Louisiana, U.S.A., 4-7 October.

Petrostreamz AS: ***Pipe-It/Streamz***, www.petrostreamz.com.

Schlumberger: ***ECLIPSE 300*** Reservoir Engineering Software. 2009. www.slb.com.

Zick Technologies: ***PhazeComp***. www.zicktech.com.

Chapter 5

Modeling CO_2 Injection in Darvish Fractured Chalk Experiment (Sw=26%)

5.1 Introduction

In this chapter, we modeled an additional Darvish (2007) CO_2 injection experiment, in which there was initial water saturation in the core, and the CO_2 was injected at a higher rate. The experiment consisted of a vertically-oriented, 60-cm-long chalk outcrop core that was initially saturated with live reservoir oil at a temperature of 130 ^oC and a pressure of 300 bar. After saturating the core with the oil and water by displacement, a small fracture volume surrounding the core was created by heating the solid Wood's metal that originally filled the space between the core and core holder. The CO_2 was then injected for 20 days. Our modeling was conducted using a compositional reservoir simulator. The 2-dimensional r-z model used a fine grid for the core and the surrounding fracture. The CO_2 injection rate and initial water saturation effect were investigated by comparing these experimental results with those of a similar experiment in which the CO_2 was injected at a lower rate with no initial water saturation (Chapter 4).

Pollack *et al.* (1988) experimentally studied the effect of the presence of an aqueous phase on the phase behavior of a CO_2/hydrocarbon system. They found that the presence of water reduces the amount of CO_2 that is available for mixing with the hydrocarbon due to the solubility of CO_2 in water. Chang, Coats and

Nolen (1998) modeled CO_2 floods, including CO_2-water solubility, for an unfractured reservoir. These authors studied secondary and tertiary water alternating gas (WAG) injection. They found that approximately 10% of the CO_2 that was injected dissolved in to the water, and this CO_2 was unavailable for mixing with the oil. The solubility effects were more pronounced for tertiary CO_2 WAG than for the secondary injection and the delayed oil recovery. We studied CO_2 solubility in water, as described in the following sections.

5.2 Rock and Fluid Properties

A chalk core from the Faxe area outcrop in Denmark, which has similar rock properties to North Sea chalk, was used in the present experiment. The core had a cylindrical shape with a length of 59.6 cm and a diameter of 4.6 cm. The core porosity and permeability have been previously reported as 44.4% and 4 md, respectively (Darvish 2007).

Relative permeabilities and capillary pressure were not measured for the core. The C_1-n-C_5 capillary pressure of the Faxe outcrop chalk core, as measured by Christoffersen (1992), was used for the core oil-gas capillary pressure. Corey-type relative permeabilities were used to model the experiment. The gas and oil exponents for the Corey-like relative permeabilities (k_{rg} and k_{rog}) were 2.4 and 3.8, respectively (Eqs. (2.19) and (2.20)). The oil and gas relative permeabilities are shown in **Fig. 5.1**. For the water and oil relative permeabilities, the same type of relative permeabilities (Eqs. (2.17) and (2.18)) were used. The oil exponent for the Corey-like relative permeability (k_{row}) was set to 2.5. The water-oil capillary pressure curve (Eq. (2.21)) and the water permeability were set as variables to match the cumulative volume of water produced. **Fig. 5.2** shows the oil and water relative permeabilities that were used in the present model.

The 13 components PR-EOS/LBC parameters that were used in this chapter are given in Tables 4.1 and 4.2.

5.3 Experimental Procedures

This section describes the experiment that was performed to study a CO_2

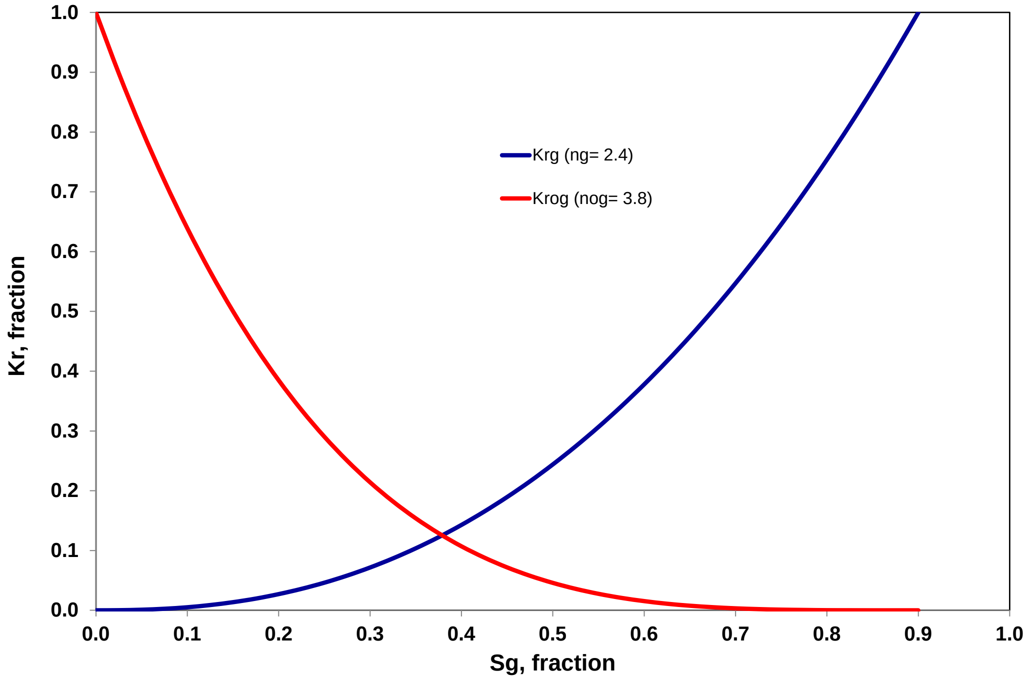

Figure 5.1 – Oil and gas relative permeability used in the matched model.

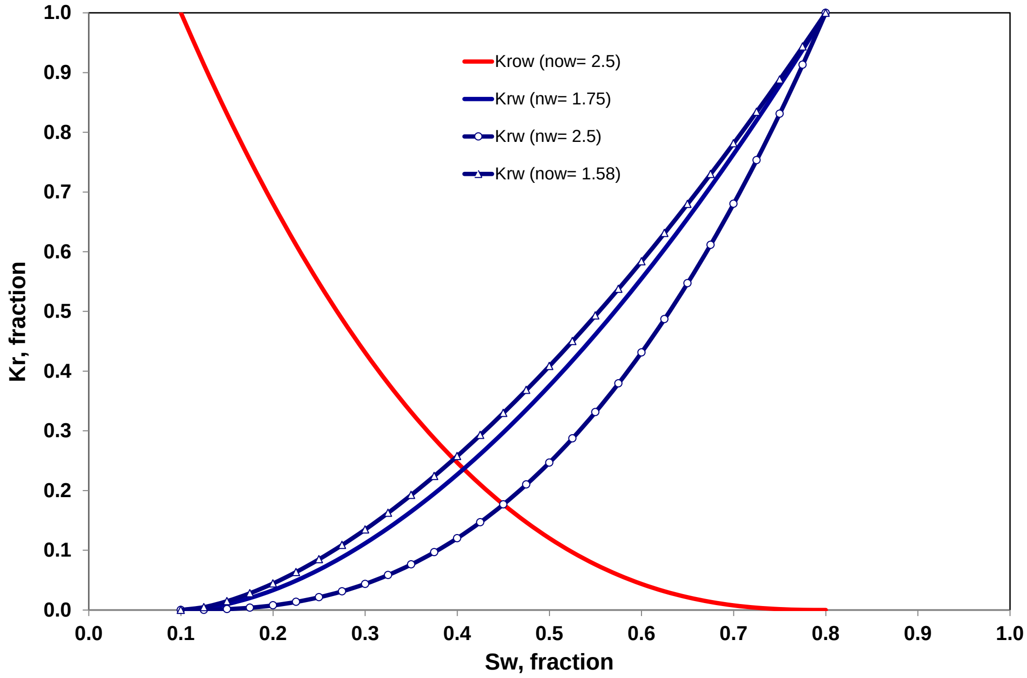

Figure 5.2 – Oil and water relative permeability used in the matched model.

injection in a fractured reservoir. The experimental procedure that is described was based on Darvish (2007) and on personal communications with Darvish.

A dried cylindrical chalk core was placed in a steel core holder. The core holder inner diameter was 5.0 cm. The core diameter was 4.6 cm, and the length was 59.6 cm. The fracture was represented by a 2 mm space between the core and the core holder. The core porosity and absolute permeability have been previously reported as 44.4% and 4 md, respectively (Darvish 2007).

Due to the large permeability contrast between the core and the surrounding space (artificial fracture), the process of initially saturating the core with live oil was complicated. The oil would flow through the high permeable space, leaving the core partially saturated with live oil. Therefore, the space between the core and the core holder wall was initially filled with Wood's metal. The metal melting point was 70 ^{o}C, and the experiment was performed at 130 ^{o}C. The metal was melted and poured into the space between the core and the core holder. The fracture was sealed with the metal and had zero permeability after the system was cooled.

The core was evacuated and pressurized with brine. Live oil was injected from in the top of the core at a constant pressure (300 bar) and temperature (40 ^{o}C), and the amount of water produced was measured. The water saturation of the core after flooding it with a 1.2 pore volume of oil was 26.3 %. The system was heated to 130 ^{o}C at a constant pressure (300 bar), and the Wood's metal was removed from the annular space by injecting oil. The oil was injected from the top of the core holder, and the metal was drained from the bottom. The fracture porosity and permeability were not measured after the metal was removed from the system; however, the pressure difference between the top and bottom of core holder was measured, which could be used to determine the fracture permeability in a model.

The oil in the fracture was replaced by CO_2. The experiment continued with a CO_2 gas injection for 20 days. The cumulative volume of CO_2 that was injected during the experiment is illustrated in **Fig. 5.3**. The fluid that was produced was diverted to a separator under ambient conditions. The mass of the separated oil was measured continually, and the component mass fraction was measured periodically.

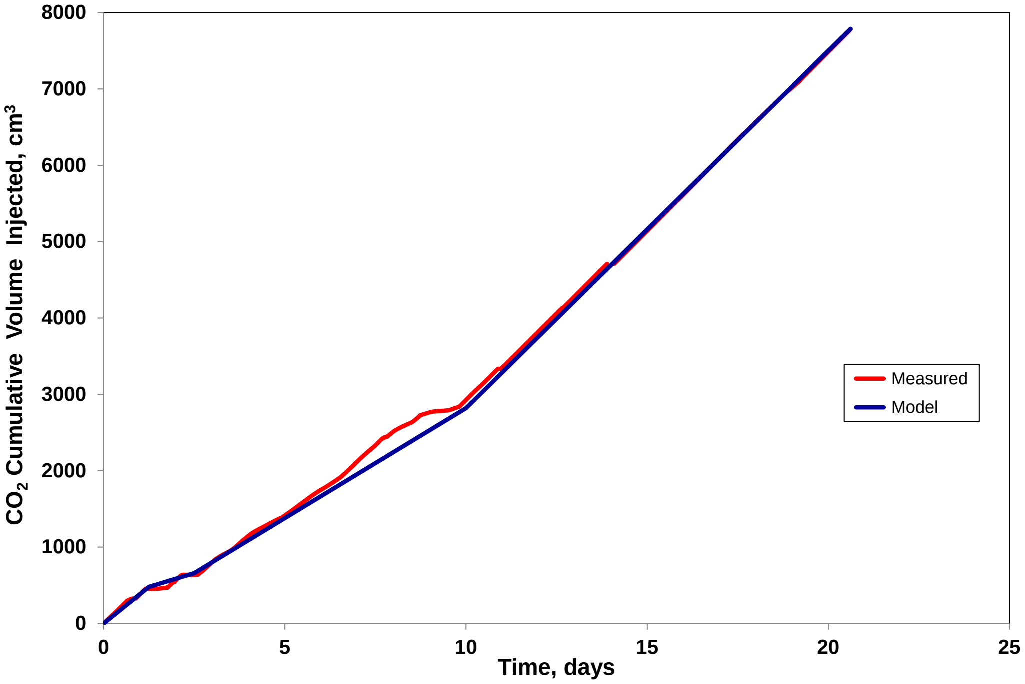

Figure 5.3 – Measured and calculated cumulative volume of CO_2 injected.

5.4 Model Description

The matrix block (core) was initially filled with oil, and the fractures were initially filled with CO_2. The fractures were assumed to have a negligible capillary pressure. The matrix and the fracture dimensions were the same as the core and fracture in the experiment. A two-dimensional, radial grid was used in which the matrix block was surrounded by two horizontal fractures (at the top and bottom) and one vertical fracture. A fine grid was required to reduce the numerical dispersion for the CO_2 gas injection. 10 and 51 grid cells were used in the radial and vertical directions, respectively, to simulate the experiment.

The *ECLIPSE 300* simulator with implicit solution method was used for all of the simulations. A 13-component PR-EOS was used. The EOS properties of the components are summarized in Tables 4.1 and 4.2.

The oil and gas relative permeabilities that were used to model the experiment are shown in Fig. 5.1. As mentioned above, the water-oil capillary pressure curve and water relative permeability were set as variables to match the cumulative volume of water that was produced. Because mobile oil, gas and water were used in the model, three-phase oil relative permeabilities were needed. Eqs. (2.23a) and (2.23b) were used.

The C_1-n-C_5 capillary pressure that was measured by Christoffersen (1992) for a similar core was used as the core capillary pressure in the model. Following Eq. (2.24), this capillary pressure was scaled using the IFT, for which the reference interfacial tension (IFT) was 1.5 mN/m. No capillary pressure was present in the fracture. The relative permeabilities were not scaled using the IFT.

The *Pipe-it/Streamz* software was used to calculate cumulative mass of produced oil from reservoir simulation result. One separator was defined to simulate the produced stream in the experiment. As in the experiment, the separator pressure was atmospheric. As mentioned above, the separator temperature was not measured during the experiment.

The oil and gas effective diffusion coefficients are given in Table 4.4. The gas diffusion coefficients were determined from the equilibrium gas at the bubble-point pressure. More details of the diffusion coefficient calculations are given in section (2.2).

5.5 Matching The Experimental Data

In this section, we describe the matching process for the measured cumulative mass of the separator oil and the cumulative volume of the water that was produced. In Chapter 4, fractured permeability was set to 80 md to get pressure difference measured during the experiment. Because the same procedure was used to initialize this experiment, we kept the fracture permeability at 80 md. A CO_2 injection experiment (Darvish 2007) using a chalk core without water saturation was matched with the two sets of the oil-gas relative permeabilities (Chapter 4). When water was present in the system, however, we found that the non-linear oil-gas relative permeabilities for the core provided a better match than the linear gas-oil relative permeabilities.

The model matched the cumulative volume of produced water with and without the water-oil capillary pressure. Because the water-oil capillary pressure was not measured, we used the water-oil imbibition capillary pressure measurements from the other North Sea chalk reservoir (Valhall) as guidelines (Webb, Black and Tjetland 2005). The Valhall water-oil imbibition capillary curve was not used in the model, but the capillary curve that was used in the model had a similar capillary pressure range, as is shown in **Fig. 5.4**. The water exponent (n_w) for the Corey-like water relative permeability (K_{rw}) was set as a variable in both cases (with and without the water-oil capillary pressure). The cumulative volume of the gas that was produced was matched, yielding n_w= 1.58 with, and n_w= 1.75 without, the water-oil capillary pressure.

No condenser or cooler was present in the outlet stream; consequently, the effective separator temperature was set as a variable during the experiment. The effective surface separator temperature was mainly affected by the producing

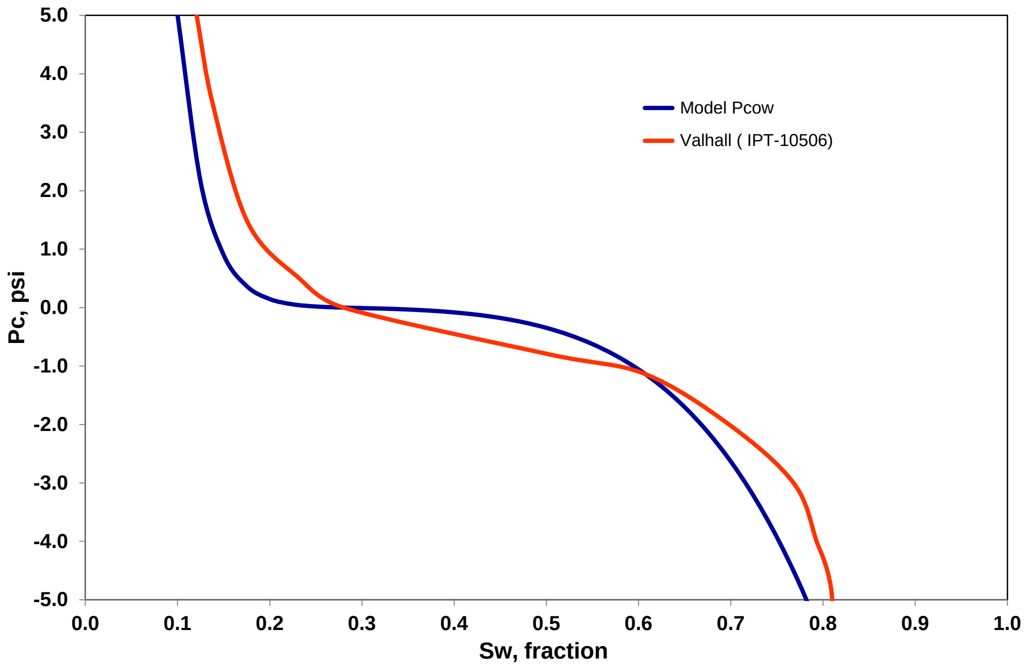

Figure 5.4 – Model and Valhall (after Webb et. al.) capillary pressure curves.

stream rate and the solid precipitation on the pipe wall (Wood's metal and wax). The fluid retention time decreased with an increasing fluid rate in the pipe, and as a result, the amount of heat exchange was smaller. In contrast, the stream rate was directly proportional to the CO_2 injection rate. The profiles of the CO_2 injection rate and the effective surface separator temperature are shown in **Figs. 5.5** and **5.6**, respectively. Except in the early stages (less than 1.3 days) of the experiment, the effective separator temperature was proportional to the injection rate. As mentioned above, the solid precipitation on the pipe wall reduced the heat exchange between the fluid and the pipe. Therefore, the heat exchange at the early stages of the experiment were higher than those in the later stages because of less solid precipitate on the pipe wall.

The other parameters in the numerical model were taken from the reported values in the experiment. The results of the model are shown in **Figs. 5.7** and **5.8**.

The heavy-component mass fractions from the experiment were compared with the numerical model results. All of the calculated mass fractions from the model follow the same trend as the measured values, as shown in **Fig. 5.9**. The

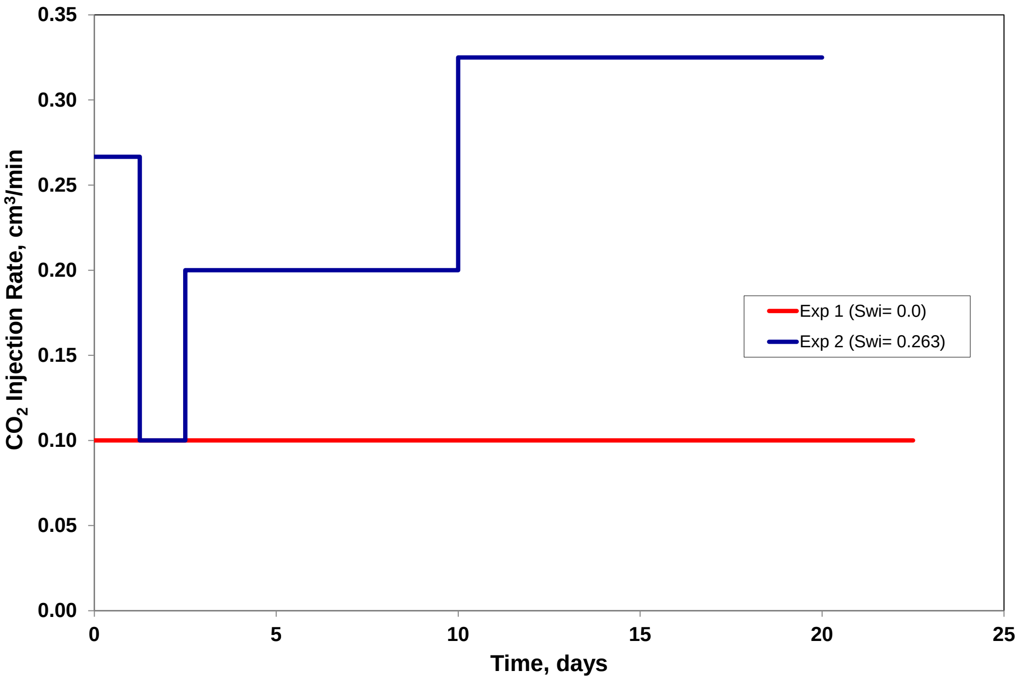

Figure 5.5 – Profile of CO_2 injection rate in experiment-1 (S_w=0.0) and experiment-2 (S_w=0.263).

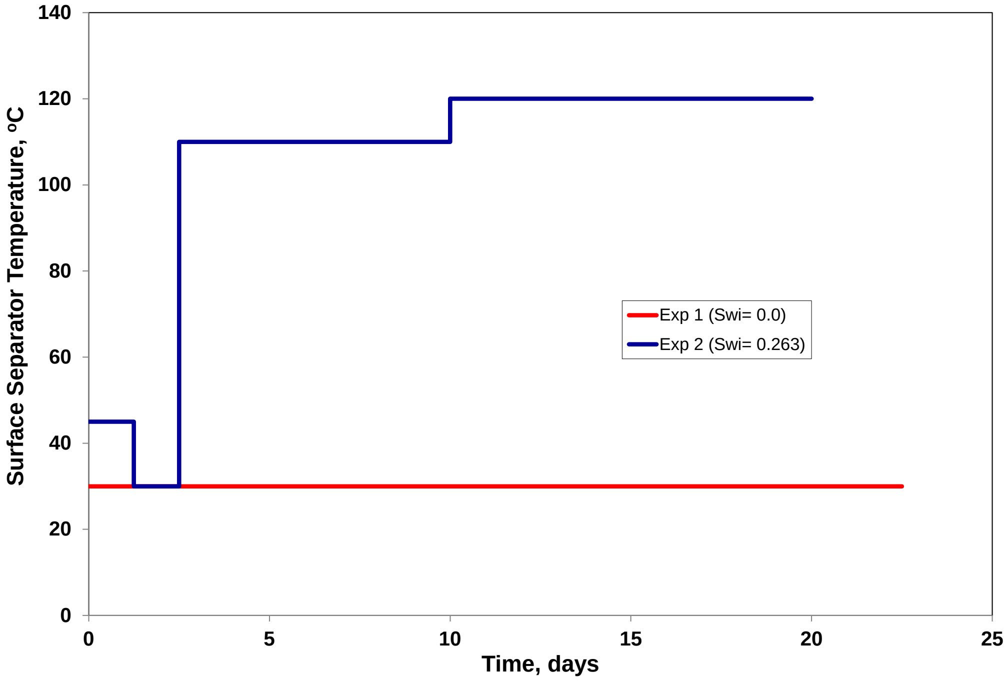

Figure 5.6 – Profile of separator temperature in experiment-1 (S_w=0.0) and experiment-2 (S_w=0.263).

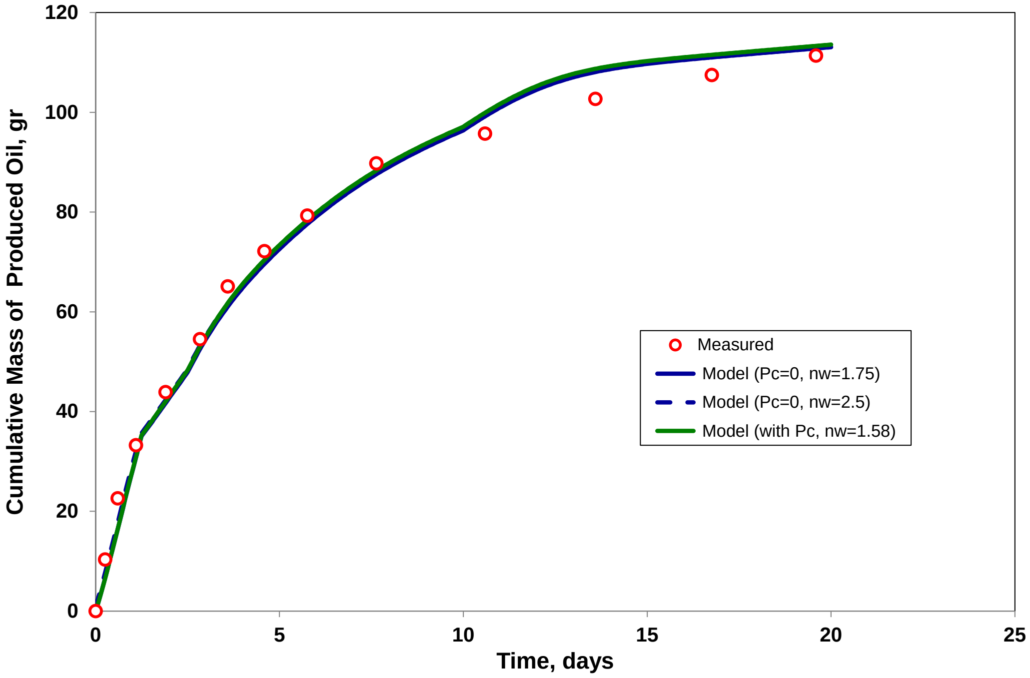

Figure 5.7 – Measured produced oil mass with matched simulation results for three core water relative permeability and with and without water-oil capillary pressure.

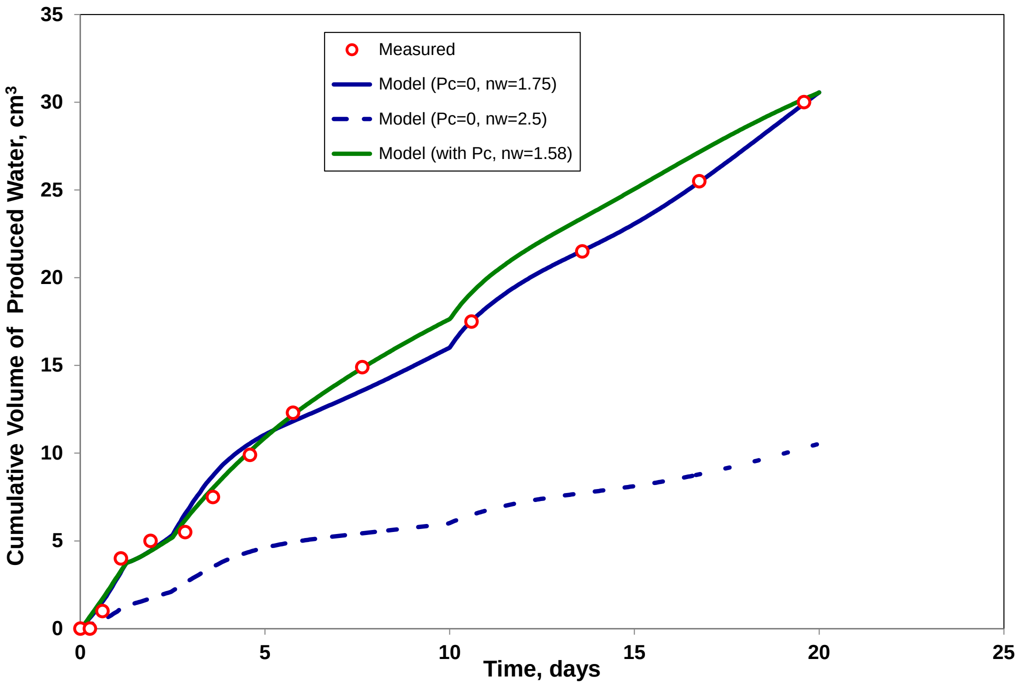

Figure 5.8 – Measured produced water volume with matched simulation results for three core water relative permeability and with and without water-oil capillary pressure.

separator temperature was set to 30 °C for this calculation because the small samples that were taken from the oil stream cooled faster and quickly reached laboratory temperature. When C_{10} and the heavier components were grouped together, the results of the numerical model and the experimental data were closer together than when they were not grouped, as shown in Fig. 5.9. This result likely indicates that the grouping of the C_{10+} components was performed somewhat differently in the laboratory than in the EOS calculation. The calculated molecular weight of the oil produced in the laboratory was compared with the molecular weight from the numerical model (**Fig. 5.10**). The calculated molecular weight was close to that in the laboratory until 8 days had elapsed. After 8 days, the molecular weight of the numerical model was lower than the calculated molecular weight of produced oil in the laboratory, possibly due to the uncertainty of determining the molecular weight of heavy-end components in the laboratory. The oil produced after 8 days mainly consisted of the C_{16+}. C_{23+} mass

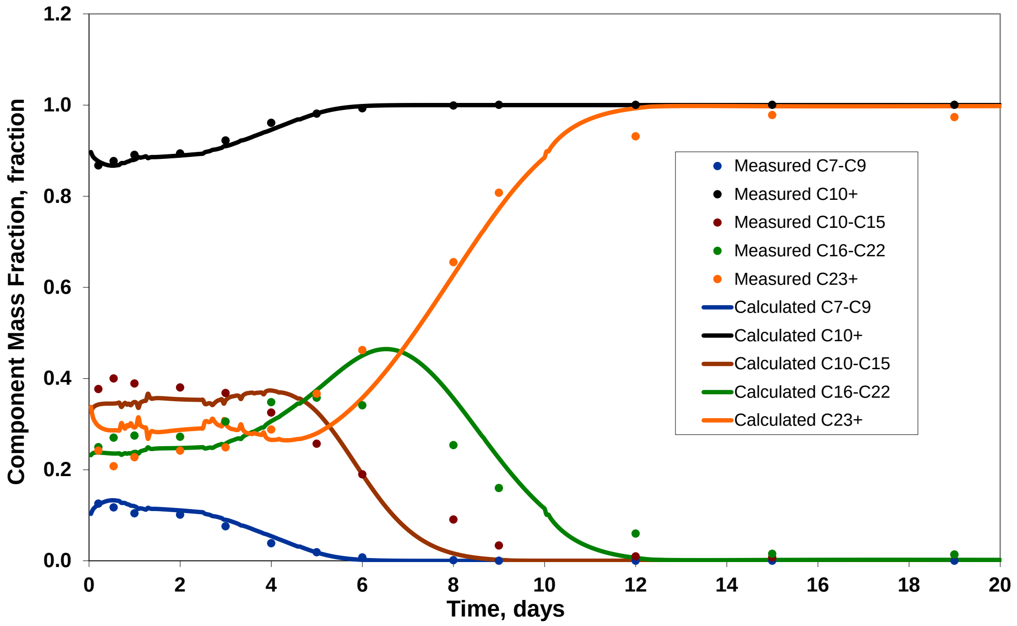

Figure 5.9 – Measured and calculated heavy components mass fraction of produced oil at separator condition.

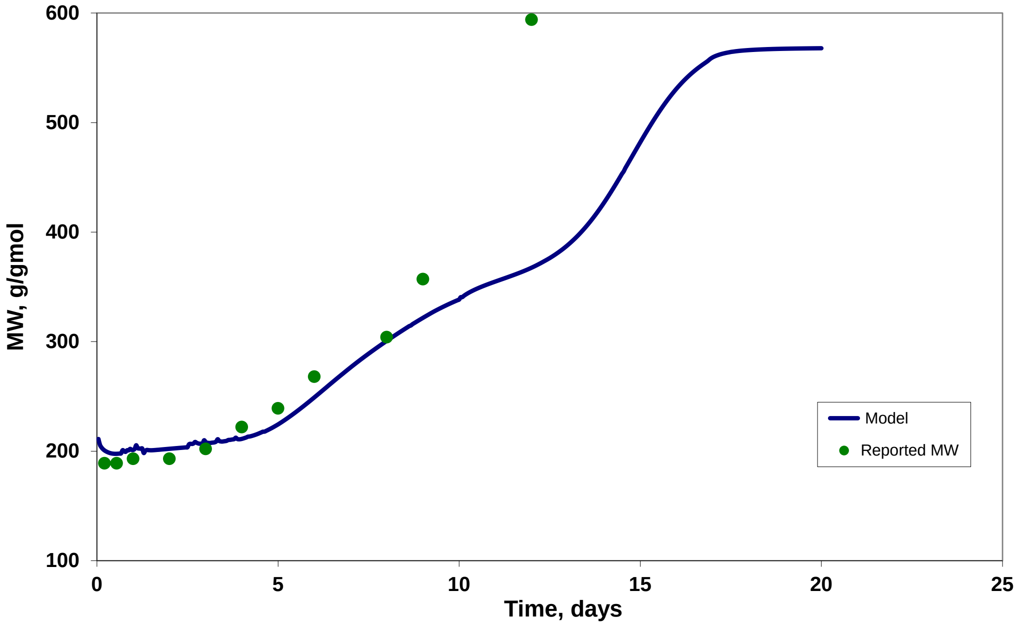

Figure 5.10 – Reported and calculated molecular weight of produced oil at separator condition.

fractions increased with time. As a result, the difference between the two molecular weights also increased with time.

5.6 CO_2 Injection Rate Effect

In this section, we describe the comparison of the modeling results from the present experiment with those of the experiment in Chapter 4. In the experiment in Chapter 4, the CO_2 injection rate (0.1 cm^3/min) was lower than that in the present study, and no initial water was present in the system. We will call the experiment that is described in this chapter "Experiment-2", and we will call the experiment from Chapter 4 "Experiment-1". Some of the CO_2 was dissolved in the water and was consequently not available to interact with the oil. Based on the results of Duan and Sun (2003), 11.5 cm^3 of CO_2 dissolved in the core water in place (116 gr). Therefore, the amount of CO_2 that dissolved into the water was considered to be negligible compared to the 7500 cm^3 of CO_2 that was injected over the 20 day period.

5.6.1 Oil Recovery

The components and the total oil recovery that were based on the component moles were calculated using Eqs. (4.3) and (4.4). Plotting the mole-based oil recovery in both of the experiments using the model results (**Fig. 5.11**) revealed that the experiment with the lower CO_2 injection rate had better efficiency per CO_2 hydrocarbon pore volume (HCPV) injected. The oil that was produced in Experiment-1 (the experiment with the lower CO_2 injection rate) was heavier than that in Experiment-2 with respect to the HCPV injected (**Fig. 5.12**). In both of these experiments, furthermore, the lighter components were produced first, as shown in **Fig. 5.13**. Consequently, the mass transfer between the CO_2 and the hydrocarbon was more efficient in Experiment-1 than in Experiment-2. Because greater amounts of CO_2 were available to interact with the oil in the core in Experiment-2, however, the oil recovered faster when the CO_2 injection rate was increased, as shown in **Fig. 5.14**. Although CO_2 and oil had less efficient mass transfer but more oil was recovered during same period of time.

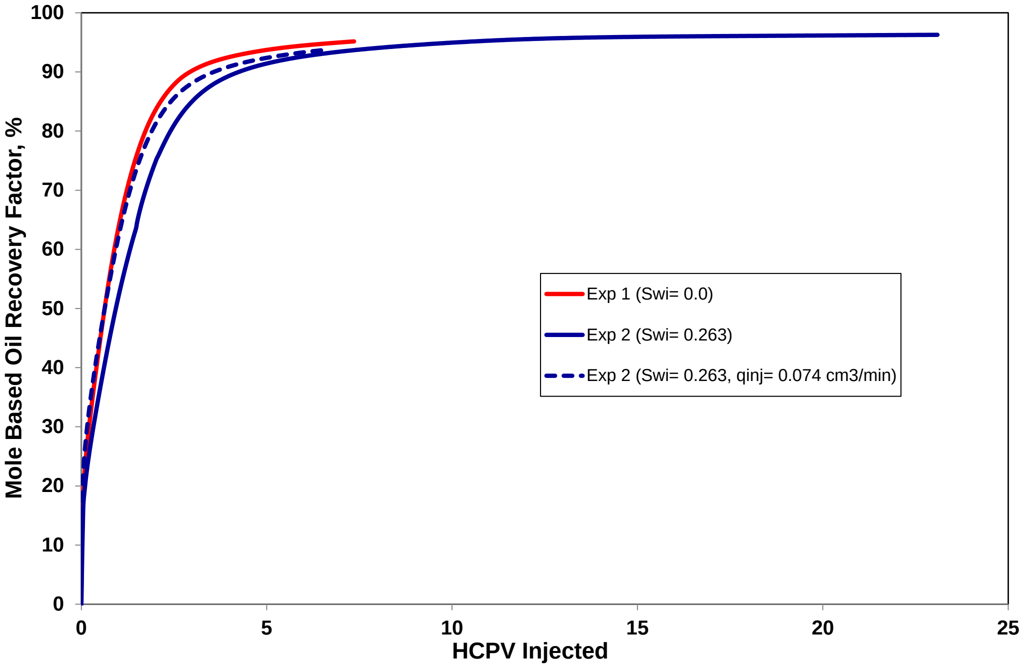

Figure 5.11 – Calculated mole based oil recovery factor of two experiments versus HCPV injected from matched model.

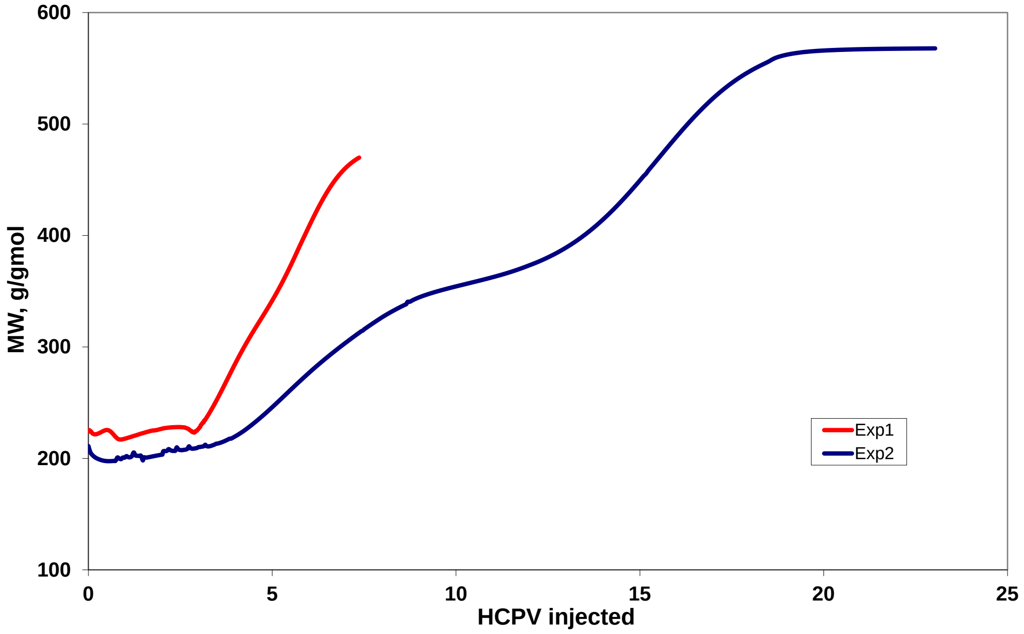

Figure 5.12 – Calculated mole based component recovery of two experiments versus HCPV injected from matched model.

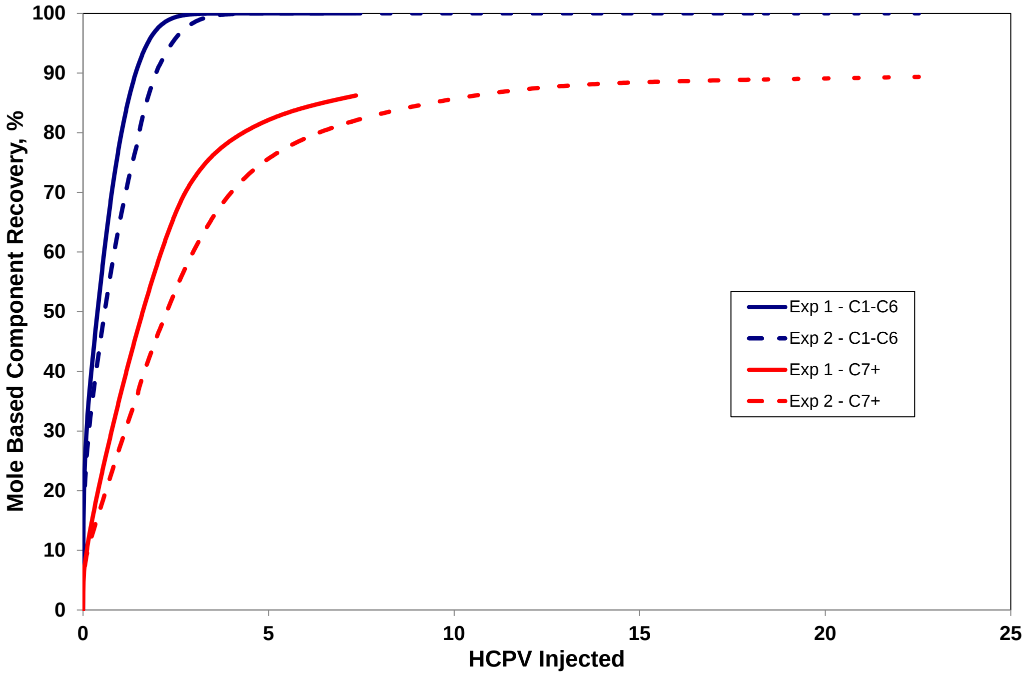

Figure 5.13 – Calculated mole based component recovery of two experiments versus HCPV injected from matched model.

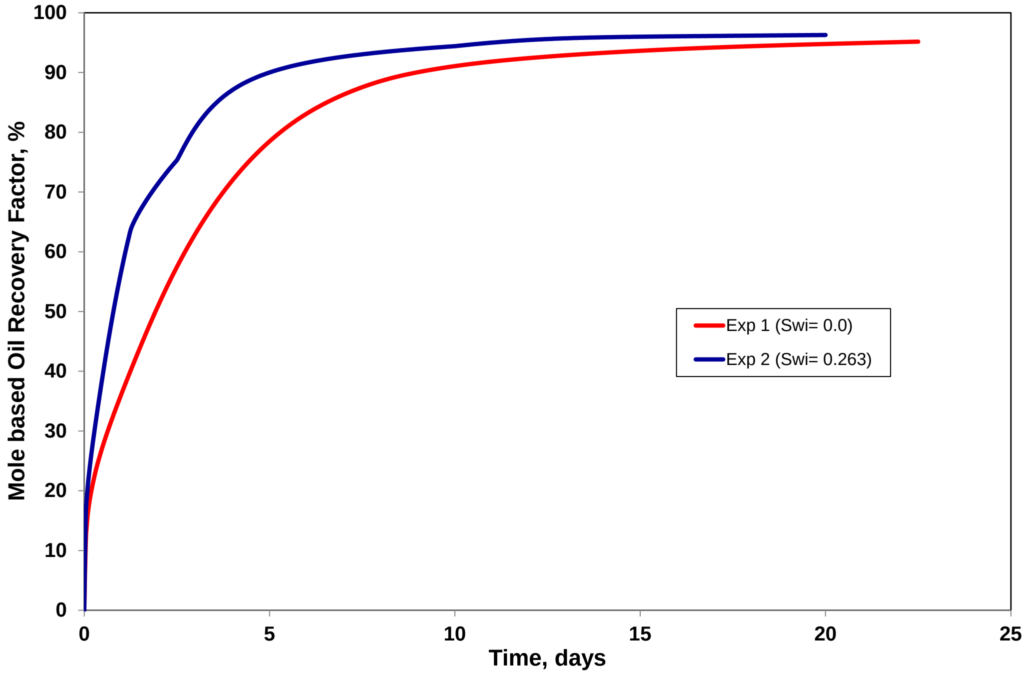

Figure 5.14 – Calculated mole based oil recovery factor of two experiments versus time from matched model.

Injection rate in Experiment-2 model was reduced to 0.074 cm^3/min to yield the same HCPV fraction injected as in Experiment-1. Results of this Experiment-2 run shows that recovery with and without water is approximately same at a given HCPV injected, when the CO_2 injection rate, expressed as $\Delta HCPV/\Delta t$, is approximately same (Fig. 5.11).

5.6.2 CO_2 Map Profile

Comparing the CO_2 map profiles from the two experiments yielded 27.5 and 78.5 % oil recovery. These results correspond to 12 hours and 5 days in Experiment-1, respectively, and to 5 hours and 2.8 days in Experiment-2, respectively. As shown in **Figs. 5.15** and **5.16**, the oil was displaced more laterally in Experiment-2 than in Experiment-1. The amount of CO_2 that flowed in the fracture (the annulus space) was greater in Experiment-2 than in Experiment-1. Therefore, the mass transfer was greater in the core grids that were adjacent to the fracture compared to the central core grids.

5.7 Grid Sensitivity

A numerical grid sensitivity analysis was performed to investigate its effect on oil recovery and water production. The ultimate oil recovery was the same for all of the grids considered, as shown in **Fig. 5.17**. However, the 5x5 ($N_x x N_z$) grid resulted in a slightly slower oil recovery. The amount of water that was produced decreased as the number of grid cells that were used in the model decreased. The 5x5 grid model does not follow the production trend of the other cases (**Fig. 5.18**).

5.8 Diffusion Coefficients Effect

Diffusion played an important role in the present experiment. The oil and gas diffusion coefficients were the parameters that controlled the diffusion mechanisms in the numerical simulation. Another important parameter was the driving force of the diffusion transport. Two major forces drive diffusion: a) concentration forces and b) chemical forces. The driving potential from the chemical force was used in all of the above models.

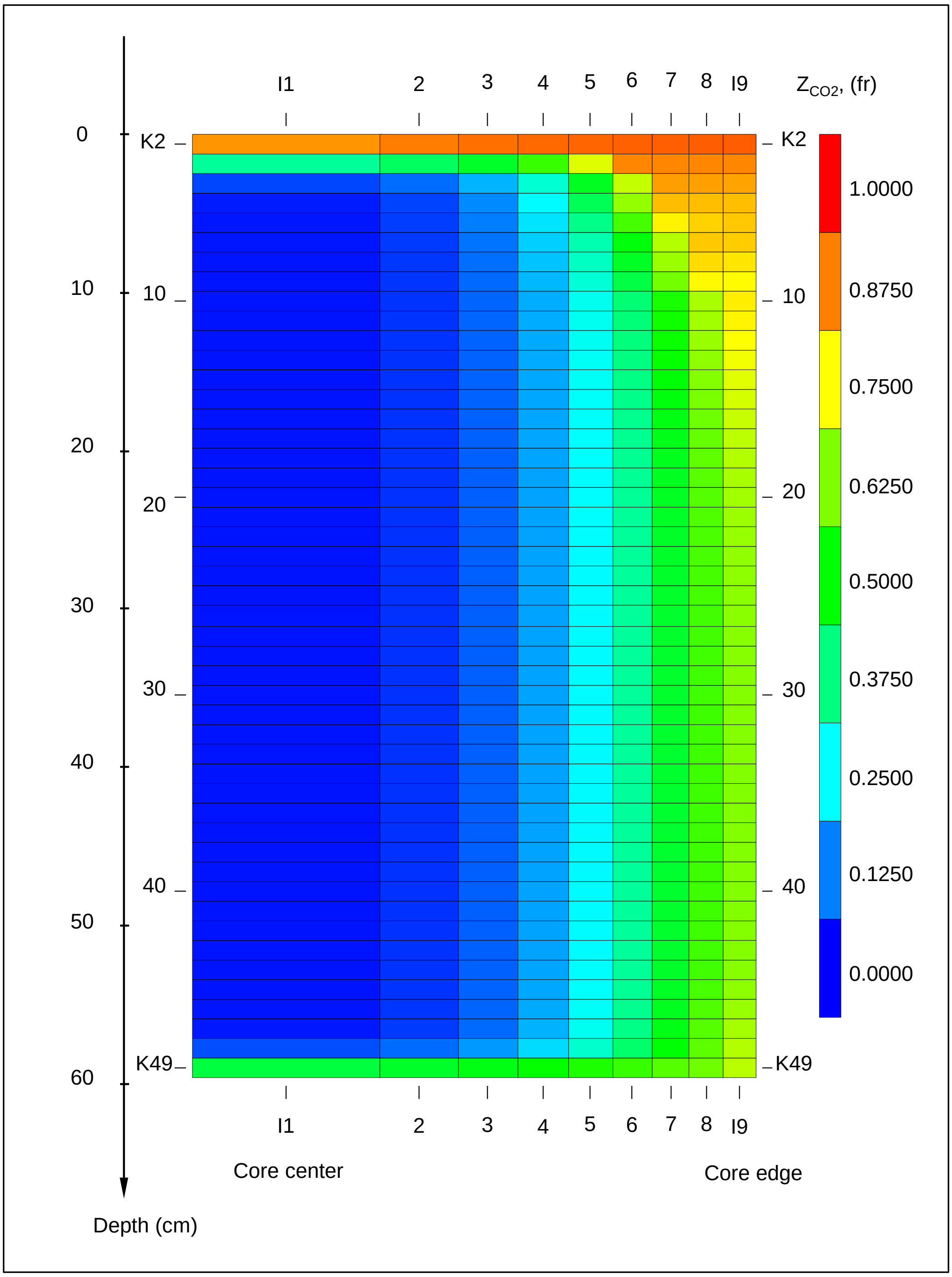

Figure 5.15 – CO_2 mole fraction profile of core after 5 hours for matched model of experiment-2 (at about 36% oil recovery).

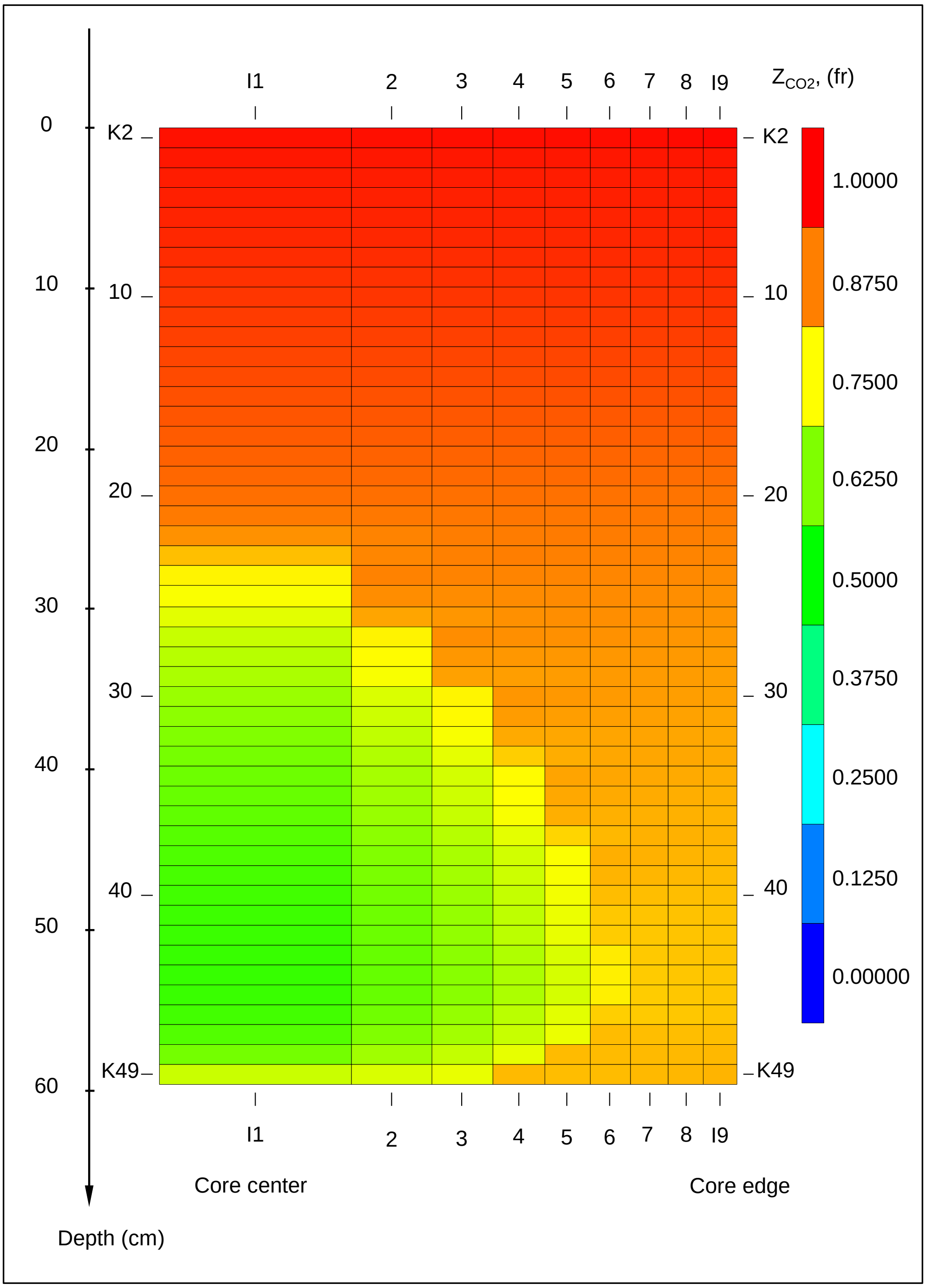

Figure 5.16 – CO_2 mole fraction profile of core after 2.8 days for matched model of experiment-2 (at about 78.5% oil recovery).

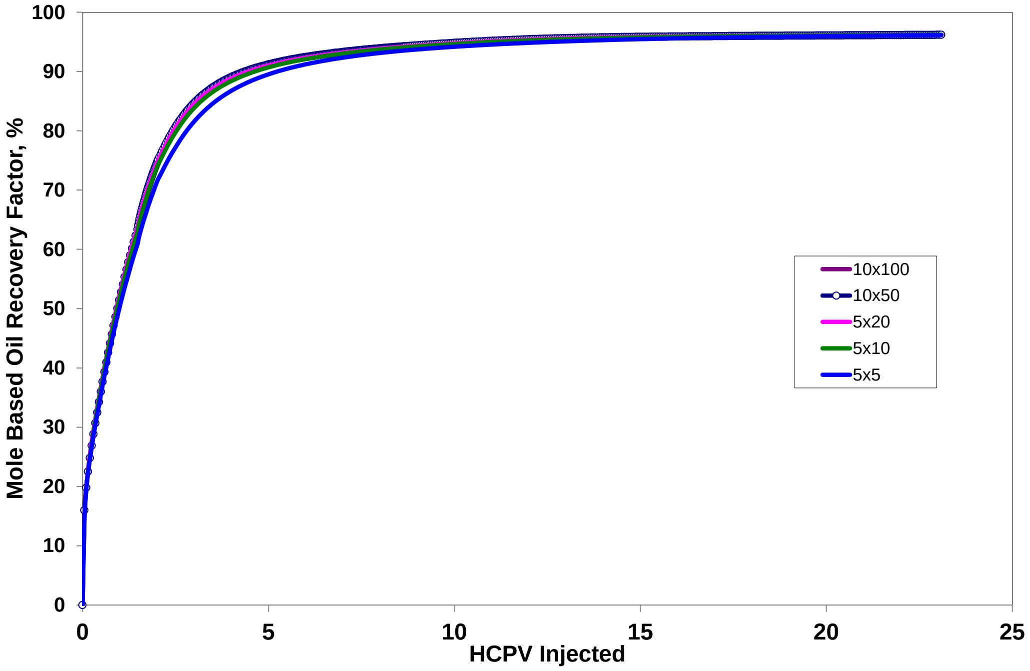

Figure 5.17 – Mole based oil recovery results from grid sensitivity models.

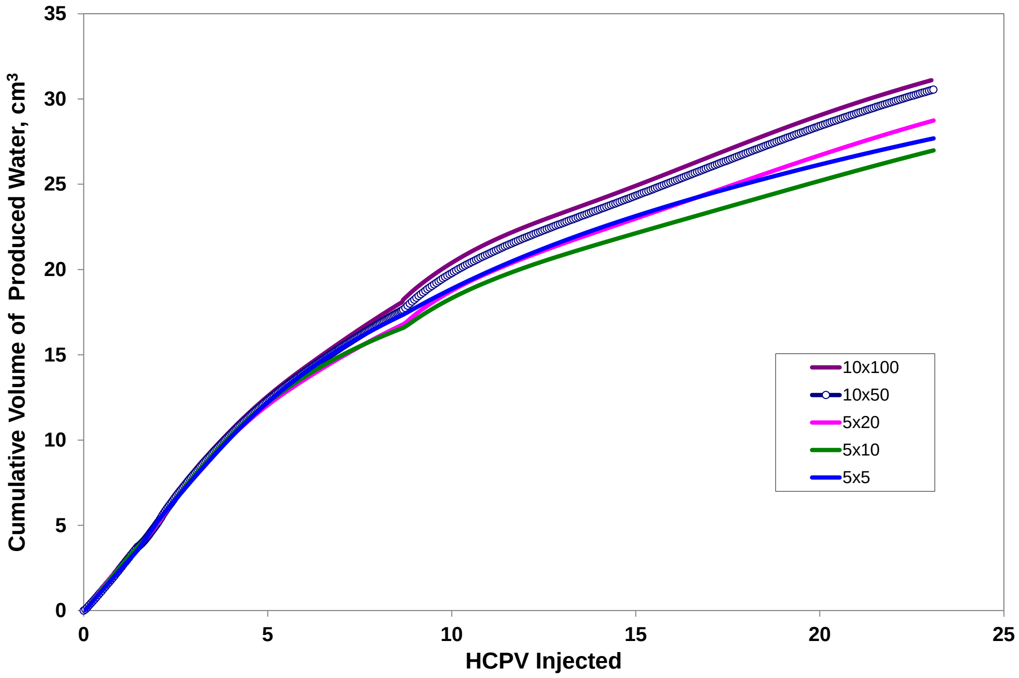

Figure 5.18 – Mole based oil recovery results from numerical sensitivity models.

The oil and gas diffusion coefficients were increased and decreased by one order of magnitude to study the effects of these adjustments on the oil recovery. As expected, increasing the diffusion coefficients increased the oil recovery rate and decreased the diffusion coefficients, which slowed down the oil recovery (**Fig. 5.19**). One model was constructed using the default oil and gas diffusion coefficients using concentration driven diffusion. The oil recovery was dramatically slower than in the other cases for which chemical potential driven diffusion was used. The ultimate oil recoveries were the same for all of the cases (Fig. 5.19).

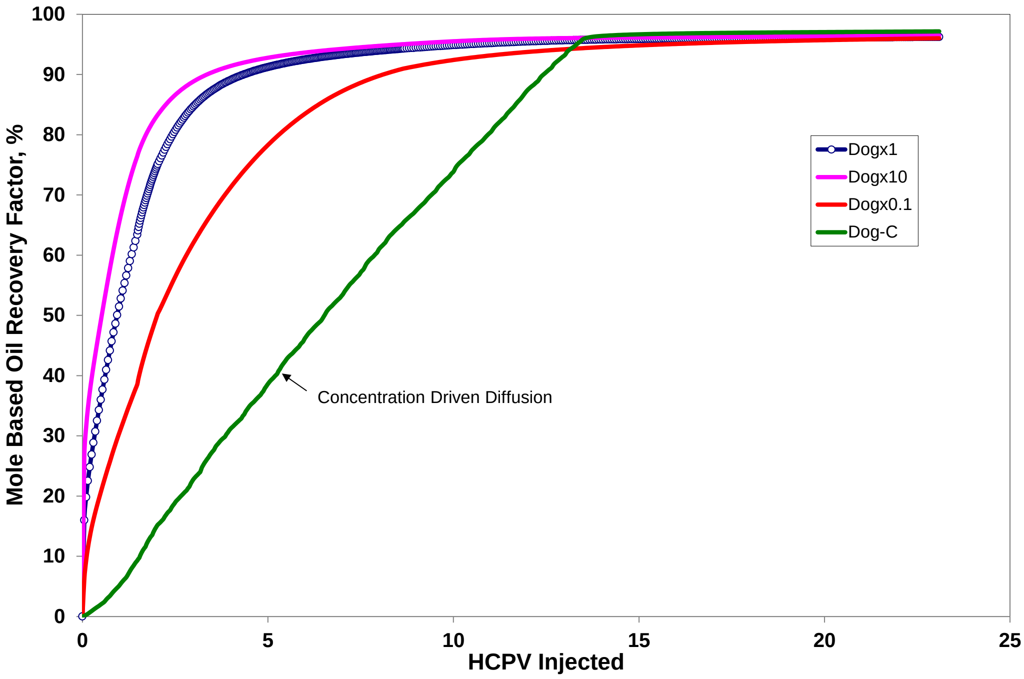

Figure 5.19 – Effect of diffusion coefficient and diffusion drive on mole based oil recovery factor.

5.9 Conclusions

The following conclusions were determined after analyzing the experimental and numerical studies.

1. The measured production data from the experiment were matched with a commercial compositional finite-difference simulator model.

2. The ultimate oil recovery was not significantly affected by the CO_2 injection rate. The rate of oil recovery increased with an increasing CO_2 injection rate in the time domain; however, the mass transfer became less efficient with respect to the CO_2 volume that was injected.
3. The initial water saturation in this experiment did not appear to affect the oil recovery.
4. The oil recovery was sensitive to the diffusion coefficients that were used in the modeling. Traditional concentration-based diffusion severely under-predicts the diffusion compared to the chemical-energy-based diffusion.
5. The oil recovery was less sensitive to numerical gridding than the water production.

5.10 References

Chang, Y., Coats B.K and Nolen, J.S. 1998. A Compositional Model for CO_2 Floods Including CO_2 Solubility in Water. SPE Reservoir Evaluation and Engineering, 1(2): 155-160. SPE-35164-PA.

Christoffersen, K. 1992. High-Pressure Experiments with Application to Naturally Fractured Chalk Reservoirs. PhD Dissertation, NTNU, Trondheim, Norway.

Darvish, G.R. 2007. Physical Effects Controlling Mass Transfer in Matrix Fracture system During CO_2 Injection in to Chalk Fractured Reservoir. PhD Dissertation, NTNU, Trondheim, Norway.

Duan, Z. and Sun, R., 2003. An Improved Model Calculating CO_2 Solubility in Pure Water and Aqueous NaCl Solution from 273 to 533 K and from 0 to 2000 bar. Chemical Geology Journal 193 (2003) 257– 271.

Petrostreamz AS: ***Pipe-It/Streamz***, www.petrostreamz.com.

Pollack N.R., Enick R.M., Mangone D.J. and Morsi B.I. 1988. Effect of an Aqueous Phase on CO_2/Tetradecane and CO_2/Maljamar-Crude-Oil Systems. SPE Reservoir Engineering 3(2) : 533-541. SPE-15400-PA.

Schlumberger: ***ECLIPSE 300*** Reservoir Engineering Software. 2009. www.slb.com.

Webb, K.J., Black, C.J.J. and Tjetland. G., 2005. A Laboratory Study Investigating Methods for Improving Oil Recovery in Carbonates. International Petroleum Technology Conference, Doha, Qatar, 21-23 November.

Chapter 6

CO_2 Injection in Naturally Fractured Reservoirs – Haft Kel Study without Diffusion

6.1 Introduction

We present results studying the enhanced-oil-recovery (EOR) potential for carbon dioxide (CO_2) injection in the naturally fractured Haft Kel field, Iran, on the basis of detailed compositional simulations of a homogeneous single matrix block surrounded by fractures. The effect of several key parameters will be study in detail—matrix permeability, matrix-block size, matrix/matrix capillary continuity (stacked blocks), and the use of injection gas mixtures of CO_2 and HC gas. However recovery in CO_2 injection cases is slow because molecular diffusion effect is not considered in this chapter.

Haft Kel field is located in the foothills of the Zagros Mountains, some 100 km east of Ahwaz city and on the east side of the Dezful embayment. The first oil well in Haft Kel was completed to a depth of 3363 ft in 1928, with an initial production rate of approximately 5700 STB/D. A field plateau rate of approximately 200,000 STB/D was maintained for several years, before the field was shut down from 1950 to 1954. Subsequently, production dropped to approximately 14000 STB/D in 1976. HC (separator) gas injection was initiated in June 1976, at a rate of 400 MMscf/D, with oil production stopped for approximately 7 years between 1980 and 1987 to allow the oil column to build from 100 to 300 ft. Since 1987, the oil column and pressure have been held constant by gas injection, with a sustained oil rate of 35000 STB/D adding an additional 100 million STB produced from 1987 through 1995 (Saidi 1996).

6.2 Description of Model

A single matrix block surrounded by fractures was used to study the matrix/fracture fluid exchange in a gravity/capillary recovery mechanism. Significant compositional variations develop within the matrix block, resulting in high recoveries.

The matrix block is initially filled with oil, and the fractures are initialized with injection gas. Zero capillary pressure and high permeability (100 darcies) of the fractures means that the viscous forces are negligible compared with gravity and capillary forces. We define a large pore volume (PV) for the fracture, to eliminate effects of model injection and production wells. The matrix block is always surrounded by injection gas, and produced oil from the matrix block always enters the fracture system. Conceptually, we are looking at a matrix block located at the no-flow boundary between an injector and a producer in which lateral pressure gradients are negligible.[1]

Haft Kel petrophysical properties and initial fluid compositions are taken from Saidi (1987). The matrix and the fracture dimensions and parameters are given in **Table 6.1.** Because of the matrix-block symmetry, only half of the matrix block is modeled. A 2D Cartesian grid is used where the matrix block is surrounded by two horizontal fractures at the top and bottom and one vertical fracture on the right side of the matrix block.

The reservoir simulator *SENSOR* is used for all simulations. An 11-component tuned Soave-Redlich-Kwong (SRK) equation of state (EOS) describes phase and volumetric behavior; the Lorenz-Bray-Clark correlation, tuned to viscosity data,

---

[1] Ringen *et al.* (2005) shows that this type of simulation model accurately represents reservoir-condition laboratory tests of gas gravity drainage for a carbonate core.

Table 6.1 – Matrix and Fracture Fixed Dimensions and Properties

Matrix width (X)	8 ft
Matrix length (Y)	8 ft
Vertical fracture width	0.01ft
Horizontal fracture height	0.01ft
Fracture permeability	100 D
Matrix porosity	10%
Fracture porosity	100%

Table 6.2 – Fluid Properties For The 11-Component SRK Characterization

Component	MW	Tc, ^oR	Pc, psia	ω	Vshift	Zc	Parachor
N2	28.01	227.16	492.84	0.037	-0.001	0.29178	59.10
CO2	44.01	547.42	1069.51	0.225	0.217	0.27433	80.00
H2S	34.08	672.12	1299.97	0.090	0.102	0.28292	80.10
C1	16.04	343.01	667.03	0.011	-0.002	0.2862	71.00
C2	30.07	549.58	706.62	0.099	0.059	0.27924	111.00
C3	44.10	665.69	616.12	0.152	0.091	0.2763	151.00
C4-C6	70.43	840.66	527.88	0.214	0.098	0.27403	216.05
C7-C14	136.82	1147.73	411.95	0.353	0.099	0.29826	384.35
C15-C21	239.68	1395.61	283.74	0.605	0.131	0.29826	657.60
C22-C29	341.31	1546.43	225.55	0.818	0.130	0.29826	855.51
C30+	487.10	1692.33	184.60	1.06576	0.09103	0.29826	1062.75

is used to calculate viscosities. EOS component properties and binary interaction parameters (BIPs) are given in **Tables 6.2** and **6.3,** respectively.

Pressure/volume/temperature (PVT) simulations needed to generate the EOS model from reported PVT data were made using *PhazeComp*. After tuning the EOS with black-oil properties reported by Saidi (1987), this PVT simulator was also used to generate saturated oil compositions for initializing the matrix block at pressures higher than and lower than the current reservoir pressure. Saturation pressure of the original oil composition was 1400 psia. Constant-composition-expansion (CCE) experiments are simulated to determine oil compositions below

Table 6.3 – BIPs for The 11-Component SRK Characterization

	N2	CO2	H2S	C1	C2	C3	C4-C6	C7-C14	C15-C21	C22-C29	C30+
N2	-										
CO2	0.0000	-									
H2S	0.0000	0.1200	-								
C1	0.0250	0.1050	0.0800	-							
C2	0.0100	0.1300	0.0700	0.0000	-						
C3	0.0900	0.1250	0.0700	0.0000	0.0000	-					
C4-C6	0.1040	0.1154	0.0544	0.0000	0.0000	0.0000	-				
C7-C14	0.1100	0.1150	0.0500	0.0000	0.0000	0.0000	0.0000	-			
C15-C21	0.1100	0.1150	0.0500	0.0000	0.0000	0.0000	0.0000	0.0000	-		
C22-C29	0.1100	0.1150	0.0500	0.0000	0.0000	0.0000	0.0000	0.0000	0.0000	-	
C30+	0.1100	0.1150	0.0500	0.0000	0.0000	0.0000	0.0000	0.0000	0.0000	0.0000	-

1400 psia.[2] Special "swelling" tests were made to calculate oil composition at higher pressures: Incipient bubblepoint gas from a lower pressure was added to the bubblepoint oil to raise the bubblepoint pressure. This process was started at 1400 psia and was repeated at 2000, 2500, and 3000 psia. The 11-component compositions for the reservoir oils and equilibrium gases at different saturation pressures are given in **Tables 6.4** and **6.5,** respectively. Other details of the simulator models are given below.

Table 6.4 – Oil Composition for The 11-Component EOS at Different Saturation Pressures

Component	1000 psi	1400 psi	2000 psi	2500 psi	3000 psi
N2	0.0004	0.0009	0.0019	0.0026	0.0033
CO2	0.0039	0.0043	0.0046	0.0048	0.0050
H2S	0.0133	0.0130	0.0122	0.0117	0.0113
C1	0.2211	0.2957	0.3873	0.4524	0.5089
C2	0.0494	0.0497	0.0490	0.0485	0.0481
C3	0.0542	0.0506	0.0460	0.0427	0.0399
C4-C6	0.1428	0.1282	0.1105	0.0979	0.0871
C7-C14	0.3761	0.3343	0.2837	0.2478	0.2167
C15-C21	0.0998	0.0887	0.0752	0.0657	0.0574
C22-C29	0.0299	0.0266	0.0225	0.0197	0.0172
C30+	0.0092	0.0082	0.0069	0.0060	0.0053
Tres= 110 ^{O}F					

---

[2] Near-identical oil compositions result from CCE, differential liberation, and constant-volume tests or from depletion, which accounts for changing gas and oil mobilities.

Table 6.5 – Equilibrium-Gas Composition for The 11-Component EOS at Different Saturation Pressures

Component	1000 psi	1400 psi	2000 psi	2500 psi	3000 psi
N2	0.0050	0.0075	0.0106	0.0111	0.0110
CO2	0.0073	0.0064	0.0058	0.0056	0.0055
H2S	0.0098	0.0082	0.0072	0.0068	0.0068
C1	0.8913	0.8999	0.9004	0.8967	0.8907
C2	0.0520	0.0451	0.0409	0.0399	0.0399
C3	0.0225	0.0201	0.0194	0.0198	0.0205
C4-C6	0.0114	0.0117	0.0137	0.0162	0.0190
C7-C14	0.0006	0.0010	0.0020	0.0037	0.0064
C15-C21	0.0000	0.0000	0.0000	0.0000	0.0001
C22-C29	0.0000	0.0000	0.0000	0.0000	0.0000
C30+	0.0000	0.0000	0.0000	0.0000	0.0000

Oil recovery factor (RF) is calculated from total average oil saturation S_o in the matrix block using Eq. (3.2)

Capillary pressure and relative permeability are taken from Saidi (1987) and were fit to the Sensor analytical capillary pressure and relative permeability models (Eq. (2.17)-(2.22)).

This capillary pressure is scaled with IFT according to Eq. (2.24) where reference interfacial tension (IFT) is 10 mN/m. There is no capillary pressure in the fracture.

6.3 Grid Sensitivity

In this section, we discuss grid effect on oil recovery using equilibrium-gas and CO_2-gas injection at 1400-psia system pressure. The only requirement for accurate representation of recovery performance for gravity/capillary equilibrium in a system with constant phase properties (densities and IFTs) is sufficient vertical gridding to provide a good integration of the final equilibrium saturation/height relationship. Therefore, the oil recovery with equilibrium gas is the same for all grids considered, as we see in **Fig. 6.1.**

The recovery performance for CO_2 injection is affected by different gridding because of changing compositional effects, as shown in Fig. 6.1. 10×50 ($N_x \times N_z$)

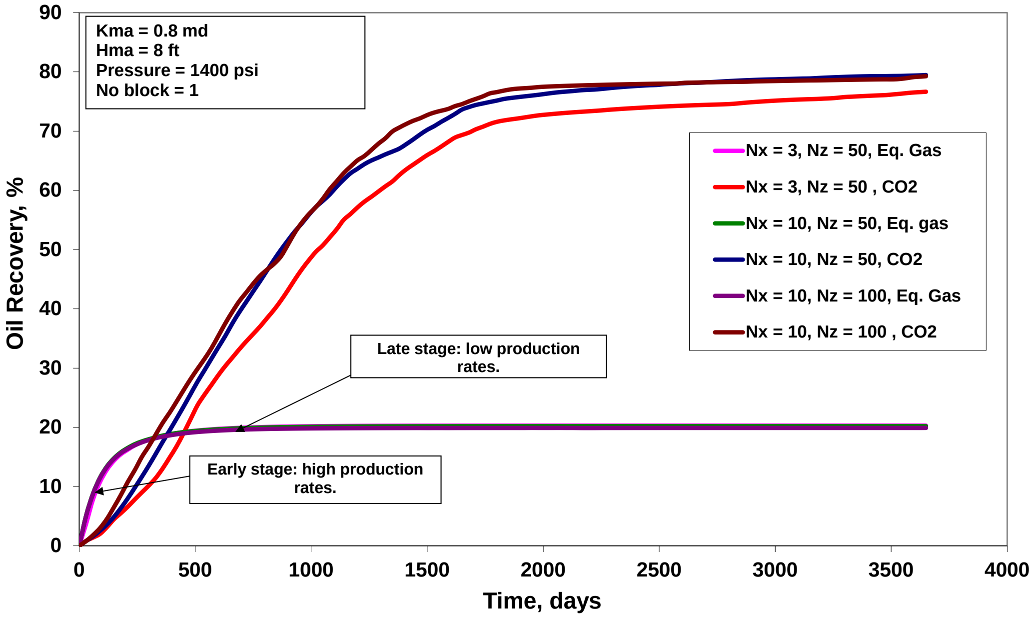

Figure 6.1 – Effect of grid cells on oil recovery vs. time for single matrix block using equilibrium-gas injection at system pressure of 1400 psia.

and 10×100 grids give higher recovery than 3×50 grids. A finer grid is needed for CO_2 injection to capture gravity and near-miscible displacement. Details of the CO_2-injection mechanism will be described in the next sections. Most equilibrium-gas-injection cases were run with a 10×50 ($N_x \times N_z$) grid, and a 10×100 grid for CO_2 injection.

6.4 Prediction of Minimum Miscibility Pressure (MMP)

1D slimtube simulations were used to determine the thermodynamic MMP. The slimtube simulations were performed at system pressures of 1000, 1400, 2000, 2500, and 3000 psia using 200, 500, and 1000 grid cells. The results of recoveries for the different runs vs. system pressure are given in **Fig. 6.2;** final recoveries are defined as 1 minus the fraction of initial oil in place remaining after 1.2 PV of CO_2 injected, divided by the initial oil in place. At each pressure, linear regression was used to fit these recoveries vs. $1/\sqrt{N}$, where N is the number of cells. Recoveries are extrapolated to infinite grid cells. The MMP is 1400 psia according to slimtube simulations interpreted as described above, which compares favorably with the PhazeComp-calculated multicell algorithm MMP of 1,350 psia for a condensing/vaporizing mechanism.

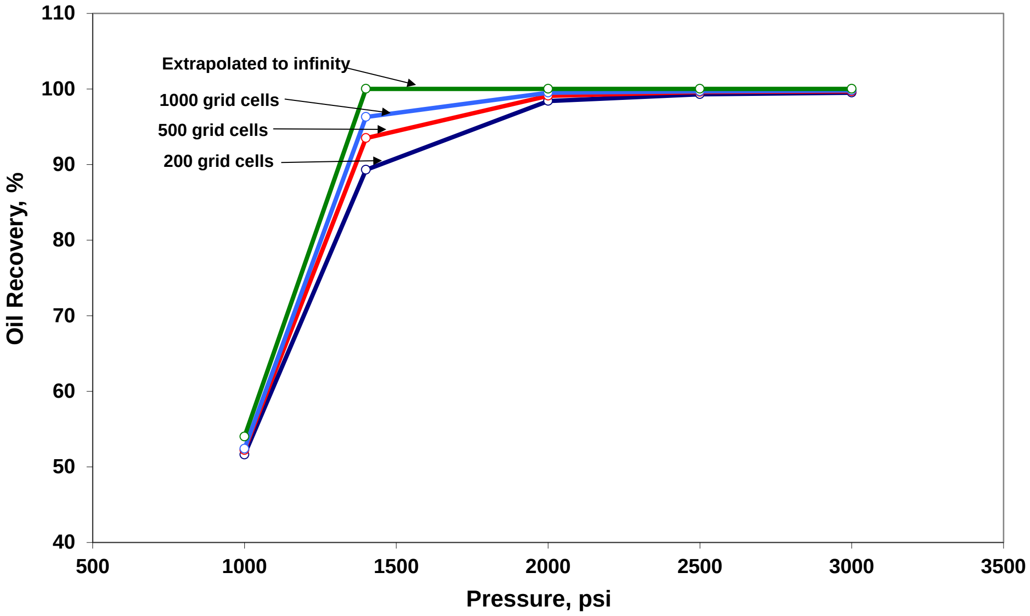

Figure 6.2 – Slimtube simulation using CO2 injection gas. Oil recovery at 1.2 PVs of gas injected vs. pressure for different number of grid cells.

6.5 Injection-Gas Mechanism

6.5.1 Equilibrium Gas in a Single Matrix Block

If the gravity forces exceed capillary forces, gas enters the top of the matrix block and oil is produced from the bottom of the matrix block. Viscous forces may be present during oil production from a matrix block. Viscous/gravity ($R_{v/g}$), Eq. (3.1), and capillary/gravity ($R_{c/g}$) dimensionless ratios are used to understand the importance of the various recovery mechanisms during production (Wylie and Mohanty 1999; Stalkup 1983; Løvoll *et al.* 2005):

$$R_{c/g} = \frac{\Delta P_{cap}}{\Delta P_{grav}} = \frac{\Delta P_{cap}}{g \Delta \rho_{og} h} \quad \ldots\ldots (6.1)$$

where $\Delta\rho_{og}$ is oil and gas density difference, g is gravity-acceleration constant, h is grid-cell height, and ΔP_{cap} is capillary pressure gradient at the displacement front.

The recovery process can be divided approximately into two main periods: a quick initial production period characterized by high oil rates when most of the oil is recovered, followed by a final long production period characterized by lower production rates.

Oil primarily flows in the vertical direction, whereas gas enters both from the top and from the sides. After 30 days when only 4% of the oil has been recovered, the gas has entered only the topmost blocks of the core. $R_{v/g}$ and $R_{c/g}$ are equal at 0.005 and 0.15, respectively. These numbers suggest that gravity drainage is the dominant mechanism. After 180 days, approximately 15% of the original oil in place is recovered and the gas front has reached the capillary holdup zone (entry height). The profile is now almost uniform in the vertical direction; however, the gas saturation behind the front is less than the ultimate equilibrium gas saturation, so there is still a significant amount of oil left to be recovered. This is illustrated in Fig. 6.1, showing that it takes only 180 days to recover 15% of the oil, whereas it takes nearly 1,000 days to reach 20% ultimate oil recovery.

The initial period with high production rates ends when the displacement front reaches the capillary holdup zone in the matrix block. At this point, the gas saturation behind the front has not reached the final equilibrium profile and there is still potential for additional oil recovery. However, the recovery of remaining oil during the last stage is slow because of low oil mobility.

The parameters controlling the rate of recovery, but which have limited impact on ultimate recovery, are (a) absolute matrix permeability, (b) shape of the relative permeability curve, and (c) matrix block-to-block flow (re-infiltration). Parameters that control the ultimate recovery are (a) pressure (because of IFT and density dependence), (b) capillary pressure curve, and (c) endpoint saturations S_{org} and S_{wc}.

The following subsections present sensitivity simulations for these parameters. Unless stated otherwise, only a single parameter is changed in each sensitivity, keeping the other properties equal to base-case values.

6.5.2 Mechanism of CO_2 in a Single Matrix Block

In this subsection, we investigate the recovery mechanism of CO_2 in a single matrix block. In general, CO_2 gas has a higher viscosity than HC gas and, therefore, a better mobility ratio. In our study, we focus on the mechanism of gravity/capillary drainage, thereby making mobility ratio a less important parameter. CO_2-gas injection reduces gas/oil IFT significantly, and this has a pronounced impact on recovery by reducing the capillary retaining forces.

As seen in **Fig. 6.3**, CO_2 is lighter than oil at lower pressures, but can be heavier than oil at higher pressures. For Haft Kel, CO_2 has a higher density than reservoir oil at pressures above 2050 psia. This characteristic results in two fundamentally different recovery mechanisms for CO_2, depending on the sign of the CO_2-oil density difference.

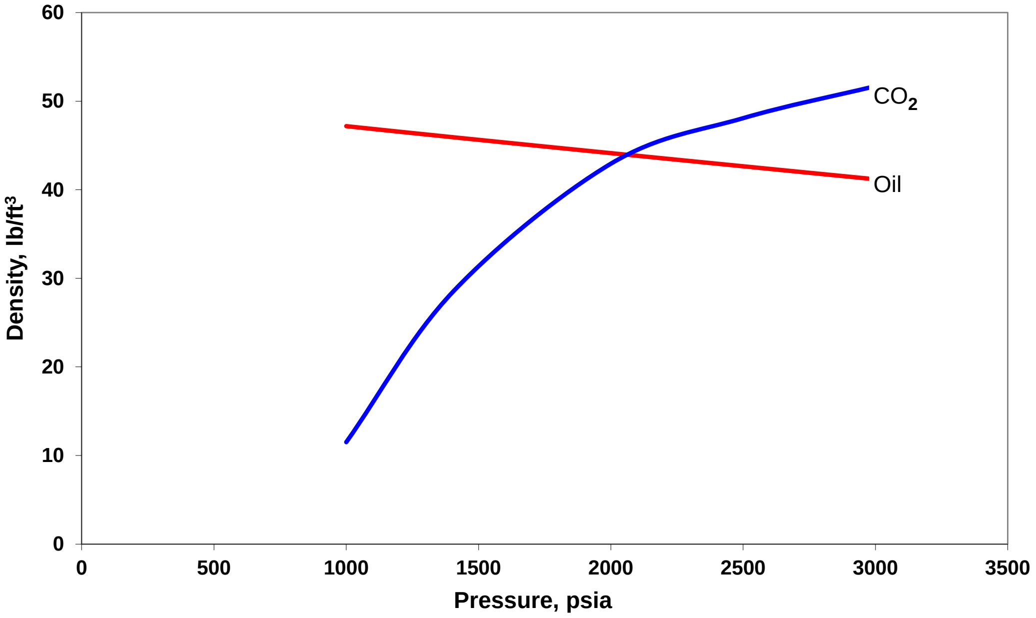

Figure 6.3 – Comparison of CO_2 and Haft Kel oil densities as a function of pressure (at reservoir temperature of 110 °F).

6.5.2.1 CO_2 Lighter Than Oil.

When CO_2 is lighter than oil, CO_2 enters from top of the matrix block as in a traditional gas gravity-drainage mechanism. As shown in **Fig. 6.4,** the recovery behavior of CO_2 injection can be divided into three periods: an initial production period of high oil rates and two longer production periods characterized by lower production rates. The final period results in significant extra oil recovery from a capillary-drive mechanism first described by Uleberg and Høier (2002). **Figs. 6.5 through 6.7** show saturation distributions during the three periods, respectively.

The first two periods are similar in shape to the equilibrium gravity/capillary mechanism, but with a more complicated recovery mechanism. Because IFT decreases more significantly in CO_2 injection, capillary entry height decreases to result in higher ultimate recoveries after the first and second periods. Viscous/gravity ($R_{v/g}$=0.004) and capillary/gravity ($R_{c/g}$=0.006) ratios clarify that gravity drainage is the dominant mechanism during this period of oil production. This is illustrated in Fig. 6.4, which shows that it takes 1,400 days to recover 70% of the oil (end Phase 1), but not before 7400 days does recovery reach 84% (end Phase 2).

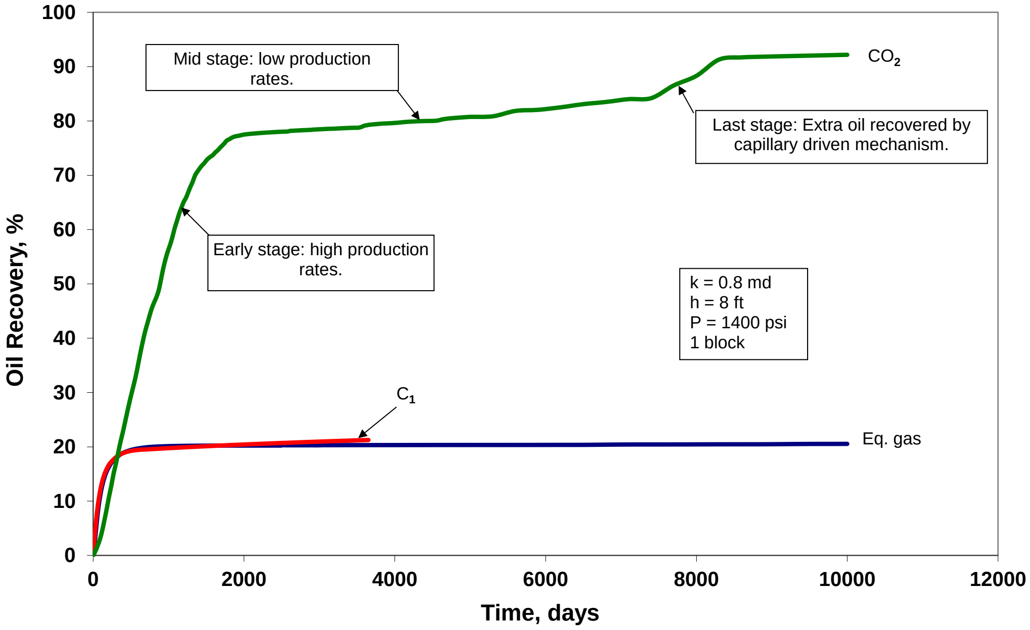

Figure 6.4 – Effect of different injection gas on oil recovery vs. time for single matrix block at system pressure of 1400 psia.

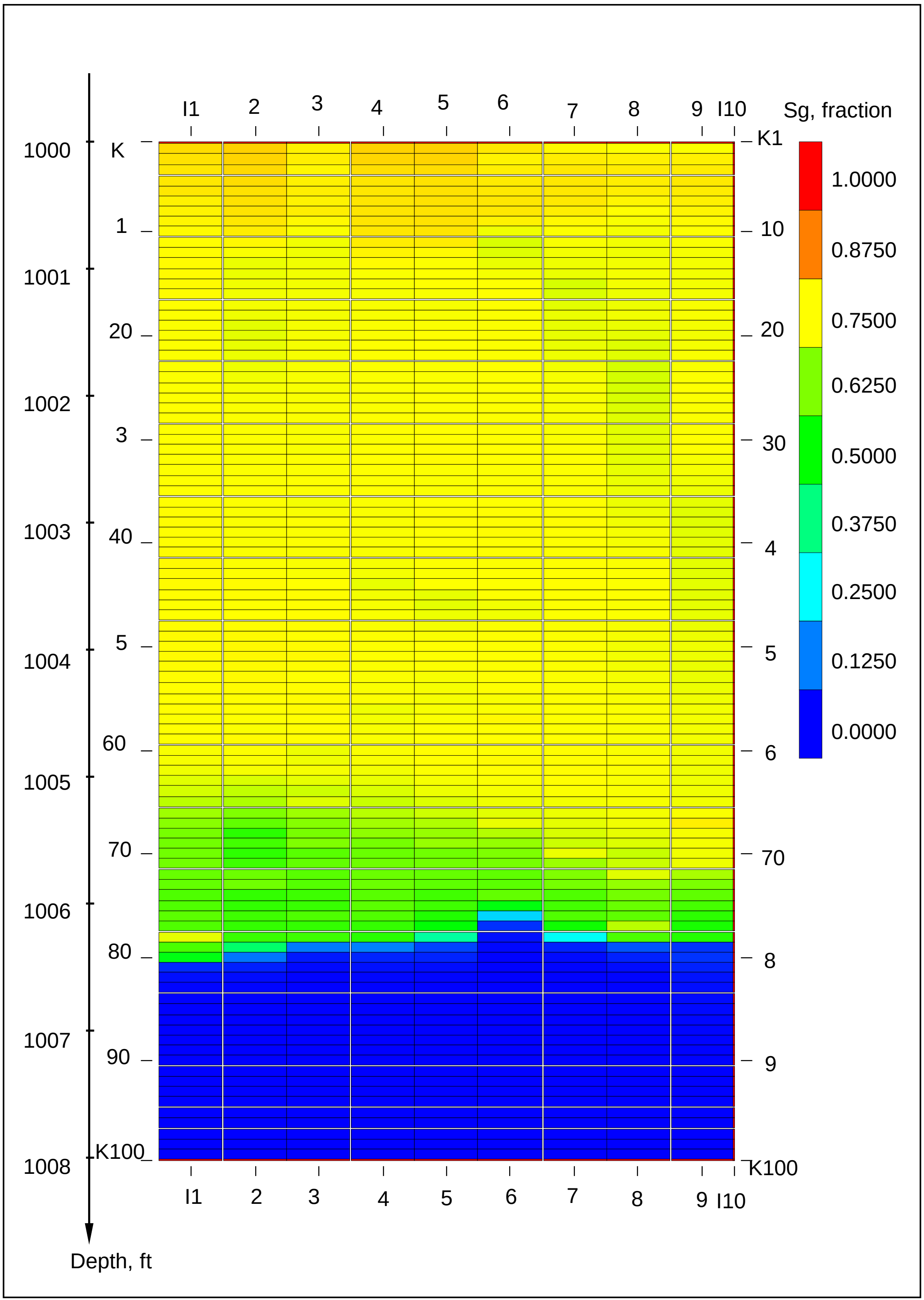

Figure 6.5 – Early stage CO$_2$ gas displacement, gas saturation profile inside matrix block after 1410 days at system pressure of 1400 psia (at 71% oil recovery).

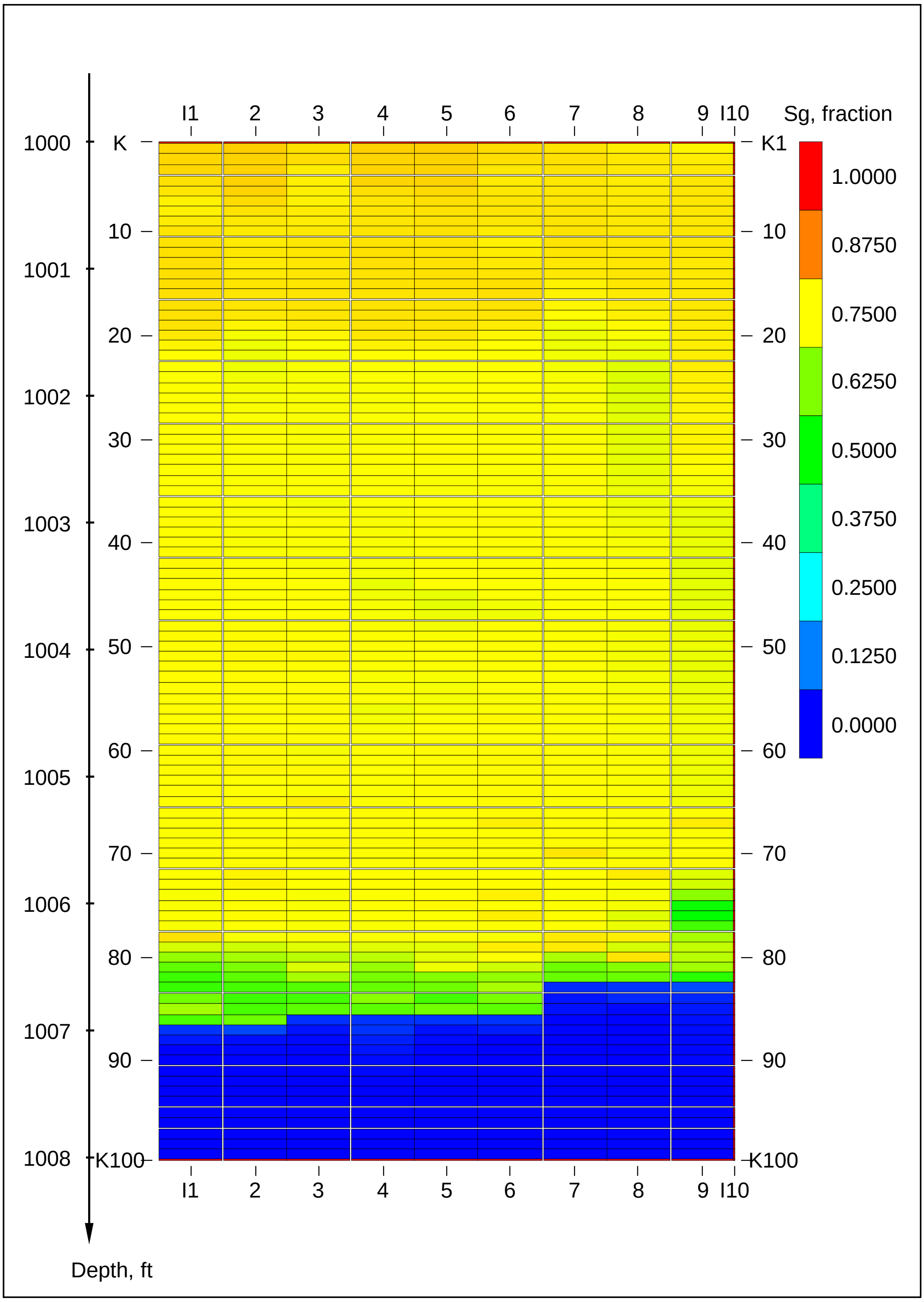

Figure 6.6 – Mid stage CO_2 gas displacement, gas saturation profile inside matrix block after 3600 days at system pressure of 1400 psia (at 79% oil recovery).

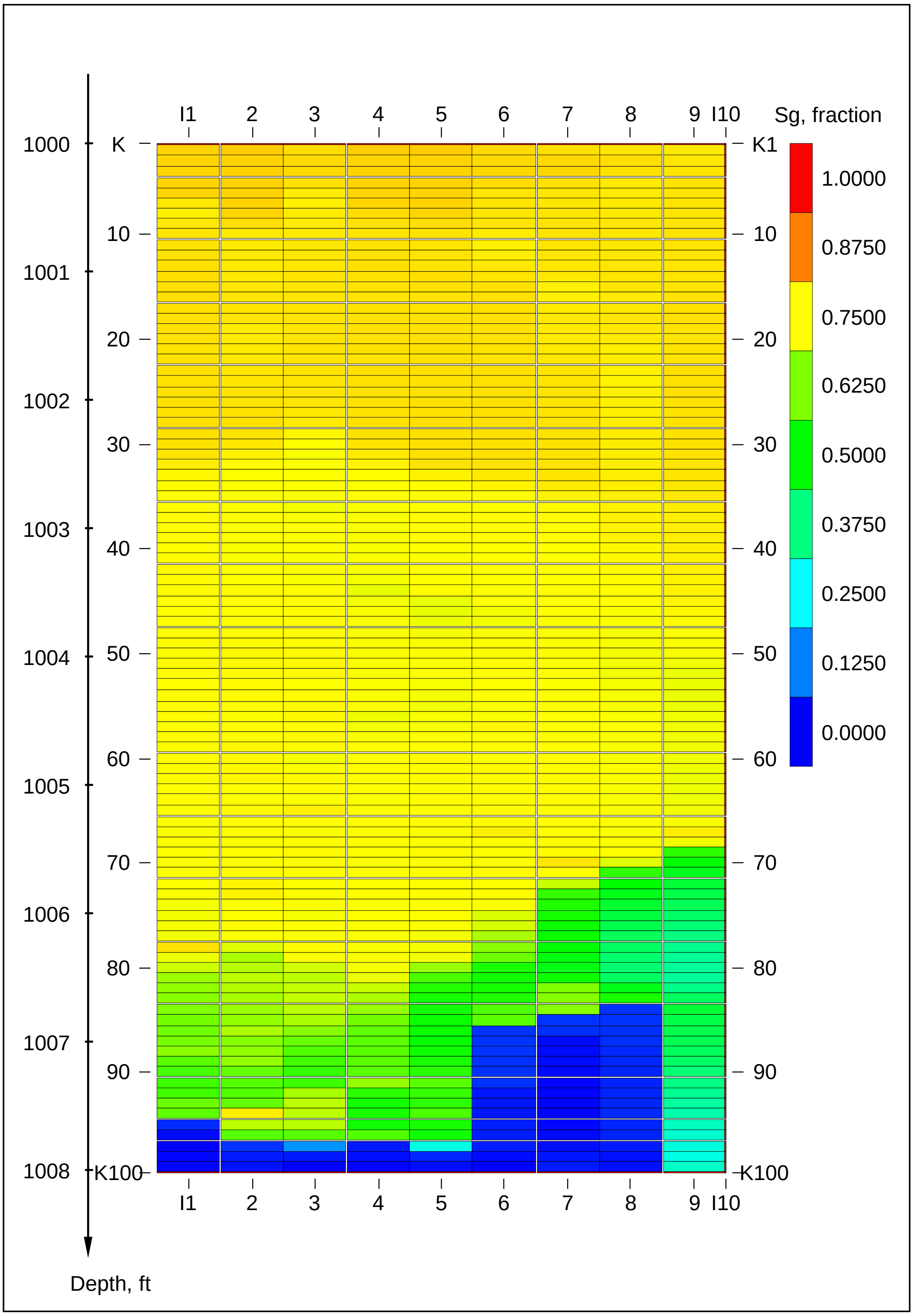

Figure 6.7 – Late stage CO$_2$ gas displacement, gas saturation profile inside matrix block after 7100 days at system pressure of 1400 psia (at 84% oil recovery).

As shown in **Fig. 6.8,** the extreme decrease in the gas/oil IFT near the displacement front results in a strong IFT and, consequently, capillary pressure gradient. Uleberg and Høier (2002) describe the resulting process, “This, combined with a relative small phase density difference near the miscible front, induces a Darcy flow of oil against gravity. As the oil flows upwards it contacts fresher and leaner gas and the intermediate and heavy components of the oil are more easily vaporized. The oil components that vaporize to the gas phase are then transported to the fracture system by: (1) injectant gas replacing the matrix block gas due to the density difference and (2) molecular diffusion due to the compositional difference between the gas in the fracture system and in the matrix block.”

“Oil is transported upwards by IFT induced Darcy flow even after the gas-oil front has reached the capillary entry height. This results in a shrinking of the oil zone at the bottom of the matrix block, and fracture gas more easily enters below the initial capillary entry height level. Eventually most of the original oil from the matrix block will be produced.”

“Increasing the system pressure makes the displacement process more miscible. The phase density differences are less and the IFT gradient near the miscible front is more pronounced, creating an even greater potential for the oil to flow upwards, and at higher rate.”

The capillary-driven mechanism transpires throughout the displacement (Periods 1, 2, a nd 3), though it is more pronounced in the late period of displacement, verified by a capillary/gravity ratio $R_{c/g}$=22.15.

In the early stage, displacement preferentially moves along the fracture side (Fig. 6.5) because there is fresh CO_2 available, with more oil vaporized and production to the fracture. The matrix-block grid cells in the vicinity of fracture have higher CO_2 concentrations. The IFT gradient at the displacement front is less toward the fracture (Fig. 6.8). For that reason, displacement is preferentially in the matrix block center during the late stage of recovery (Fig. 6.7).

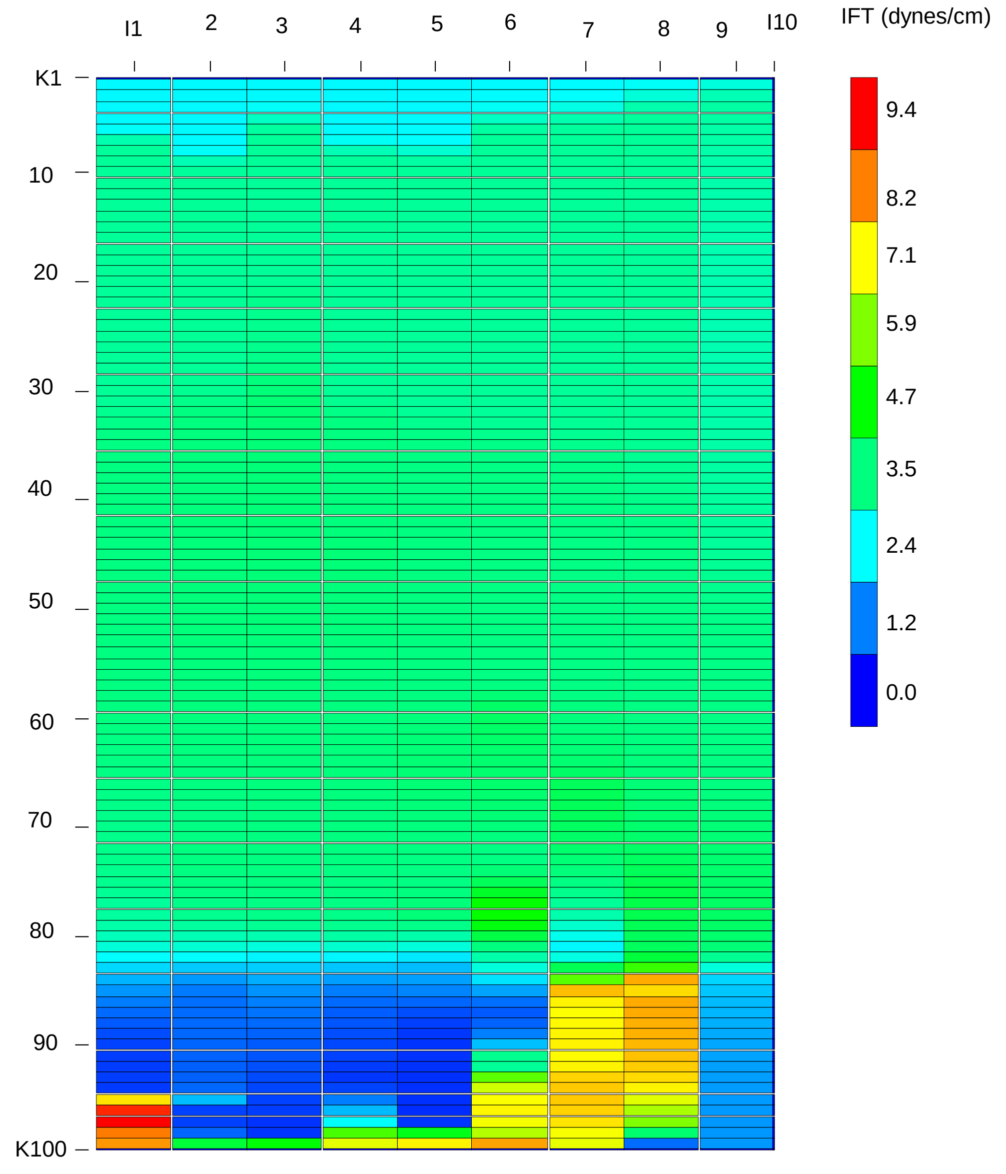

Figure 6.8 – Late stage CO$_2$ gas displacement, interfacial tension profile inside matrix block after 7100 days at system pressure of 1400 psia (at 84% oil recovery).

6.5.2.2 CO_2 Heavier Than Oil.

At early times, CO_2 dissolves into the oil phase and some lighter oil components vaporize into the CO_2-rich gas phase. This results in increasing oil and gas densities in the matrix block, with very-low density differences near the upward-moving front. As shown in **Fig. 6.9,** IFT decreases dramatically at the displacement front, from 3.8 to 0.06 mN/m implying that the process is near miscible (system pressure of 2500 psia is far above the thermodynamic MMP of 1350 psia[3]).

Before the upward-moving front reaches the top of the matrix block, three characteristic phases coexist in the matrix block. The original oil phase exists in the upper section of the matrix block, ahead of the front. Behind the front, a gas phase and an equilibrium oil phase exist, though the phase compositions vary significantly from the matrix bottom to the front.

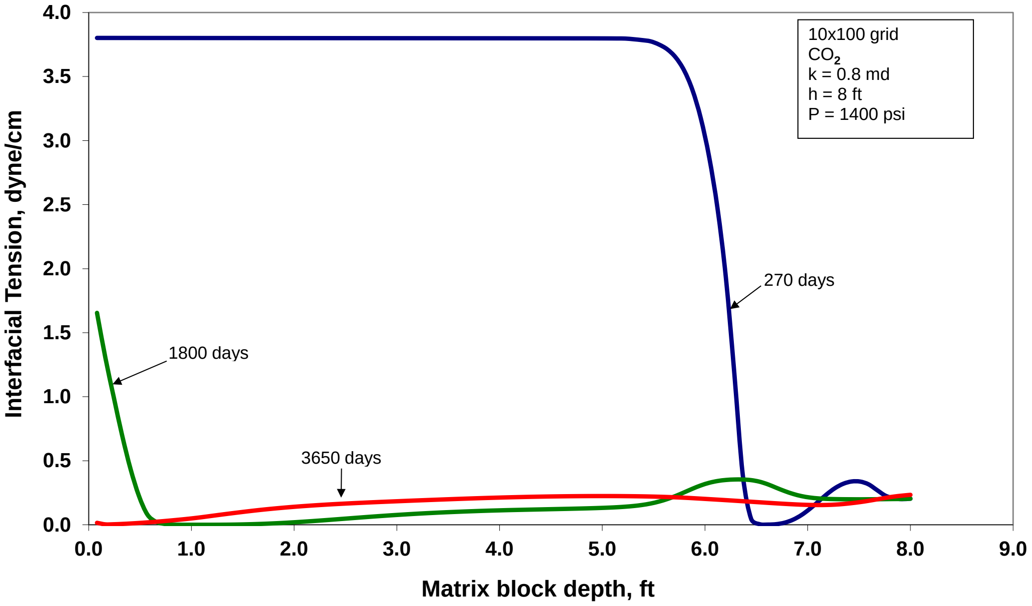

Figure 6.9 – IFT profile for single matrix block using CO_2 injection gas at system pressure of 2500 psia.

---

[3] We did not study the front's approach to miscibility as grid refinement is increased to large numbers and dispersivity is reduced toward zero (an assumption in the thermodynamic MMP).

The front moves upward as the frontal gas pushes original oil from the top of the matrix block, as seen in **Fig. 6.10.** Behind the front we find a complex flow mechanism where remaining oil eventually becomes heavier as it is vaporized by the gas. This oil starts flowing downward out the bottom of the matrix block, but at a low rate because of low mobility.

When the gas front reaches the top of the matrix block, CO_2 starts to enter from the top and the remaining oil is produced slowly from the bottom of the matrix block by gravity drainage; the remaining oil is denser than CO_2 but has low mobility.

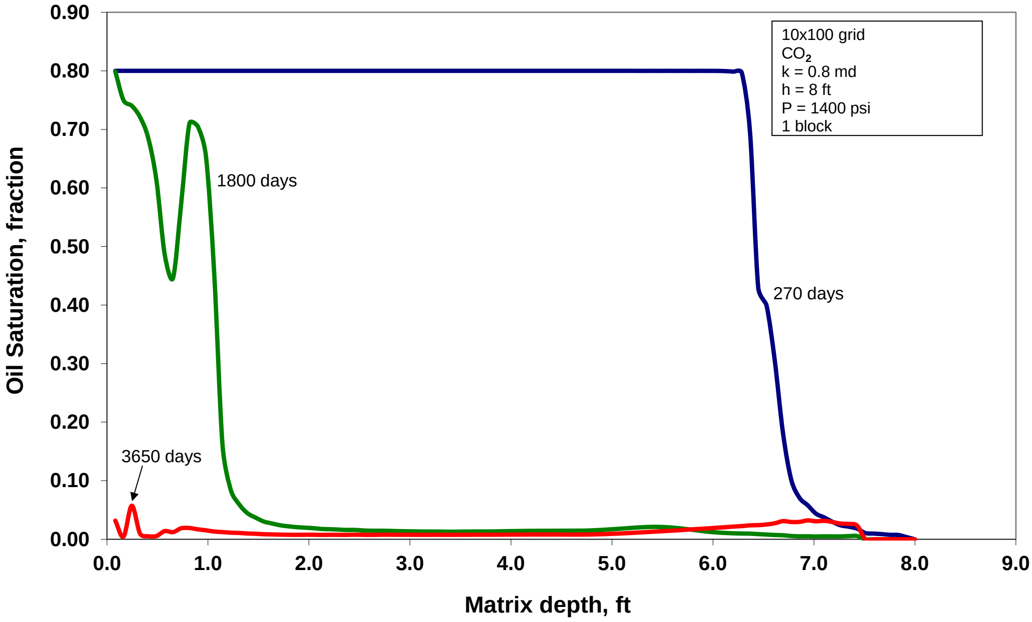

Figure 6.10 – Oil saturation profile for single matrix block using CO_2 injection gas at system pressure of 2500 psia.

6.6 Injection-Gas Effect

In this section, we study different injection gases for a single matrix block. We examine equilibrium-gas, dry-gas (C_1), and CO_2 injection at a system pressure of 1400 psia. Results are shown in Fig. 6.4. The CO_2 injection case has highest ultimate oil recovery (recovery at 10000 days), approximately 92%, while the equilibrium gas and dry gas have the same oil recovery of approximately 20%.

As mentioned earlier, 1,400 psia is the thermodynamic MMP for CO_2 with Haft Kel oil.

6.6.1 CO_2-Dilution Effect

Because the Haft Kel field has a large gas cap, injected gas may dilute with gas-cap equilibrium gas because of convective and diffusive flow in the fracture system. CO_2 concentration at a given fracture location in the reservoir will depend on many effects, including gravity segregation, gas/gas diffusion, gas-injection rate, matrix-block permeability, gas-cap size, and location of injector perforations. Fracture gas compositions surrounding matrix blocks may vary substantially, with associated impact on oil recovery.[4]

We studied several CO_2 mixtures—i.e., 50, 80, and 90 mol% CO_2 mixed with equilibrium gas at 1400 psia. As shown in **Fig. 6.11,** the ultimate oil recoveries for these three gases were 24.5, 34.5, and 52%, respectively. Reduced oil recoveries are related to increased gas/oil IFT and less-efficient condensing/vaporizing behavior near the displacement front (i.e., an increase in MMP) as CO_2 concentration decreased in the injection gas.

6.6.2 Tertiary Recovery by CO_2 Injection

Haft Kel dry-gas injection started in 1976. Dry-gas injection behaves very similar to equilibrium-gas injection, with similar recovery performance. Basically, the injected dry gas changes composition when it contacts reservoir oil, with a resulting gas composition that is very close to the incipient gas composition of the original oil. In this section, we present results from our study of recovery performance when CO_2 is injected following dry-gas injection.

Different concentrations of CO_2 were mixed with HC (equilibrium or dry) injection gas, the resulting mixture being injected into the fracture system following an initial period of HC-only gas injection. Two wells were used in

---

[4] We suspect that gravity segregation in the fracture system may segregate the injected CO_2 into a “blanket” of high-CO_2 gas on the top of the fracture oil column, with a HC gas floating on the CO_2 blanket.

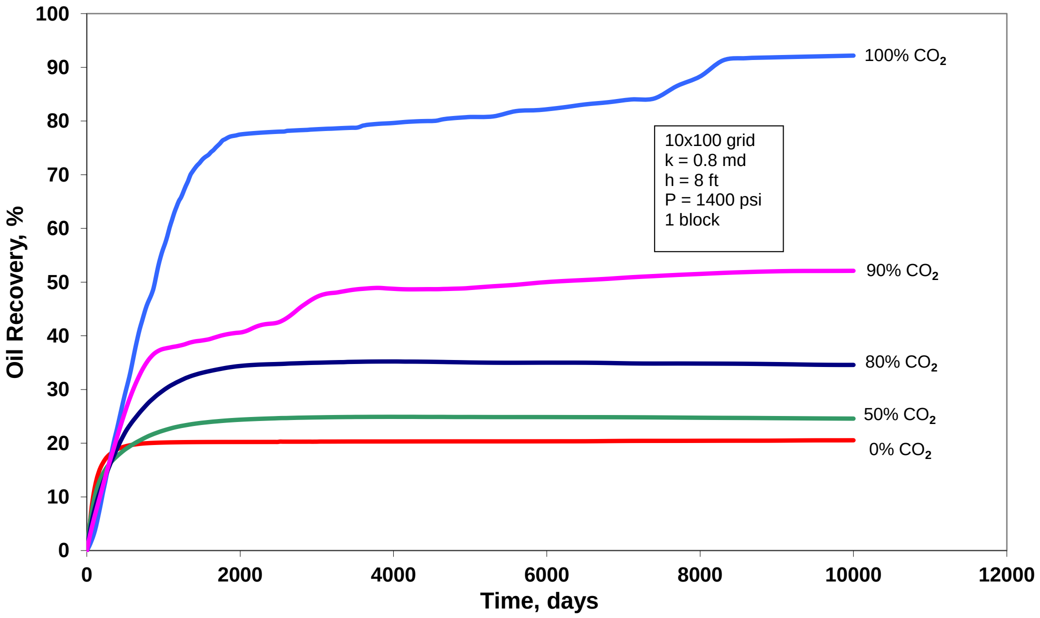

Figure 6.11 – Effect of CO_2 dilution on oil recovery vs. time for single matrix block at system pressure of 1400 psia.

these simulations, allowing injection-gas composition to change with time. The injection well was perforated in the top fracture, and the producer was perforated in the bottom fracture. The injection well was controlled by a constant bottomhole pressure, and the producer was controlled by constant gas-production rate of 0.353 Mscf/D.

Injection gases with 100, 90, 80, and 50 mol% CO_2 mixed with equilibrium gas at reservoir pressure of 1400 psia were injected after first injecting equilibrium gas only into the matrix block. Equilibrium gas was injected for 1500 days to ensure that the equilibrium-gas displacement was complete. This was followed by injection with a CO_2-rich gas. Results are given in **Fig. 6.12.** The ultimate oil recoveries for 100 (pure), 90, 80, and 50 mol% CO_2 mixtures were 93, 51, 36, and 26%, respectively.

These ultimate oil recoveries are close to those found where CO_2-rich gases were injected without first injecting equilibrium HC gas. However, the recovery mechanism is slightly different. First, oil recovery drops as a result of CO_2

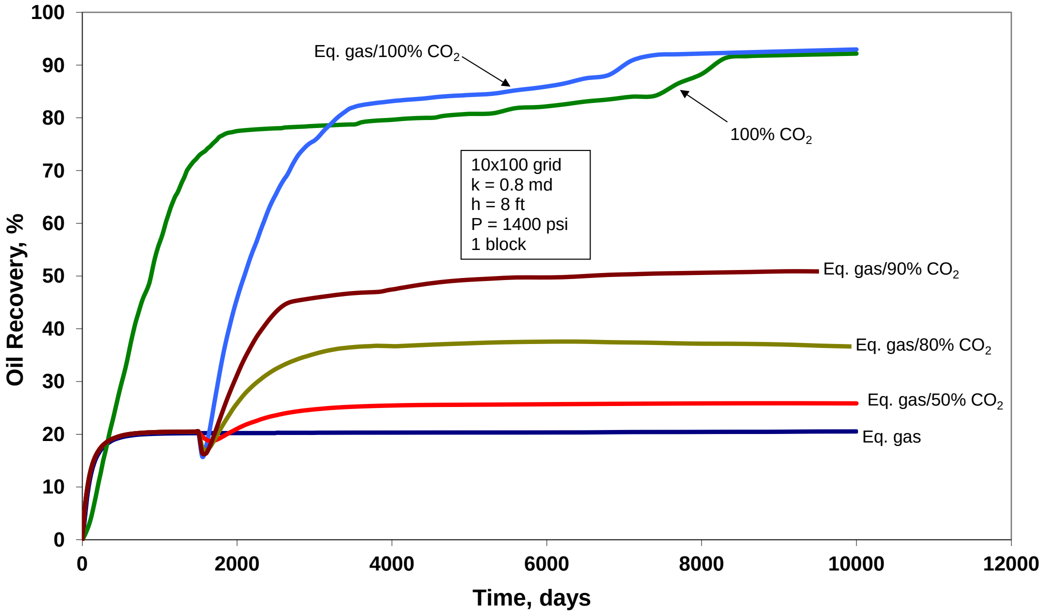

Figure 6.12 – Effect of injection gas, inject different concentration of CO_2 after equilibrium and Methane injection on oil recovery vs. time for single matrix block at system pressure of 1400 psia.

swelling in the matrix block with associated oil-saturation increase, leading to lower oil recovery, based on Eq. (3.2). Second, the injected CO_2 gas at 1400 psia is lighter than oil but heavier than the initial HC gas in the matrix block. Consequently the CO_2-rich gas cannot enter from the top or from the bottom of matrix block. Instead, it enters from the side of the matrix block by exchanging composition with gas in the matrix. The front for CO_2 mixed with matrix-block gas moves in both horizontal and vertical directions. After CO_2 enters into the matrix block, gravity/capillary drainage becomes strong and oil produces from the bottom of the matrix block.

6.6.3 Reservoir-Pressure Effect

The effect of reservoir pressure on oil recovery for equilibrium gas, CO_2, and different mixtures of CO_2 and equilibrium injection gas is studied in this section. Different models are used, with the system pressure of 1000, 1400, 2000, 2500, and 3000 psia. The equilibrium-gas models use 10×50 ($N_x \times N_z$) grid cells; for each pressure, the matrix block is initialized with saturated oil and the fracture is initialized with equilibrium gas. CO_2-injection models contain 10×100 grid cells, and for each pressure case, the matrix block is initialized with saturated oil and the fracture is initialized with CO_2.

For the equilibrium-gas cases, gas/oil IFT decreases with increasing reservoir pressure. As a result, the capillary entry height is lowered and ultimate oil recovery increases. As shown in **Fig. 6.13,** oil recovery increases from 14% at 1000 psia to 50% at 3,000 psia, corresponding to a change in gas/oil IFT from 13.55 to 2.24 mN/m.

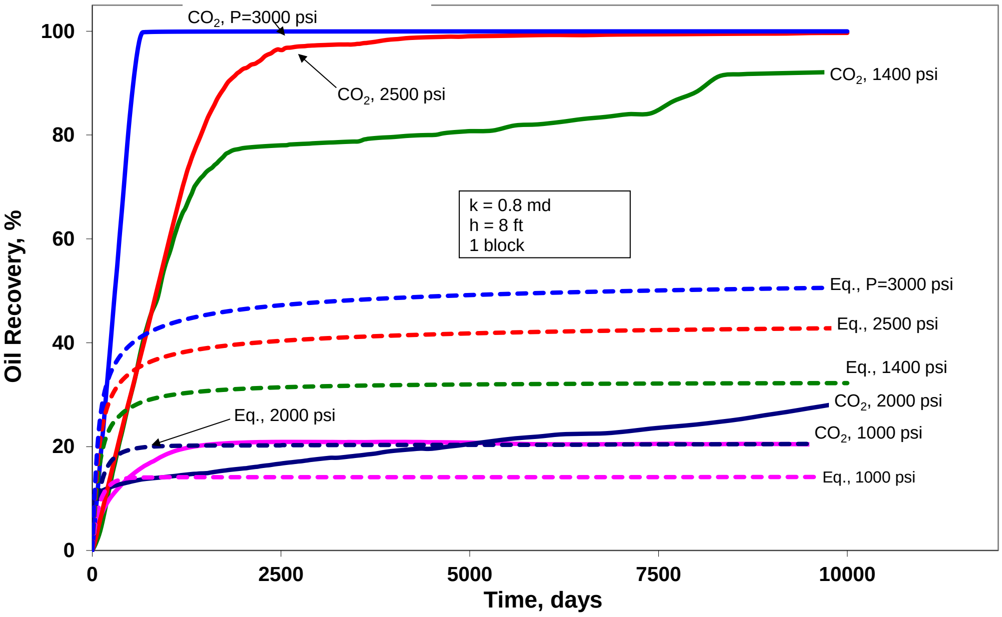

Figure 6.13 – Effect of reservoir pressure on oil recovery vs. time for single matrix block system using equilibrium gas (dash line) and CO_2 (solid line) injection.

For CO_2 injection, we find that oil recovery generally increases with reservoir pressure, reaching nearly 100% near the thermodynamic MMP of 1400 psia. A significant anomaly is seen at 2000 psia, where recovery is less than 30% after 10000 days (when all other runs had essentially reached ultimate recovery), as seen in Fig. 6.13. CO_2 and oil densities are approximately equal at 2000 psia, as shown in Fig. 6.3, and consequently gravity drainage is slowed radically.

Mixtures of CO_2 and equilibrium gas at 2000 psia show higher oil recovery than pure CO_2 **(Fig. 6.14)** because gas/oil density differences are higher than for pure CO_2. Fig. 6.14 shows that oil recovery rises toward 100% as the thermodynamic MMP is approached. MMP increases with decreasing CO_2 content in the injection gas, and the RF-pressure trend toward near-100% recovery becomes less steep.

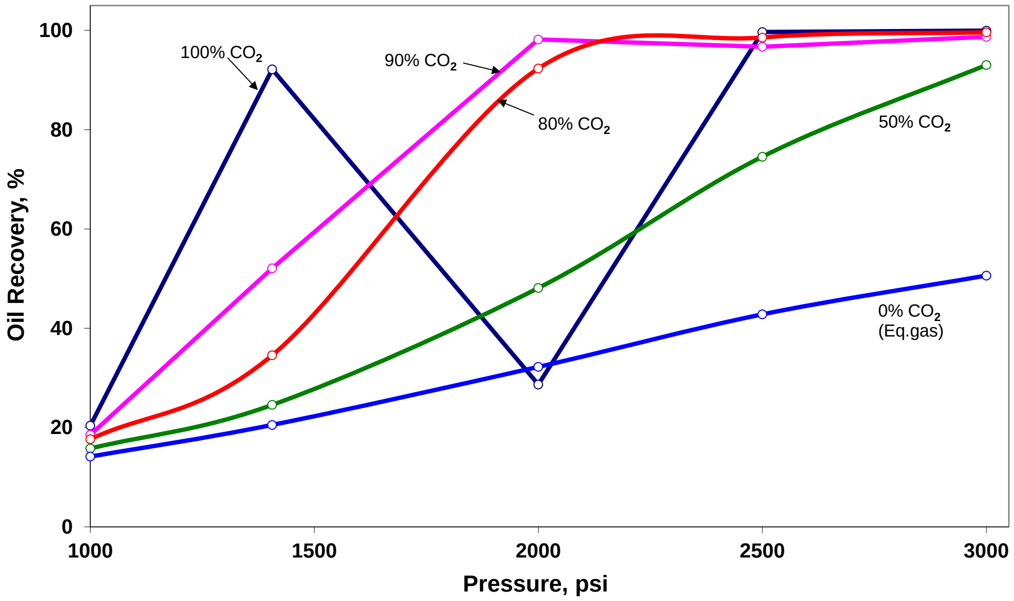

Figure 6.14 – Comparison of CO_2 injection gas with equilibrium gas oil recovery at 10000 days vs. reservoir pressure for Single matrix block system.

6.7 Matrix-Block Height Effect

The matrix-block height is a critical parameter for gas injection in fractured reservoirs. If the matrix-block height is smaller than the initial capillary entry height, no gas can enter (unless by diffusion).

Haft Kel block size varies from 6 to 14 ft, as reported by Saidi (1996). We considered four matrix-block heights—6, 8, 10, and 14 ft—to study the effect of matrix-block height on oil-recovery performance for equilibrium gas (dashed line) and CO_2 (solid line), as shown in **Fig. 6.15.**

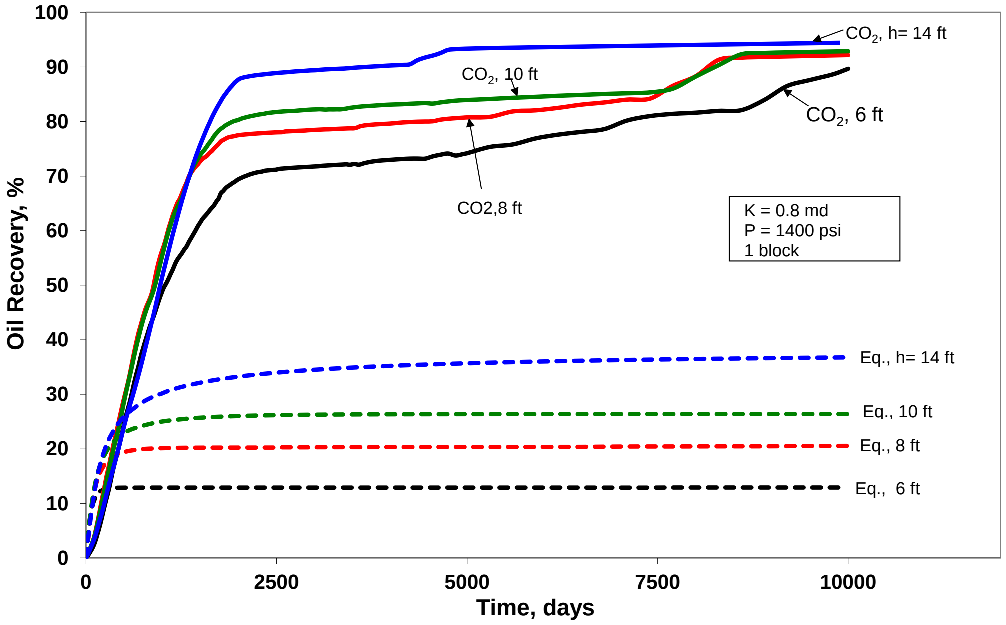

Figure 6.15 – Effect of matrix block height on oil recovery vs. time for single matrix block using equilibrium (dash line) and CO$_2$ (solid line) injection gas at system pressure of 1400 psia.

When equilibrium gas is injected, the ultimate oil recovery increases significantly with increasing stack height for small matrix blocks close to the capillary entry height. The ultimate recovery approaches an asymptotic value given by the saturation endpoints, S_{org} and S_{wc}, and the effect of matrix-block height on the final recovery is not significant for very tall matrix stack heights. The stack height does not have a strong effect on the oil-production rate, meaning that the time to reach a given recovery increases with stack height (because of changes of amount of fluids in place). Previous studies (Saidi 1996; Behbahani *et al.* 1996) on Haft Kel field pointed out that the oil recovery by immiscible HC gas varies between 15 and 32%. As seen in Fig. 6.15, the lowest and highest oil recoveries are 12.9 and 36.7% for 6- and 14-ft matrix blocks, respectively.

For CO$_2$ injection, the ultimate oil recovery is approximately the same for all stack heights. First, the capillary entry height in CO$_2$ injection is lower than the capillary entry height of equilibrium-gas injection, caused by low IFT in a developed condensing/vaporizing near-miscible process. Furthermore, the oil below capillary entry height is produced by the dynamic gravity/capillary-drive mechanism, as described by Uleberg and Hoier (2002). Ultimate recovery from this mechanism is not greatly affected by matrix-block height, as shown in Fig. 6.15.

6.8 Matrix-Block-Permeability Effect

The matrix permeability controls the rate of recovery from a matrix block, and the ratio between the matrix and fracture permeability determines if viscous displacement (Darcy flow by pressure gradients) is important or not. If injection fluid mainly flows in the fracture, then viscous force is negligible in low-permeability matrix block. Matthai and Belayneh (2004) studied the effects of matrix/fracture permeability ratio on fracture/matrix flow partitioning, and their results indicate that at a ratio of fracture permeability to matrix permeability of 10^4 and lower, viscous force becomes important. Porosity and capillary pressure are assumed to be constant in all cases.

In Haft Kel, matrix-block permeability varies from 1 to 0.05 md. For equilibrium-gas injection, the rate of oil recovery increases with increasing matrix-block permeability, but ultimate oil recovery is the same, as shown in **Fig. 6.16.** As shown in Fig. 6.16, CO_2 has the same effect but it is more pronounced because the rate of oil recovery in CO_2 injection is slower than the rate of oil recovery for equilibrium-gas injection.

Interestingly, there is a linear relationship between the time to reach a given oil recovery and the matrix permeability, when plotted on log-log paper. This is seen in **Fig. 6.17,** where the times to reach specific recoveries of 10, 15, and 20% are considered. The lines have the same slope for both equilibrium gas and CO_2. Fig. 6.17 is useful to find the time to reach a given oil recovery for a wide range of matrix-block permeabilities.

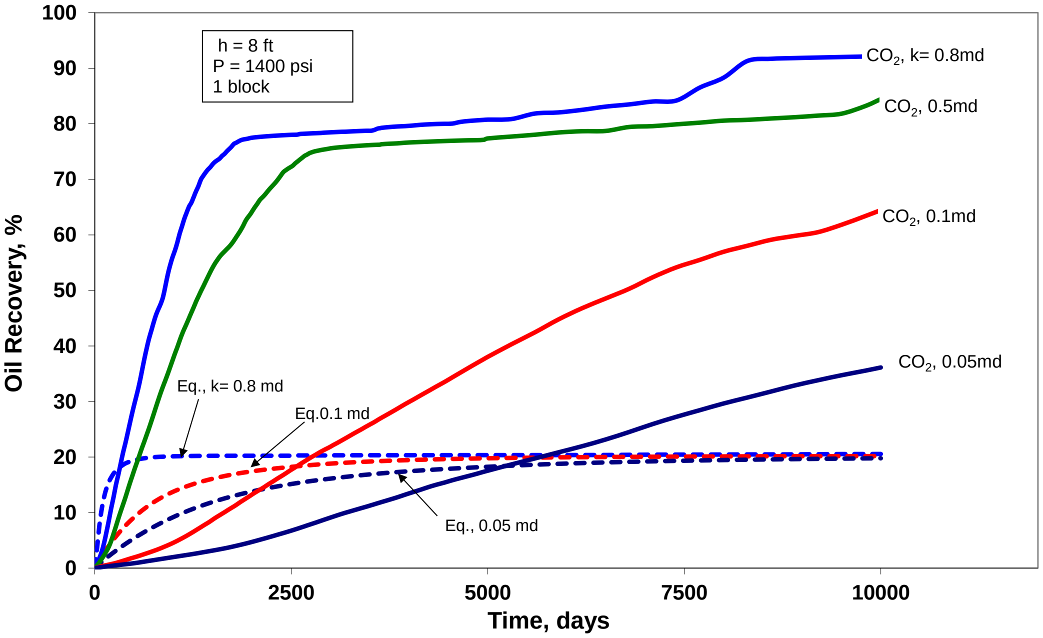

Figure 6.16 – Effect of matrix block permeability on oil recovery vs. time for single matrix block using equilibrium (dash line) and CO_2 (solid line) injection gas at system pressure of 1400 psia.

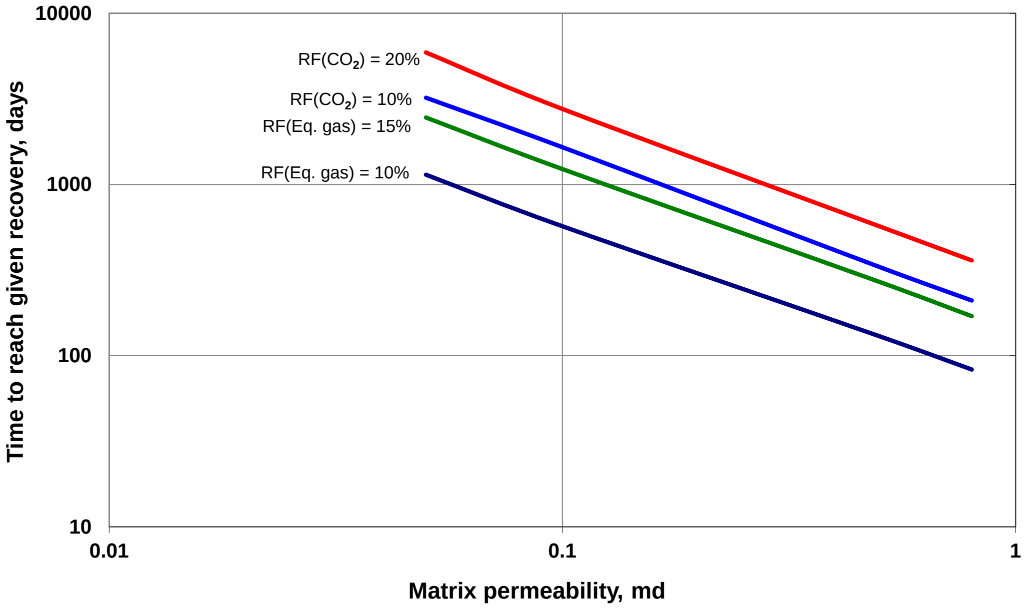

Figure 6.17 – Time of reaching certain oil recovery vs. Matrix block permeability for single matrix block using equilibrium and CO_2 injection gas at system pressure of 1400 psia.

6.9 Block-to-Block Interaction

Oil produced from one matrix block may flow into an underlying matrix block. Oil reinfiltration may result from physical contact between the blocks (permeable contact points) or by oil produced from one block entering another block because of gravity/capillary interaction, liquid bridges, or film flow. We studied the effect of vertical block-to-block interaction using taller effective matrix-block heights.

In our model, the matrix blocks are 8 ft in height, and are separated by horizontal fractures. The top, bottom, and side fractures are defined with a large PV to provide the gas needed to inject and to eliminate injection and production wells. Thin horizontal fractures were gridded to represent the connection of one matrix block with another.

For equilibrium gas we studied 1, 5, 10, 20, and 40 stacked matrix blocks using 3×1×25 grid cells for each matrix block. **Fig. 6.18** illustrates the total oil recoveries for different stacked matrix blocks. Total oil recovery is the arithmetic average of oil recovery for all matrix blocks. This figure shows significant delay of oil production because of oil reinfiltration.

Another series of stacked matrix blocks were studied to compare CO_2 injection with equilibrium gas. The CO_2-injection cases have higher total oil recoveries than equilibrium-gas cases, as shown in **Fig. 6.19.** Fig. 6.19 shows that the shape of oil recovery for stacked blocks does not include the final stage of single-block oil recovery in which the extra oil is recovered exclusively by the dynamic gravity/capillary mechanism.

The cases shown here represent 100% reinfiltration. It is likely that the degree of reinfiltration is less in the field. Many factors can reduce block-to-block flow significantly, such as interbedded layers of nonfractured impermeable rock (shales and mineral-filled fractures), sloped fractures, and viscous forces.

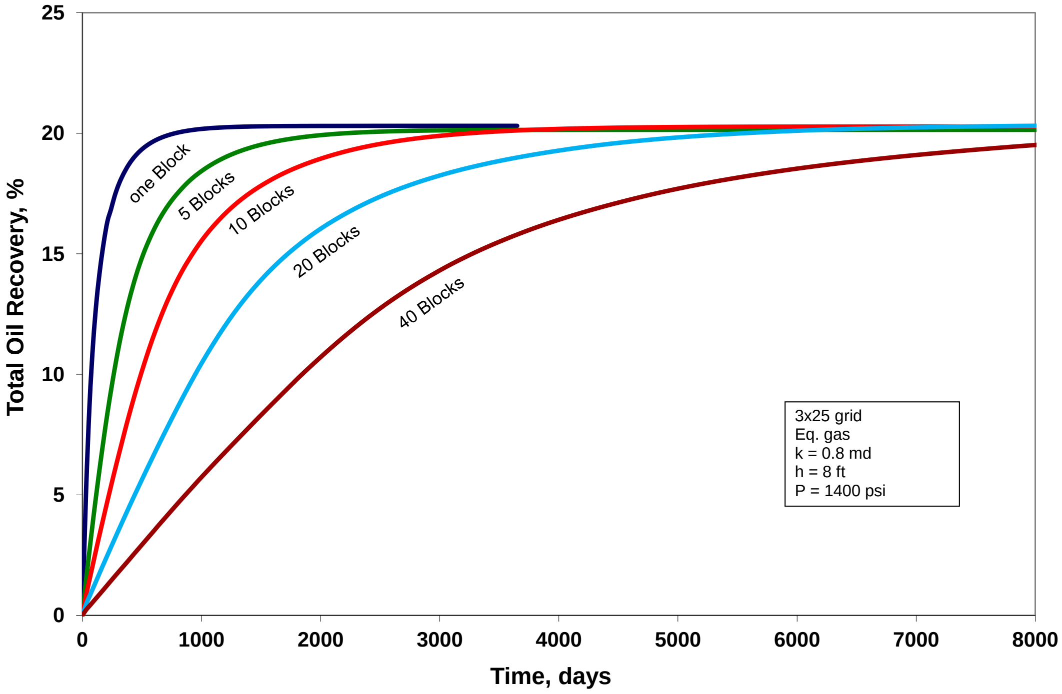

Figure 6.18 – Total oil recovery vs. time for different number of stacked matrix blocks using equilibrium gas injection at system pressure of 1400 psia.

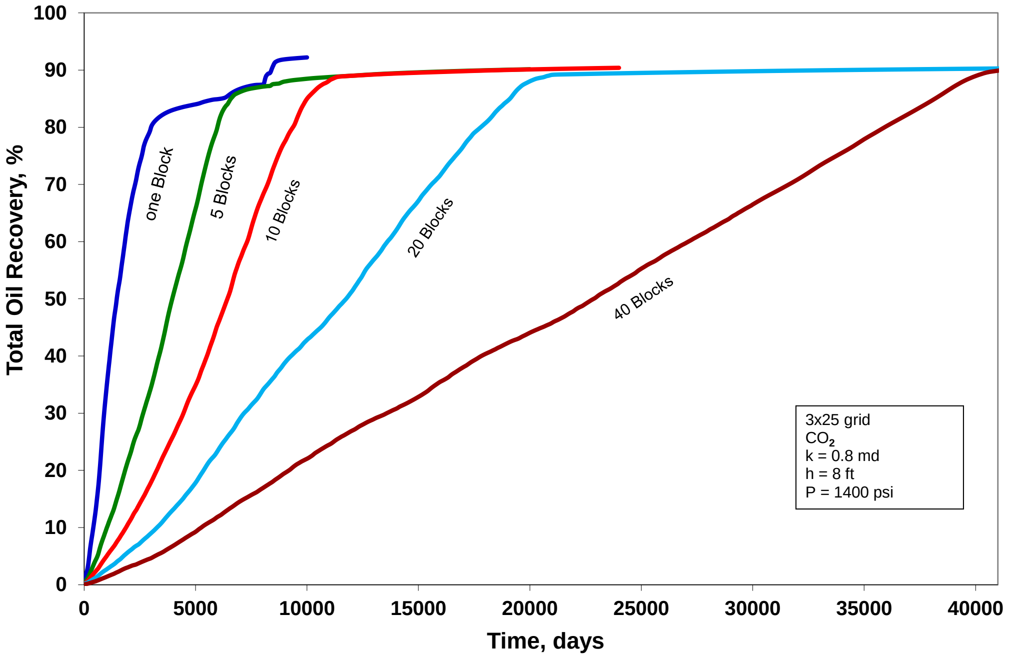

Figure 6.19 – Total oil recovery vs. time for different number of stacked matrix blocks using CO_2 gas injection at system pressure of 1400 psia.

6.10 Conclusions

Oil-recovery performance was quantified for the Haft Kel oil system using compositional modeling of a matrix block surrounded by a gas-filled fracture. Simulations were performed for a wide range of petrophysical properties, matrix-block sizes, injection gas, varying initial conditions of pressure, and saturation pressure.

Some of the most interesting observations and conclusions concerned CO_2 injection include:

1. Grid refinement is needed for accurate modeling of nonequilibrium gas injection because of a complex gravity/capillary recovery mechanism with significant IFT and capillary pressure gradients.
2. CO_2 is heavier than the Haft Kel oil at pressures greater than 2,050 psia. When CO_2 gas is lighter than oil, CO_2 gas enters from the top of the matrix block and drains oil downward, as found with all other injection gases.
3. When pure CO_2 is heavier than the reservoir oil, CO_2 gas initially enters from the bottom of the matrix block. Unusual saturation gradients develop, with near-initial oil saturation at the top of the matrix block remaining until the upward-moving gas front reaches the top. Gradually, the oil at the bottom of the matrix becomes heavier than its equilibrium HC/CO_2 matrix gas mixture, resulting in “normal” gravity segregation.
4. Despite high ultimate oil recovery with CO_2, the process is slow (compared with nonequilibrium HC gases) and particularly when the CO_2-gas and reservoir-oil densities are similar.
5. Ultimate oil recovery increases with increasing reservoir pressure and CO_2 concentration in injection gas.
6. CO_2 injection in Haft Kel field can lead to significant additional oil production, even after dry-gas injection.

6.11 References

Behbahani, H.S.-Z., Kharrat, R., and Vossoughi S. 1996. Case History of a Unique Gas Injection Scheme and its Simulation Using Material Balance Based Simulator. Paper SPE 35631 presented at the SPE Gas Technology Conference, Calgary, 28 April–1 May. doi: 10.2118/35631-MS.

Coats Engineering: ***SENSOR***, www.coatsengineering.com.

Løvoll, G., Meheust, Y., Måløy, K. L., Aker, E., and Schmittbuhl, J. 2005. Competition of gravity, capillary and viscous forces during drainage in a two-dimensional porous medium, a pore scale study. Energy **30** (6): 861–872. doi:10.1016/j.energy.2004.03.100.

Matthai, S.K. and Belayneh, M. 2004. Fluid flow partitioning between fractures and a permeable rock matrix. Geophys. Res. Lett. **31:** L07602. doi:10.1029/2003GL019027.

Ringen, J.K., Haugse, V., Høier, L., Berge, L.I., and Reed, J. 2005. Experimental and Numerical Studies of Gas Injection in Fractured Carbonates: Pressure and Compositional Effects. Paper presented at the 2005 International Symposium of Society of Core Analysts, Toronto, Canada, 21–25 August.

Saidi, A.M. 1987. Reservoir Engineering of Fractured Reservoirs: Fundamental and Practical Aspects, 764–770. Paris: TOTAL Edition Press.

Saidi, A.M. 1996. Twenty Years of Gas Injection History into Well-Fractured Haft Kel Field (Iran). Paper SPE 35309 presented at the International Petroleum Conference and Exhibition of Mexico, Villahermosa, Mexico, 5–7 March. doi: 10.2118/35309-MS.

Stalkup, F.I. Jr. 1983. Miscible Displacement. Henry L. Doherty Monograph Series, SPE, Richardson, Texas, USA **8**.

Uleberg, K. and Høier, L. 2002. Miscible Gas Injection in Fractured Reservoirs. Paper SPE 75136 presented at the SPE/DOE Improved Oil Recovery Symposium, Tulsa, 13–17 April. doi: 10.2118/75136-MS.

Wylie, P.L. and Mohanty, K.K. 1999. Effect of Wettability on Oil Recovery by Near-Miscible Gas Injection. SPE Res Eval & Eng **2** (6): 558–564. SPE-59476-PA. doi: 10.2118/59476-PA.

Zick Technologies: ***PhazeComp***. www.zicktech.com.

Chapter 7

CO_2 Injection in Naturally Fractured Reservoirs – Lab and Field Modeling Studies with Diffusion

7.1 Introduction

Based on detailed compositional simulations of matrix/fracture systems, we study the effect of molecular diffusion on oil recovery by CO_2 injection for small-scale laboratory experiments and field-scale systems. We consider reservoir conditions that lead to a range of recovery mechanisms from immiscible to near-miscible.

Laboratory experimentation is a useful approach to understand the recovery mechanism of CO_2 injection in fractured oil reservoirs because an unusual combination of complex physical phenomena exists. A fundamental problem with this approach is scaling the results to field conditions, and particularly matrix block size which is often many (5-100) times larger than laboratory cores. Diffusion is clearly affected by matrix block dimensions, and any effect of diffusion on the recovery mechanism will be scale dependent. In this chapter we provide guidelines and computational examples of laboratory tests to study CO_2 recovery processes, including diffusion. We also study the change in recovery processes as matrix/fracture dimensions approach field scale.

We recommend using reservoir core or outcrop samples similar to reservoir rock, with dimensions (5-25 in^2 horizontal area and 10-30 in high). A synthetic model oil can be constructed to mimic PVT properties of the actual reservoir oil, and in particular the minimum miscibility pressure (MMP) as defined by a traditional 1D multi-contact displacement process – MMP_{1D}, reduced gas-oil interfacial tensions (IFT) and oil-gas density differences. The core should be placed in a container with annular space representing the fracture. CO_2 is injected at various rates into the annular space at relevant reservoir pressures, both above and below the MMP_{1D}.

In this work, the effect of several key parameters will be studied – matrix permeability, matrix block size, CO_2 injection rate and reservoir pressure. One of the key results is the effect of diffusion on oil recovery, and how it varies with matrix block size and CO_2 injection rate.

7.2 Description of Matrix/Fracture Models

7.2.1 Haft Kel Field-Scale Model

For the Haft Kel field-scale matrix/fracture system, a single matrix block surrounded by fractures was used to study compositional mass exchange and recovery mechanisms. Significant compositional variations develop within the matrix block, resulting in high recoveries (chapter 6).

Haft Kel petrophysical properties and initial fluid compositions are taken from Saidi (1987). The matrix is represented by an 8-ft cube with 0.8 md isotropic permeability and default fracture width of 0.01 ft (0.30 cm) having 100 D permeability. Due to the matrix block symmetry, only half of the matrix block is modeled. A 2D Cartesian grid is used where the matrix block is surrounded by two horizontal fractures on the top and bottom and one vertical fracture on the right side of the matrix block.

The matrix block is initially filled with oil and the fractures are initialized with injection gas. Zero capillary pressure and high permeability of the fractures means that viscous forces are negligible compared to gravity and capillary forces in the matrix. Injection rate was investigated using production and gas injection wells at the bottom and top fracture, respectively. The production well is pressure controlled and the injection well is rate controlled. Conceptually we are looking at a matrix block located at the no-flow boundary between an injector and a producer where lateral pressure gradients are negligible. All models use an 11x1x102 (N_x N_y N_z) grid where the I=1-10 and K=2-101 grid cells represent a half matrix block.

Eclipse 300 is used for all simulations. An 11-component tuned SRK (Soave-Redlich-Kwong) equation of state (EOS) describes phase and volumetric behavior; the Lorenz-Bray-Clark correlation, tuned to viscosity data, is used to calculate viscosities. EOS component properties and binary interaction parameters (BIPs) are given in Tables 6.2 and 6.3 Unfortunately, CO_2-oil PVT data were not available to tune the EOS model, thereby making CO_2-oil phase behavior predictions somewhat uncertain.

7.2.2 Laboratory Model.

For the laboratory test simulations, a 2D Cartesian grid is used, where the core is surrounded by horizontal fractures on the top and bottom, and one vertical fracture on the right side of the core. Fine gridding is needed for CO_2 injection (chapter 6). The core has a square 0.2x0.2-ft top and bottom surface shape with a total core height of 2 ft (60.96 cm). Core permeability was 0.8 md and porosity was 10%.

A simple, synthetic oil consisting of methane (C_1) and normal pentane (n-C_5) was used, this synthetic oil having similar MMP_{1D} as the Haft Kel reservoir oil, about 1400 psia. EOS component properties and BIPs of the synthetic oil are given in **Tables 7.1** and **7.2**.

Table 7.1 – Fluid Properties for The 3 Component SRK Characterization

Component	MW	Tc, °R	Pc, psia	ω	Vshift	Zc	Parachor
CO2	44.01	547.42	1069.51	0.225	0.217	0.27433	80.00
C1	16.04	343.01	667.03	0.011	-0.002	0.2862	71.00
n-C5	70.91	846.25	503.20	0.229	0.119	0.27119	205.17

Table 7.2 – Binary Interaction Coefficients for The 3 Component SRK Characterization

	CO2	C1	n-C5
CO2	-		
C1	0.1200	-	
n-C5	0.1500	0.0000	-

Capillary pressure and relative permeability of the Haft Kel and lab models are similar, taken from Saidi (1987). Laboratory capillary pressures were scaled with gas-oil IFT by Eq. (2.24) where the gas-oil laboratory IFT, equal to 10 mN/m. Relative permeabilies were not scaled with IFT.

Oil and gas effective diffusion coefficients are given in **Table 7.3** and **7.4**. Gas diffusion coefficients were determined from equilibrium gas at bubble point pressure. More details of diffusion coefficient calculation are given in section (2.2). Liquid density of C_1-n-C_5 mixture was 427.91 kg/m^3 at 1500 psia which led to the liquid diffusion coefficients in Table 7.3. Pressure and composition dependency of diffusion coefficients was not considered.

Table 7.3 – Oil Composition for The 3 Component EOS at Different Saturation Pressures and Diffusion Coefficients

Component	1000 psia			1250 psia			1500 psia		
	X_i mole fr.	D_{io} cm^2/s	D_{ig} cm^2/s	X_i mole fr.	D_{io} cm^2/s	D_{ig} cm^2/s	X_i mole fr.	D_{io} cm^2/s	D_{ig} cm^2/s
CO2	0.0000	1.54E-05	2.25E-04	0.0000	1.65E-05	1.75E-04	0.0000	1.81E-05	1.39E-04
C1	0.2735	1.99E-05	2.92E-04	0.3419	2.01E-05	1.13E-04	0.4099	2.07E-05	9.03E-05
n-C5	0.7265	1.99E-05	2.92E-04	0.6581	2.01E-05	1.13E-04	0.5901	2.07E-05	9.03E-05
Texp= 185 °F									

Table 7.4 – Oil Composition for The 11 Component EOS at Different Saturation Pressures and Diffusion Coefficients

Component	1000 psia			1250 psia			1500 psia		
	X_i mole fr.	D_{ig} cm^2/s	D_{io} cm^2/s	X_i mole fr.	D_{ig} cm^2/s	D_{io} cm^2/s	X_i mole fr.	D_{ig} cm^2/s	D_{io} cm^2/s
N2	0.0004	2.34E-03	3.63E-05	0.0009	1.84E-03	3.42E-05	0.0011	1.49E-03	3.26E-05
CO2	0.0039	1.72E-03	2.44E-05	0.0043	1.35E-03	2.31E-05	0.0043	1.09E-03	2.20E-05
H2S	0.0133	1.70E-03	2.49E-05	0.0130	1.33E-03	2.36E-05	0.0128	1.08E-03	2.25E-05
C1	0.2211	1.57E-03	3.42E-05	0.2957	1.22E-03	3.10E-05	0.3113	9.90E-04	2.83E-05
C2	0.0494	1.62E-03	2.46E-05	0.0497	1.27E-03	2.32E-05	0.0496	1.03E-03	2.21E-05
C3	0.0542	1.28E-03	1.87E-05	0.0506	1.00E-03	1.77E-05	0.0499	8.14E-04	1.69E-05
C4-C6	0.1428	9.77E-04	1.34E-05	0.1282	7.65E-04	1.28E-05	0.1251	6.23E-04	1.23E-05
C7-C14	0.3761	6.57E-04	1.07E-05	0.3343	5.15E-04	1.04E-05	0.3257	4.20E-04	1.01E-05
C15-C21	0.0998	4.60E-04	6.82E-06	0.0887	3.60E-04	6.48E-06	0.0864	2.93E-04	6.20E-06
C22-C29	0.0299	3.69E-04	5.17E-06	0.0266	2.89E-04	4.90E-06	0.0259	2.35E-04	4.68E-06
C30+	0.0092	3.00E-04	4.13E-06	0.0082	2.35E-04	3.91E-06	0.0079	1.92E-04	3.74E-06
Tres= 110 ^oF									

Oil recovery factor (RF) is calculated from total average oil saturation S_o in the matrix block using Eq. (3.2).

7.3 CO_2 Displacement Mechanism

In this section we discuss the recovery performance for the laboratory system and for the Haft Kel single matrix block.

7.3.1 Lab Test Recovery Performance

System pressure was 1000 psia (68.95 bara) and CO_2 injection rate was 0.5 cm^3/hr. Models were run with and without diffusion. **Fig. 7.1** shows that 100% of the synthetic oil is recovered after 3 days when diffusion is included. Neglecting diffusion reduces recovery to only 12.2 % after 10 days, and leads to a laterally-uniform displacement with final recovery controlled by the vertical balance of capillary and gravity forces. **Fig. 7.2** shows an oil saturation map at 1 day (60% recovery) for the 1000 psia model run with synthetic oil using diffusion. The oil saturation is spatially non-uniform, caused by CO_2 entry into the matrix through a complex process controlled by capillary-gravity drainage and diffusion.

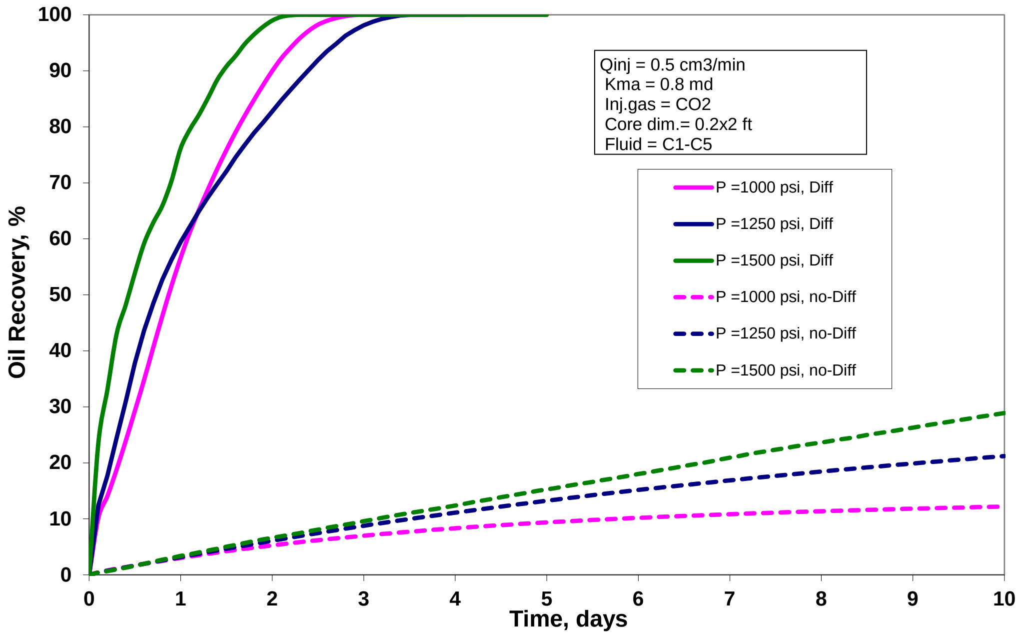

Figure 7.1 – Effect of reservoir pressure on oil recovery vs. time for C_1-C_5 lab system using CO_2 injection with (solid lines) and without diffusion (dash lines).

Fig. 7.3 shows oil recovery performance including diffusion for a lab core saturated with Haft Kel oil[1]. The oil recovery and rate of recovery are significantly lower than the synthetic-oil core test. Because of relatively small core dimensions, an important component of oil recovery in laboratory tests will be the *vaporizing-diffusion mechanism (VDM)*. Where gas saturation has been established in the core, CO_2 vaporizes the oil components which are then transported out of the core by diffusion, as fresh CO_2 enters the fracture. The VDM is dominant for synthetic oil systems, but less efficient for real oils which have a large range of heavier components that (a) vaporize less (with lower equilibrium K-values) and (b) diffuse slower in the gas phase, with decreasing efficiency as a function of molecular weight.

The oil saturation profile in **Fig. 7.4** shows a saturation map at 16 days (17% recovery) for the 1000 psia lab test model with Haft Kel oil. The *capillary-*

---

[1] All Haft Kel fluid in lab-test models were run with diffusion, because in the models without diffusion capillary threshold height is larger than the core height and CO_2 will not enter into the core.

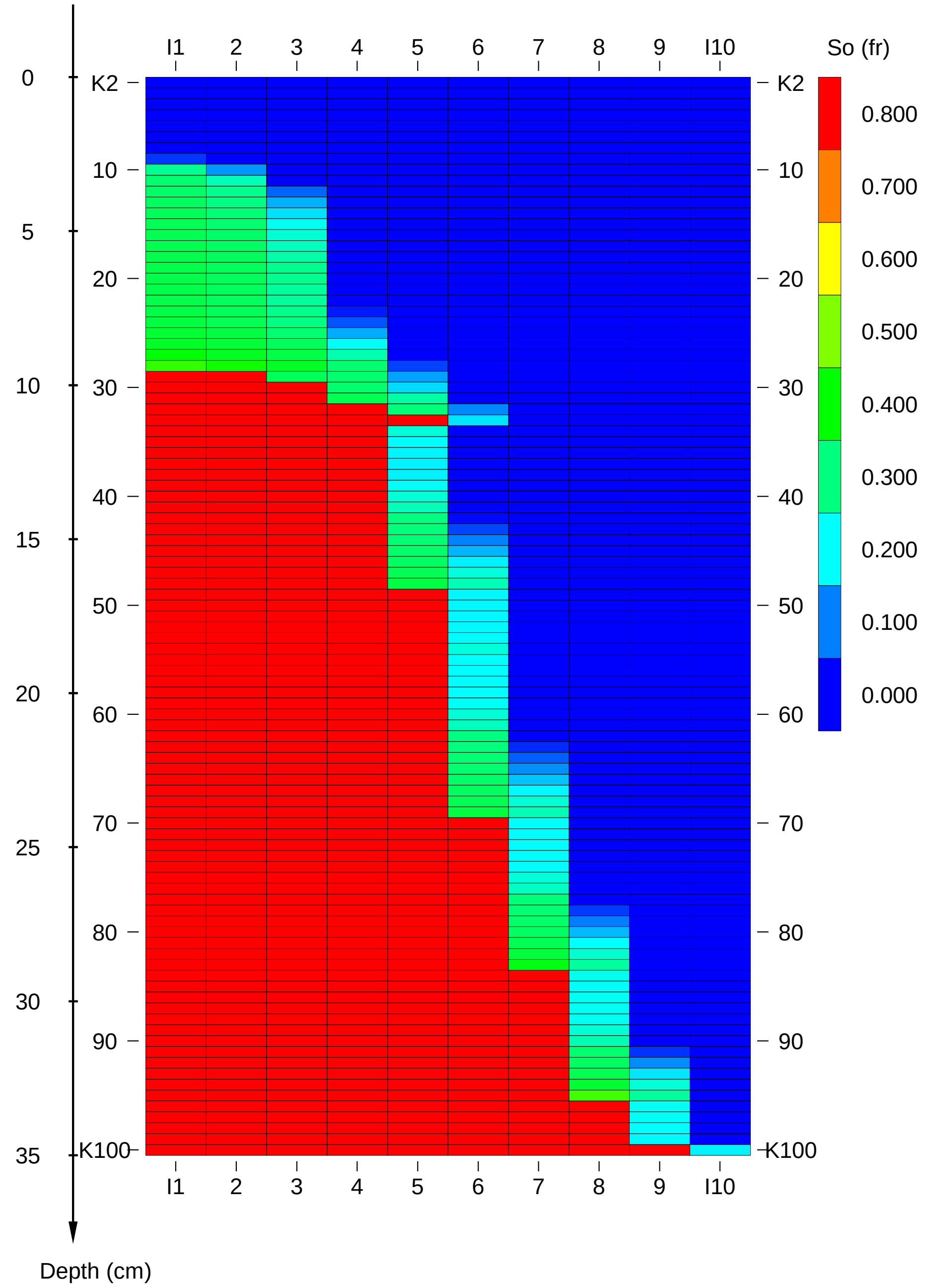

Figure 7.2 – CO_2 gas displacement with diffusion, core oil saturation profile after 1 day for C_1-C_5 lab system at 1000 psia (at about 60% oil recovery).

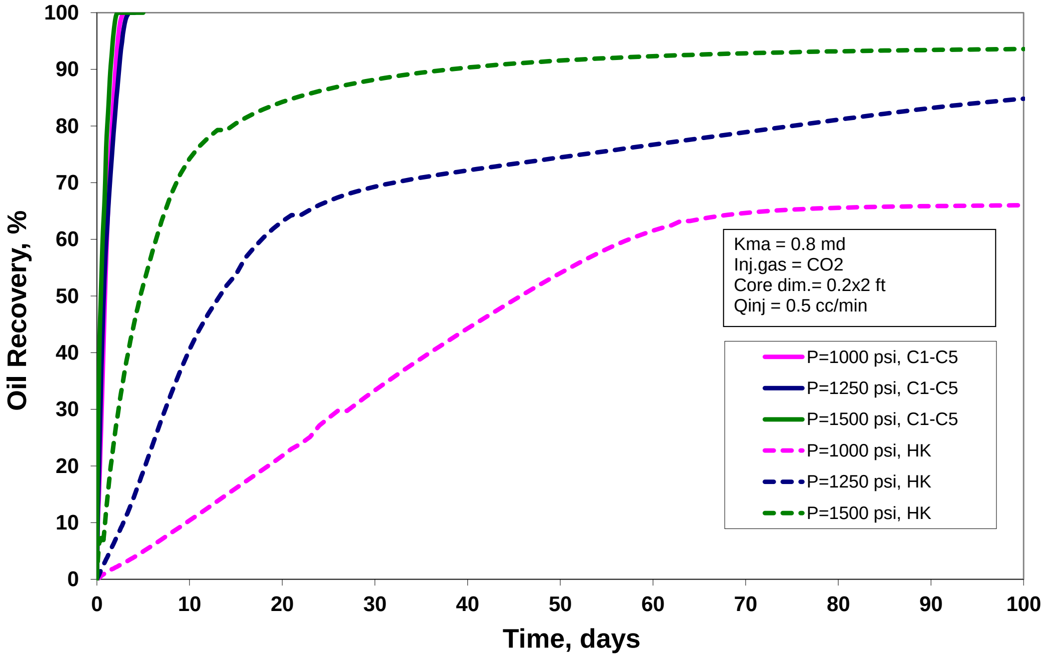

Figure 7.3 – Comparison of reservoir pressure effect on oil recovery vs. time for C_1-C_5 (solid lines) and Haft Kel (dash lines) lab system using CO_2 injection with diffusion.

gravity drive mechanism (CGDM) is more pronounced, with less lateral variations and more-gradual saturation changes than seen with the synthetic oil system. Fig. 7.3 clearly suggests a strong effect of pressure on oil recovery for the Haft Kel oil system, this being linked to strong IFT variations that result from near-critical phase behavior with strong influence of composition and pressure on heavier-component K-values.

7.3.2 Field-Scale (Haft Kel) Recovery Performance

With the reservoir pressure set to 1000 psia (68.95 bara) and CO_2 injection rate of 3 M scf/D, model runs (with Haft Kel oil) were made with and without diffusion. For the model run without diffusion, near-ultimate recovery of ~22% was achieved after 5 years, as shown with red lines in **Fig. 7.5**. Oil recovery with molecular diffusion was ~72% (near-ultimate recovery) after 10 years. The oil saturation profile shown in **Fig. 7.6**, for the run with diffusion, shows that the

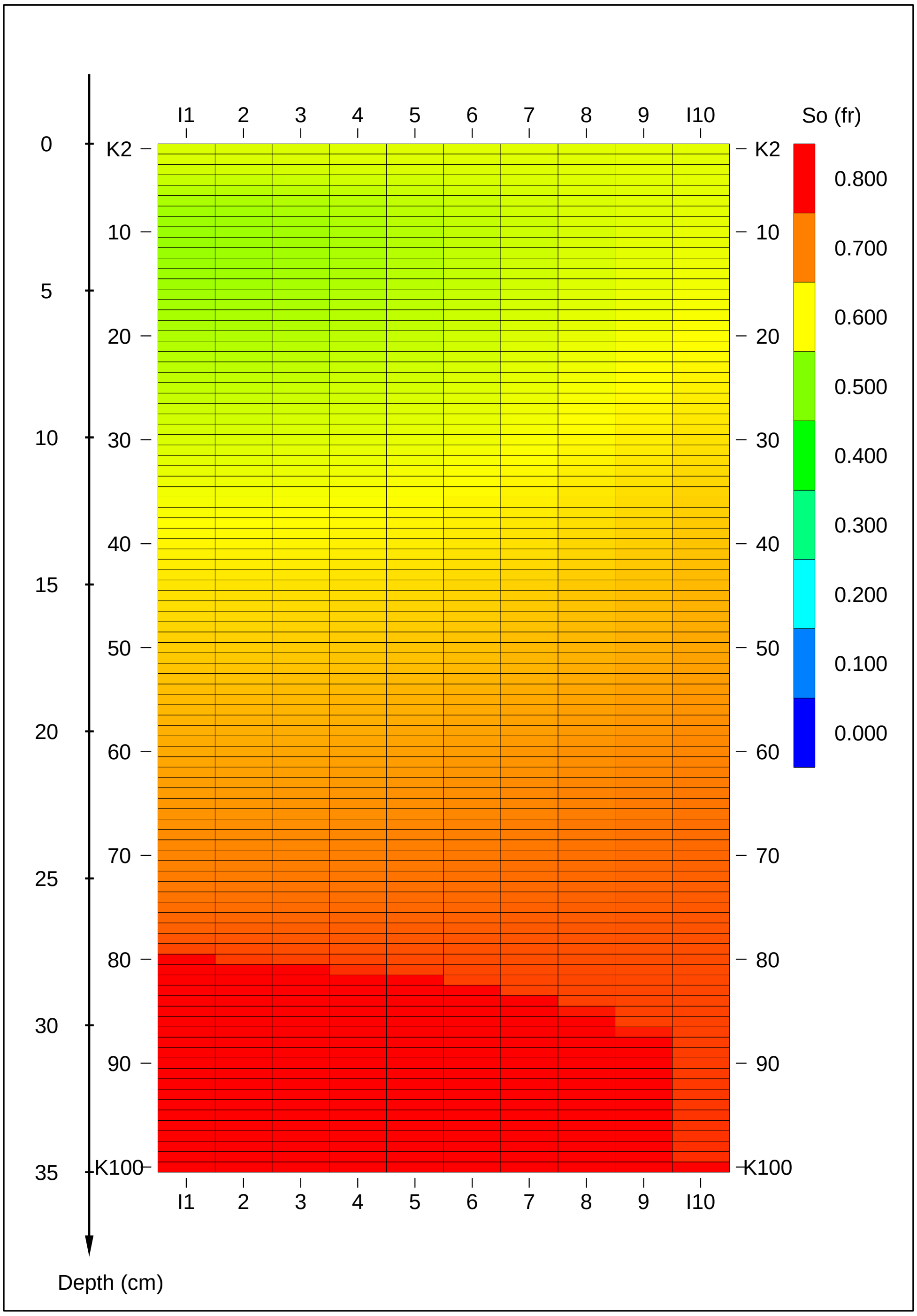

Figure 7.4 – CO_2 gas displacement, oil saturation profile inside core after 16 days for Haft Kel lab system at 1000 psia (at about 17% oil recovery).

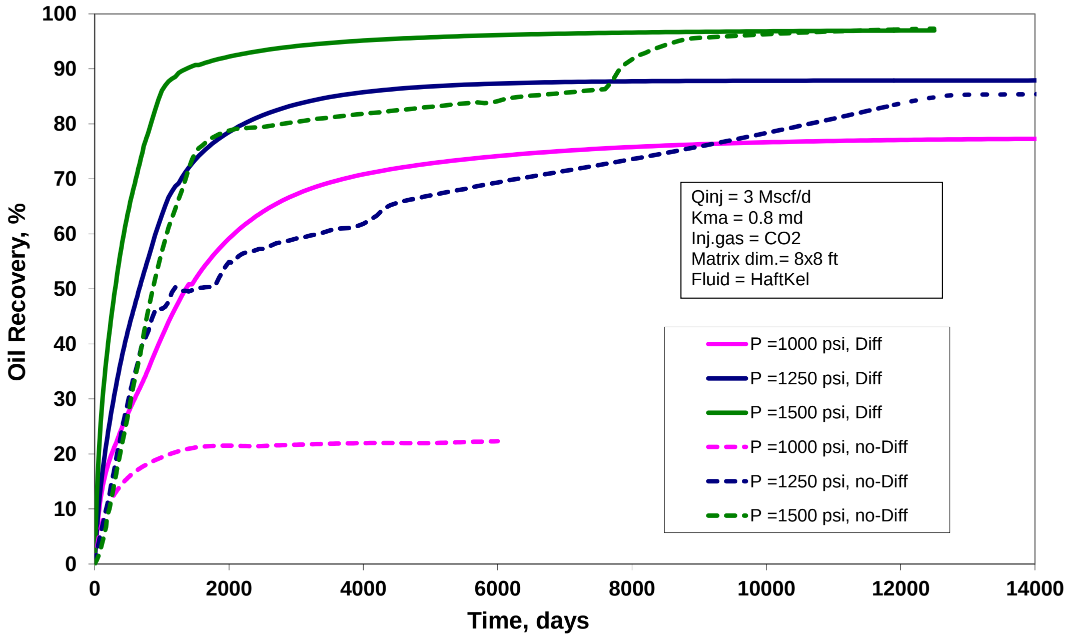

Figure 7.5 – Effect of reservoir pressure on oil recovery vs. time for 8-ft cube Haft Kel single matrix block system using CO_2 injection with (solid lines) and without diffusion (dash lines).

displacement front is laterally non-uniform (somewhat similar to the lab test with Haft Kel oil seen in Fig. 7.4).

7.4 Reservoir Pressure Sensitivity

In this section we study the effect of reservoir pressure on lab- and field-scale systems – at 1000, 1250 and 1500 psia. For each pressure the matrix block/core is initialized with saturated oil and the fracture is initialized with CO_2. Matrix properties, injection rate, and gridding are the same as described above model for the lab- and field-scale models, respectively.

7.4.1 Core Model

The simple C_1-C_5 oil recoveries are 100% after short time (2-3 days) for all pressures (Fig. 7.1). The vaporizing-diffusion mechanism is very effective for this system. For Haft Kel reservoir oil however, the ultimate recovery and the rate of recovery increase significantly with pressure in the lab-test model with

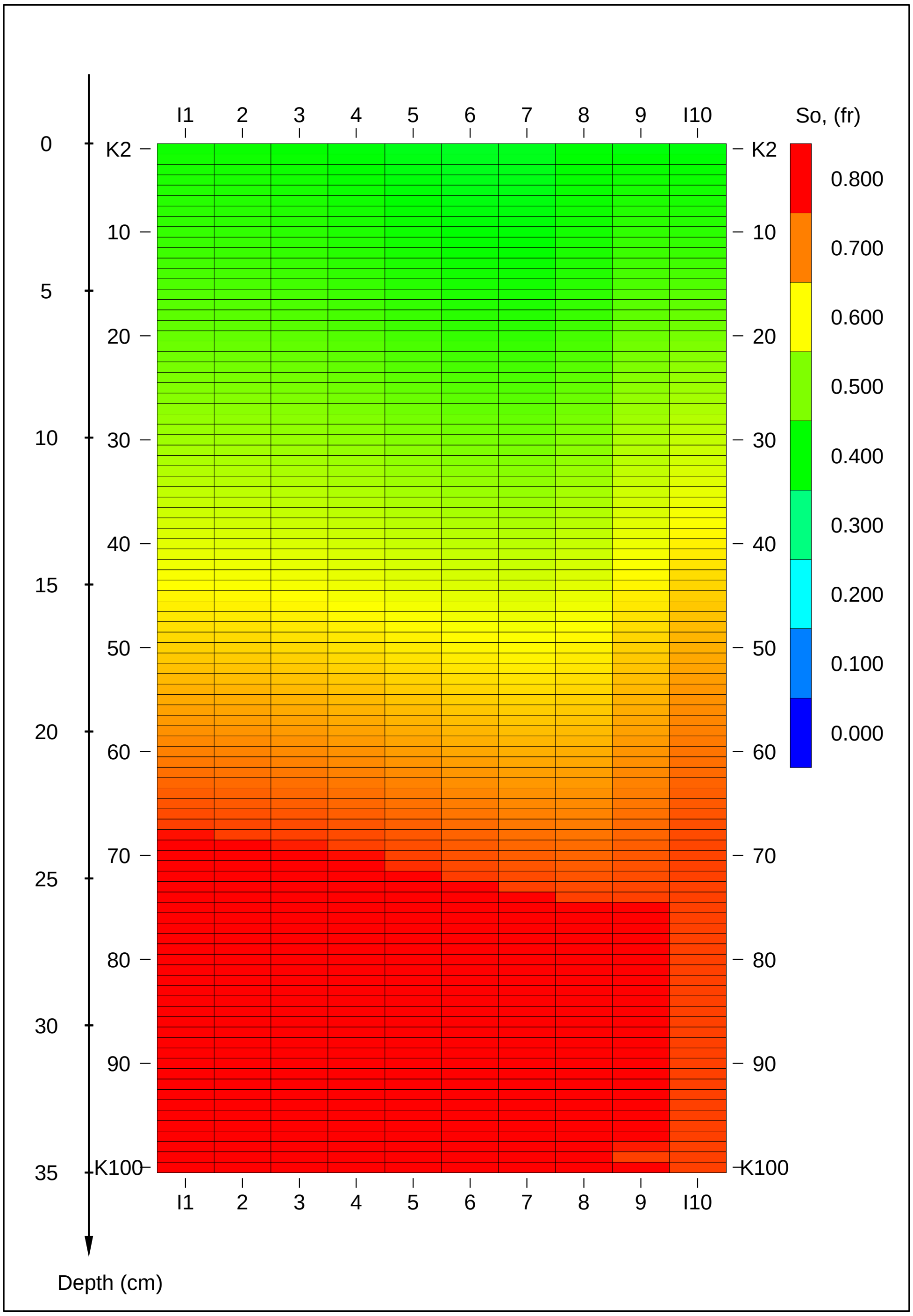

Figure 7.6 – CO_2 gas displacement, matrix block oil saturation profile after 300 days for 8-ft cube Haft Kel single matrix block system at 1000 psia (at about 21.5 % oil recovery).

reservoir oil, as shown in Fig. 7.3. The same conclusion was reported by Er, Babadagli and Zhenghe (2010).

7.4.2 Field-Scale Matrix

For the Haft Kel field-scale single matrix block model, a similar ultimate recovery was found with and without diffusion, for 1250 and 1500 psia, though rate of recovery is much higher with diffusion. For 1000 psia reservoir pressure, the ultimate recovery with diffusion is 78% vs. 22% without diffusion – mainly because CO_2 is able to penetrate the matrix below the threshold capillary height. For all simulations including diffusion, the total recovery and the rate of recovery increase with increasing pressure (Fig. 7.5).

Cases with diffusion show that CO_2 recovers oil below the capillary threshold height, and that unrecovered oil saturation decreases with increasing reservoir pressure (**Fig. 7.7**). Higher pressures result in more vaporization, with vaporized oil components being transported by gas diffusion from the matrix block. Detailed displacement mechanisms of models with no diffusion (capillary-gravity drive) are previously in chapter 6. Thus mechanism would only be dominant in field with very large matrix blocks where diffusion is insufficient.

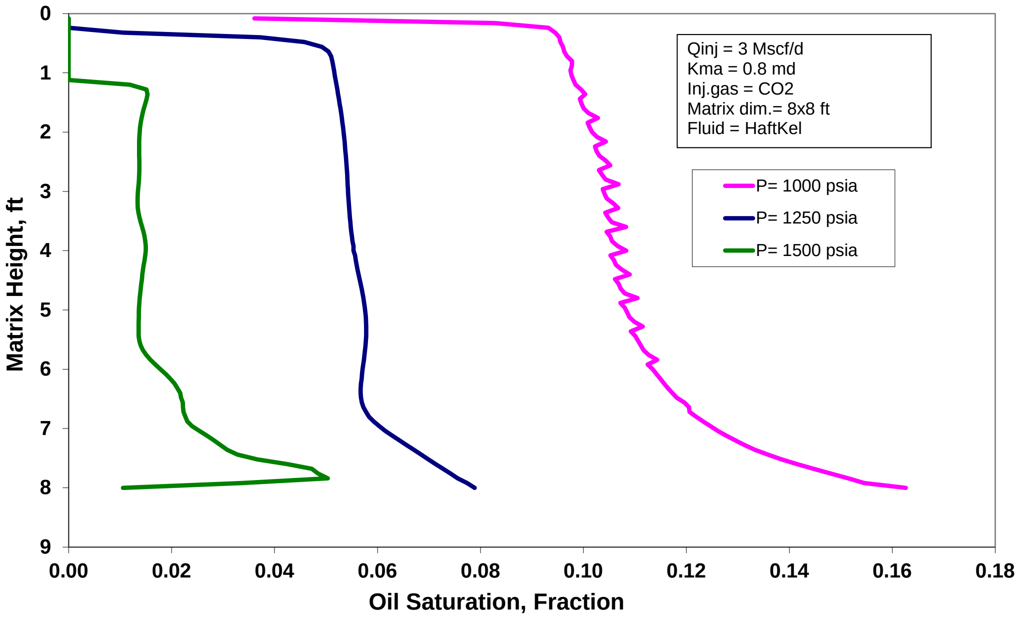

Figure 7.7 – Oil saturation profile for 8-ft cube Haft Kel single matrix block using CO_2 injection gas at 10000 days.

7.5 Matrix Block Permeability Sensitivity

We studied the effect of matrix block permeability for the field-scale Haft Kel system at pressures of 1000, 1250 and 1500 psia, including diffusion. Two matrix block permeabilities were used, 0.8 and 5 md. For each pressure the matrix block is initialized with saturated oil and the fracture is initialized with CO_2. All models are run with an 11x1x102 grid. Injection rate is 3 Mscf/D.

The rate of oil recovery increases with increasing matrix block permeability for all reservoir pressures, but ultimate oil recovery is not affected significantly, as shown in **Fig. 7.8**. Similar results were obtained for models with no diffusion (Section 6.8).

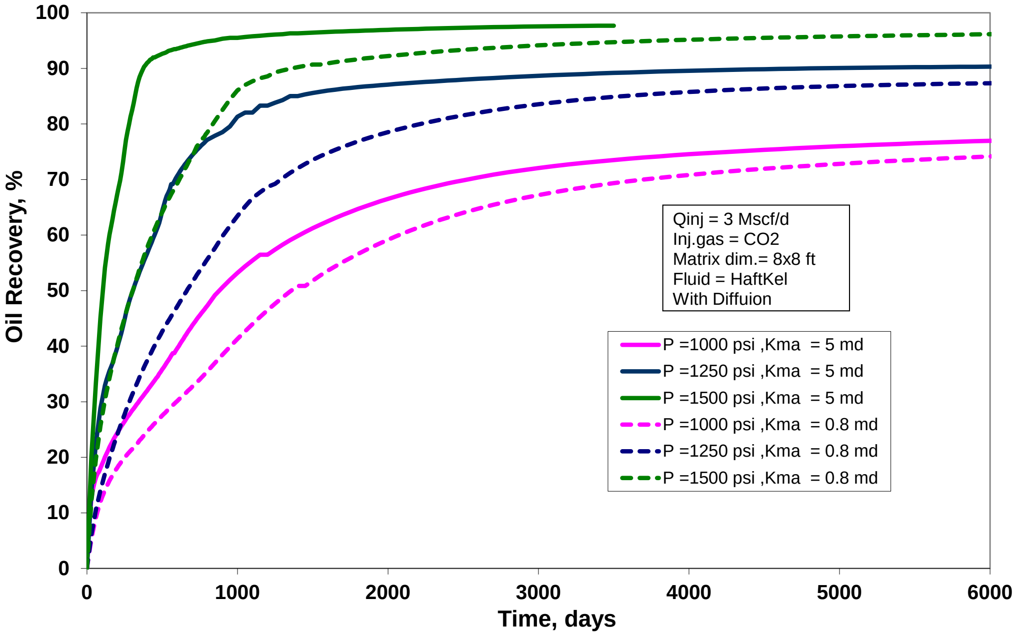

Figure 7.8 – Effect of matrix block permeability on oil recovery vs. time for 8-ft cube Haft Kel single matrix block using CO_2 injection gas at various system pressure.

7.6 Matrix Block Size Sensitivity

We consider cubic matrix blocks with dimensions of 8-, 16- and 35 ft. Models were run with system pressure of 1000 and 1500 psia using 0.8 md matrix block permeability. For each case the matrix block is initialized with saturated oil at system pressure, and the fracture is initialized with CO_2. All models use the

11x1x102 grid. Injection rate is 3 Mscf/D. Cases are run with and without diffusion.

Fig. 7.9 shows recovery performance at 1000 psia, comparing behavior with and without diffusion for different matrix blocks sizes. Higher recoveries (>50%) result mainly from the vaporizing-diffusion mechanism. For the larger matrix block size of 35 ft we see that VDM is a slower, less-effective recovery process, with similar recovery performance with and without diffusion. For the smaller matrix block size of 8 ft we see that VDM is a fast and efficient recovery process; without diffusion, much lower ultimate oil recovery results because remaining oil trapped by capillary-gravity equilibrium cannot be recovered.

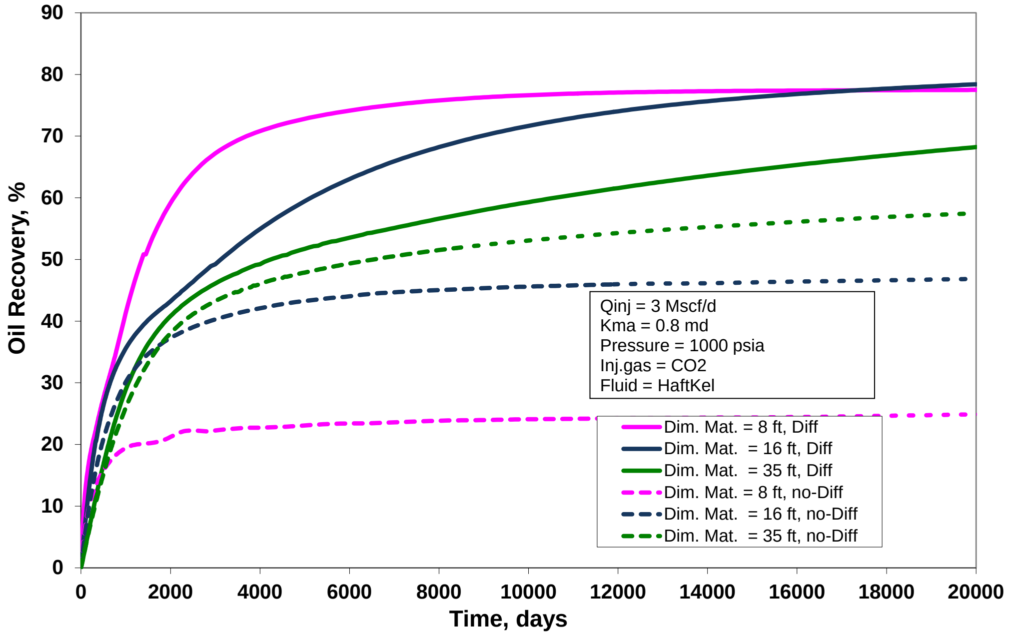

Figure 7.9 – Effect of matrix block dimension on oil recovery vs. time for Haft Kel single matrix block using CO_2 injection gas at system pressure of 1000 psia.

Fig. 7.10 shows recovery performance at 1500 psia, comparing behavior with and without diffusion for different matrix blocks sizes. We see that capillary-gravity drive is more significant for all cases, with smaller and larger matrix block sizes. The impact of diffusion is much less, yielding only a slight acceleration in recoveries. IFTs become very low at 1500 psia through CO_2-oil

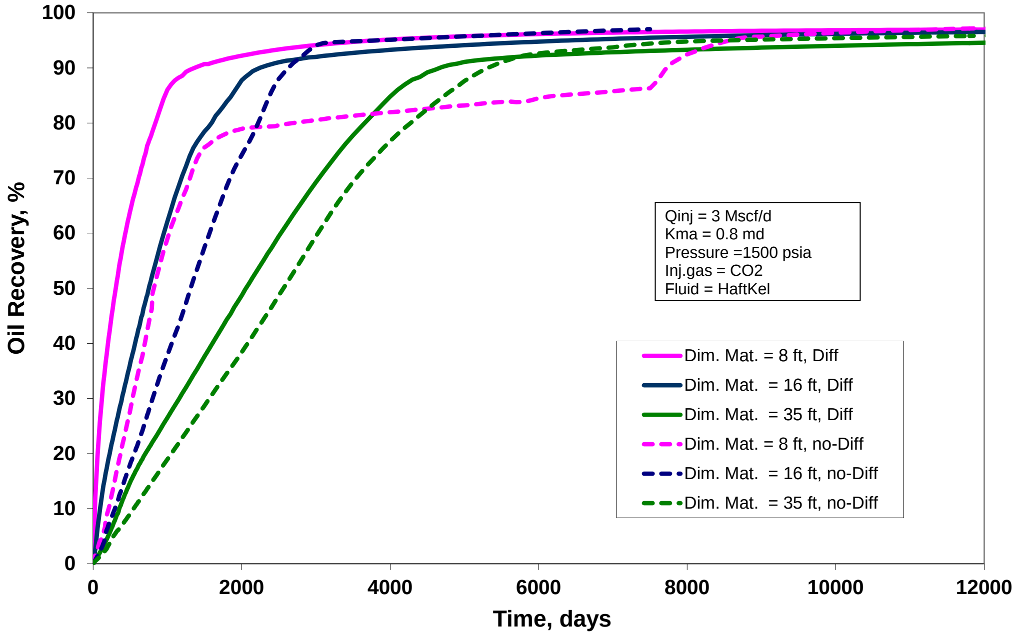

Figure 7.10 – Effect of matrix block dimension on oil recovery vs. time for Haft Kel single matrix block using CO$_2$ injection gas at system pressure of 1500 psia.

interaction and near-critical phase behavior, reducing capillary retaining forces significantly.

Figs. 7.9 and 7.10 clearly show that the relative importance of vaporizing-diffusion recovery and capillary-gravity drainage recovery can vary significantly, according to pressure (phase behavior effects) and matrix block size.

7.7 Injection Rate Sensitivity

Availability of fresh CO$_2$ in fractures surrounding the matrix block has a large impact on total fracture/matrix mass transfer, and consequently the rate of oil recovery. CO$_2$ injection rate is investigated for both lab-scale and field-scale systems.

For the lab scale model, 0.8 and 5 md core are considered. System pressure is 1000 psia. CO$_2$ injection rates of 0.5, 0.1 and 0.03 cm^3/min injection rates are used. Cases with and without diffusion are studied.

For the field-scale simulations, we consider an 8-ft cubic matrix block with system pressure of 1000 and 1500 psia. Matrix block permeability is 0.8 md. For each pressure the matrix block is initialized with saturated oil, and the fracture is initialized with CO_2. For the case with 1000 psia reservoir pressure, three injection rates are used: 3, 0.3 and 0.03 Mscf/D, while for 1500 psia reservoir pressure, two injection rates are used: 3 and 0.3 Mscf/D.

As seen in **Figs. 7.11, 7.12** and **7.13** diffusion has a huge effect on rate of recovery for lab-scale simulations. Oil recoveries are delayed dramatically by decreasing injection rate. The lack of fresh CO_2 slows down the vaporizing-diffusion mass transfer mechanism.

The strong dependence of recovery on diffusion in lab core test leads to an important lab-design potential. Using lab oil systems with 3-5 pure components representing oil can provide component production data that is useful to verify the model's capability to describe the VDM accurately. As the synthetic oil composition is changed, the overall recovery mechanism can also be altered to move from VDM to a mixed VDM/CGDM mechanism.

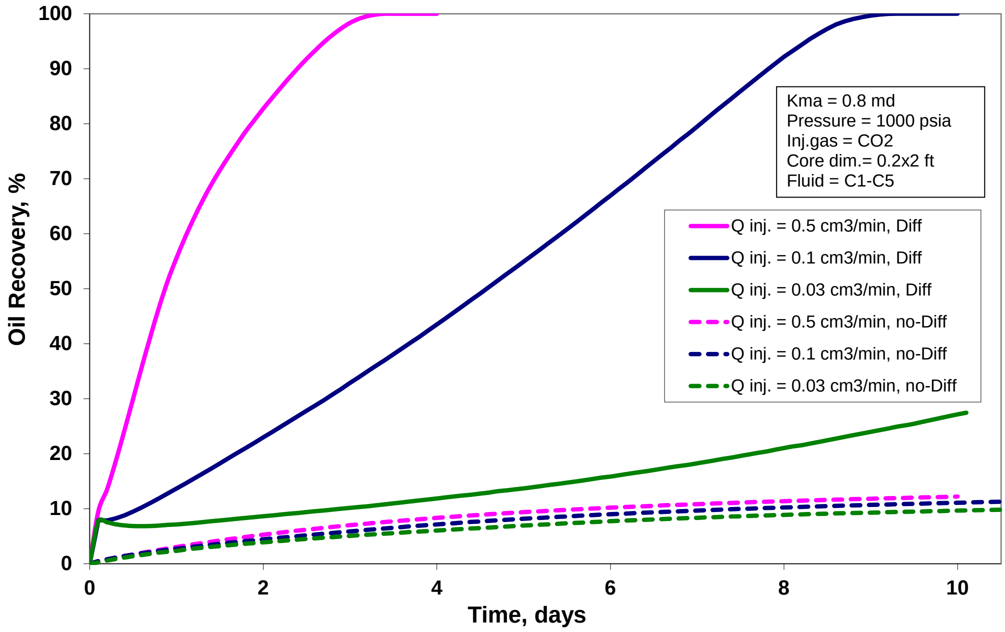

Figure 7.11 – Effect of injection rate on 0.8 md core during CO_2 gas injection for C_1-C_5 lab system at 1000 psia.

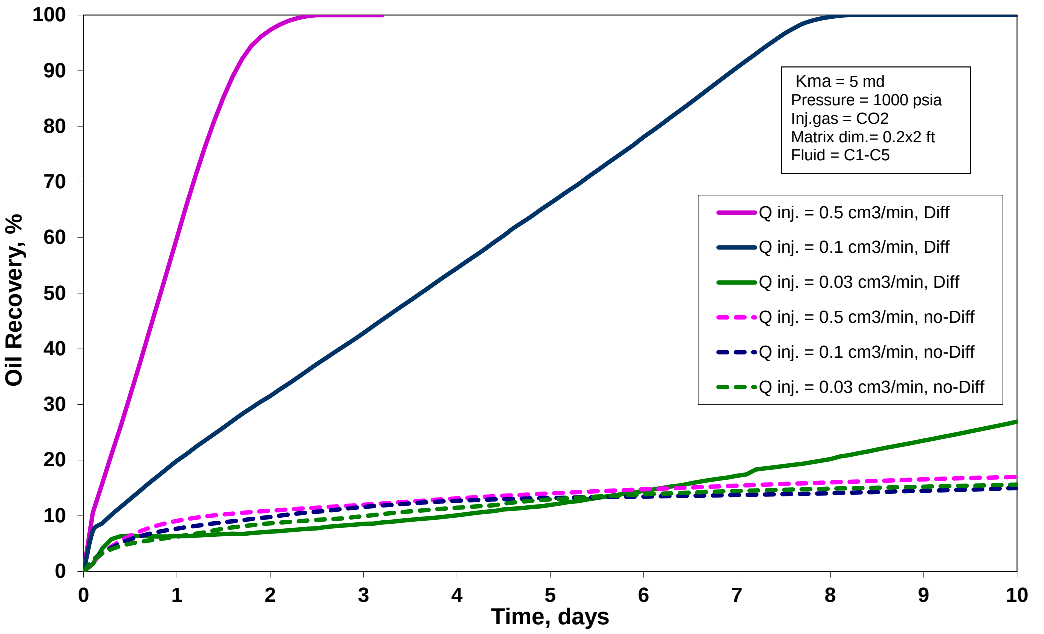

Figure 7.12 – Effect of injection rate on 5 md core during CO_2 gas injection for C_1-C_5 lab system at 1000 psia.

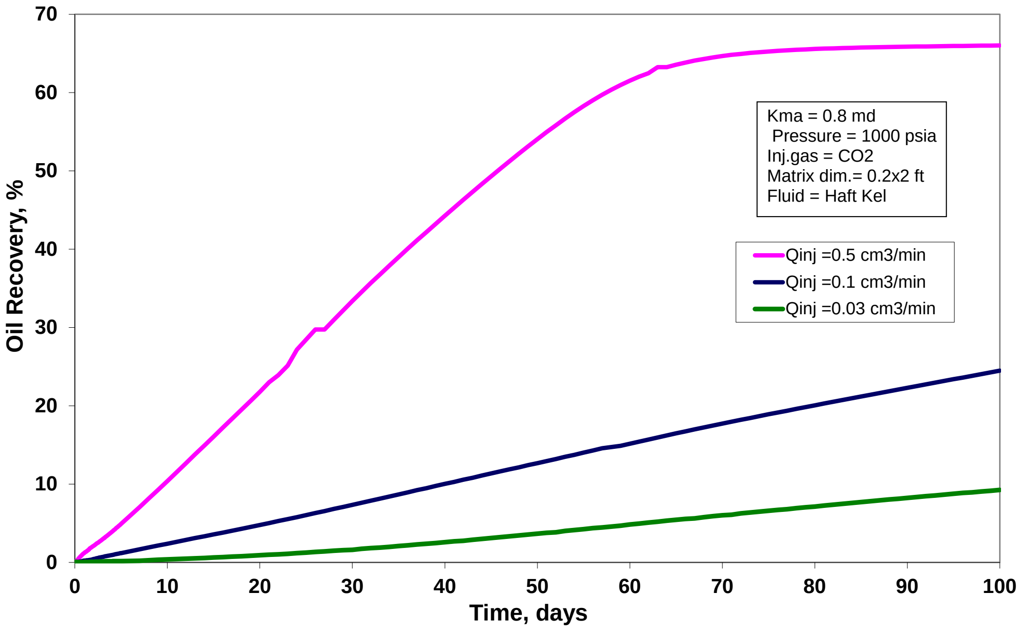

Figure 7.13 – Effect of injection rate on 0.8 md core during CO_2 gas injection for Haft Kel lab system at 1000 psia.

For a single matrix block in the field-scale simulations, CO_2 injection rate of 3 and 0.3 M scf/D give similar results, though the rate of recovery is somewhat slower for 0.3 Mscf/D. A dramatic decrease in the rate of recovery is seen for 0.03 Mscf/D at 1000 psia.[2] Results are shown in **Figs. 7.14** and 7.**15**. It is clear that the actual distribution, movement, and composition of gas in the fractures of a naturally-fractured reservoir will not be as simple as modeled in this study.

We have only considered the potential adverse effect of low CO_2 "injection rate" – i.e. conditions whereby the fracture is not replenished continuously with fresh CO_2. The modeling of CO_2 concentration in the fracture system needs to be studied further, as reduced CO_2 concentrations will reduce the effectiveness of both vaporizing-diffusion and capillary-gravity drainage processes.

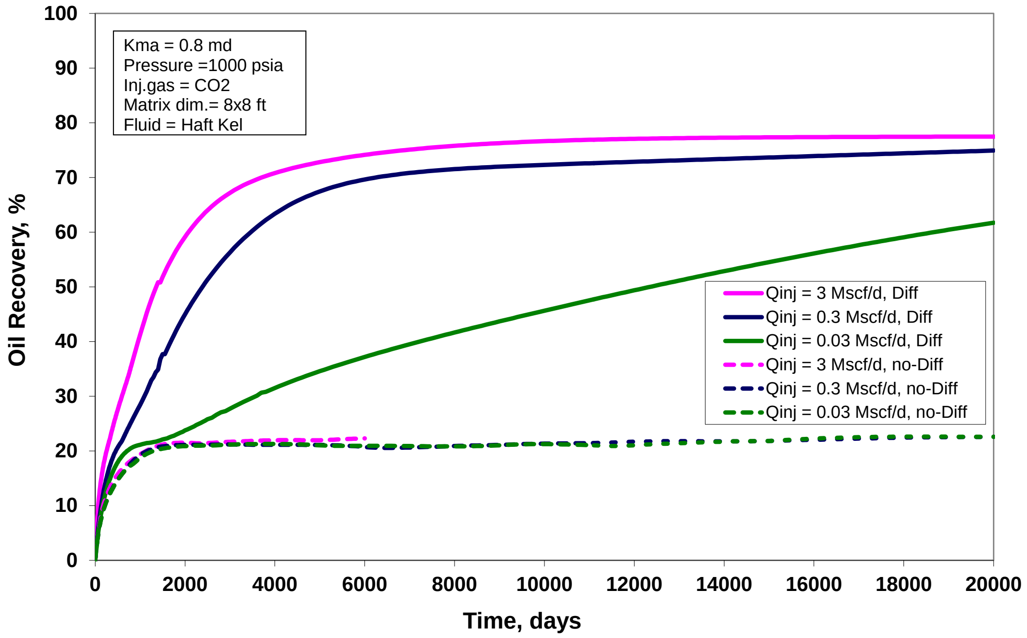

Figure 7.14 – Effect of injection rate on 0.8 md single matrix block during CO_2 gas injection for 8-ft cube Haft Kel system at 1000 psia.

---

[2] Gas injection rate of 0.03 Mscf/D at 1500 psia resulted in unstable simulation results, and are therefore not presented here.

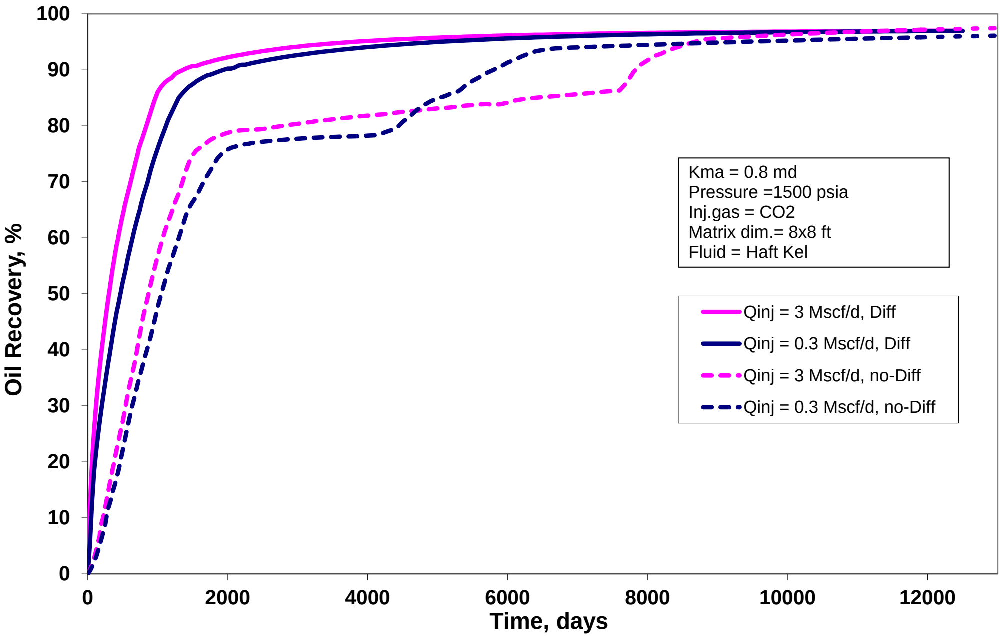

Figure 7.15 – Effect of injection rate on 0.8 md single matrix block during CO_2 gas injection for 8-ft cube Haft Kel system at 1500 psia.

7.8 Conclusions

Conclusions from our numerical model studies include:

1. Diffusion has a significant acceleration effect on oil recovery for all cases studied. The impact is related to (a) vaporized heavier components extracted from the oil and transported from matrix to fracture by diffusion, and (b) CO_2 movement into the matrix block, with subsequent effect on IFT and, thereby, capillary-gravity, and capillary-induced displacement.
2. Ultimate oil recovery increases by CO_2 injection with increasing reservoir pressure in a single matrix block fractured system.
3. Ultimate oil recovery is independent of pressure for the synthetic C_1-C_5 oil studied for lab-scale systems in the range of 1000-1500 psia (with thermodynamic MMP ~1400 psia).

4. Oil recovery rate is affected by CO_2 injection (replenishment) rate, mainly because the vaporizing-diffusion process is slowed, but also because IFT changes are lessened.

7.9 References

Er, V., Babadagli, T and Zhenghe X. 2010. Pore-Scale Investigation of the Matrix-Fracture Interaction during CO_2 Injection in Naturally Fractured Oil Reservoir. Energy Fuels 2010, 24: 1421-1430.

Saidi, A.M.1987. Reservoir Engineering of Fractured Reservoirs. TOTAL Edition Press, Paris, P 764-770.

Schlumberger: ***ECLIPSE 300*** Reservoir Engineering Software. 2009. www.slb.com.

Appendix A

Simulator Input Data Sets

Input Data Set Used to Model Karimaie Experiment in Chapter 3

SENSOR input data set

Note:

Compositional production of well streams were processed using *Pipe-it/Steamz* with separator varying with time (section 3.6.4 and Table 3.5).

```
TITLE
  Simulating Chalk core done by Hassan
  Experiment 4 in page 128
  Full radial block model
  4 Component EOS
  Base:
    Nx  = 10
    Nz  = 50
    Kma = 5.0 md
    Hma = 19.6 cm= 0.643 ft
    Porosity= 0.44-0.48
    Matrix diameter = 3.8 cm =0.12467154 ft
    Pinit = 220 bara=3190.83 psia
    Inj gas = Eq gas
    No blocks = 1
    Displacement=2D
ENDTITLE

C -----------------------------------------------------------------------------------------
C Dimension and Solution Options
C -----------------------------------------------------------------------------------------

GRID  10 1 51

CPU

 IMPLICIT

MAPSX 1 1 2 3
MAPSY 1 1 2 3
MAPSPRINT 1 X Y P SO SG GG GO TENS TX TZ PV PCGO VISO !  Initialization output

C --------------------------------------------------------------------------------------
C Grid Block Properties
C --------------------------------------------------------------------------------------
RADIAL
    5                      ! equal volume block option
    0. 0.06233577   0.06889743   ! Nx-1 equal vol blocks to 0.060695 ft + 1 annulus block
    360
DEPTH CON
 1000
THICKNESS ZVAR
 0.00328083 48*0.013396723 0.001640415  0.001640415
KX CON
 100000
MOD
 1 10 1 1  1 51  =  26.25560264 ! 16.71049
 1 9  1 1  2 49  = 5

KY EQUALS KX
KZ EQUALS KX

POROS CON
  1.00
MOD
 1 10  1 1  1 51  =  0.936092035
 1 9  1 1  2 49  =   0.44468662
C ----------------------------------------------------------------------------------------
C Regions: Region 1 = Matrix, Region 2 = Fracture
C ----------------------------------------------------------------------------------------

ROCKTYPE CON           ! Rock (saturation table) regions
  2
MOD
 1 9  1 1  2 49  = 1

REGION CON             ! Fluid in place regions
  2
MOD
 1 9  1 1  2 49  = 1

INITREG CON            ! Initialization regions
  2
MOD
 1 9  1 1  2 49  = 1

C ----------------------------------------------------------------------------------------
```

```
C Rel-perm and capillary pressure data
C ---------------------------------------------------------------------------------------

! Rock type 1 (Matrix-Chalk)
KRANALYTICAL 1
   0.0    0.0     0.050799489   0.0           ! Swc  Sorw  Sorg  Sgc 0.10557
   1.0    1.0     1                     ! krw(Sorw)  krg(Swc)  kro(Swc)
   1.0    1.0     1.0   1.0             ! nw now ng nog
   0.087  2.088   3.337 PCGO            ! c1 c2 c3 gas-oil (C1-nC5 Pc) , ref=1.5

! Rock type 2 (Fracture, Pc = 0)
KRANALYTICAL 2
 0.0  0.0  0.0  0.0              ! Swc  Sorw  Sorg  Sgc
 1.0  1.0  1.0                   ! krw(Sorw)  krg(Swc)  kro(Swc)
 1.0  1.0  1.0  1.0              ! nw now ng nog
! Interfacial tension scaling
 TENSION  1.5   300                 ! ref_tension, max_tension

C ---------------------------------------------------------------------------------------
C Fluid PVT data
C ---------------------------------------------------------------------------------------

PVTEOS SRK
185    ! Reservoir temperature (deg F)

CPT      MW       TC      PC    ZCRIT    SHIFT     AC      PCHOR    OMEGA     OMEGB
C1     16.043   343.01  667.03  0.2862   -0.00247  0.011   64.23    0.42748   0.08664
n-C7   100.2    972.36  397.4   0.2611   0.14347   0.35   281.33    0.42748   0.08664
CO2    44.01    547.42  1069.5  0.27433  0.21749   0.225    80      0.42748   0.08664
N2     28.014   227.16  492.84  0.29178  -0.0009   0.037    59.1    0.42748   0.08664

BIN
0.01574     0.12        0.02
0.15        0.08
0

C ----------------------------------------------------------------------------
C Initialization
C ----------------------------------------------------------------------------
INITIAL 1
!   depth psat     C1            n-C7         CO2     N2
DEPTH
1000   3190.83    0.684404     0.315596      0.0000  0.0000
PINIT  3190.83
ZINIT  1000

INITIAL  2
!   depth psat         C1           n-C7       CO2       N2
DEPTH
1000   3190.83    0.684404     0.315596      0.0000  0.0000
PINIT  3190.83
ZINIT  1000
ENDINIT
C we can define well under one keyword or separate them to each well
 WELL
    I    J       K       PI
  PROD                          !name of oil produce well
    1    1      51       1     ! perforated location
    2    1      51       1
    3    1      51       1
    4    1      51       1
    5    1      51       1
    6    1      51       1
    7    1      51       1
    8    1      51       1
    9    1      51       1

   GINJ                          !name of gas injection well
    1    1       1       1      ! perforated location
    2    1       1       1
    3    1       1       1
    4    1       1       1
    5    1       1       1
    6    1       1       1
    7    1       1       1
    8    1       1       1
    9    1       1       1
```

```
 INJGAS                          !Equilibrium gas
  GINJ
0.92857147   0.07142853    0.0000  0.0000
WELLTYPE                          !define well type and unit for that
  PROD       STBOIL               !Oil producer  STB/day
  GINJ        -2                  ! Gas injection well RB/day
RATE
  PROD      200                  !rate of the Gas produce  well
  GINJ     0.00905733            !injection rate 1 cm3/min (5 cm3/min=0.045286631 )
  BHP
  PROD      3190.83
  GINJ      319000.83            !BHP of the  gas injection well

C ---------------------------------------------------------------------------------------
C Output specifications
C ---------------------------------------------------------------------------------------
 PSM
MAPSFREQ 1

MAPSFILE  SAT SG SO TENS GO GG
MAPSFILEFREQ 1    ! maps written to fort.71
SUMFREQ 1
WELLFREQ 1
 WELLSUM
C - Time step control
C         days    freq
 TIME     0.0150
RATE
 GINJ       0.0035

C         days    freq
 TIME     0.080

 RATE
 GINJ      0.000905733       !injection rate 0.1 cm3/min

TIME       0.1
TIME       4.2     0.1

 INJGAS                          !CO2 gas
  GINJ
   0.0000   0.0000    1.0000  0.0000
 RATE
  GINJ    0.000905733  ! 0.0033               !injection rate 0.364 cm3/min 0.0033

 TIME      4.5      0.1

 RATE
  GINJ    0.000905733  ! 0.000634013            !injection rate 0.07 cm3/min 0.000634013

 DTSTART 0.001
 DTMAX 0.001
 TIME      6.4      0.1

END
```

Input Data Set Used to Model Darvish Experiment in Chapter 4

ECLIPSE 300 input data set

```
--RUNSPEC section--------------------------------------------------
NOECHO
RUNSPEC
--TITLE
--IMPES
FULLIMP

DIMENS
   10    1    51  /
RADIAL
-- Phases present
OIL
GAS
OPTIONS3
--switch 19    21     26     46   68    74         146
18*     0  1* 200 4*  2  19* 200 21* 1  5*  1  71*  5  11*   1*  / 14*  1

--Enables molecular diffusion
DIFFUSE
-- Units
LAB
-- Define Compnent in EOS
COMPS
13   /
REGDIMS
-- Max.FIPREG  FIPREG
     2          2     0    2/
TABDIMS
--No.sat.tab  No.pvt.tab  max.sat.nods  max.sat.nods  Max.FIPREG
2              1             50           50            2/
EQLDIMS
----Eqrgn  Deptab
    2      50    /
WELLDIMS
5  10  20  20  20  20/
MISCIBLE
/
-- To unified output files
UNIFOUT
MULTSAVE
0 /
UNIFIN
--Grid section--------------------------------------------------------
GRID
--Requests output of an INIT file (Need for FloViz)
INIT
RPTGRID
DR DZ PERMR PERMZ PORO PORV TRANR  TRANZ NNC /
MINPORV
0.000000001/
INRAD
0.1E-03/
--  SPECIFY GRID BLOCK DIMENSIONS IN THE R DIRECTION
DRV
0.7666634    0.3175650    0.2436724    0.2054291    0.1809841
0.1636227    0.1504676    0.1400495    0.1315395    0.1999991/  cm
DTHETAV
 360.0/
DZV
 0.099999698 48*1.2427 2*0.049999849  / cm
EQUALS
  TOPS      1              1 10 1 1 1 1 /
  PORO      0.94           1 10 1 1 1 51   /     Fracture porosity0.94
  PORO      0.438        1 9 1 1 2 49   /     Martix porosity 0.438   0.444
  PERMR     80        1 10 1 1 1 51 /       Fracture permeabiliy  16.2
  PERMR     4            1 9 1 1 2 49 /       Martix permeabiliy
/
COPY
      'PERMR'    'PERMTHT'  /   1  10  1  1  1  51
      'PERMR'    'PERMZ'   /
/
GRIDFILE
2 /

PROPS    ==============================================================
EOS
PR79 /
```

```
-- Reservoir temperatures Deg C
RTEMP
 130  /
CNAMES
N2  CO2  C1   C2   C3   C4   C5   C6   C7-C9   C10-C15   C16-C22    C23-C34    C35+    /

-- Molecular Weights
MW
28.014 44.010 16.043 30.070 44.097 58.123 72.150 84.135 110.403 167.317 244.898 347.728
578.832 /

-- Critical temperatures Deg K
TCRIT
126.20  304.12 190.56 305.32 369.83 416.49 465.10 511.14 577.75 682.95 782.17 874.10 1024.78
/

-- Critical pressures atm
PCRIT
33.5357 72.7757 45.3886 48.0829 41.9245 36.6942 33.3165 31.7778 27.5412 20.4465 15.0670
11.4071 10.0720 /

-- Acentric factors
ACF
0.03700 0.22500 0.01100 0.09900 0.15200 0.19299 0.24053 0.25984 0.32623 0.49183 0.70817
0.97132 1.40544/

-- Critical Z-factors
ZCRIT
0.29178 0.27433 0.28620 0.27924 0.27630 0.27792 0.27032 0.26759 0.25962 0.24406 0.22710
0.20735 0.17549 /

-- Parachors (Dynes/cm)
PARACHOR
59.10  80.00  71.00 111.00 151.00 189.90 229.20 236.92 299.97 436.56 622.75 869.55 1424.20 /

-- Critical Viscosity Z-factors
ZCRITVIS
0.29178 0.29278 0.28620 0.27924 0.27630 0.27792 0.27032 0.29954 0.27966 0.25667 0.24019
0.23267 0.22163  /

-- Parameter EoS Shift Coefficients
SSHIFT
-0.16758 -0.00573 -0.14996 -0.06280 -0.06381 -0.05795 -0.04271 -0.00273 0.02683 0.09061
0.14892 0.18839 0.0726 /

-- Binary Interaction Coefficients
BIC
0.00000
0.02500 0.21000
0.01000 0.26000  0.00000
0.09000 0.25000  0.00000 0.0000
0.09500 0.23492  0.00000 0.0000 0.0000
0.10508 0.23000  0.00000 0.0000 0.0000 0.0000
0.11000 0.23000  0.00000 0.0000 0.0000 0.0000 0.0000
0.11000 0.10425 -0.04464 0.0000 0.0000 0.0000 0.0000 0.0000
0.11000 0.09498 -0.06761 0.0000 0.0000 0.0000 0.0000 0.0000 0.0000
0.11000 0.08535 -0.08963 0.0000 0.0000 0.0000 0.0000 0.0000 0.0000 0.0000
0.11000 0.07660 -0.10795 0.0000 0.0000 0.0000 0.0000 0.0000 0.0000 0.0000 0.0000
0.11000 0.06659  0.19401 0.0000 0.0000 0.0000 0.0000 0.0000 0.0000 0.0000 0.0000 0.00000  /

--Interfacial tension scaling
MISCSTR
--ref_tension, max_tension
1.5   300  10/
-- (IFT.ref/IFT)^n; n=1
MISCEXP
0/

SGOF
--Sg        Krg        Krog      Pcog (atm)
  0.0000    0.0000    1.0000    0.0000
  1.0000    1.0000    0.0000    0.0000
  / --table 1 (fracture)
  0.0000    0.0000    1.0000     0.0000
  0.0500    0.0500    0.9500     0.0059
  0.1000    0.1000    0.9000     0.0060
  0.1500    0.1500    0.8500     0.0062
```

```
  0.2000    0.2000    0.8000     0.0066
  0.2500    0.2500    0.7500     0.0073
  0.3000    0.3000    0.7000     0.0085
  0.3500    0.3500    0.6500     0.0102
  0.4000    0.4000    0.6000     0.0126
  0.4500    0.4500    0.5500     0.0158
  0.5000    0.5000    0.5000     0.0200
  0.5500    0.5500    0.4500     0.0252
  0.6000    0.6000    0.4000     0.0318
  0.6500    0.6500    0.3500     0.0397
  0.7000    0.7000    0.3000     0.0491
  0.7500    0.7500    0.2500     0.0603
  0.8000    0.8000    0.2000     0.0734
  0.8500    0.8500    0.1500     0.0885
  0.9000    0.9000    0.1000     0.1059
  0.9500    0.9500    0.0500     0.1253
  1.0000    1.0000    0.0000     0.1480
  / --table 2 (Matrix)

DIFFAGAS
-- N2        CO2       C1        C2        C3        C4        C5        C6        C7-C9
C10-C15   C16-C22   C23-C34   C35+     (cm2/hr)
0.186 1.151 0.971 0.943 0.884     0.753 0.651 0.590 0.511 0.377     0.276 0.206 0.155 /-new
EOS

DIFFAOIL
-- N2        CO2       C1        C2        C3        C4        C5        C6        C7-C9
C10-C15   C16-C22   C23-C34   C35+     (cm2/hr)
0.011 0.027 0.029 0.027 0.022     0.018 0.016 0.014 0.012 0.010     0.008 0.006 0.005 / New
EOS

REGIONS    ==========================================================

-- Regoin 2= Matrix
-- Regoin 1= Fracture
EQUALS
FIPNUM 1   / Fliud In Place reg. no.
FIPNUM 2  1 9 1 1 2 49 / Fliud In Place reg. no.
SATNUM 1   / Saturation reg. no.
SATNUM 2  1 9 1 1 2 49 / Saturation reg. no.
EQLNUM 1   /
EQLNUM 2  1 9 1 1 2 49 /
/

SOLUTION ==============================================================

DATUMR
 1.0 1.01 /
PRESSURE
 510*296.077 /  atma
EQUALS
SWAT  0/
SOIL  0.0/
SOIL  1.0  1 9 1 1 2 49/
/
NEI
0.00 1.00 0.00  0.00  0.00  0.00  0.00   0.00  0.00   0.00     0.00   0.00   0.00  /
0.0012 0.0085 0.4480 0.0767 0.0426 0.0318 0.0220 0.0211 0.0797 0.0986 0.0652 0.0538 0.0509 /

RPTSOL
PRESSURE  SOIL SGAS PCOG PSAT XMF YMF /

RPTRST
 BASIC=2 SOIL PCOG /

SUMMARY ===============================================================

--data be written to the Summary file only at report time
RPTONLY
-- ****************************
-- * PSM SUMMARY include file *
-- ****************************
--INCLUDE
--'REZA_PSM.SUMMARY' /
RUNSUM
--ALL
FOPR
```

```
FOPT
FGPT
FOMT
FOMR
FGMT
FGMR
--FONPT
--FGNPT
--/
FOE
ROE
/
ROSAT
/
ROIP
/
ROIPL
/
RUNSUM
EXCEL

SCHEDULE =============================================================
-------- THE SCHEDULE SECTION DEFINES THE OPERATIONS TO BE SIMULATED
------------------------------------------------------------------------
--Define Separator condition
SEPCOND
LABSEP       ''          1    130  296.077 /
/
WELSPECS
PROD Field 1 1 1* GAS /
GINJ Field 1 1 1* GAS /
/
WSEPCOND
PROD    LABSEP /
/

WCONPROD
--Wellname   status  control  oil-s.rate  wat-s.rate  gas-s.rate  liq-s.rate  res.rate   BHP
--Unit                         stb/d       stb/d       stb/d       stb/d      rcm3/hr   atma
PROD         OPEN     BHP       4*                                             1000  296.077/
/

WCONINJE
--Wellname  type  status  control  Surf.rate  res.rate    BHP
--Unit                              cm3/hr    rcm3/hr      atma
GINJ        GAS   OPEN     RESV      1*       6.00       2900/
/

-- defining gas injection composition
WELLSTRE
--well St.name  Z-C1      Z-nC7        Z-CO2    Z-N2
CO2-gas     0.000   1.00  0.00   0.00      0.000   0.000  0.00   0.00     0.000   0.000
0.00   0.000   0.00 / 0.00
/

WINJGAS
-- Well name   Stream  Stream name
GINJ       STREAM   CO2-gas/
/


WELLCOMP
--Well name  I  J   K1  K2  SatTable
PROD        1  1   51  51  1*   0.00010    /
PROD        2  1   51  51  1*   0.1999985  /
PROD        3  1   51  51  1*   0.1999985  /
PROD        4  1   51  51  1*   0.1999985  /
PROD        5  1   51  51  1*   0.1999985  /
PROD        6  1   51  51  1*   0.1999985  /
PROD        7  1   51  51  1*   0.1999985  /
PROD        8  1   51  51  1*   0.1999985  /
PROD        9  1   51  51  1*   0.1999985  /
GINJ       1  1   1  1  1*   0.00010    /
GINJ       2  1   1  1  1*   0.1999985  /
GINJ       3  1   1  1  1*   0.1999985  /
GINJ       4  1   1  1  1*   0.1999985  /
GINJ       5  1   1  1  1*   0.1999985  /
```

```
GINJ       6  1   1  1  1*   0.1999985  /
GINJ       7  1   1  1  1*   0.1999985  /
GINJ       8  1   1  1  1*   0.1999985  /
GINJ       9  1   1  1  1*   0.1999985  /
/
-- Creat Restart file
RPTRST
 BASIC=2  SOIL/
RPTPRINT
8*/
RPTSCHED
'CPU=1'   'FIP=3'   'SOIL' XFW FUGG  FUGO  'ZMF'  XMF YMF PRES  PCOG  KRO KRG /

--TUNING
--8* /
--4*  /
--20 1*  /20  1*  2*20
-- Uint= Hr

TSTEP
1.0 /
WCONINJE
--Wellname  type  status  control  Surf.rate  res.rate    BHP
--Unit                              scm3/hr    rcm3/hr      atma
GINJ        GAS   OPEN     RESV      1*       6.00       2900/
/
--TSCRIT
--0.001 0.001  0.1 /
-- Uint= Hr
TSTEP
539*1 /
--1/
END
```

Input Data Set Used to Tune EOS of Darvish Experiment in Chapter 4

Phaze Comp input data set

```
====================================================================
* PhazeComp file generated by PhzGUI 9/3/2009
====================================================================

TEST1 ALL ; Automatic stability test of all single-phase solutions
TEST2 ALL ; Automatic stability test of all two-phase solutions
STAB  ON

VARIABLE DUMMY 1.0 0.9999 1.001 ; Ensures that a REG file is generated by post-processor

--------------------------------------------------------------------
; Initial Definition of Aliases
--------------------------------------------------------------------
Define   satp   0.000E+0
Define   rvol   0.000E+0
Define   lrvol   0.000E+0
Define   lden   0.000E+0
Define   gden   0.000E+0
Define   gz   0.000E+0
Define   lvis   0.000E+0
Define   gvis   0.000E+0
Define   mr   0.000E+0
Define   gsg   0.000E+0
Define   comp   0.000E+0
Define   K30   0.000E+0
Define   gor   0.000E+0
Define   lden_vis   0.000E+0
Define   com-vis   0.000E+0
--------------------------------------------------------------------
; Char Lab-C10+
--------------------------------------------------------------------
CHAR       Lab-C10+
EOS        PR
Comp       Mw
N2
CO2
C1
C2
C3
I-C4
N-C4
I-C5
N-C5
C6         85.48
C7         93.03
C8         106.27
C9         120.99
C10p       1.000

END
--------------------------------------------------------------------
; Char SCN-C35+
--------------------------------------------------------------------
; Soreide parameters
SOREIDE
Factor     2.570E-1
Sg0        2.900E-1
Mw0        66.000
Exponent   1.570E-1

; Gamma Distribution
GAMMA
Split      C10p       C10
Shape       9.100E-1
Bound        128.0  ;128.500
Average    293.500
Origin       5.33E-1
END

VARIABLE   Cf          2.52194e-01  ; 0.2   0.3     ;   2.570E-1     2.52194e-01
REPLACE    SOREIDE    Factor     BY         Cf


; Twu MW damping factor
REPLACE    TWUMW      by         1.000

CHAR       SCN-C35+
```

```
EOS         PR
Comp    Mw      Tc    Pc    AF    VS    VC       A    B    Tb    SG     Zc     ZcVisc      Pchor     LMw
                R   Psia           cm3/gmol            R
N2
CO2
C1
C2
C3
I-C4
N-C4
I-C5
N-C5
C6                                                                    0.28256
C7                                                                    0.27041
C8                                                                    0.26309
C9                                                                    0.25630
C10                                                                   0.25211
C11                                                                   0.24590
C12                                                                   0.24168
C13                                                                   0.23797
C14                                                                   0.23468
C15                                                                   0.23177
C16                                                                   0.22919
C17                                                                   0.22690
C18                                                                   0.22489
C19                                                                   0.22312
C20                                                                   0.22158
C21                                                                   0.22024
C22                                                                   0.21909
C23                                                                   0.21811
C24                                                                   0.21728
C25                                                                   0.21660
C26                                                                   0.21605
C27                                                                   0.21563
C28                                                                   0.21531
C29                                                                   0.21510
C30                                                                   0.21498
C31                                                                   0.21495
C32                                                                   0.21500
C33                                                                   0.21512
C34                                                                   0.21531
C35+                                                                  0.26359


BIPS  N2 CO2 C1 C2 C3 I-C4 N-C4 I-C5 N-C5 C6 C7 C8 C9 C10 C11 C12 C13 C14 C15 C16 C17 C18 C19
C20 C21 C22 C23  C24 C25 C26 C27 C28 C29 C30 C31 C32 C33 C34 C35+
N2
CO2   0.00E+0
C1    2.50E-2 1.05E-1
C2    1.00E-2 1.30E-1 0
C3    9.00E-2 1.25E-1 0 0
I-C4  9.50E-2 1.20E-1 0 0 0
N-C4  9.50E-2 1.15E-0 0 0 0 0
I-C5  1.00E-1 1.15E-1 0 0 0 0 0
N-C5  1.10E-1 1.15E-1 0 0 0 0 0 0
C6    1.10E-1 1.15E-0 0 0 0 0 0 0 0
C7    1.10E-1 1.15E-1 0 0 0 0 0 0 0 0
C8    1.10E-1 1.15E-0 0 0 0 0 0 0 0 0 0
C9    1.10E-1 1.15E-0 0 0 0 0 0 0 0 0 0 0
C10   1.10E-1 1.15E-0 0 0 0 0 0 0 0 0 0 0 0
C11   1.10E-1 1.15E-0 0 0 0 0 0 0 0 0 0 0 0 0
C12   1.10E-1 1.15E-0 0 0 0 0 0 0 0 0 0 0 0 0 0
C13   1.10E-1 1.15E-0 0 0 0 0 0 0 0 0 0 0 0 0 0 0
C14   1.10E-1 1.15E-0 0 0 0 0 0 0 0 0 0 0 0 0 0 0 0
C15   1.10E-1 1.15E-0 0 0 0 0 0 0 0 0 0 0 0 0 0 0 0 0
C16   1.10E-1 1.15E-0 0 0 0 0 0 0 0 0 0 0 0 0 0 0 0 0 0
C17   1.10E-1 1.15E-0 0 0 0 0 0 0 0 0 0 0 0 0 0 0 0 0 0 0
C18   1.10E-1 1.15E-0 0 0 0 0 0 0 0 0 0 0 0 0 0 0 0 0 0 0 0
C19   1.10E-1 1.15E-0 0 0 0 0 0 0 0 0 0 0 0 0 0 0 0 0 0 0 0 0
C20   1.10E-1 1.15E-0 0 0 0 0 0 0 0 0 0 0 0 0 0 0 0 0 0 0 0 0 0
C21   1.10E-1 1.15E-0 0 0 0 0 0 0 0 0 0 0 0 0 0 0 0 0 0 0 0 0 0 0
C22   1.10E-1 1.15E-0 0 0 0 0 0 0 0 0 0 0 0 0 0 0 0 0 0 0 0 0 0 0 0
C23   1.10E-1 1.15E-0 0 0 0 0 0 0 0 0 0 0 0 0 0 0 0 0 0 0 0 0 0 0 0 0
C24   1.10E-1 1.15E-0 0 0 0 0 0 0 0 0 0 0 0 0 0 0 0 0 0 0 0 0 0 0 0 0 0
C25   1.10E-1 1.15E-0 0 0 0 0 0 0 0 0 0 0 0 0 0 0 0 0 0 0 0 0 0 0 0 0 0 0
C26   1.10E-1 1.15E-0 0 0 0 0 0 0 0 0 0 0 0 0 0 0 0 0 0 0 0 0 0 0 0 0 0 0 0
```

```
C27   1.10E-1 1.15E-0 0 0 0 0 0 0 0 0 0 0 0 0 0 0 0 0 0 0 0 0 0 0 0 0 0 0 0 0
C28   1.10E-1 1.15E-1 0 0 0 0 0 0 0 0 0 0 0 0 0 0 0 0 0 0 0 0 0 0 0 0 0 0 0 0 0
C29   1.10E-1 1.15E-0 0 0 0 0 0 0 0 0 0 0 0 0 0 0 0 0 0 0 0 0 0 0 0 0 0 0 0 0 0 0
C30   1.10E-1 1.15E-0 0 0 0 0 0 0 0 0 0 0 0 0 0 0 0 0 0 0 0 0 0 0 0 0 0 0 0 0 0 0 0
C31   1.10E-1 1.15E-1 0 0 0 0 0 0 0 0 0 0 0 0 0 0 0 0 0 0 0 0 0 0 0 0 0 0 0 0 0 0 0 0
C32   1.10E-1 1.15E-1 0 0 0 0 0 0 0 0 0 0 0 0 0 0 0 0 0 0 0 0 0 0 0 0 0 0 0 0 0 0 0 0 0
C33   1.10E-1 1.15E-1 0 0 0 0 0 0 0 0 0 0 0 0 0 0 0 0 0 0 0 0 0 0 0 0 0 0 0 0 0 0 0 0 0 0
C34   1.10E-1 1.15E-1 0 0 0 0 0 0 0 0 0 0 0 0 0 0 0 0 0 0 0 0 0 0 0 0 0 0 0 0 0 0 0 0 0 0 0
C35+  1.10E-1 1.15E-1 0 0 0 0 0 0 0 0 0 0 0 0 0 0 0 0 0 0 0 0 0 0 0 0 0 0 0 0 0 0 0 0 0 0 0 0

CORRELATE

; Modified Chueh-Praunitz BIP correlation

 CHUEU      C1         with       C7         to         C35+       by       6.000
 Multiply   BIPS       of         C1         with       C7     to    C35+  by 1.800E-1

VARIABLE   CO2-CPLUS-CHUEU-EXP     1.42308e+00  ;  1.5   1   6       ; kdef

CHUEU      CO2     WITH       C7         TO         C35+       BY   CO2-CPLUS-CHUEU-EXP


VARIABLE   CO2-C1-FAC        2.00000e+00  ; 1.5   -2.0   2
VARIABLE   CO2-C2C6-FAC      2.00000e+00  ; 1   -2   2
VARIABLE   CO2-CPLUS-FAC     3.50096e-01  ; 1    0  3.0       ; k = kdef * fac + inc
VARIABLE   CO2-CPLUS-INC     1.21955e-01  ; 0.1  0  0.25
;VARIABLE   BIP-CO2-C35+-INC  7.61145e-02  ;  0.0   -0.1  0.2


MULTIPLY BIPS OF CO2 WITH C1 BY CO2-C1-FAC
MULTIPLY BIPS OF CO2 WITH C2 TO C6 BY CO2-C2C6-FAC
MULTIPLY BIPS OF CO2 WITH C7 TO C35+ BY -1                 ; A way of getting CO2-HC BIPs to
decrease with HC
MULTIPLY BIPS OF CO2 WITH C7 TO C35+ BY CO2-CPLUS-FAC
INCREASE BIPS OF CO2 WITH C7 TO C35+ BY CO2-CPLUS-INC

;INCREASE BIPS OF CO2 WITH C35+ BY BIP-CO2-C35+-INC



; Variable Definitions
;          Name       Initial    Lower      Upper
Variable   TC-C35+                1.01665e+00   ;     0.920     1.0200
Variable   PC-C35+                1.25000e+00      ; 1.1500     1.2500
Variable   BIP_C1_C7_C35_SCN-C35+  -1.43368e+00  ;   -2.000     2.000  ;-1.31893e-02
Variable   BIP_C1-C35+   1.94920e-01   ;    -.2000     .2000



Multiply   TC              C35+       by         TC-C35+
Multiply   PC              C35+       by         PC-C35+

; BIPs Regression
; Type     BIPS       of         Comp       with  First  to  Last     by Variable

Multiply  BIPS  of    C1    with   C7    to    C34       by         BIP_C1_C7_C35_SCN-C35+
Replace   BIPS     of         C1                C35+       by         BIP_C1-C35+

 Variable   Zc-vis-C6      1.69776e-02 ; -0.2   0.2
 Variable   Zc-visC35+    -4.19643e-02 ;   -0.2   0.22
 Variable   Zc-visCO2      1.84508e-02 ;  -0.2   0.20

 Increase    ZcVis   of   C6   to   C34   BY   Zc-vis-C6
 Increase    ZcVis   of   C35+   BY   Zc-visC35+
 Increase     ZcVis   of   CO2   BY   Zc-visCO2

LUMP       C10+       C10        26*1       ; C10 C11 … C34 C35+
LUMP       C4         I-C4       N-C4
LUMP       C5         I-C5       N-C5
LUMP       C7-C9      C7         C8         C9
LUMP       C10-C15    C10        6*1        ; C10 C11... C15
LUMP       C16-C22    C16        7*1        ; C16 C17 … C22
LUMP       C23-C34    C23        12*1       ; C23 C24 … C34

END
```

```
--------------------------------------------------------------------
; Char C35+
--------------------------------------------------------------------
CHAR       EOS-C35+
Basis      SCN-C35+
EOS        PR
Comp       Mw         Tc         Pc         AF         VS         A          B          Tb
SG         Zc         ZcVisc     Pchor      LMw
                      K          bar                                                     K
N2
CO2
C1
C2
C3
C4
C5
C6
C7-C9
C10-C15
C16-C22
C23-C34
C35+



BIPS       N2         CO2        C1         C2         C3         C4         C5         C6
C7-C9      C10-C15    C16-C22    C23-C34    C35+
N2
CO2
C1
C2
C3
C4
C5
C6
C7-C9
C10-C15
C16-C22
C23-C34
C35+
; Lump C5- C1 C2 C3 C4 C5

Variable   VSC7   7.48906e-01     ; -2   2
Variable   VSCO2 -3.00000e+00     ;1    -3   3

Multiply    VS   of   C7-C9   to   C35+   BY   VSC7
Multiply   VS   of   CO2   BY   VSCO2

END
--------------------------------------------------------------------
; FEED Lab-C10+
--------------------------------------------------------------------
Restore    Lab-C10+

;          Name       Type       N2         CO2        C1         C2         C3         I-C4
;N-C4       I-C5       N-C5       C6         C7         C8         C9         C10p  ;   MW+
Mix    SEPG  Moles 2.000E-1   1.370      72.620     12.320     6.480      1.250      2.790
7.700E-1 9.800E-1 7.600E-1 3.400E-1 1.000E-1   1.000E-2   0.000E+0   ;   293.500

Mix   SEPO  Moles 0.000E+0   0.000E+0   3.000E-2   1.800E-1   6.800E-1   3.800E-1   1.380
1.030   1.820      4.100      5.360      8.330      6.560      70.150     ;          293.500

Mix   Recm-oil  Moles  1.200E-1   8.300E-1   44.150     7.560      4.210      9.100E-1
2.240  8.700E-1   1.310  2.070   2.310  3.330  2.580  27.510 ;  293.500    99.170
--------------------------------------------------------------------
; CNV Lab-C10+
--------------------------------------------------------------------
; Gamma Distribution
GAMMA
Split      C10p       C10
Shape       9.100E-1
Bound      128  ;128.500
Average    293.500
Origin     5.33E-1
END

CONSERVE   Mass
```

```
RESTORE    Lab-C10+
MULTIPLY   Mass       of         C10p       in         SEPG       by         293.500
RESTORE    SCN-C35+
REPLACE    Gamma      Average    by         293.500
MIX        SEPG       1 Mole     SEPG

RESTORE    Lab-C10+
MULTIPLY   Mass       of         C10p       in         SEPO       by         293.500
RESTORE    SCN-C35+
REPLACE    Gamma      Average    by         293.500
MIX        SEPO       1 Mole     SEPO

RESTORE    Lab-C10+
MULTIPLY   Mass       of         C10p       in         Recm-oil   by         293.500
RESTORE    SCN-C35+
REPLACE    Gamma      Average    by         293.500
MIX        Recm-oil   1 Mole     Recm-oil

--------------------------------------------------------------------
; Global weight factors used in regression
--------------------------------------------------------------------
Define   satp     0.000E+0
Define   lrvol    0.000E+0
Define   lden     0.000E+0
Define   gden     0.000E+0
Define   gz       0.000E+0
Define   lvis     0.000E+0
Define   lvis-1   0.000E+0
Define   gvis     0.000E+0
Define   mr       0.000E+0
Define   gsg      0.000E+0
Define   comp     0.000E+0
Define   K30      0.000E+0
Define   gor      0.000E+0
Define   lden_vis 0.000E+0
Define   com-vis  0.000E+0
Define   x-co2    0 ; 1.000E+0
--------------------------------------------------------------------
; EXP GOR correction
--------------------------------------------------------------------
Restore    EOS-C35+

Variable   fg       6.15723e-01 ; 6.15171e-01    0.61515    0.61518   ; 6.17242e-01


; GOR correction -SEPG
Multiply   moles      of         N2         to         C35+       in         SEPG       by
fg
Mix        Recm-oil   1 Tank     SEPG       SEPO       1.000      TMOLE

Mix        Feed       Recm-oil   1.000      Mole
TEMP       130.000    C
Psat
CCE
Basis      1.000      mole
Press      Temp       GOR        WT
psia       F          scf/bbl
14.700     60.000     735.700    ?gor?
END

END

--------------------------------------------------------------------
; EXP CCE: Recm-oil
--------------------------------------------------------------------
Restore    EOS-C35+

Mix        Feed       Recm-oil   1.000      Mole
Temp       130.000    C
Pres       000    bara

CCE
ID         "CCE: Recm-oil"
Basis      1.000      Mole
Satp       242.000    bara       Weight   ?satp?
PRES  LSAT  GZ  K-C16-C22   K-C23-C34  K-C35+  K-C1  K-CO2 K-C2 K-C3  K-C4  K-C5 K-C6
```

```
bara       %
WT         0; ?lrvol?    ?gz?
           100.000
232.244    96.932
221.802    93.949
206.687    90.199
194.321    87.216
182.779    83.977
171.237    80.313
160.244    77.074
138.534    69.574
112.427    59.347
92.916     50.313
81.924     45.199

End

;DLE: Recm-oil

Restore    EOS-C35+

Mix        Feed       Recm-oil   1.000      Mole
Temp       130.000    C
Pres       0.000E+0   bara

DLE
ID         " ;DLE: Recm-oil"
Basis      1.480      bbl
Satp       242.000    bara       Weight     ?satp?
PRES       TEMP       MR         LVOL       LDEN       GSG        GZ         WT
bara       C          SCF        bbl        g/cc
WT         0.000E+0   ?mr?       ?lrvol?    ?lden?     ?gsg?      ?gz?
395.077    130.000               1.432
384.923    130.000               1.435
375.385    130.000               1.437
364.923    130.000               1.441
354.154    130.000               1.444
344.000    130.000               1.447
333.538    130.000               1.450
323.385    130.000               1.453
313.538    130.000               1.456
304.000    130.000               1.459
294.154    130.000               1.462
283.692    130.000               1.465
273.231    130.000               1.469
263.385    130.000               1.472
252.308    130.000               1.476
242.000    130.000               1.480      6.700E-1
232.000    130.000               1.457
221.846    130.000               1.433
206.462    130.000               1.405

;CCE: Recm-oil
Mix        Feed       Recm-oil   1.000      Mole
Temp       130.000    C
Pres       242.000    bara

CCE
ID         ";CCE: Recm-oil"
Basis      1.000      Mole
Satp       242.000    bara       Weight     ?satp?
PRES       DEN        LDEN
bara       g/cc       g/cc
WT         ?lden?
395.000    6.930E-1
375.000    6.903E-1
350.000    6.872E-1
325.000    6.839E-1
300.000    6.804E-1
275.000    6.761E-1
250.000    6.719E-1
242.000    6.705E-1
230.000    6.596E-1
220.000    6.501E-1
210.000    6.383E-1

END
```

```
--------------------------------------------------------------------
; EXP Swelling test Oil-CO2
--------------------------------------------------------------------
Restore    EOS-C35+

Mix        Feed       Recm-oil   1 Mole
Temp       130.450    C
Pres       250.38   bara   ; 250.380
Mix        Injectant  CO2

SWELL        ID         "CO2 swelling test"
Basis      1.000      Mole
Stg   Press     RMI     PSAT   LSAT  IFT    EQL  EQV LDens  Z-CO2  WT  ; CO2 mol. Injected
      bara              bara    %   dyne/cm          g/cc              ;
WT                     ?satp?   00
1.000       0.000E+0   242     100                                     ;     0.000E+0
2.000       3.780E-1   288     100                                     ;     9.600E-2
3.000       6.024E-1   317     100              CO2-36                 ;     1.530E-1
4.000       8.386E-1   340     100                                     ;     2.130E-1
5.000       1.437      387     100              CO2-57                 ;     3.650E-1
6.000       1.752      410     100              CO2-62  CO2-63         ;     4.450E-1
7.000       2.220      450     0                        CO2-67         ;     5.640E-1
End


Mix  CRIT-MIX  CO2-62  1  Mole

Variable  Fg-crit    9.93852e-01; 0.9985   0.995  0.999  ; 0.284514
Multiply       moles   of   N2  to  C35+    in  CRIT-MIX  by  Fg-crit
Mix  Feed  1 Tank  CRIT-MIX  CO2-67        1 TMOLE
TEMP  130.45  C
Pres  0  bara
CCE
ID  " Critical ponit"
Basis  1  mole
PRES  TEMP  K-C16-C22  K-C23-C34  K-C35+  K-C1  K-CO2 K-C2  K-C3  K-C4   K-C5     K-C6
bara   C
WT     0    ?K30?     ?K30?       ?K30? ?K30?  ?K30?  ?K30? ?K30? ?K30? ?K30?     ?K30?
     130.45   1         1          1    1      1       1     1     1      1         1
END

;CCE test Oil-CO2
Mix        Feed       CO2-36     1.000      Mole
Temp       130.450    C
Pres       0    bara

CCE
ID         "CCE-CO2-36"
Basis      1.000      Mole
Satp       317.000    bara       Weight     ?satp?
PRES       LSAT
bara       %
WT         ?lrvol?
           100.00
296.981    93.618
266.053    84.444
237.776    76.966
208.616    69.288
180.781    61.211
160.898    55.328
132.622    46.054
100.810    34.487
92.415     31.296
END



Mix        Feed       CO2-57     1.000      Mole
Temp       130.450    C
Pres       0    bara
CCE
ID         "CCE-CO2-57"
Basis      1.000      Mole
Satp       387.000    bara       Weight     ?satp?
PRES       LSAT
bara       %
WT         ?lrvol?
```

```
           100.000
376.735    89.238
346.122    74.170
321.020    68.431
298.980    64.126
272.041    58.984
251.224    54.918
219.388    49.178
201.633    45.112
181.429    40.807
156.327    34.469
129.388    27.653
END



Mix        Feed       CO2-62     1.000      Mole
Temp       130.450    C
Pres       0    bara
CCE
ID         "CCE-CO2-62"
Basis      1.000      Mole
Satp       410.000    bara       Weight     ?satp?
PRES       LSAT
bara       %
WT         ?lrvol?
           100.000
399        85.16
389        71.88
379        68.16
351        62.89
306        56.64
261        49.80
225        43.95
189        38.09
146        27.73
END



Mix        Feed       CO2-67     1.000      Mole
Temp       130.450    C
Pres       0    bara

CCE
ID         "CCE-CO2-67"
Basis      1.000      Mole
Satp       450.000    bara       Weight     ?satp?
PRES       LSAT
bara       %
WT         ?lrvol?
           0.000E+0
449.6
445
423.404    31.101
405.728    45.639
399.100    48.194
383.633    50.573
359.329    50.308
335.025    48.811
307.774    47.577
266.530    42.731
247.381    40.529
212.766    35.595
174.468    29.075
152.373    25.463
106.710    16.212
93.453     13.480
END

Restore   EOS-C35+
Mix   Feed   CO2   1 Mole
Temp   130.45   C
Pres   450   bara
Mix    Injectant    Recm-oil

SWELL   ID   "CO2 swelling test"
```

```
Basis   1   Mole
Stg   Press   RMI    Psat  LSAT     IFT       EQV       Dens   Z-CO2  WT
      bara           bara   %     dyne/cm             g/cc
WT             0    ?satp?  1
1     450    0.000          0                                         0
2            0.058          0                 CO2-95                  0
3            0.143    605   0                 CO2-87
4            0.319    516   0                 CO2-75
End
```

```
Mix        Feed       CO2-87     1.000      Mole
Temp       130.450    C
Pres       0    bara
CCE
ID         "CCE-CO2-87"
Basis      1.000      Mole
Satp       605.000    bara       Weight   0; ?satp?
PRES      LSAT
bara       %
WT       ?lrvol?
         0.000
502      3.70
483      5.07
454      7.02
401      9.94
362      11.31
317      12.87
269      13.65
241      12.87
210      11.50

END
```

```
Mix        Feed       CO2-75     1.000      Mole
Temp       130.450    C
Pres       0    bara
CCE
ID         "CCE-CO2-75"
Basis      1.000      Mole
Satp       516.000    bara       Weight   0 ; ?satp?
PRES      LSAT
bara       %
WT       ?lrvol?
           0.000
469       12.09
446       19.49
398       27.10
355       30.60
318       31.58
283       30.80
243       27.88
212       25.15
184       21.83
173       20.47
112       12.28
END
```

```
Mix        Feed       CO2-95     1.000      Mole
Temp       130.450    C
Pres       0    bara
CCE
ID         "CCE-CO2-95"
Basis      1.000      Mole
Satp       320.000    bara       Weight    0; ?satp?
PRES      LSAT
bara       %
WT         ?lrvol?
          0.000
318       1.36
291       1.75
252       2.53
225       2.34
203       2.73
```

```
182       2.53
END


--------------------------------------------------------------------
; EXP Viscosity
--------------------------------------------------------------------
Restore    EOS-C35+

Mix        Feed       Recm-oil   1.000      Mole
Temp       130.000    C
Pres       300.000    bara

DLE
ID         "Viscosity-Recm-oil"
Basis      1.000      Mole
Satp       242.000    bara       Weight     0.000E+0
PRES       TEMP       LVIS       LDEN       GDEN    GMDens      LMDens     ; Weight
bara       C          cp         g/cc       g/cc   gmol/cm3    gmol/cm3
WT         0.000E+0   ?lvis-1?     ?lden?
300.000    130.000    3.500E-1   6.800E-1

END
--------------------------------------------------------------------
; Creating mixtrure for Viscosity Experiment
--------------------------------------------------------------------
Restore    EOS-C35+
 Variable   fg-6    5.20019e-02  ;   0.000E+0   1.000 ;  5.18564e-02
 Variable   fg-11   1.10495e-01  ;   0.000E+0   1.000 ;  1.10359e-01
 Variable   fg-17   1.71006e-01  ;   0.000E+0   1.000 ;  1.70879e-01
 Variable   fg-27   2.65806e-01  ;   0.000E+0   1.000 ;  2.65693e-01
 Variable   fg-46   4.87789e-01  ;   0.000E+0   1.000 ;  4.90852e-01
 Variable   fg-58   6.63342e-01  ;   0.000E+0   1.000 ;  6.67081e-01
 Variable   fg-65   8.29761e-01  ;   0.000E+0   1.000 ;  8.41806e-01


 Mix  CO2-6 CO2
 Multiply   moles      of         CO2        in         CO2-6       by         fg-6
 Mix        CO2-6   1 Tank     CO2-6       Recm-oil       1.000      TMOLE

 Mix        Feed       CO2-6      1.000      Mole
 Temp       130.000    C
 Pres       300.000    bara
 DLE        ID         "Viscosity-CO2-6"
 Basis      1.000      Mole
 PRES       TEMP       LVIS       LDEN         X-CO2
 bara       C          cp         g/cc
 WT         0.000E+0   ?lvis?   ?lden_vis?   ?x-co2?
300.000    130.000    3.300E-1   6.650E-1     0.06

End


 Mix  CO2-11.8 CO2
 Multiply   moles      of         CO2        in         CO2-11.8       by         fg-11
 Mix        CO2-11.8   1 Tank     CO2-11.8       Recm-oil       1.000      TMOLE

 Mix        Feed       CO2-11.8      1.000      Mole
 Temp       130.000    C
 Pres       300.000    bara
 DLE        ID         "Mixture of X-CO2 = 11.8"
 Basis      1.000      Mole
 PRES       TEMP       LVIS       LDEN         X-CO2
 bara       C          cp         g/cc
 WT         0.000E+0   ?lvis?  ?lden_vis?  ?x-co2?
300.000    130.000    3.100E-1   0.650     0.118

End


 Mix  CO2-17.8 CO2
 Multiply   moles      of         CO2        in         CO2-17.8       by         fg-17
 Mix        CO2-17.8   1 Tank     CO2-17.8       Recm-oil       1.000      TMOLE

 Mix        Feed       CO2-17.8      1.000      Mole
 Temp       130.000    C
 Pres       300.000    bara
```

```
 DLE        ID         "Mixture of X-CO2 = 17.8"
 Basis      1.000      Mole
 PRES       TEMP       LVIS       LDEN         X-CO2
 bara       C          cp         g/cc
 WT         0.000E+0   ?lvis?  ?lden_vis?    ?x-co2?
300.000    130.000    2.800E-1   0.635        0.178

End


 Mix  CO2-27.2 CO2
 Multiply   moles      of         CO2        in         CO2-27.2       by         fg-27
 Mix        CO2-27.2   1 Tank     CO2-27.2       Recm-oil       1.000      TMOLE

 Mix        Feed       CO2-27.2      1.000      Mole
 Temp       130.000    C
 Pres       300.000    bara
 DLE        ID         "Mixture of X-CO2 = 27.2"
 Basis      1.000      Mole
 PRES       TEMP       LVIS       LDEN         X-CO2
 bara       C          cp         g/cc
 WT         0.000E+0   ?lvis?   ?lden_vis?   ?x-co2?
300.000    130.000    1.800E-1   0.612        0.272

End


 Mix  CO2-46.8 CO2
 Multiply   moles      of         CO2        in         CO2-46.8       by         fg-46
 Mix        CO2-46.8   1 Tank     CO2-46.8       Recm-oil       1.000      TMOLE

 Mix        Feed       CO2-46.8      1.000      Mole
 Temp       130.000    C
 Pres       300.000    bara
 DLE        ID         "Mixture of X-CO2 = 11.8"
 Basis      1.000      Mole
 PRES       TEMP       LVIS       LDEN         X-CO2
 bara       C          cp         g/cc
 WT         0.000E+0   ?lvis-1?   ?lden_vis?   ?x-co2?
300.000    130.000    2.400E-1   0.624        0.468

End


 Mix  CO2-58.1 CO2
 Multiply   moles      of         CO2        in         CO2-58.1       by         fg-58
 Mix        CO2-58.1   1 Tank     CO2-58.1       Recm-oil       1.000      TMOLE

 Mix        Feed       CO2-58.1      1.000      Mole
 Temp       130.000    C
 Pres       300.000    bara
 DLE        ID         "Mixture of X-CO2 = 58.1"
 Basis      1.000      Mole
 PRES       TEMP       LVIS       LDEN         X-CO2
 bara       C          cp         g/cc
 WT         0.000E+0   ?lvis?   ?lden_vis?   ?x-co2?
300.000    130.000    2.900E-1   0.735        0.581

End


 Mix  CO2-65.9 CO2
 Multiply   moles      of         CO2        in         CO2-65.9       by         fg-65
 Mix        CO2-65.9   1 Tank     CO2-65.9       Recm-oil       1.000      TMOLE

 Mix        Feed       CO2-65.9      1.000      Mole
 Temp       130.000    C
 Pres       300.000    bara
 DLE        ID         "Mixture of X-CO2 = 65.9"
 Basis      1.000      Mole
 PRES       TEMP       LVIS       LDEN         X-CO2
 bara       C          cp         g/cc
 WT         0.000E+0   ?lvis-1?   ?lden_vis?    ?x-co2?
300.000    130.000    3.700E-1   0.759         0.659

End
```

```
Mix Feed CO2
Temp 130 C
Pres 450 bara
CCE
Pres  Temp  GDens  LDens  Dens  Lvis   Vis   GMDens      LMDens
bara   C    g/cc   g/cc   g/cc   cp    cp   gmol/cm3    gmol/cm3
WT     0     0      0
450   130   0.7    0.7
300   130
 End

Mix        Feed       Recm-oil   1.000      Mole

Temp       130.000    C
Pres       300.000    bara
Mix  Solvent CO2
MMP  50
;MMP 100
;MMP 500

END
```

Input Data Set Used to Model Haft Kel Matrix-Fracture System (without Diffusion) in Chapter 6

Base case SENSOR input data set

```
TITLE
  Haft kel simulation without diffusion
  Half block model
  11 Component EOS
  Base:
   - A1 : Nx  = 10
   - B1 : Nz  = 50
   - C1 : Kma = 0.8 md
   - D1 : Hma = 8 ft
   - E1 : Pinit = 1400 psia
   - F1 : Inj gas = Eq gas
   - G1 : No blocKs = 1
   - H1 : Displacement=2D
ENDTITLE

C ------------------------------------------------------------------------------------------
C Dimension and Solution Options
C ------------------------------------------------------------------------------------------

GRID  10 1 50

CPU

IMPLICIT

MAPSPRINT 1  SO P GG GO TENS X Y TENS TX TZ PCGO    ! Initialization output

C ---------------------------------------------------------------------------------------
C Grid Block Properties
C ---------------------------------------------------------------------------------------
DELX XVAR
 9*0.4444444 0.01
DELY CON
 8
DEPTH CON
 1000
THICKNESS ZVAR
 0.01 48*0.166667 0.01
KX CON
  100000
MOD
 1 9  1 1  2 49  = 0.8
KY EQUALS KX
KZ EQUALS KX
POROS CON
  1.
MOD
 1 9  1 1  2 49  = 0.10

C -----------------------------------------------------------------------------------------
C Regions: Region 1 = Matrix, Region 2 = Fracture
C -----------------------------------------------------------------------------------------
ROCKTYPE CON           ! Rock (saturation table) regions
  2
MOD
 1 9  1 1  2 49  = 1
REGION CON             ! Initialization regions
  2
MOD
 1 9  1 1  2 49  = 1
INITREG CON            ! Fluid in place regions
  2
MOD
 1 9  1 1  2 49  = 1

C -----------------------------------------------------------------------------------------
C Rel-perm and capillary pressure data
C -----------------------------------------------------------------------------------------
! Rock type 1 (Matrix)
KRANALYTICAL 1
 0.2  0.2  0.2  0.05              ! Swc  Sorw  Sorg  Sgc
 1.0  0.653  1                    ! krw(Sorw)  krg(Swc)  kro(Swc)
 2.0  2.0  1.3  3.98              ! nw now ng nog
 0.397 4.166 1.079 PCGO           ! c1 c2 c3 gas-oil

! Rock type 2 (Fracture, Pc = 0)
KRANALYTICAL 2
```

```
 0.0  0.0  0.0  0.0              ! Swc  Sorw  Sorg  Sgc
 1.0  1.0  1.0                   ! krw(Sorw)  krg(Swc)  kro(Swc)
 1.0  1.0  1.0  1.0              ! nw now ng nog

! Interfacial tension scaling
TENSION  10  30                  ! ref_tension, max_tension

C ---------------------------------------------------------------------------------------
C Fluid PVT data
C ---------------------------------------------------------------------------------------
PVTEOS SRK
110                              ! Reservoir temperature deg F

CPT          PC    TC       MW      AC       SHIFT   ZCRIT     PCHOR   OMEGA       OMEGB
C          psia        R
N2        492.84  227.16   28.014  0.03700 -0.00090 0.29178    59.10  0.4274700  0.0866400
CO2      1069.51  547.42   44.010  0.22500  0.21749 0.27433    80.00  0.4274700  0.0866400
H2S      1299.97  672.12   34.082  0.09000  0.10153 0.28292    80.10  0.4274700  0.0866400
C1        667.03  343.01   16.043  0.01100 -0.00247 0.28620    71.00  0.4274700  0.0866400
C2        706.62  549.58   30.070  0.09900  0.05894 0.27924   111.00  0.4274700  0.0866400
C3        616.12  665.69   44.097  0.15200  0.09075 0.27630   151.00  0.4274700  0.0866400
C4-C6     527.88  840.66   70.433  0.21405  0.09829 0.27403   216.05  0.4274802  0.0866404
C7-C14    411.95 1147.73  136.819  0.35302  0.09872 0.29826   384.35  0.4274802  0.0866404
C15-C21   283.74 1395.61  239.679  0.60452  0.13147 0.29826   657.60  0.4274801  0.0866403
C22-C29   225.55 1546.43  341.306  0.81842  0.12980 0.29826   855.51  0.4274801  0.0866404
C30+      184.60 1692.33  487.101  1.06576  0.09103 0.29826  1062.75  0.4274810  0.0866404

BIN
0.00000 0.00000 0.02500 0.01000 0.09000 0.10401 0.11000 0.11000 0.11000 0.11000
        0.12000 0.10500 0.13000 0.12500 0.11541 0.11500 0.11500 0.11500 0.11500
                0.08000 0.07000 0.07000 0.05436 0.05000 0.05000 0.05000 0.05000
                        0.00000 0.00000 0.00000 0.00000 0.00000 0.00000 0.00000
                                0.00000 0.00000 0.00000 0.00000 0.00000 0.00000
                                        0.00000 0.00000 0.00000 0.00000 0.00000
                                                0.00000 0.00000 0.00000 0.00000
                                                        0.00000 0.00000 0.00000
                                                                0.00000 0.00000
                                                                        0.00000

C ----------------------------------------------------------------------------
C Initialisation
C ----------------------------------------------------------------------------

INITIAL 1
!depth psat   N2     CO2    H2S    C1    C2    C3   C4-C6  C7-C14  C15-C21 C22-C29  C30+
DEPTH
1000 1406 0.000936 0.004250 0.012956 0.295681 0.049689 0.050642 0.128152 0.334292 0.088677
0.026569 0.008156
PINIT  1406
ZINIT  1000

INITIAL  2
!depth psat   N2     CO2    H2S    C1    C2    C3   C4-C6  C7-C14  C15-C21 C22-C29  C30+
DEPTH
1000 1406 0.00753 0.00645 0.00820 0.89991 0.04511 0.02012 0.01169 0.00098 0.000 0.000 0.000
PINIT  1406
ZINIT  1000
ENDINIT

MODIFY PV
 10 10  1 1 2 49 * 1E8    ! Vertical fracture
 1  10  1 1 1 1 * 1E8        ! Top fracture
 1  10  1 1  50 50 * 1E8   ! Bottom fracture

C ---------------------------------------------------------------------------------------
C Output specifications
C ---------------------------------------------------------------------------------------
! PSM
MAPSFREQ 1
MAPSFILE  SAT SG SO TENS GO GG
MAPSFILEFREQ 1    ! maps written to fort.71

C         days    freq
TIME      3650     30
TIME      5000    100
TIME      10000   300
END
```

Input Data Set Used to Model Haft Kel Matrix-Fracture System (with Diffusion) in Chapter 7

Base case ECLIPSE 300 input data set

```
RUNSPEC

--  Using Haft Kel rock type and matrix dimension
--  Half block model
--  11 Component EOS
--  Diff-f2g3h2-ecl:
--    - A1 : Nx  = 10
--    - B1 : Nz  = 100
--    - C1 : Kma = 0.8 md
--    - D1 : Matrix Dim. = 8x8 ft
--    - E1 : Pinit = 1000 psia
--    - F1 : Inj gas = CO2 gas
--    - G3 : Diffusion = Chemical potential
--    - H2 : Fluid = Haft Kel

MESSAGES
8* 100000 /


--IMPES
FULLIMP

DIMENS
   11    1    102  /

-- Phases present
WATER
OIL
GAS

OPTIONS3
--switch 4        19     26    68    74
4*       14*  0  6*  2  41* 1  5* 1 /


--Enables molecular diffusion
DIFFUSE

-- Units
FIELD

-- Define Component in EOS
COMPS
11   /

REGDIMS
-- Max.FIPREG  FIPREG
     2          2     0    2/

TABDIMS
--No.sat.tab  No.pvt.tab  max.sat.nods  max.sat.nods  Max.FIPREG
2              1             50           50            2/

EQLDIMS
----Eqrgn  Deptab
  2      50    /

WELLDIMS
5  20  3*  20/

MISCIBLE
/
RSSPEC

FMTOUT

-- To unified output files
UNIFOUT

GRID     ===============================================================

--Requests output of an INIT file (Need for FloViz)
INIT

RPTGRID
DX DZ PERMR PERMZ PORO PORV TRANR  TRANZ NNC /
```

```
MINPORV
0.000000001/
--  SPECIFY GRID BLOCK DIMENSIONS IN THE R DIRECTION
DXV
10*0.4 0.01  / ft
DYV
 8.0/
DZV
0.01 100*0.08 0.01  / FT

EQUALS
  TOPS      10000     1 11 1 1 1 1 /
  PORO      1.0       1 11 1 1 1 102   /     Fracture porosity
  PORO      0.10      1 10 1 1 2 101   /     Martix porosity
  PERMX     100000    1 11 1 1 1 102 /       Fracture permeabiliy
  PERMX     0.8       1 10 1 1 2 101  /       Martix permeabiliy
/
COPY
      'PERMX'    'PERMY'  /
      'PERMX'    'PERMZ'   /
/
GRIDFILE
2 /
PROPS    ==============================================================
MESSAGES
8* 100000 /
EOS
SRK /
-- Reservoir temperatures Deg F
RTEMP
 110  /
CNAMES
N2   CO2   H2S   C1   C2   C3   C4-C6   C7-C14   C15-C21   C22-C29   C30+   /

-- Critical temperatures Deg R
TCRIT
227.16  547.42  672.12  343.01  549.58  665.69  840.66  1147.73  1395.61  1546.43  1692.33 /

-- Critical pressures psia
PCRIT
492.84  1069.51  1299.97  667.03  706.62  616.12  527.88  411.95  283.74  225.55  184.6   /

-- Critical Z-factors
ZCRIT
0.29178 0.27433 0.28292 0.2862 0.27924 0.2763 0.27403 0.25616 0.23658 0.22253 0.20718 /


ZCRITVIS
0.29178 0.27433 0.28292 0.2862 0.27924 0.2763 0.27403 0.29826 0.29826 0.29826 0.29826 /


-- 3-Parameter EoS Shift Coefficients
SSHIFT
-0.0009 0.21749 0.10153  -0.00247 0.05894 0.09075 0.09829 0.09872 0.13147 0.1298 0.09103 /

-- Acentric factors
ACF
0.037  0.225  0.09  0.011  0.099  0.152  0.21405  0.35302  0.60452  0.81842  1.06576 /

-- Molecular Weights
MW
28.014  44.01  34.082  16.043  30.07  44.097  70.433  136.819  239.679  341.306  487.101  /

-- Parachors (Dynes/cm)
PARACHOR
59.1   80   80.1   71   111   151   216.05   384.35   657.6   855.51   1062.75  /

-- Binary Interaction Coefficients
BIC
0.00000
0.00000   0.12000
0.02500   0.10500   0.08000
0.01000   0.13000   0.07000   0.0000
0.09000   0.12500   0.07000   0.0000  0.0000
0.10401   0.11541   0.05436   0.0000  0.0000  0.0000
0.11000   0.11500   0.05000   0.0000  0.0000  0.0000   0.0000
0.11000   0.11500   0.05000   0.0000  0.0000  0.0000   0.0000  0.0000
```

```
0.11000   0.11500   0.05000   0.0000  0.0000  0.0000   0.0000  0.0000   0.0000
0.11000   0.11500   0.05000   0.0000  0.0000  0.0000   0.0000  0.0000   0.0000   0.0000  /

--Interfacial tension scaling
MISCSTR
--ref_tension, max_tension
10   30  107/
-- (IFT/IFT.ref)^n in rel perm.; n=MISCEXP
MISCEXP
0/

SGOF
--Sg        Krg        Krog      Pcog
  0.0      0.0        1.0        0.0
  0.01     0.0        0.99       0.0
  0.1      0.1        0.9        0.0
  0.2      0.2        0.8        0.0
  0.3      0.3        0.7        0.0
  0.4      0.4        0.6        0.0
  0.5      0.5        0.5        0.0
  0.6      0.6        0.4        0.0
  0.7      0.7        0.3        0.0
  0.8      0.8        0.2        0.0
  0.9      0.9        0.1        0.0
  1.0      1.0        0.0        0.0  / table 1 (fracture)
  0.0000    0.0000    1.0000     0.397
  0.0400    0.0000    0.7599     0.561
  0.0500    0.0000    0.7073     0.606
  0.1200    0.0448    0.4114     0.935
  0.1600    0.0806    0.2910     1.131
  0.2000    0.1206    0.1991     1.330
  0.2400    0.1640    0.1309     1.533
  0.2800    0.2102    0.0819     1.739
  0.3200    0.2589    0.0482     1.947
  0.3600    0.3099    0.0261     2.157
  0.4000    0.3629    0.0126     2.369
  0.4400    0.4177    0.0052     2.583
  0.4800    0.4742    0.0017     2.798
  0.5200    0.5323    0.0003     3.014
  0.5600    0.5919    0.0000     3.232
  0.6000    0.6530    0.0000     3.451
  0.6400    0.7154    0.0000     3.672
  0.6800    0.7791    0.0000     3.893
  0.7200    0.8440    0.0000     4.115
  0.7600    0.9101    0.0000     4.339
  0.8000    1.0000    0.0000     4.563    / table 2 (Matrix)

SWOF
--Sw        Krw        Krow      Pcow
  0.0      0.0        1.0        0
  0.01     0.0        0.99       0
  0.1      0.1        0.9        0.0
  0.2      0.2        0.8        0
  0.3      0.3        0.7        0
  0.4      0.4        0.6        0
  0.5      0.5        0.5        0
  0.6      0.6        0.4        0
  0.7      0.7        0.3        0
  0.8      0.8        0.2        0.0
  0.9      0.9        0.1        0.0
  1.0      1.0        0.0        0.0          / table 1 (fracture)
  0.2000    0.0000    1.0000     0.000
  0.2400    0.0044    0.8711     0.000
  0.2800    0.0178    0.7511     0.000
  0.3200    0.0400    0.6400     0.000
  0.3600    0.0711    0.5378     0.000
  0.4000    0.1111    0.4444     0.000
  0.4400    0.1600    0.3600     0.000
  0.4800    0.2178    0.2844     0.000
  0.5200    0.2844    0.2178     0.000
  0.5600    0.3600    0.1600     0.000
  0.6000    0.4444    0.1111     0.000
  0.6400    0.5378    0.0711     0.000
  0.6800    0.6400    0.0400     0.000
  0.7200    0.7511    0.0178     0.000
  0.7600    0.8711    0.0044     0.000
  0.8000    1.0000    0.0000     0.000
```

```
  0.8400    1.0000    0.0000     0.000
  0.8800    1.0000    0.0000     0.000
  0.9200    1.0000    0.0000     0.000
  0.9600    1.0000    0.0000     0.000
  1.0000    1.0000    0.0000     0.000      / table 2 (Matrix)


FACTLI
1  0.9/

DIFFAGAS
-- N2     CO2     H2S     C1      C2      C3      C4-C6  C7-C14  C15-C21  C22-C29  C30+
(field units: 1 cm2/s = 92.9979 ft2/Day)
0.02180 0.01598 0.01579 0.01459 0.01508 0.01191 0.00908  0.00611  0.00427 0.00343 0.00279/


DIFFAOIL
-- N2     CO2     H2S     C1      C2      C3      C4-C6  C7-C14  C15-C21  C22-C29  C30+     -
--(field units: 1 cm2/s = 92.9979 ft2/Day)
0.00034 0.00023 0.00023 0.00032 0.00023 0.00017 0.00012 0.00010 0.00006 0.00005 0.00004/

REGIONS    ============================================================
-- Regoin 2= Matrix
-- Regoin 1= Fracture
EQUALS
FIPNUM 1   / Fliud In Place reg. no.
FIPNUM 2  1 10 1 1 2 101 / Fliud In Place reg. no.
SATNUM 1   / Saturation reg. no.
SATNUM 2  1 10 1 1 2 101 / Saturation reg. no.
EQLNUM 1   /
EQLNUM 2  1 10 1 1 2 101 /
/

SOLUTION ============================================================
DATUMR
10000.0 10000.01 /
PRESSURE
1122*1000 /
EQUALS
SWAT  0/
SWAT  0.2  1 10 1 1 2 101/
SOIL  0.0/
SOIL  0.8  1 10 1 1 2 101/
/
--N2     CO2     H2S     C1      C2      C3      C4-C6  C7-C14  C15-C21  C22-C29  C30+
NEI
0.0000  1.0000  0.0000  0.0000  0.0000  0.0000  0.0000  0.0000  0.0000  0.0000  0.0000/
0.000430 0.003867 0.013348 0.221131 0.049395 0.054161 0.142768 0.376053 0.099776 0.029894
0.009177 /

RPTSOL
PRESSURE  SOIL SGAS PSAT XMF YMF ZMF/

RPTRST
 BASIC=2 SOIL PCOG/


SUMMARY ============================================================
MESSAGES
8* 100000 /
--data be written to the Summary file only at report time
RPTONLY
--ALL
FOPR
FOPT
FGPT
FPR

ROSAT
/
ROIP
/
ROIPL
/

WBHP
/
```

```
WGPR
/
WGIR
/

RUNSUM
EXCEL

SCHEDULE ============================================================
-------- THE SCHEDULE SECTION DEFINES THE OPERATIONS TO BE SIMULATED
-----------------------------------------------------------------------
MESSAGES
8* 100000 /

WELSPECS
PROD Field 1 1 1* GAS /
GINJ Field 1 1 1* GAS /
/
-- defining gas injection composition
WELLSTRE
--well St.name  N2  CO2   H2S    C1   C2   C3  C4-C6  C7-C14  C15-C21  C22-C29   C30+
--EQV 0.00497991 0.00730661 0.00982485 0.89132114 0.05203481 0.02252617 0.0113755
--0.00063026   0.00000075  0.0000       0.0000 /
CO2-gas 0.0000 1.0000 0.0000 0.0000 0.0000 0.0000 0.0000 0.0000 0.0000 0.0000 0.0000/
 /

COMPDAT
--Well name  I  J   K1  K2   Status   SatTable   PI
PROD        1  1   102  102  OPEN  1      100  /
PROD        2  1   102  102  OPEN  1      100  /
PROD        3  1   102  102  OPEN  1      100  /
PROD        4  1   102  102  OPEN  1      100  /
PROD        5  1   102  102  OPEN  1      100  /
PROD        6  1   102  102  OPEN  1      100  /
PROD        7  1   102  102  OPEN  1      100  /
PROD        8  1   102  102  OPEN  1      100  /
PROD        9  1   102  102  OPEN  1      100  /
PROD        10 1   102  102  OPEN  1      100  /
PROD        11 1   102  102  OPEN  1      100  /
GINJ        1  1   1    1    OPEN  1      100  /
GINJ        2  1   1    1    OPEN  1      100  /
GINJ        3  1   1    1    OPEN  1      100  /
GINJ        4  1   1    1    OPEN  1      100  /
GINJ        5  1   1    1    OPEN  1      100  /
GINJ        6  1   1    1    OPEN  1      100  /
GINJ        7  1   1    1    OPEN  1      100  /
GINJ        8  1   1    1    OPEN  1      100  /
GINJ        9  1   1    1    OPEN  1      100  /
GINJ        10 1   1    1    OPEN  1      100  /
GINJ        11 1   1    1    OPEN  1      100  /
/



WCONPROD
--Wellname   status  control  oil-s.rate  wat-s.rate  gas-s.rate  liq-s.rate  res.rate    BHP
--Unit                         stb/d       stb/d       Mscf/d       stb/d      rbbl/d
psia
PROD         OPEN     BHP       2*                      50.00         2*
1000.50/  GRAT
/

WCONINJE
--Wellname  type  status  control  Surf.rate  res.rate    BHP
--Unit                              Mscf/d     rbbl/d     psia
GINJ        GAS   OPEN     RATE      3.0          1*    100000.0/
/

WINJGAS
-- Well name   Stream  Stream name
GINJ           STREAM     CO2-gas/
/

-- Creat Restart file
RPTRST
 BASIC=2  SOIL/
```

```
RPTPRINT
8*/

RPTSCHED
'CPU=1'   'FIP=3'   'SOIL' PRES 'WELLS=5'   PSAT  PCOG  STEN   'ZMF'  XMF YMF   DENG DENO   /
IFTGO KRO KRG  MULT

--TUNING
--8* /
--4*  /
--2*  200000 /

TSCRIT
--ini  min   max
0.001 0.001   /0.2

--TSTEP
--5*1 /

TSTEP
12*10 68*10   34*50  60*100 60*100 55*100  30*1000 / 2000 days


END
```

Input Data Set Used to Model Laboratory System with Synthetic C_1-C_5 mixture (with Diffusion) in Chapter 7

Base case ECLIPSE 300 input data set

```
RUNSPEC

--  Using Haft kel rock type and matrix dimension
--  Lab model
--  4 Component EOS
--  Diff-d2f2g3-ecl:
--   - A1 : Nx  = 10
--   - B1 : Nz  = 100
--   - C1 : Kma = 0.8 md
--   - D2 : Matrix Dim. = 0.2x2 ft
--   - E1 : Pinit = 1000 psia =68.05 atma
--   - F2 : Inj gas = CO2 gas
--   - G3 : Diffusion = Chemical potential

FULLIMP
DIMENS
   11    1    102  /

-- Phases present
WATER
OIL
GAS

OPTIONS3
--switch 19    21     26     46   68    74
 18*     0  1* 200 4*  2  19* 200 21* 1  5* 1 /

--Enables molecular diffusion
DIFFUSE

CART
-- Units
--FIELD
LAB

-- Define Compnent in EOS
COMPS
4   /

REGDIMS
-- Max.FIPREG  FIPREG
     2          2     0    2/

TABDIMS
--No.sat.tab  No.pvt.tab  max.sat.nods  max.sat.nods  Max.FIPREG
2              1             50           50            2/

EQLDIMS
----Eqrgn  Deptab
  2      50    /

WELLDIMS
5  20  3*  20/

MISCIBLE
/

RSSPEC
FMTOUT
-- To unified output files
UNIFOUT

GRID     ===============================================================
--Requests output of an INIT file (Need for FloViz)
INIT

RPTGRID
DX DZ PERMR PERMZ PORO PORV TRANR  TRANZ NNC /

MINPORV
0.000000001/


--  SPECIFY GRID BLOCK DIMENSIONS IN THE R DIRECTION
DXV
10*0.3048 0.3048  / cm
DYV
```

```
 6.096/
DZV
0.3048 100*0.6096 0.3048   / cm
EQUALS
  TOPS      1         1 11 1 1 1 1 /
  PORO      1.0       1 11 1 1 1 102   /     Fracture porosity
  PORO      0.10      1 10 1 1 2 101   /     Martix porosity
  PERMX     100000    1 11 1 1 1 102 /       Fracture permeabiliy
  PERMX     0.8       1 10 1 1 2 101  /       Martix permeabiliy
/
COPY
      'PERMX'    'PERMY'  /
      'PERMX'    'PERMZ'   /
/
GRIDFILE
2 /

PROPS    ==============================================================
EOS
SRK /
-- Reservoir temperatures Deg C
RTEMP
 85  /

CNAMES
C1    C5  CO2  N2    /

-- Critical temperatures Deg K
TCRIT
    190.56       470.14       304.12       126.20          /

-- Critical pressures atma
PCRIT
   45.3886       34.2407       72.7757       33.5357          /

-- Critical Z-factors
ZCRIT
      0.2862       0.27119       0.27433       0.29178       /

-- 3-Parameter EoS Shift Coefficients
SSHIFT
      -0.00247       0.11942       0.21749       -0.0009      /

-- Acentric factors
ACF
      0.011       0.22895       0.225       0.037      /

-- Molecular Weights
MW
     16.043       70.905       44.01       28.014        /

-- Parachors (Dynes/cm)
PARACHOR
    71       205.17       80       59.1       /

-- Binary Interaction Coefficients

BIC
 0.0
 0.12000       0.15000
 0.02000       0.08000       0.00000/

--Interfacial tension scaling
MISCSTR
--ref_tension, max_tension
10   30  114/

-- (IFT/IFT.ref)^n in rel perm.; n=MISCEXP
MISCEXP
0/

SGOF
--Sg        Krg        Krog      Pcog
  0.0      0.0        1.0        0
  0.01     0.0        0.99       0
  0.1      0.1        0.9        0.0
  0.2      0.2        0.8        0
```

```
  0.3      0.3        0.7        0
  0.4      0.4        0.6        0
  0.5      0.5        0.5        0
  0.6      0.6        0.4        0
  0.7      0.7        0.3        0
  0.8      0.8        0.2        0.0
  0.9      0.9        0.1        0.0
  1.0      1.0        0.0        0.0  / table 1 (fracture)
  0.0000    0.0000    1.0000     0.0270
  0.0400    0.0000    0.7599     0.0382
  0.0500    0.0000    0.7073     0.0412
  0.1200    0.0448    0.4114     0.0636
  0.1600    0.0806    0.2910     0.0770
  0.2000    0.1206    0.1991     0.0905
  0.2400    0.1640    0.1309     0.1043
  0.2800    0.2102    0.0819     0.1183
  0.3200    0.2589    0.0482     0.1325
  0.3600    0.3099    0.0261     0.1468
  0.4000    0.3629    0.0126     0.1612
  0.4400    0.4177    0.0052     0.1758
  0.4800    0.4742    0.0017     0.1904
  0.5200    0.5323    0.0003     0.2051
  0.5600    0.5919    0.0000     0.2199
  0.6000    0.6530    0.0000     0.2348
  0.6400    0.7154    0.0000     0.2499
  0.6800    0.7791    0.0000     0.2649
  0.7200    0.8440    0.0000     0.2800
  0.7600    0.9101    0.0000     0.2953
  0.8000    1.0000    0.0000     0.3105  /      table 2 (Matrix)

SWOF
--Sw        Krw        Krow      Pcow
  0.0      0.0        1.0        0
  0.01     0.0        0.99       0
  0.1      0.1        0.9        0.0
  0.2      0.2        0.8        0
  0.3      0.3        0.7        0
  0.4      0.4        0.6        0
  0.5      0.5        0.5        0
  0.6      0.6        0.4        0
  0.7      0.7        0.3        0
  0.8      0.8        0.2        0.0
  0.9      0.9        0.1        0.0
  1.0      1.0        0.0        0.0          / table 1 (fracture)
  0.2000    0.0000    1.0000     0.000
  0.2400    0.0044    0.8711     0.000
  0.2800    0.0178    0.7511     0.000
  0.3200    0.0400    0.6400     0.000
  0.3600    0.0711    0.5378     0.000
  0.4000    0.1111    0.4444     0.000
  0.4400    0.1600    0.3600     0.000
  0.4800    0.2178    0.2844     0.000
  0.5200    0.2844    0.2178     0.000
  0.5600    0.3600    0.1600     0.000
  0.6000    0.4444    0.1111     0.000
  0.6400    0.5378    0.0711     0.000
  0.6800    0.6400    0.0400     0.000
  0.7200    0.7511    0.0178     0.000
  0.7600    0.8711    0.0044     0.000
  0.8000    1.0000    0.0000     0.000
  0.8400    1.0000    0.0000     0.000
  0.8800    1.0000    0.0000     0.000
  0.9200    1.0000    0.0000     0.000
  0.9600    1.0000    0.0000     0.000
  1.0000    1.0000    0.0000     0.000      / table 2 (Matrix)


FACTLI
1  0.9/

DIFFAGAS
-- C1     C5      CO2        N2  (cm2/hr)
1.0505    1.0505    0.8087    0.000/

DIFFAOIL
-- C1     C5      CO2        N2  (cm2/hr)
0.07152    0.07152    0.05539    0.000/
```

```
REGIONS    ==============================================================
-- Regoin 2= Matrix
-- Regoin 1= Fracture
EQUALS
FIPNUM 1   / Fliud In Place reg. no.
FIPNUM 2  1 10 1 1 2 101 / Fliud In Place reg. no.
SATNUM 1   / Saturation reg. no.
SATNUM 2  1 10 1 1 2 101 / Saturation reg. no.
EQLNUM 1   /
EQLNUM 2  1 10 1 1 2 101 /
/

SOLUTION =============================================================
DATUMR
 1.0 1.01 /

PRESSURE
 1122*68.05 /  atma
EQUALS
 SWAT  0/
 SWAT  0.2  1 10 1 1 2 101/
 SOIL  0.0/
 SOIL  0.8  1 10 1 1 2 101/
 /

NEI
0.0000       0.0000       1.0000   0.0000/
0.27350364   0.72649636  0.0000  0.0000/

RPTSOL
PRESSURE  SOIL SGAS PSAT XMF YMF ZMF/

RPTRST
 BASIC=2 SOIL PCOG/

SUMMARY  =============================================================
--data be written to the Summary file only at report time
RPTONLY
--ALL
FOPR
FOPT
FGPT
FPR
ROSAT
/
ROIP
/
ROIPL
/
WBHP
/
WGPR
/
WGIR
/

RUNSUM
EXCEL

SCHEDULE =============================================================
-------- THE SCHEDULE SECTION DEFINES THE OPERATIONS TO BE SIMULATED
------------------------------------------------------------------------
WELSPECS
PROD Field 1 1 1* GAS /
GINJ Field 1 1 1* GAS /
/
-- defining gas injection composition
WELLSTRE
--well St.name  Z-C1      Z-nC7        Z-CO2    Z-N2
EQV         0.86284482   0.13715518   0.0000  0.0000/
CO2-gas     0.0000       0.0000       1.0000   0.0000 /
/

COMPDAT
--Well name  I  J   K1  K2   Status   SatTable   PI
PROD        1  1   102  102  OPEN  1      10000000  /
```

```
GINJ        1  1   1    1    OPEN  1      10000000  /
/

WCONPROD
--Wellname   status  control  oil-s.rate  wat-s.rate  gas-s.rate  liq-s.rate  res.rate    BHP
--Unit                         scc/hr       scc/hr       scc/hr      scc/hr    rcc/hr    atma
PROD      OPEN       BHP     2*                             2*                  600    68.05/
/

WCONINJE
--Wellname  type  status  control  Surf.rate  res.rate    BHP
--Unit                              scc/hr     rcc/hr    atma
GINJ        GAS   OPEN    RESV      1*           30     1000.00/
/

WINJGAS
-- Well name   Stream  Stream name
GINJ       STREAM   CO2-gas/
/

-- Creat Restart file
RPTRST
 BASIC=2  SOIL/

RPTPRINT
8*/

RPTSCHED
'CPU=1'   'FIP=3'   'SOIL' PRES 'WELLS=5'   PSAT  PCOG  STEN  KRO KRG 'ZMF'  XMF YMF    MULT
/  IFTGO

TUNING
8* /
4*  /
50 1*  2000 /

TSCRIT
--ini  min   max
0.05  0.05   0.05 /

TSTEP
50*2.4  /

END
```

Appendix B

Papers

Paper I

CO_2 EOR Potential in Naturally-Fractured Haft Kel Field, Iran

SPE Reservoir Evaluation and Engineering: 720-729. SPE-139528-PA

CO_2 EOR Potential in Naturally Fractured Haft Kel Field, Iran

Sayyed Ahmad Alavian, NTNU, and **Curtis H. Whitson,** SPE, NTNU/PERA

Summary

We present results studying the enhanced-oil-recovery (EOR) potential for carbon dioxide (CO_2) injection in the naturally fractured Haft Kel field, Iran, on the basis of detailed compositional simulations of a homogeneous single matrix block surrounded by fractures. Oil recoveries from CO_2 injection in this idealized model approach 90% for reservoir pressures of 1,400 psia and higher (i.e., at and above current reservoir pressure of 1,500–1,800 psia). It is expected that heterogeneity will reduce recovery on the field scale. This compares with 15–25% recoveries reported for gas-cap expansion and/or injection of hydrocarbon (HC) gas.

Fundamentally different recovery mechanisms develop above and below 2,000 psia, the pressure at which CO_2 density equals the reservoir-oil density. At lower pressures, CO_2 is less dense than reservoir oil and traditional gas/oil gravity segregation results, with a highly efficient process driven by gravity, compositional effects, and interfacial-tension (IFT) gradients that cause capillary-induced oil flow. At pressures greater than 2,000 psia, CO_2 density is greater than reservoir-oil density, resulting in an unusual gravity-drainage mechanism whereby CO_2 enters the bottom of a matrix block and pushes oil out the sides and top of the matrix block.

The effect of several key parameters has been studied in detail—matrix permeability, matrix-block size, matrix/matrix capillary continuity (stacked blocks), and the use of mixtures of CO_2 and HC gas. One of the key results is how the rate of recovery differs for combined injection of HC gas and CO_2, and how it varies for CO_2 injection for different model parameters.

EOR results are affected by grid sensitivity. Grid effects have been quantified and compared for different model parameters. Final EOR assessment is made using models in which sufficient grid refinement is used to minimize grid sensitivity.

Introduction

When an oil-saturated matrix block is surrounded by gas in the fracture, oil will drain from the matrix as a result of density difference between the gas and the oil. However, drainage can occur only if the matrix-block height is greater than the capillary-entry height.

The ultimate oil recovery from a single matrix block under gravity drainage depends on the balance between two forces: gravity, which is a direct function of the matrix-block height and the density difference between the two phases, and capillary force, which is a function of size distribution of matrix pores and pore throats and of IFT. Other factors not considered in this study also affect the ultimate oil recovery of fractured reservoirs, such as block-to-block continuity, molecular diffusion, regional pressure gradients, fracture orientation, and fracture flow/convection.

Most literature on gas injection in fractured reservoirs considers immiscible gas, and only a few treat miscible-gas injection in fractured reservoirs. Uleberg and Høier (2002) studied miscible HC gas injection in a fractured reservoir. They report high oil recovery caused by a capillary-driven mechanism. Tan and Firoozabadi (1995) and Jamshidnezhad (2004) studied first-contact-miscible recovery in fractured porous media using 1D modeling. The main purpose of this study is to investigate CO_2 recovery mechanisms in a naturally fractured reservoir.

Haft Kel field is located in the foothills of the Zagros Mountains, some 100 km east of Ahwaz city and on the east side of the Dezful embayment. The first oil well in Haft Kel was completed to a depth of 3,363 ft in 1928, with an initial production rate of approximately 5,700 STB/D. A field plateau rate of approximately 200,000 STB/D was maintained for several years, before the field was shut down from 1950 to 1954. Subsequently, production dropped to approximately 14,000 STB/D in 1976. HC (separator) gas injection was initiated in June 1976, at a rate of 400 MMscf/D, with oil production stopped for approximately 7 years between 1980 and 1987 to allow the oil column to build from 100 to 300 ft. Since 1987, the oil column and pressure have been held constant by gas injection, with a sustained oil rate of 35,000 STB/D adding an additional 100 million STB produced from 1987 through 1995 (Saidi 1996).

Description of Model

A single matrix block surrounded by fractures was used to study the matrix/fracture fluid exchange in a gravity/capillary recovery mechanism. Significant compositional variations develop within the matrix block, resulting in high recoveries.

The matrix block is initially filled with oil, and the fractures are initialized with injection gas. Zero capillary pressure and high permeability (100 darcies) of the fractures means that the viscous forces are negligible compared with gravity and capillary forces. We define a large pore volume (PV) for the fracture, to eliminate effects of model injection and production wells. The matrix block is always surrounded by injection gas, and produced oil from the matrix block always enters the fracture system. Conceptually, we are looking at a matrix block located at the no-flow boundary between an injector and a producer in which lateral pressure gradients are negligible.[1]

Haft Kel petrophysical properties and initial fluid compositions are taken from Saidi (1987). The matrix and the fracture dimensions and parameters are given in **Table 1.** Because of the matrix-block symmetry, only half of the matrix block is modeled. A 2D Cartesian grid is used where the matrix block is surrounded by two horizontal fractures at the top and bottom and one vertical fracture on the right side of the matrix block.

The reservoir simulator Sensor is used for all simulations. An 11-component tuned Soave-Redlich-Kwong (SRK) equation of state (EOS) describes phase and volumetric behavior; the Lorenz-Bray-Clark correlation, tuned to viscosity data, is used to calculate viscosities. EOS component properties and binary interaction parameters (BIPs) are given in **Tables 2 and 3,** respectively.

Pressure/volume/temperature (PVT) simulations needed to generate the EOS model from reported PVT data were made using PhazeComp. After tuning the EOS with black-oil properties reported by Saidi (1987), this PVT simulator was also used to generate saturated oil compositions for initializing the matrix block at pressures higher than and lower than the current reservoir pressure. Saturation pressure of the original oil composition was 1,400 psia. Constant-composition-expansion (CCE) experiments are simulated to determine oil compositions below 1,400 psia.[2] Special "swelling" tests were made to calculate oil composition

This paper (SPE 139528) was revised for publication from paper IPTC 10641, first presented at the International Petroleum Technology Conference, Doha, 21–23 November 2009 and revised for publication. Original manuscript received for review 24 August 2009. Revised manuscript received for review 8 April 2010. Paper peer approved 19 April 2010.

---

[1] Ringen et al. (2005) shows that this type of simulation model accurately represents reservoir-condition laboratory tests of gas gravity drainage for a carbonate core.

[2] Near-identical oil compositions result from CCE, differential liberation, and constant-volume tests or from depletion, which accounts for changing gas and oil mobilities.

TABLE 1—MATRIX AND FRACTURE FIXED DIMENSIONS AND PROPERTIES

Matrix width (*X*)	8 ft
Matrix length (*Y*)	8 ft
Vertical fracture width	0.01 ft
Horizontal fracture height	0.01 ft
Fracture permeability	100 darcies
Matrix porosity	10%
Fracture porosity	100%

at higher pressures: Incipient bubblepoint gas from a lower pressure was added to the bubblepoint oil to raise the bubblepoint pressure. This process was started at 1,400 psia and was repeated at 2,000, 2,500, and 3,000 psia. The 11-component compositions for the reservoir oils and equilibrium gases at different saturation pressures are given in **Tables 4 and 5,** respectively. Other details of the simulator models are given below.

Oil recovery factor (RF) is calculated from total average oil saturation S_o in the matrix block using the relation

$$\mathrm{RF} = \left(1 - \frac{S_o}{S_{oi}}\right). \qquad (1)$$

TABLE 2—FLUID PROPERTIES FOR THE 11-COMPONENT SRK CHARACTERIZATION

Component	MW	*Tc* (°R)	*Pc* (psia)	*ω*	Vshift	*Zc*	Parachor	Ω*a*
N_2	28.01	227.16	492.84	0.037	–0.001	0.29178	59.10	0.427
CO_2	44.01	547.42	1,069.51	0.225	0.217	0.27433	80.00	0.427
H_2S	34.08	672.12	1,299.97	0.090	0.102	0.28292	80.10	0.427
C_1	16.04	343.01	667.03	0.011	–0.002	0.2862	71.00	0.427
C_2	30.07	549.58	706.62	0.099	0.059	0.27924	111.00	0.427
C_3	44.10	665.69	616.12	0.152	0.091	0.2763	151.00	0.427
C_4–C_6	70.43	840.66	527.88	0.214	0.098	0.27403	216.05	0.427
C_7–C_{14}	136.82	1147.73	411.95	0.353	0.099	0.29826	384.35	0.427
C_{15}–C_{21}	239.68	1395.61	283.74	0.605	0.131	0.29826	657.60	0.427
C_{22}–C_{29}	341.31	1546.43	225.55	0.818	0.130	0.29826	855.51	0.427
C_{30+}	487.10	1692.33	184.60	1.06576	0.09103	0.29826	1062.75	0.427

TABLE 3—BICs FOR THE 11-COMPONENT SRK CHARACTERIZATION

	N_2	CO_2	H_2S	C_1	C_2	C_3	C_4–C_6	C_7–C_{14}	C_{15}–C_{21}	C_{22}–C_{29}
N_2	–									
CO_2	0.0000	–								
H_2S	0.0000	0.1200	–							
C_1	0.0250	0.1050	0.0800	–						
C_2	0.0100	0.1300	0.0700	0.0000	–					
C_3	0.0900	0.1250	0.0700	0.0000	0.0000	–				
C_4–C_6	0.1040	0.1154	0.0544	0.0000	0.0000	0.0000	–			
C_7–C_{14}	0.1100	0.1150	0.0500	0.0000	0.0000	0.0000	0.0000	–		
C_{15}–C_{21}	0.1100	0.1150	0.0500	0.0000	0.0000	0.0000	0.0000	0.0000	–	
C_{22}–C_{29}	0.1100	0.1150	0.0500	0.0000	0.0000	0.0000	0.0000	0.0000	0.0000	–
C_{30+}	0.1100	0.1150	0.0500	0.0000	0.0000	0.0000	0.0000	0.0000	0.0000	0.0000

TABLE 4—OIL COMPOSITION FOR THE 11-COMPONENT EOS AT DIFFERENT SATURATION PRESSURES

Component	1,000 psi	1,400 psi	2,000 psi	2,500 psi	3,000 psi
N_2	0.0004	0.0009	0.0019	0.0026	0.0033
CO_2	0.0039	0.0043	0.0046	0.0048	0.0050
H_2S	0.0133	0.0130	0.0122	0.0117	0.0113
C_1	0.2211	0.2957	0.3873	0.4524	0.5089
C_2	0.0494	0.0497	0.0490	0.0485	0.0481
C_3	0.0542	0.0506	0.0460	0.0427	0.0399
C_4–C_6	0.1428	0.1282	0.1105	0.0979	0.0871
C_7–C_{14}	0.3761	0.3343	0.2837	0.2478	0.2167
C_{15}–C_{21}	0.0998	0.0887	0.0752	0.0657	0.0574
C_{22}–C_{29}	0.0299	0.0266	0.0225	0.0197	0.0172
C_{30+}	0.0092	0.0082	0.0069	0.0060	0.0053

Tres = 110°F.

TABLE 5—EQUILIBRIUM-GAS COMPOSITION FOR THE 11-COMPONENT EOS AT DIFFERENT SATURATION PRESSURES

Component	1,000 psi	1,400 psi	2,000 psi	2,500 psi	3,000 psi
N_2	0.0050	0.0075	0.0106	0.0111	0.0110
CO_2	0.0073	0.0064	0.0058	0.0056	0.0055
H_2S	0.0098	0.0082	0.0072	0.0068	0.0068
C_1	0.8913	0.8999	0.9004	0.8967	0.8907
C_2	0.0520	0.0451	0.0409	0.0399	0.0399
C_3	0.0225	0.0201	0.0194	0.0198	0.0205
C_4–C_6	0.0114	0.0117	0.0137	0.0162	0.0190
C_7–C_{14}	0.0006	0.0010	0.0020	0.0037	0.0064
C_{15}–C_{21}	0.0000	0.0000	0.0000	0.0000	0.0001
C_{22}–C_{29}	0.0000	0.0000	0.0000	0.0000	0.0000
C_{30+}	0.0000	0.0000	0.0000	0.0000	0.0000

Capillary pressure and relative permeability are taken from Saidi (1987) and were fit to the Sensor analytical capillary pressure and relative permeability models.

Laboratory capillary pressures were scaled with IFT according to

$$P_c = \left(\frac{\sigma}{\sigma_{\text{lab}}}\right) P_{c,\text{lab}}, \quad \dots\dots\dots\dots\dots\dots (2)$$

where $P_{c,\text{lab}}$ is laboratory-reported capillary pressure, σ_{lab} is the laboratory gas/oil IFT (equal to 10 mN/m), and σ is reservoir gas/oil IFT calculated from

$$\sigma = \left[\sum P_i \left(x_i \frac{\rho_o}{M_o} - y_i \frac{\rho_g}{M_g}\right)\right]^4. \quad \dots\dots\dots\dots\dots (3)$$

Grid Sensitivity

In this section, we discuss grid effect on oil recovery using equilibrium-gas and CO_2-gas injection at 1,400-psia system pressure. The only requirement for accurate representation of recovery performance for gravity/capillary equilibrium in a system with constant phase properties (densities and IFTs) is sufficient vertical gridding to provide a good integration of the final equilibrium saturation/height relationship. Therefore, the oil recovery with equilibrium gas is the same for all grids considered, as we see in **Fig. 1.**

The recovery performance for CO_2 injection is affected by different gridding because of changing compositional effects, as shown in Fig. 1. 10×50 (N_x×N_z) and 10×100 grids give higher recovery than 3×50 grids. A finer grid is needed for CO_2 injection to capture gravity and near-miscible displacement. Details of the CO_2-injection mechanism will described in the next sections. Most equilibrium-gas-injection cases were run with a 10×50 (N_x×N_z) grid, and a 10×100 grid for CO_2 injection.

Prediction of Minimum Miscibility Pressure (MMP)

1D slimtube simulations were used to determine the thermodynamic MMP. The slimtube simulations were performed at system pressures of 1,000, 1,400, 2,000, 2,500, and 3,000 psia using 200, 500, and 1,000 grid cells. The results of recoveries for the different runs vs. system pressure are given in **Fig. 2;** final recoveries are

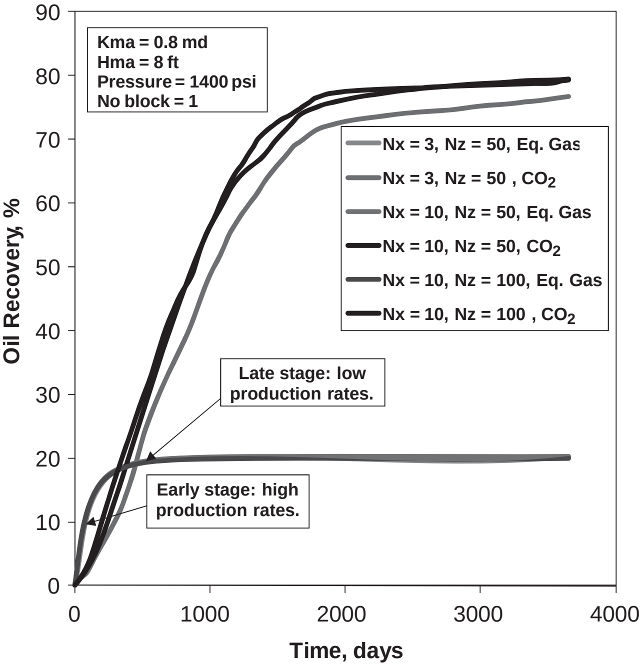

Fig. 1—Effect of grid cells on oil recovery vs. time for single matrix block using equilibrium-gas injection at system pressure of 1,400 psia.

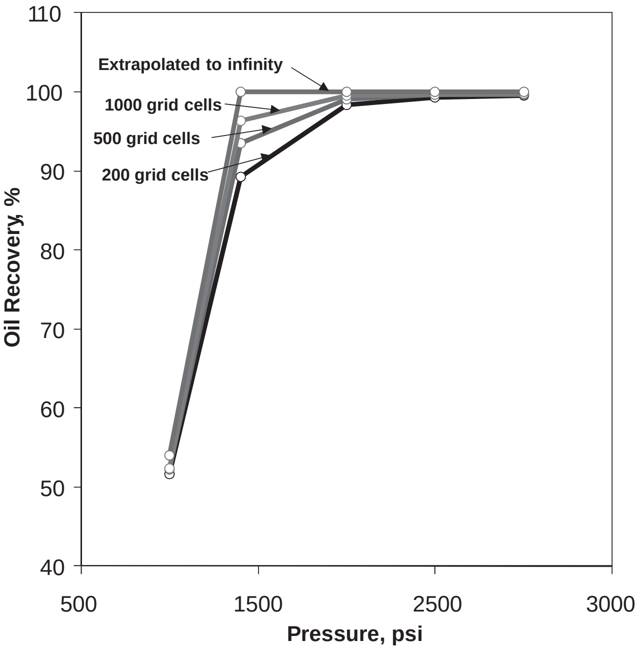

Fig. 2—Slimtube simulation using CO_2 injection gas. Oil recovery at 1.2 PVs of gas injected vs. pressure for different number of grid cells.

defined as 1 minus the fraction of initial oil in place remaining after 1.2 PV of CO_2 injected, divided by the initial oil in place. At each pressure, linear regression was used to fit these recoveries vs. $1/\sqrt{N}$, where N is the number of cells. Recoveries are extrapolated to infinite grid cells. The MMP is 1,400 psia according to slimtube simulations interpreted as described in the preceding, which compares favorably with the PhazeComp-calculated multicell algorithm MMP of 1,350 psia for a condensing/vaporizing mechanism.

Injection-Gas Mechanism

Equilibrium Gas in a Single Matrix Block. If the gravity forces exceed capillary forces, gas enters the top of the matrix block and oil is produced from the bottom of the matrix block. Viscous forces may be present during oil production from a matrix block. Viscous/gravity ($R_{v/g}$) and capillary/gravity ($R_{c/g}$) dimensionless ratios are used to understand the importance of the various recovery mechanisms during production (Wylie and Mohanty 1999; Stalkup 1983; Løvoll et al. 2005):

$$R_{v/g} = \frac{\Delta P_{\text{visc}}}{\Delta P_{\text{grav}}} = \frac{u\mu}{kg\Delta\rho_{og}} \quad \dots\dots\dots\dots (4)$$

and

$$R_{c/g} = \frac{\Delta P_{\text{cap}}}{\Delta P_{\text{grav}}} = \frac{\Delta P_{\text{cap}}}{g\Delta\rho_{og}h}, \quad \dots\dots\dots\dots (5)$$

where u is linear Darcy velocity in z-direction, μ is oil viscosity, k is matrix-block permeability, $\Delta\rho_{og}$ is oil and gas density difference, g is gravity-acceleration constant, h is grid-cell height, and ΔP_{cap} is capillary pressure gradient at the displacement front.

The recovery process can be divided into approximately two main periods: a quick initial production period characterized by high oil rates when most of the oil is recovered, followed by a final long production period characterized by lower production rates.

Oil primarily flows in the vertical direction, whereas gas enters both from the top and from the sides. After 30 days when only 4% of the oil has been recovered, the gas has entered only the topmost blocks of the core. $R_{v/g}$ and $R_{c/g}$ are equal at 0.005 and 0.15, respectively. These numbers suggest that gravity drainage is the dominant mechanism. After 180 days, approximately 15% of the original oil in place is recovered and the gas front has reached the capillary holdup zone (entry height). The profile is now almost uniform in the vertical direction; however, the gas saturation behind the front is less than the ultimate equilibrium gas saturation, so there is still a significant amount of oil left to be recovered. This is illustrated in Fig. 1, showing that it takes only 180 days to recover 15% of the oil, whereas it takes nearly 1,000 days to reach 20% ultimate oil recovery.

The initial period with high production rates ends when the displacement front reaches the capillary holdup zone in the matrix block. At this point, the gas saturation behind the front has not reached the final equilibrium profile and there is still potential for additional oil recovery. However, the recovery of remaining oil during the last stage is slow because of low oil mobility.

The parameters controlling the rate of recovery, but which have limited impact on ultimate recovery, are (a) absolute matrix permeability, (b) shape of the relative permeability curve, and (c) matrix block-to-block flow (re-infiltration). Parameters that control the ultimate recovery are (a) pressure (because of IFT and density dependence), (b) capillary pressure curve, and (c) endpoint saturations S_{org} and S_{wc}.

The following subsections present sensitivity simulations for these parameters. Unless stated otherwise, only a single parameter is changed in each sensitivity, keeping the other properties equal to base-case values.

Mechanism of CO_2 in a Single Matrix Block. In this subsection, we investigate the recovery mechanism of CO_2 in a single matrix block. In general, CO_2 gas has a higher viscosity than HC gas and, therefore, a better mobility ratio. In our study, we focus on the mechanism of gravity/capillary drainage, thereby making mobility ratio a less important parameter. CO_2-gas injection reduces gas/oil IFT significantly, and this has a pronounced impact on recovery by reducing the capillary retaining forces.

As seen in **Fig. 3,** CO_2 is lighter than oil at lower pressures, but can be heavier than oil at higher pressures. For Haft Kel, CO_2 has a higher density than reservoir oil at pressures above 2,050 psia. This characteristic results in two fundamentally different recovery mechanisms for CO_2, depending on the sign of the CO_2-oil density difference.

CO_2 Lighter Than Oil. When CO_2 is lighter than oil, CO_2 enters from top of the matrix block as in a traditional gas gravity-drainage mechanism. As shown in **Fig. 4,** the recovery behavior of CO_2

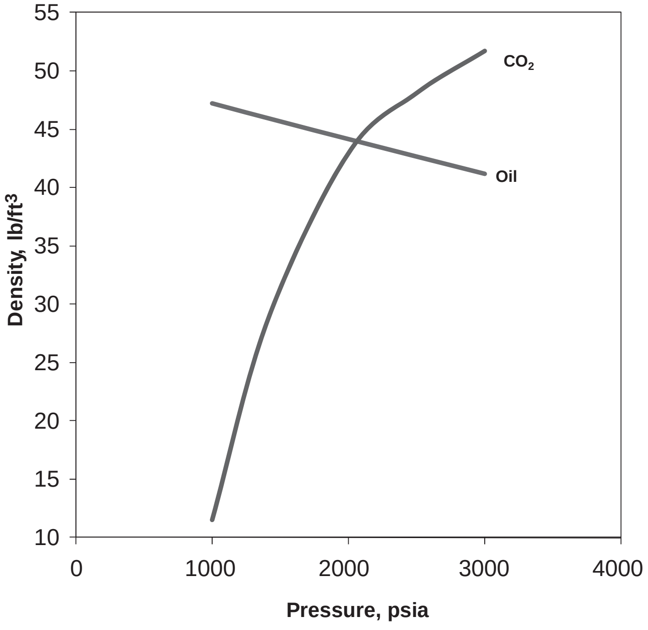

Fig. 3—Comparison of CO_2 and Haft Kel oil densities as a function of pressure (at reservoir temperature of 110°F).

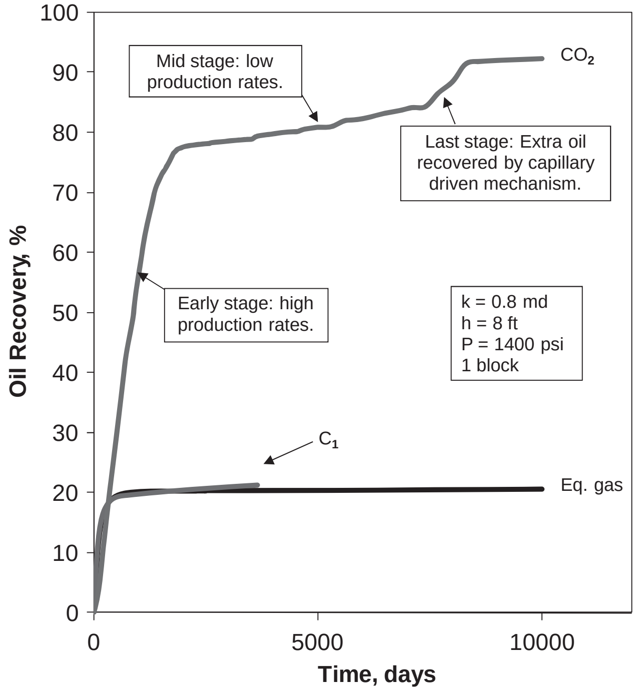

Fig. 4—Effect of different injection gas on oil recovery vs. time for single matrix block at system pressure of 1,400 psia.

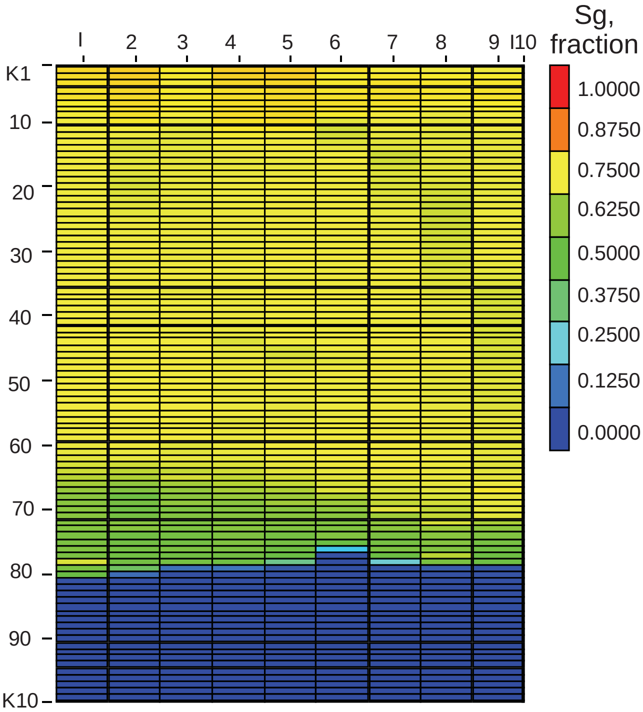

Fig. 5—Early-stage CO_2-gas displacement, gas-saturation profile inside matrix block after 1,410 days at system pressure of 1,400 psia (at 71% oil recovery).

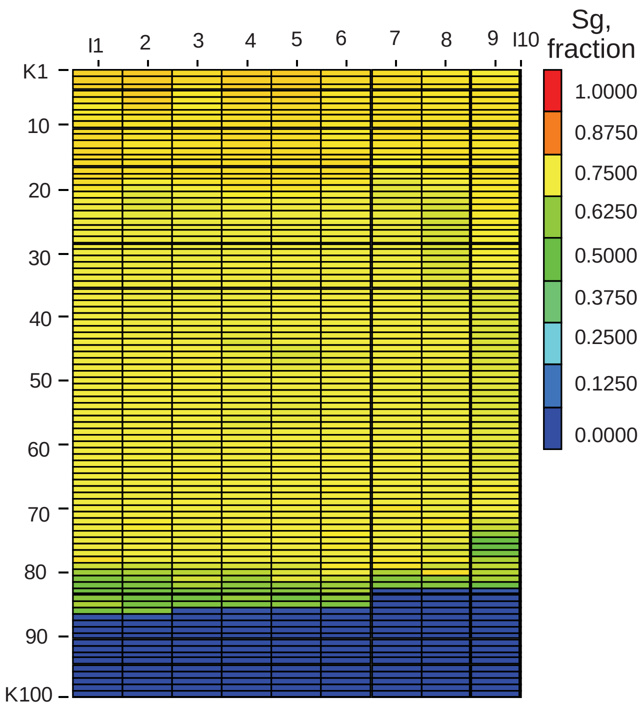

Fig. 6—Midstage CO_2-gas displacement, gas-saturation profile inside matrix block after 3,600 days at system pressure of 1,400 psia (at 79% oil recovery).

injection can be divided into three periods: an initial production period of high oil rates and two longer production periods characterized by lower production rates. The final period results in significant extra oil recovery from a capillary-drive mechanism first described by Uleberg and Høier (2002). **Figs. 5 through 7** show saturation distributions during the three periods, respectively.

The first two periods are similar in shape to the equilibrium gravity/capillary mechanism, but with a more complicated recovery mechanism. Because IFT decreases more significantly in CO_2 injection, capillary entry height decreases to result in higher ultimate recoveries after the first and second periods. Viscous/gravity ($R_{v/g}$=0.004) and capillary/gravity ($R_{c/g}$=0.006) ratios clarify that gravity drainage is the dominant mechanism during this period of oil production. This is illustrated in Fig. 4, which shows that it takes 1,400 days to recover 70% of the oil (end Phase 1), but not before 7,400 days does recovery reach 84% (end Phase 2).

As shown in **Fig. 8,** the extreme decrease in the gas/oil IFT near the displacement front results in a strong IFT and, consequently,

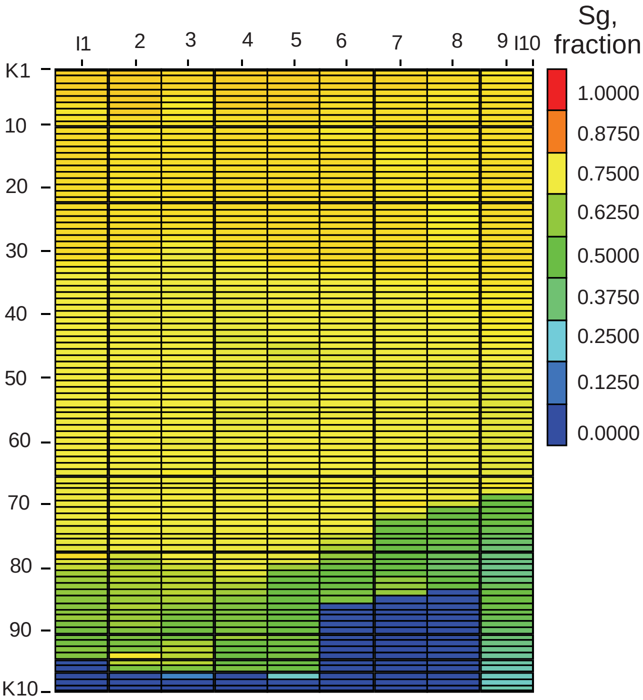

Fig. 7—Late-stage CO_2 gas-displacement, gas-saturation profile inside matrix block after 7,400 days at system pressure of 1,400 psia (at 84% oil recovery).

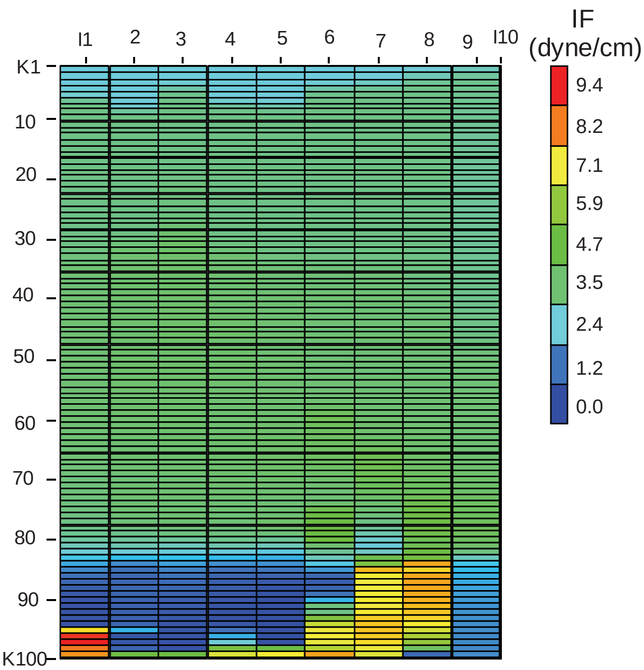

Fig. 8—Late-stage CO_2-gas-displacement, IFT profile inside matrix block after 7,400 days at system pressure of 1,400 psia (at 84% oil recovery).

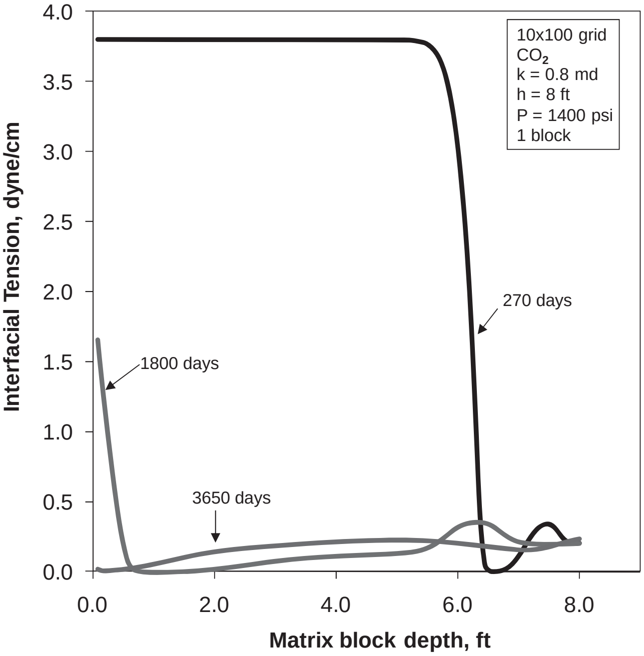

Fig. 9—IFT profile for single matrix block using CO_2 injection gas at system pressure of 2,500 psia.

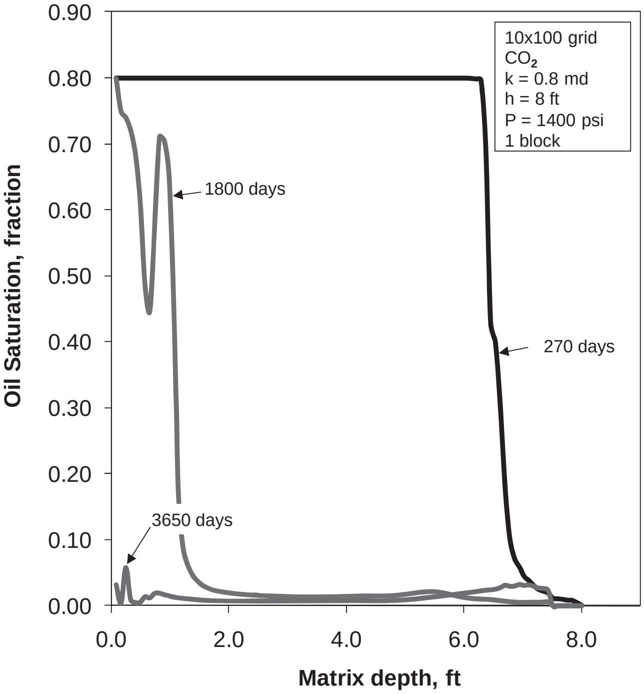

Fig. 10—Oil-saturation profile for single matrix block using CO_2 injection gas at system pressure of 2,500 psia.

capillary pressure gradient. Uleberg and Høier (2002) describe the resulting process, “This, combined with a relative small phase density difference near the miscible front, induces a Darcy flow of oil against gravity. As the oil flows upwards it contacts fresher and leaner gas and the intermediate and heavy components of the oil are more easily vaporized. The oil components that vaporize to the gas phase are then transported to the fracture system by: (1) injectant gas replacing the matrix block gas due to the density difference and (2) molecular diffusion due to the compositional difference between the gas in the fracture system and in the matrix block.

Oil is transported upwards by IFT induced Darcy flows even after the gas-oil front has reached the capillary entry height. This results in a shrinking of the oil zone at the bottom of the matrix block, and fracture gas more easily enters below the initial capillary entry height level. Eventually most of the original oil from the matrix block will be produced.

Increasing the system pressure makes the displacement process more miscible. The phase density differences are less and the IFT gradient near the miscible front is more pronounced, creating an even greater potential for the oil to flow upwards, and at higher rate.”

The capillary-driven mechanism transpires throughout the displacement (Periods 1, 2, and 3), though it is more pronounced in the late period of displacement, verified by a capillary/gravity ratio $R_{c/g}$=22.15.

In the early stage, displacement preferentially moves along the fracture side (Fig. 5) because there is fresh CO_2 available, with more oil vaporized and production to the fracture. The matrix-block grid cells in the vicinity of fracture have higher CO_2 concentrations. The IFT gradient at the displacement front is less toward the fracture (Fig. 8). For that reason, displacement is preferentially in the matrix block center during the late stage of recovery (Fig. 7).

CO_2 Heavier Than Oil. At early times, CO_2 dissolves into the oil phase and some lighter oil components vaporize into the CO_2-rich gas phase. This results in increasing oil and gas densities in the matrix block, with very-low density differences near the upward-moving front. As shown in **Fig. 9,** IFT decreases dramatically at the displacement front, from 3.8 to 0.06 mN/m implying that the process is near miscible (system pressure of 2,500 psia is far above the thermodynamic MMP of 1,350 psia[3]).

Before the upward-moving front reaches the top of the matrix block, three characteristic phases coexist in the matrix block. The original oil phase exists in the upper section of the matrix block, ahead of the front. Behind the front, a gas phase and an equilibrium oil phase exist, though the phase compositions vary significantly from the matrix bottom to the front.

The front moves upward as the frontal gas pushes original oil from the top of the matrix block, as seen in **Fig. 10.** Behind the front we find a complex flow mechanism where remaining oil eventually becomes heavier as it is vaporized by the gas. This oil starts flowing downward out the bottom of the matrix block, but at a low rate because of low mobility.

When the gas front reaches the top of the matrix block, CO_2 starts to enter from the top and the remaining oil is produced slowly from the bottom of the matrix block by gravity drainage; the remaining oil is denser than CO_2 but has low mobility.

Injection-Gas Effect

In this section, we study different injection gases for a single matrix block. We examine equilibrium-gas, dry-gas (C_1), and CO_2 injection at a system pressure of 1,400 psia. Results are shown in Fig. 4. The CO_2 injection case has highest ultimate oil recovery (recovery at 10,000 days), approximately 92%, while the equilibrium gas and dry gas have the same oil recovery of approximately 20%. As mentioned earlier, 1,400 psia is the thermodynamic MMP for CO_2 with Haft Kel oil.

CO_2-Dilution Effect. Because the Haft Kel field has a large gas cap, injected gas may dilute with gas-cap equilibrium gas because of convective and diffusive flow in the fracture system. CO_2 concentration at a given fracture location in the reservoir will depend on many effects, including gravity segregation, gas/gas diffusion, gas-injection rate, matrix-block permeability, gas-cap size, and location of injector perforations. Fracture gas compositions surrounding matrix blocks may vary substantially, with associated impact on oil recovery.[4]

We studied several CO_2 mixtures—i.e., 50, 80, and 90 mol% CO_2 mixed with equilibrium gas at 1,400 psia. As shown in **Fig. 11,** the ultimate oil recoveries for these three gases were 24.5, 34.5, and

---

[3] We did not study the front's approach to miscibility as grid refinement is increased to large numbers and dispersivity is reduced toward zero (an assumption in the thermodynamic MMP).

[4] We suspect that gravity segregation in the fracture system may segregate injected CO_2 into a “blanket” of high-CO_2 gas on the top of the fracture oil column, with a HC gas floating on the CO_2 blanket.

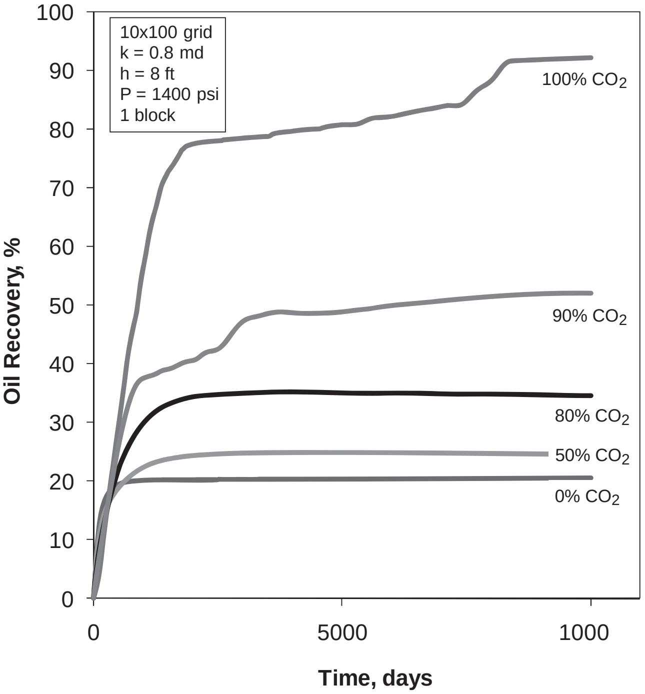

Fig. 11—Effect of CO_2 dilution on oil recovery vs. time for single matrix block at system pressure of 1,400 psia.

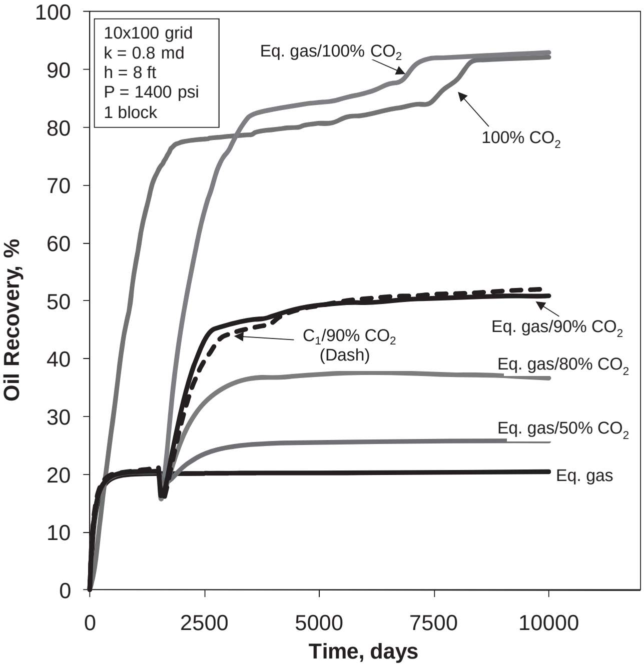

Fig. 12—Effect of injection gas, injecting different concentrations of CO_2 after equilibrium-gas (solid) and methane (dash line) injection, on oil recovery vs. time for single matrix block at system pressure of 1,400 psia.

52%, respectively. Reduced oil recoveries are related to increased gas/oil IFT and less-efficient condensing/vaporizing behavior near the displacement front (i.e., an increase in MMP) as CO_2 concentration decreased in the injection gas.

Tertiary Recovery by CO_2 Injection. Haft Kel dry-gas injection started in 1976. Dry-gas injection behaves very similar to equilibrium-gas injection, with similar recovery performance. Basically, the injected dry gas changes composition when it contacts reservoir oil, with a resulting gas composition that is very close to the incipient gas composition of the original oil. In this section, we present results from our study of recovery performance when CO_2 is injected following dry-gas injection.

Different concentrations of CO_2 were mixed with HC (equilibrium or dry) injection gas, the resulting mixture being injected into the fracture system following an initial period of HC-only gas injection. Two wells were used in these simulations, allowing injection-gas composition to change with time. The injection well was perforated in the top fracture, and the producer was perforated in the bottom fracture. The injection well was controlled by a constant bottomhole pressure, and the producer was controlled by constant gas-production rate of 0.353 Mscf/D.

Injection gases with 100, 90, 80, and 50 mol% CO_2 mixed with equilibrium gas at reservoir pressure of 1,400 psia were injected after first injecting equilibrium gas only into the matrix block. Equilibrium gas was injected for 1,500 days to ensure that the equilibrium-gas displacement was complete. This was followed by injection with a CO_2-rich gas. Results are given in **Fig. 12.** The ultimate oil recoveries for 100 (pure), 90, 80, and 50 mol% CO_2 mixtures were 93, 51, 36, and 26%, respectively.

These ultimate oil recoveries are close to those found where CO_2-rich gases were injected without first injecting equilibrium HC gas. However, the recovery mechanism is slightly different. First, oil recovery drops as a result of CO_2 swelling in the matrix block with associated oil-saturation increase, leading to lower oil recovery, based on Eq. 1. Second, the injected CO_2 gas at 1,400 psia is lighter than oil but heavier than the initial HC gas in the matrix block. Consequently the CO_2-rich gas cannot enter from the top or from the bottom of matrix block. Instead, it enters from the side of the matrix block by exchanging composition with gas in the matrix. The front for CO_2 mixed with matrix-block gas moves in both horizontal and vertical directions. After CO_2 enters into the matrix block, gravity/capillary drainage becomes strong and oil produces from the bottom of the matrix block.

Similar simulations were made using dry injection gas (instead of equilibrium gas) initially, and mixed with CO_2. The results are given in Fig. 12. The mechanism and recoveries are similar to results using equilibrium HC gas.

Reservoir-Pressure Effect. The effect of reservoir pressure on oil recovery for equilibrium gas, CO_2, and different mixtures of CO_2 and equilibrium injection gas is studied in this section. Different models are used, with the system pressure of 1,000, 1,400, 2,000, 2,500, and 3,000 psia. The equilibrium-gas models use 10×50 ($N_x \times N_z$) grid cells; for each pressure, the matrix block is initialized with saturated oil and the fracture is initialized with equilibrium gas. CO_2-injection models contain 10×100 grid cells, and for each pressure case, the matrix block is initialized with saturated oil and the fracture is initialized with CO_2.

For the equilibrium-gas cases, gas/oil IFT decreases with increasing reservoir pressure. As a result, the capillary entry height is lowered and ultimate oil recovery increases. As shown in **Fig. 13,** oil recovery increases from 14% at 1,000 psia to 50% at 3,000 psia, corresponding to a change in gas/oil IFT from 13.55 to 2.24 mN/m.

For CO_2 injection, we find that oil recovery generally increases with reservoir pressure, reaching nearly 100% near the thermodynamic MMP of 1,400 psia. A significant anomaly is seen at 2,000 psia, where recovery is less than 30% after 10,000 days (when all other runs had essentially reached ultimate recovery), as seen in Fig. 13. CO_2 and oil densities are approximately equal at 2,000 psia, as shown in Fig. 6, and consequently gravity drainage is slowed radically.

Mixtures of CO_2 and equilibrium gas at 2,000 psia show higher oil recovery than pure CO_2 **(Fig. 14)** because gas-/oil-density differences are higher than for pure CO_2. Fig. 14 shows that oil recovery rises toward 100% as the thermodynamic MMP is approached. MMP increases with decreasing CO_2 content in the injection gas, and the RF-pressure trend toward near-100% recovery becomes less steep.

Matrix-Block Height Effect

The matrix-block height is a critical parameter for gas injection in fractured reservoirs. If the matrix-block height is smaller than the initial capillary entry height, no gas can enter (unless by diffusion).

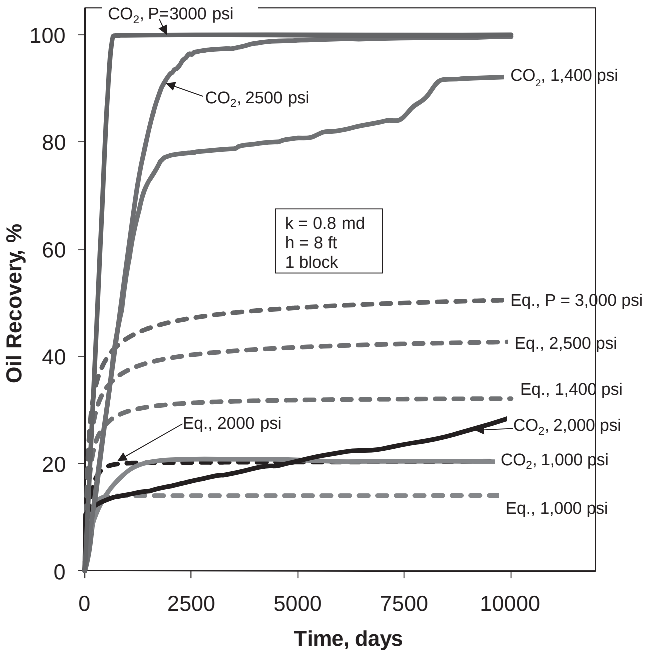

Fig. 13—Effect of reservoir pressure on oil recovery vs. time for single-matrix-block system using equilibrium-gas (dash line) and CO$_2$ (solid line) injection.

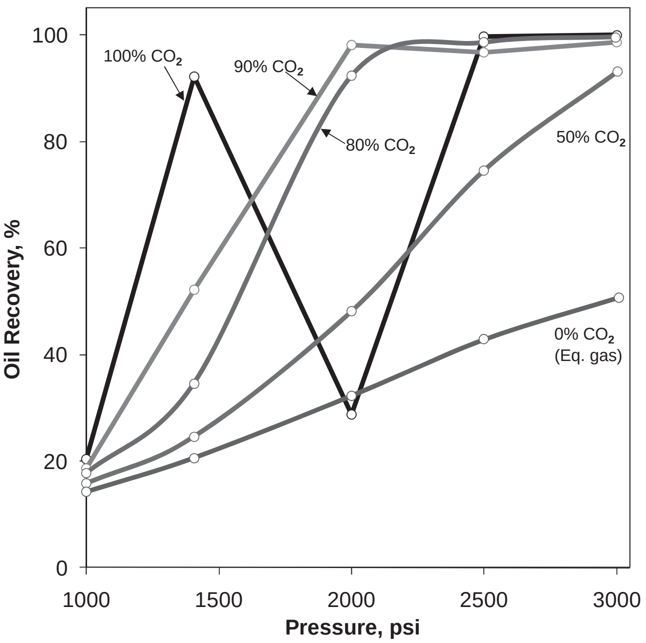

Fig. 14—Comparison of CO$_2$-injection-gas with equilibrium-gas oil recovery at 10,000 days vs. reservoir pressure for a single-matrix-block system.

Haft Kel block size varies from 6 to 14 ft, as reported by Saidi (1996). We considered four matrix-block heights—6, 8, 10, and 14 ft—to study the effect of matrix-block height on oil-recovery performance for equilibrium gas (dashed line) and CO$_2$ (solid line), as shown in **Fig. 15.**

When equilibrium gas is injected, the ultimate oil recovery increases significantly with increasing stack height for small matrix blocks close to the capillary entry height. The ultimate recovery approaches an asymptotic value given by the saturation endpoints, S_{org} and S_{wc}, and the effect of matrix-block height on the final recovery is not significant for very tall matrix stack heights. The stack height does not have a strong effect on the oil-production rate, meaning that the time to reach a given recovery increases with stack height (because of changes of amount of fluids in place). Previous studies (Saidi 1996; Behbahani et al. 1996) on Haft Kel field pointed out that the oil recovery by immiscible HC gas varies between 15 and 32%. As seen in Fig. 15, the lowest and highest oil recoveries are 12.9 and 36.7% for 6- and 14-ft matrix blocks, respectively.

For CO$_2$ injection, the ultimate oil recovery is approximately the same for all stack heights. First, the capillary entry height in CO$_2$ injection is lower than the capillary entry height of equilibrium-gas injection, caused by low IFT in a developed condensing/vaporizing near-miscible process. Furthermore, the oil below capillary entry height is produced by the dynamic gravity/capillary-drive mechanism, as described by Uleberg and Hoier (2002). Ultimate recovery from this mechanism is not greatly affected by matrix-block height, as shown in Fig. 15.

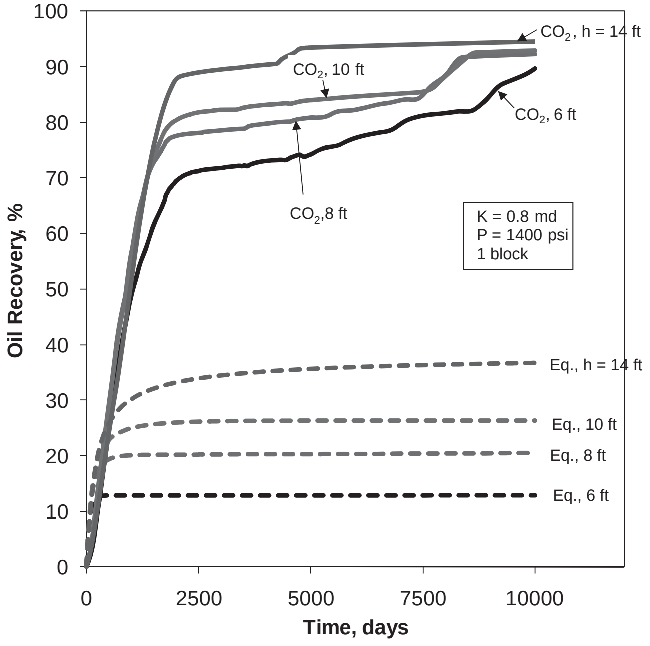

Fig. 15—Effect of matrix-block height on oil recovery vs. time for single matrix block using equilibrium (dash line) and CO$_2$ (solid line) injection gas at system pressure of 1,400 psia.

Matrix-Block-Permeability Effect

The matrix permeability controls the rate of recovery from a matrix block, and the ratio between the matrix and fracture permeability determines if viscous displacement (Darcy flow by pressure gradients) is important or not. If injection fluid mainly flows in the fracture, then viscous force is negligible in low-permeability matrix block. Matthai and Belayneh (2004) studied the effects of matrix-/fracture-permeability ratio on fracture/matrix flow partitioning, and their results indicate that at a ratio of fracture permeability to matrix permeability of 10^4 and lower, viscous force becomes important. Porosity and capillary pressure are assumed to be constant in all cases.

In Haft Kel, matrix-block permeability varies from 1 to 0.05 md. For equilibrium-gas injection, the rate of oil recovery increases with increasing matrix-block permeability, but ultimate oil recovery is the same, as shown in **Fig. 16.**

As shown in Fig. 16, CO$_2$ has the same effect but it is more pronounced because the rate of oil recovery in CO$_2$ injection is slower than the rate of oil recovery for equilibrium-gas injection.

Interestingly, there is a linear relationship between the time to reach a given oil recovery and the matrix permeability, when plotted on log-log paper. This is seen in **Fig. 17,** where the times to reach specific recoveries of 10, 15, and 20% are considered. The lines have the same slope for both equilibrium gas and CO$_2$.

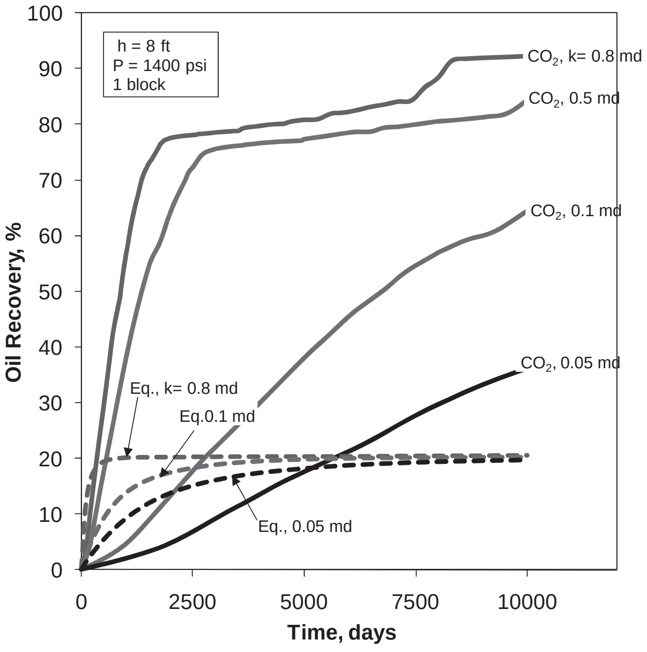

Fig. 16—Effect of matrix-block permeability on oil recovery vs. time for single matrix block using equilibrium (dash line) and CO$_2$ (solid line) injection gas at system pressure of 1,400 psia.

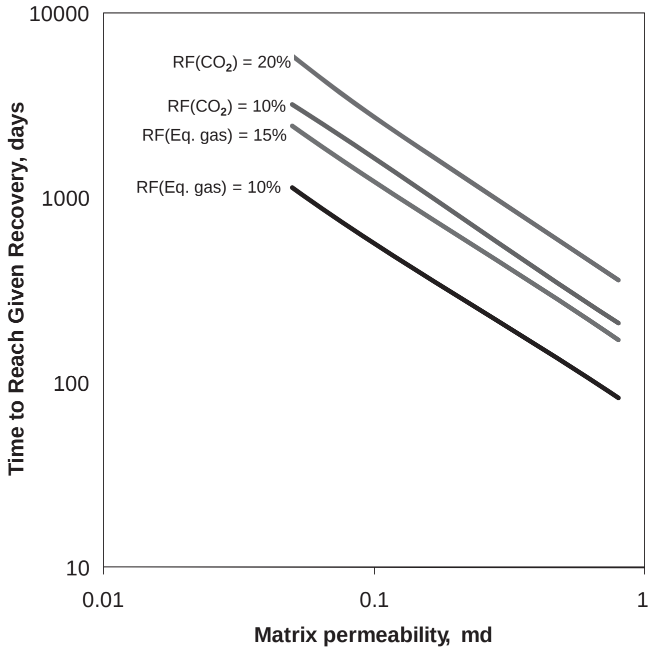

Fig. 17—Time of reaching certain oil recovery vs. matrix-block permeability for single matrix block using equilibrium and CO$_2$ injection gas at system pressure of 1,400 psia.

Fig. 17 is useful to find the time to reach a given oil recovery for a wide range of matrix-block permeabilities.

Block-to-Block Interaction

Oil produced from one matrix block may flow into an underlying matrix block. Oil reinfiltration may result from physical contact between the blocks (permeable contact points) or by oil produced from one block entering another block because of gravity/capillary interaction, liquid bridges, or film flow. We studied the effect of vertical block-to-block interaction using taller effective matrix-block heights.

In our model, the matrix blocks are 8 ft in height, and are separated by horizontal fractures. The top, bottom, and side fractures are defined with a large PV to provide the gas needed to inject and to eliminate injection and production wells. Thin horizontal fractures were gridded to represent the connection of one matrix block with another.

For equilibrium gas we studied 1, 5, 10, 20, and 40 stacked matrix blocks using 3×1×25 grid cells for each matrix block. **Fig. 18** illustrates the total oil recoveries for different stacked matrix blocks. Total oil recovery is the arithmetic average of oil recovery for all matrix blocks. This figure shows significant delay of oil production because of oil reinfiltration.

Another series of stacked matrix blocks were studied to compare CO$_2$ injection with equilibrium gas. The CO$_2$-injection cases have higher total oil recoveries than equilibrium-gas cases, as shown in **Fig. 19.** Fig. 19 shows that the shape of oil recovery for stacked blocks does not include the final stage of single-block oil recovery in which the extra oil is recovered exclusively by the dynamic gravity/capillary mechanism.

The cases shown here represent 100% reinfiltration. It is likely that the degree of reinfiltration is less in the field. Many factors can reduce block-to-block flow significantly, such as interbedded layers of nonfractured impermeable rock (shales and mineral-filled fractures), sloped fractures, and viscous forces.

Conclusions

Oil-recovery performance was quantified for the Haft Kel oil system using compositional modeling of a matrix block surrounded by a gas-filled fracture. Simulations were performed for a wide range of petrophysical properties, matrix-block sizes, injection gas, varying initial conditions of pressure, and saturation pressure.

Some of the most interesting observations and conclusions concerned CO$_2$ injection include:

1. Grid refinement is needed for accurate modeling of nonequilibrium gas injection because of a complex gravity/capillary recovery mechanism with significant IFT and capillary pressure gradients.
2. CO$_2$ is heavier than the Haft Kel oil at pressures greater than 2,050 psia. When CO$_2$ gas is lighter than oil, CO$_2$ gas enters from the top of the matrix block and drains oil downward, as found with all other injection gases.

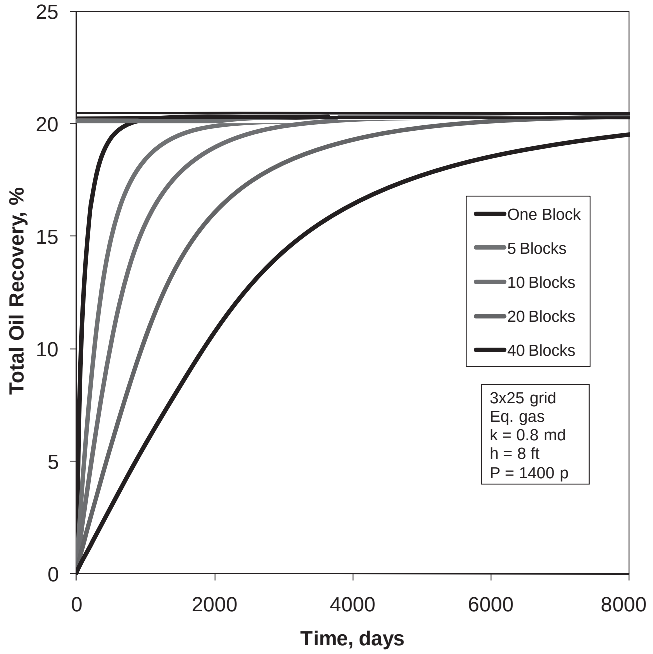

Fig. 18—Total oil recovery vs. time for different number of stacked matrix blocks using equilibrium-gas injection at system pressure of 1,400 psia.

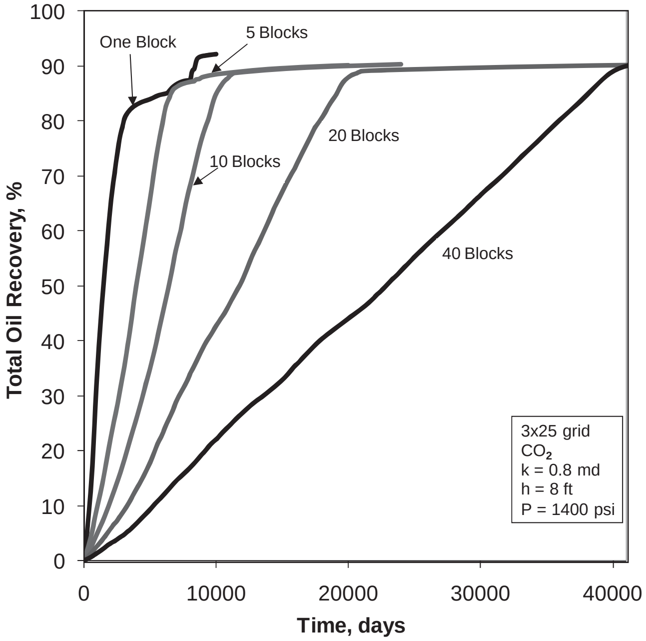

Fig. 19—Total oil recovery vs. time for different number of stacked matrix blocks using CO_2-gas injection at system pressure of 1,400 psia.

3. When pure CO_2 is heavier than the reservoir oil, CO_2 gas initially enters from the bottom of the matrix block. Unusual saturation gradients develop, with near-initial oil saturation at the top of the matrix block remaining until the upward-moving gas front reaches the top. Gradually, the oil at the bottom of the matrix becomes heavier than its equilibrium HC/CO_2 matrix gas mixture, resulting in "normal" gravity segregation.
4. Despite high ultimate oil recovery with CO_2, the process is relatively slow (compared with nonequilibrium HC gases) and particularly when the CO_2-gas and reservoir-oil densities are similar.
5. Ultimate oil recovery increases with increasing reservoir pressure and CO_2 concentration in injection gas.
6. CO_2 injection in Haft Kel field can lead to significant additional oil production, even after dry-gas injection.

Nomenclature

g = gravity-acceleration constant
h = height of grid cell, L, ft
k = matrix-block permeability, L^2, md
M_g = gas molecular weight
M_o = oil molecular weight
N = number of grid cells
N_x = number of grid cells in x-direction
N_z = number of grid cells in z-direction
P_c = capillary pressure, m/Lt^2, psia
$P_{c,\text{lab}}$ = measured capillary pressure, m/Lt^2, psia
P_{cgo} = drainage gas/oil capillary pressure, m/Lt^2, psia
P_i = parachor of component i
$R_{c/g}$ = capillary - to gravity-force ratio
$R_{v/g}$ = viscous- to gravity-force ratio
RF = oil-recovery factor
S_g = gas saturation
S_o = oil saturation
S_{oini} = initial oil saturation
S_{org} = residual-oil saturation to gas
S_{wc} = connate-water saturation, fraction
u = linear Darcy velocity, L/t^2, ft/sec^2
x_i = oil mole fraction of component i
y_i = gas mole fraction of component i
ΔP_{cap} = capillary pressure gradient in displacement front, m/Lt^2, psia
$\Delta\rho_{og}$ = oil and gas density difference, m/L^3, lbm/ft^3
ρ_g = gas density, m/L^3, lbm/ft^3
ρ_o = oil density, m/L^3, lbm/ft^3
σ = gas/oil IFT, m/t^2, dyne/cm
σ_{lab} = reference gas/oil IFT, m/t^2, dyne/cm

References

Behbahani, H.S.-Z., Kharrat, R., and Vossoughi S. 1996. Case History of a Unique Gas Injection Scheme and its Simulation Using Material Balance Based Simulator. Paper SPE 35631 presented at the SPE Gas Technology Conference, Calgary, 28 April–1 May. doi: 10.2118/35631-MS.

Jamshidnezhad, M. 2004. Vertical Miscible Displacement of Oil From Fractured Reservoir. Paper SPE 88791 presented at the Abu Dhabi International Conference and Exhibition, Abu Dhabi, UAE, 10–13 October. doi: 10.2118/88791-MS.

Løvoll, G., Meheust, Y., Måløy, K.L., Aker, E., and Schmittbuhl, J. 2005. Competition of gravity, capillary and viscous forces during drainage in a two-dimensional porous medium, a pore scale study. *Energy* **30** (6): 861–872. doi: 10.1016/j.energy.2004.03.100.

Matthai, S.K. and Belayneh, M. 2004. Fluid flow partitioning between fractures and a permeable rock matrix. *Geophys. Res. Lett.* **31:** L07602. doi: 10.1029/2003GL019027.

PhazeComp. Zick Technologies. www.zicktech.com.

Ringen, J.K., Haugse, V., Høier, L., Berge, L.I., and Reed, J. 2005. Experimental and Numerical Studies of Gas Injection in Fractured Carbonates: Pressure and Compositional Effects. Paper presented at the 2005 International Symposium of Society of Core Analysts, Toronto, Canada, 21–25 August.

Saidi, A.M. 1987. *Reservoir Engineering of Fractured Reservoirs: Fundamental and Practical Aspects*, 764–770. Paris: TOTAL Edition Press.

Saidi, A.M. 1996. Twenty Years of Gas Injection History Into Well-Fractured Haft Kel Field (Iran). Paper SPE 35309 presented at the International Petroleum Conference and Exhibition of Mexico, Villahermosa, Mexico, 5–7 March. doi: 10.2118/35309-MS.

Sensor. Coats Engineering Inc. www.coatsengineering.com.

Stalkup, F.I. Jr. 1983. *Miscible Displacement*. Henry L. Doherty Monograph Series, SPE, Richardson, Texas, USA **8.**

Tan, C.T. and Firoozabadi, A. 1995. Theoretical Analysis of Miscible Displacement in Fractured Porous Media by a One-Dimensional model: Part I- Theory. *J. Can Pet Tech* **34** (2): 17–27. JCPT Paper No. 95-02-01. doi: 10.2118/95-02-01.

Uleberg, K. and Høier, L. 2002. Miscible Gas Injection in Fractured Reservoirs. Paper SPE 75136 presented at the SPE/DOE Improved Oil Recovery Symposium, Tulsa, 13–17 April. doi: 10.2118/75136-MS.

Wylie, P.L. and Mohanty, K.K. 1999. Effect of Wettability on Oil Recovery by Near-Miscible Gas Injection. *SPE Res Eval & Eng* **2** (6): 558–564. SPE-59476-PA. doi: 10.2118/59476-PA.

SI Metric Conversion Factors

bbl	× 1.589 873	E–01 = m^3
dyne	× 1.0*	E–02 = mN
ft	× 3.048*	E–01 = m
ft^3	× 2.831 685	E–02 = m^3
°F	(°F + 459.67)/1.8	= K
lbm	× 4.535 924	E–01 = kg

*Conversion factor is exact.

Sayyed Ahmad Alavian is PhD student in Norwegian U. of Science and Technology (NTNU). E-mail: alavian@ntnu.no. He holds an MS degree in petroleum engineering from NTNU. Alavian's main area of work involves compositional reservoir simulation and PVT. **Curtis H. Whitson** is professor of petroleum engineering and applied geophysics at NTNU. E-mail: curtis.h.whitson@ntnu.no. He holds a BS degree from Stanford U. and Doctor of Technology degree from NTNU. Whitson coauthored the book Well Performance (2nd Ed. Prentice-Hall 1991), as well as the Phase Behavior monograph for SPE (2000).

Numerical Modeling CO_2 Injection in a Fractured Chalk Experiment

Journal of Petroleum Science and Engineering, Volume 77, Issue 2, May 2011, Pages 172-182

Paper II

Journal of Petroleum Science and Engineering 77 (2011) 172–182

Contents lists available at ScienceDirect

Journal of Petroleum Science and Engineering

journal homepage: www.elsevier.com/locate/petrol

Numerical modeling CO_2 injection in a fractured chalk experiment

S.A. Alavian [a,*], C.H. Whitson [a,b]

[a] Department of Petroleum Engineering and Applied Geophysics, Norwegian University of Science and Technology (NTNU), S.P Andersens 15A, 7491, Trondheim, Norway
[b] PERA, S.P Andersens 15A, 7491, Trondheim, Norway

ARTICLE INFO

Article history:
Received 13 November 2009
Accepted 27 February 2011
Available online 15 March 2011

Keywords:
Fracture reservoir
Numerical modeling of CO_2 injection experiment

ABSTRACT

This paper presents a numerical modeling study of CO_2 injection in a chalk core based on experimental data, as reported by Karimaie (2007). The experiment consisted of a vertically-oriented 19.6 cm long chalk outcrop core initially saturated with reservoir synthetic oil consisting of C_1 and n-C_7 at a temperature of 85 °C and pressure of 220 bar. After saturating the core with the oil mixture by displacement, a small “fracture” volume surrounding the core was created by heating the solid Wood's metal that originally filled the volume between the core and core holder.

Gas injection was conducted initially using an equilibrium C_1–n-C_7 gas at 220 bar. This gas should have had no recovery by thermodynamic mass transfer, only from immiscible Darcy-controlled displacement driven by pressure gradients and gravity-capillary forces. Once oil production ceased in this first displacement, a second period with pure CO_2 gas injection followed.

Our numerical modeling was conducted with a compositional reservoir simulator. The 2-dimensional r-z model used fine grids for the core matrix and the surrounding fracture. Automated history matching was used to match the experimental data (surface volumetric oil production profile). The match to reported production data gave a high degree of confidence in the model. Oil recovery improved significantly with CO_2 injection.

Our numerical model study indicates that the recovery mechanism in the Karimaie experiment was dominated by Darcy displacement because of a low conductivity in the surrounding fracture, with little impact of capillary–gravity displacement. Another observation made in our study was the strong influence of surface separator temperature on surface oil volumetric production. Finally, gas-injection rate changes had a significant impact on recovery performance for CO_2 injection. Gravity–capillary recovery mechanism was of minor importance in the Karimaie experiments.

1. Introduction

CO_2 injection has previously been considered as an efficient EOR (enhanced oil recovery) method in naturally fractured reservoirs. Alavian and Whitson (2005) study the EOR potential for CO_2 injection in the naturally-fractured Haft Kel field, Iran, based on detailed compositional simulations of the matrix–fracture system. It would be useful to experimentally investigate the efficiency of CO_2 injection in naturally fractured reservoirs having previously undergone natural gas recovery displacement.

Few experiments are reported in the literature studying gravity drainage induced by CO_2 injection in fractured reservoirs. Li et al. (2000) perform CO_2 injection after water flooding in a dead oil system. They studied water imbibition followed by CO_2 gravity drainage experiment on artificially fractured cores. They report that CO_2 gravity drainage significantly increased oil recovery after water flooding for their system. They found that CO_2 gravity drainage declines as the rock permeability decreases and initial water saturation increases. Asghari and Torabi (2008) conducted miscible and immiscible CO_2 gravity drainage experiments with dead oil (n-C_{10}). They showed that miscible CO_2 injection improves oil recovery, but they could not match laboratory experiment with a simulation model.

Karimaie (2007) performed equilibrium gas injection followed by CO_2 injection in a series of experiments on chalk and carbonate cores at reservoir conditions, where the cores were initially saturated with live synthetic oil.

In a fractured system, matrix permeability controls the rate of recovery. The pressure gradients along fractures are negligible for high permeability fractures where most injected gas flows through the fracture space and the main production mechanism from the matrix is gravity drainage. That means the ratio between the matrix and fracture permeability determines whether viscous displacement (Darcy flow by pressure gradients) governs the displacement, or not. Therefore, fracture permeability should be sufficiently high in an experiment to eliminate viscous displacement in the core. Uncertainty analysis and sources of experimental error had to be studied to understand and simulate the Karimaie experiment.

---

* Corresponding author at: S.P.Andersens vei 15A, 7491, Trondheim, Norway. Tel.: +47 735 94919; fax: +47 73944472.
E-mail address: alavian@ntnu.no (S.A. Alavian).

0920-4105/$ – see front matter © 2011 Elsevier B.V. All rights reserved.
doi:10.1016/j.petrol.2011.02.014

2. Rock and fluid properties

Chalk core from Faxe area outcrop in Denmark was used in the Karimaie experiment, with similar rock properties to North Sea chalk. The core had a cylindrical shape with a length of 19.6 cm and 3.8 cm in diameter. Core porosity and permeability were reported as 44% and 5 md, respectively (Karimaie, 2007; Karimaie and Torsæter, 2010).

Relative permeabilities were not reported by Karimaie (2007) and Karimaie and Torsæter (2010). The capillary pressure curve presented (Karimaie, 2007) was water–oil drainage capillary pressure of Ekofisk chalk core measured by Talukdar (2002). In our modeling study, we used instead a C_1–n-C_5 capillary pressure data set from Faxe outcrop chalk core measured by Christoffersen (1992). The water–oil capillary pressure curve was measured with a centrifuge, while the C_1–n-C_5 capillary curve was measured by a high-pressure, porous-plate method. Porosity and permeability of the core used to interpret the water–oil P_{cow} curve was 31% (anomonously low for outcrop chalk) and 1.94 md, respectively. Porosity and permeability of the core used to obtain C_1–n-C_5 P_{cgo} curve were 46.5% and 5 md, respectively. Reference IFT of the water–oil system was not reported, whereas C_1–n-C_5 was reported and equal to 1.5 mN/m. Reference IFT was used to scale capillary pressure. We found it more appropriate to use the C_1–n-C_5 capillary pressure.

Reported compositions were not measured. 33% of C_1 with 67% of n-C_7 mass fraction were mixed and then flashed at $P = 220$ bar and $T = 85$ °C. The liquid phase was used as live oil for the experiment and gas injected as equilibrium gas. Karimaie simulated the above process in a PVT simulator to calculate reported EOS oil and gas compositions. Using his reported equation of state (EOS) we were not able to reproduce his reported oil and gas compositions (Table 1). Given this finding, the reported oil and gas compositions and EOS were not used in our study. Bubble point pressure, oil density and interfacial tension (IFT) were measured by the SINTEF PVT lab. *PhazeComp* (Zick Technologies, 2010) PVT software using the SRK EOS was used to determine the laboratory oil composition with a 220 bar saturation pressure at 85 °C. The resulting oil composition consisted of 68.44 and 31.56 mol% of C_1 and n-C_7, respectively. Deviation of calculated oil density (0.413 g/cm^3) at 220 bar was about 1.6% which is in the range of laboratory measurement error. The EOS together with parachor method was tuned to match measured IFT at 220 bar (0.15 mN/m). EOS parameters used in this study are given in Tables 2 and 3.

3. Experimental procedure

This section describes an experiment originally designed to study gravity drainage in a fracture–matrix system by injecting equilibrium gas followed by CO_2. The experimental procedure is described by Karimaie (2007), Karimaie and Torsæter (2010) and personal communication with Karimaie. Uncertainties and possible sources of lab error are discussed in the next section.

A dried cylindrical chalk core was placed in a steel core holder. The core holder inner length and diameter were 20 cm and 4.2 cm respectively. The core diameter was 3.8 cm and had 19.6 cm in length. The fracture was represented by a 2 mm space between core and core holder. Core porosity was reported as 44%, and absolute permeability measured with n-heptane (n-C_7) at room temperature was ~5 md (Karimaie, 2007; Karimaie and Torsæter, 2010).

Table 1
Comparison of reported oil and gas compositions by Karimaie (2007) and recalculated compositions using his reported EOS.

Component	Calculated compositions from reported EOS		Reported compositions	
	X_i	y_i	x_i	y_i
C_1	0.6885	0.9197	0.7034	0.8825
nC_7	0.3115	0.0803	0.2966	0.1175

Table 2
EOS properties for the SRK characterization.

Component	MW	Tc, K	Pc, bara	Zc	Vshift	ω	Parachor
CO_2	44.01	304.12	73.74	0.2743	0.2175	0.225	80.00
C_1	16.04	190.56	45.99	0.2862	−0.0025	0.011	64.23
n-C_7	100.20	540.20	27.40	0.2611	0.1435	0.350	281.33

Due to large permeability contrast between the core and the surrounding space (artificial fracture), it was complicated to saturate the core with live oil. Oil would flow through the high permeable space leaving the core only partially saturated with live oil. Therefore, the space between the core and the core holder wall was initially filled with Wood's metal. The metal melting point is 70 °C; the experiment was conducted at 85 °C. Prior to saturating the core, the Wood's metal was melted and poured into the space between the core and core holder. The fracture was sealed with the metal and had zero permeability after cooling the system.

The core was evacuated and saturated with dead n-C_7. The dead n-C_7 oil was injected at several injection rates to determine absolute permeability. The system was then pressurized and live oil was injected into the core at a rate of 0.1 cm^3/min. During injection, the pressure was kept above 220 bar (saturation pressure) and three pore volumes of live oil were injected. Then the system was heated to 85 °C at a constant pressure and Wood's metal was removed from the annular space by injecting live oil. Oil was injected from the top and the melted Wood's metal drained from the bottom of the core holder. Fracture porosity was not measured after the metal was removed from the system. Total core + fracture permeability was not measured after removal of the Wood's metal.

Oil in the fracture was replaced by equilibrium gas. Reported gas injection rate at the beginning of displacement was 5 cm^3/min and was later reduced to 0.1 cm^3/min. The time at which the rate was changed was not reported. The experiment continued with equilibrium gas injection until no more oil was produced. After 4.2 days of equilibrium gas injection, CO_2 injection was started and lasted for 2.2 days.

With respect to measured surface oil production, Karimaie and Torsæter (2010) state "The standard volumes of liquid and gas obtained were measured after passing two step condensers at a constant temperature of 5 °C (41 °F) and −4 °C (24.8 °F), respectively, to condense any heavy hydrocarbons that may have been carried along with it".

4. Uncertainties and error sources

Core porosity defines the fluid in place, but had no direct impact on the fluid displacement process. Core diameter varied between 3.8 and 3.7 cm along the core height. Core diameter variation caused uncertainty in core and fracture pore volume, justifying our use of core (matrix) and fracture porosity as uncertainties used as regression parameters.

Ideally, the study of gravity drainage requires that viscous displacement in the core be eliminated or minimized. Unfortunately,

Table 3
SRK binary interaction parameters.

	CO2	C1	n-C7
CO_2	0.00000	0.12000	0.15000
C_1	0.12000	0.00000	0.01574
n-C_7	0.15000	0.01574	0.00000

Table 4
Measured cumulative oil and gas production.

Time days	Cumulative oil production (cm^3)	Cumulative gas production (L)	Time (day)	Cumulative oil production (cm^3)	Cumulative gas production (L)
0.000	0.0	0.00	2.339	68.0	65.96
0.010	6.0	0.05	2.397	68.0	67.03
0.016	8.0	0.10	2.470	70.0	68.49
0.020	10.0	0.89	2.523	70.0	69.87
0.027	12.0	3.27	2.589	71.0	70.95
0.037	14.0	5.34	3.084	76.0	85.39
0.044	16.0	9.20	3.318	76.0	90.59
0.051	18.0	12.68	3.350	76.0	91.00
0.057	20.0	15.87	3.517	78.0	96.75
0.066	22.0	17.10	4.130	82.0	116.83
0.083	24.0	18.05	4.233*	83.0	117.87
0.182	27.0	18.78	4.264	83.0	122.43
0.191	28.0	18.87	4.277	84.0	123.38
0.244	28.0	19.33	4.291	84.0	124.09
0.368	32.0	21.46	4.391	85.0	133.47
0.757	40.0	30.01	4.410	86.0	138.29
0.908	46.0	38.37	4.437	87.0	140.20
1.128	46.0	38.89	4.462	88.0	145.10
1.141	46.0	39.06	4.483	88.0	145.68
1.208	52.0	44.38	4.606	88.0	147.12
1.254	52.0	44.81	4.639	88.0	150.54
1.280	52.0	45.22	4.668	88.0	151.11
1.313	60.0	54.67	5.154	90.0	166.10
1.462	60.0	56.03	5.187	90.0	166.32
1.487	61.0	56.61	5.458	90.0	169.08
1.506	62.0	56.89	5.500	90.0	172.01
2.037	64.0	59.50	5.520	90.0	172.17
2.085	64.0	60.12	6.129	90.5	191.71
2.108	65.0	60.50	6.229	90.5	197.84
2.116	65.0	60.90	6.379	90.5	202.16
2.320	68.0	65.42			

* CO2 injection start.

it was observed in the Karamaie experiments that some Wood's metal remained in the space between the core and core holder. Reported fracture porosity was 93%, and fracture permeability may have been reduced. Porosity reduction of the fracture will affect fracture pore volume. Fracture permeability reduction could affect the recovery mechanism, changing from gravity-dominant to viscous-dominant for gas injection.

Another uncertainty is surface separation efficiency in the lab tests, and the correct modeling of the separation process. It was reported that produced stream passed through a two-step condenser 5 °C (41 °F) and −4 °C (24.8 °F). But according to direct discussion with Karamaie and observation of the laboratory system, the stream was passed through coiled pipe in an ice–fresh–water bath (condenser) and then flashed to a measuring cylinder at atmospheric pressure. The

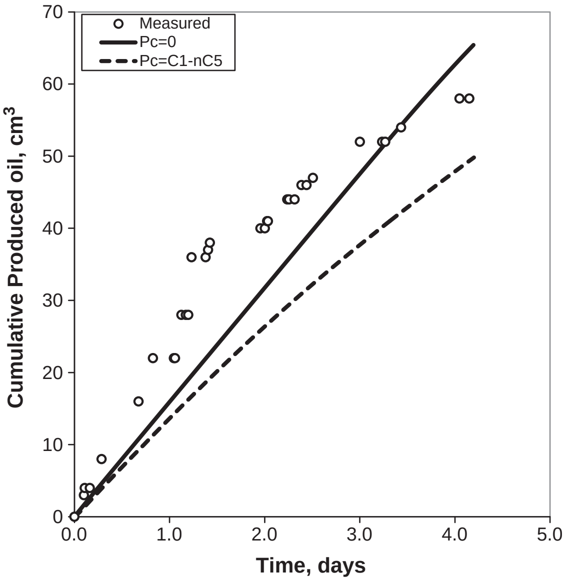

Fig. 1. Measured oil production without considering early produced oil and simulation result of assuming gravity-drainage mechanism.

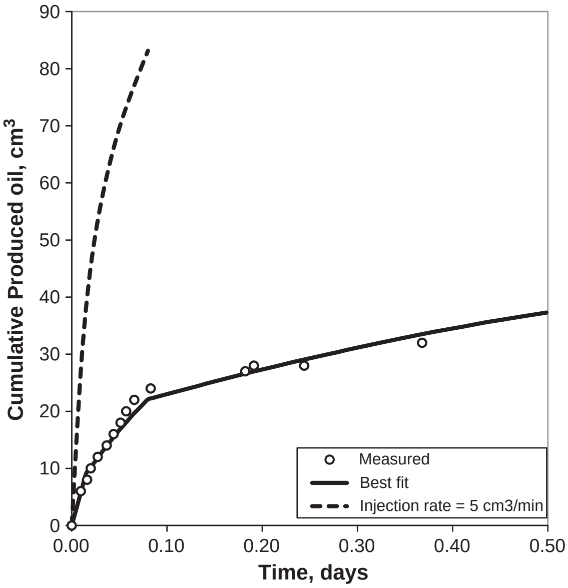

Fig. 2. Early measured oil production of the experiment and simulation results of 5 cm^3/min injection rate and best fit.

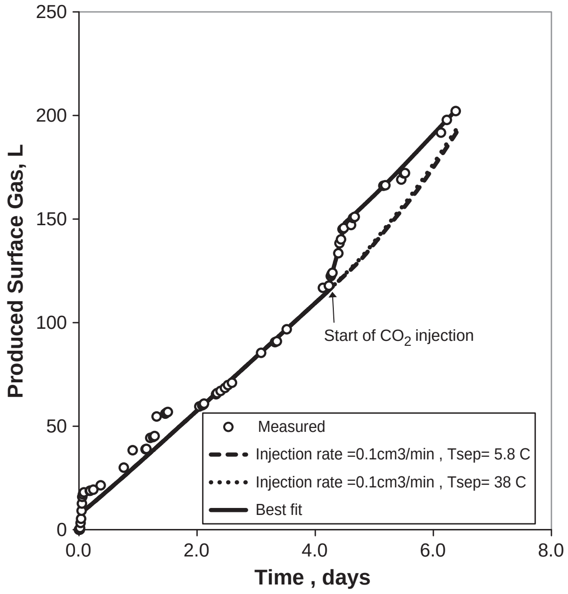

Fig. 3. Measured gas production with matched simulation result and results of 0.1 cm^3/min injection rate.

measuring cylinder was placed in and ice-brine bath. Stream temperature might not reach 5 °C (41 °F) after passing through the condenser. The whole stream was not passed through a −4 °C (24.8 °F) condenser, only the flashed liquid was cooled. According to these observations, temperature of the gas–oil separation was not known with any accuracy, and it is difficult to model accurately.

5. Model description

The matrix block and fractures were initially filled with oil. The fractures were assumed to have negligible capillary pressure. The matrix and the fractures dimensions were the same as core and fracture in the experiment. A two-dimensional radial gridded model was used, where the matrix block was surrounded by two horizontal fractures at the top and bottom and one vertical fracture. Fine gridding was needed for CO_2 gas injection to reduce numerical dispersion and achieve better results (Alavian and Whitson, 2005). Ten and 51 grid cells were used in radial and vertical directions, respectively.

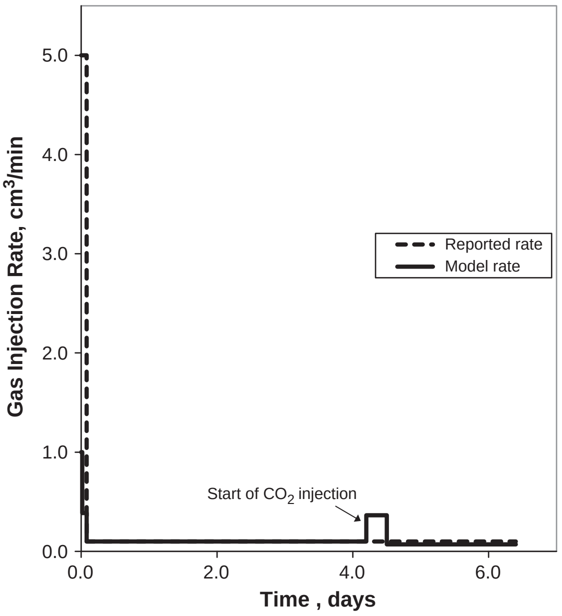

Fig. 4. Reported and model gas injection rate profile during the experiment.

The *SENSOR* (Coats Engineering, 2010) and *Eclipse 300* simulators with implicit solution method were used for simulation models. *Eclipse 300* was used to examine diffusion effects on the production behavior. A 3-component SRK EOS was used. The EOS properties of the components are summarized in Table 2 and the binary interaction parameters are given in Table 3. SENSOR (Coats Engineering, 2010) and *Eclipse 300* models gave the same results without diffusion.

An analytical capillary pressure and relative permeability formulation were used (Coats, 2008). C_1–n-C_5 capillary pressure measured by Christoffersen (1992) at a similar core was taken as core capillary pressure in the model. This capillary pressure was scaled with IFT according to the equation (Coats, 2008):

$$P_c = \left(\frac{\sigma}{\sigma_{ref}}\right) P_{c,lab}, \tag{1}$$

where $P_{c,lab}$ is original capillary pressure input in the model, σ_{ref} is reference interfacial tension (IFT) which is equal to 1.5 mN/m and σ is IFT which is calculated from the following equation (Coats, 2008):

$$\sigma_{go} = \left[\sum P_i \left(x_i \frac{\rho_o}{M_o} - y_i \frac{\rho_g}{M_g}\right)\right]^4. \tag{2}$$

There was no capillary pressure in the fracture. *Eclipse 300* had the same formulation for scaling capillary pressure and calculating IFT.

The *Pipe-It/Streamz* (Petrostreamz AS, 2010) software was used to calculate cumulative oil and gas production from reservoir simulation results. One separator was defined to simulate produced stream in the experiment. Atmospheric pressure was considered as separator pressures same as the experiment. As mentioned above separator temperature was not measured during the experiment, thus, it was used as a regression parameter.

6. Matching experimental data

6.1. Fracture permeability

In our work, measured cumulative oil production from the outset of injection (Table 4) was history-matched. Karimaie (2007) and Karimaie and Torsæter (2010) report recovery factors based on the assumption that injected gas replaces only oil in the space between the core and core holder at early times, and that no oil was produced from the core during that time. That means the oil production before 0.083 day (about 2 h) amounting to 24 cm^3 in Table 4 (compared with 90.5 cm^3 total production during entire test) was neglected in their oil recovery calculation. Their assumption of zero flow resistance in the fracture was shown to be suspect, if not wrong, based on our analysis. Together with some uncertainty in core porosity (i.e. initial oil in place

Table 5
Regression Variables.

Relative permeability	Final		Initial Value	Lower limit	Upper limit
	n = 1	n = 2			
Residual oil saturation (%)	5.1	5.8	10.0	5.0	20.0
Fracture permeability (md)	26.3	20.4	30.0	10.0	100.0
Core porosity (%)	44.5	48.0	44.0	44.0	48.0
Fracture porosity (%)	93.6	89.1	90.0	85.0	100.0
Separator temperature of equilibrium gas injection (oC)	5.8	7.0	5.0	−4.0	15.6

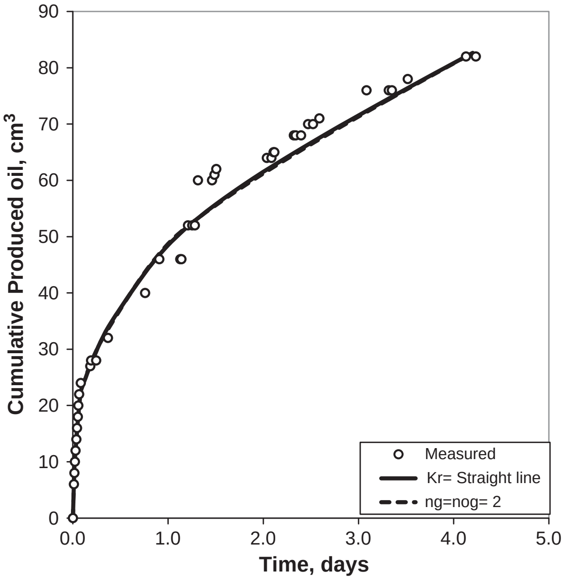

Fig. 5. Measured oil production with matched simulation results of equilibrium gas injection period.

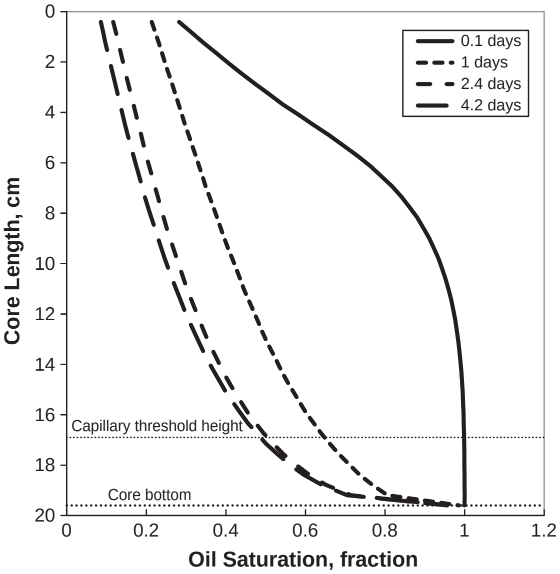

Fig. 7. Core oil saturation profile during equilibrium gas injection period from numerical model with linear core relative permeability.

in the core), we decided not to use the Karimaie-reported oil recovery factors in history matching, but instead to match reported surface oil volumes produced from the outset of injection.

To illustrate the impact of fracture flow resistance on oil recovery from the core in the Karimaie experiments, we setup two comparison models where the matrix block is filled initially with oil, and the fracture was initialized with equilibrium injection gas. This condition corresponds to the Karimaie *assumption* at the end of the 0.083 days when all the oil had been removed from the fracture and gas had yet to enter the core.

The fractures had zero capillary pressure and high permeability (100 D) to ensure that flow resistance in the fracture was negligible and that oil recovery from the core was controlled by capillary–gravity drainage. Core porosity and separator temperature were set to 44% and 5 °C (41 °F), respectively, in both models. One model used a capillary pressure curve, where gas drainage was expected only if the core height was greater than the capillary entry height (2.7 cm). In the other model we assumed zero capillary pressure in the core, to provide an extreme (albeit unphysical) case of oil drainage from the core.

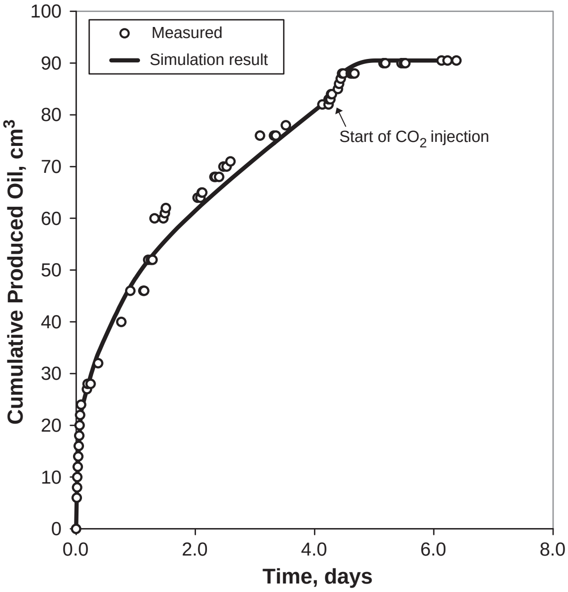

Fig. 6. Measured oil production with matched simulation result of equilibrium gas injection and CO_2 injection periods.

Our first model used a chalk capillary pressure curve, the shape of which dictates the rate of oil recovery from the core as gravity and capillary forces balance. Clearly, there exists some uncertainty in the capillary pressure curve and its scaling with IFT (constant for the equilibrium gas injection test). Fig. 1 shows predicted oil production compared with the reported oil recovery by Karimaie using oil production data after 0.083 days. Predictions are significantly lower than reported.

As an extreme treatment of core capillary pressure, we used zero capillary pressure in a second model. The only driving force of recovery is now gravity. Fig. 1 shows that even in the absence of capillary pressure in the core, predicted oil recovery was lower than reported recoveries up to 3 days, and had a very different production rate profile than reported.

Our conclusion, as shown in the final model history match of the Karimaie data, was that the oil production from the core starts immediately after gas was injected, and that the core and fracture jointly produce oil over a period significantly longer than 0.083 days. The fracture resistance was found to be significant, and far lighter than justifying the assumption of an infinite conductivity fracture.

6.2. Equilibrium gas injection rates

It was reported that equilibrium gas was injected at high rate (5 cm^3/min) from the top and then decreased to 0.1 cm^3/min after 0.083 days. Fig. 2 clearly shows a rate change at 0.015 days. However, using 5 cm^3/min injection rate in the model during the time period up to 0.083 days leads to significantly higher oil production than reported experimentally. Our final model used the following injection rates: 1 cm^3/min ($0<t<0.015$ days = 22 min), 0.386 cm^3/min ($0.0150<t<0.083$ days = 120 min), and 0.1 cm^3/min ($t>0.083$ days); this is to be compared with reported injection rates: 5 cm^3/min ($0<t<0.083$ days), and 0.1 cm^3/min ($t>0.083$ days).

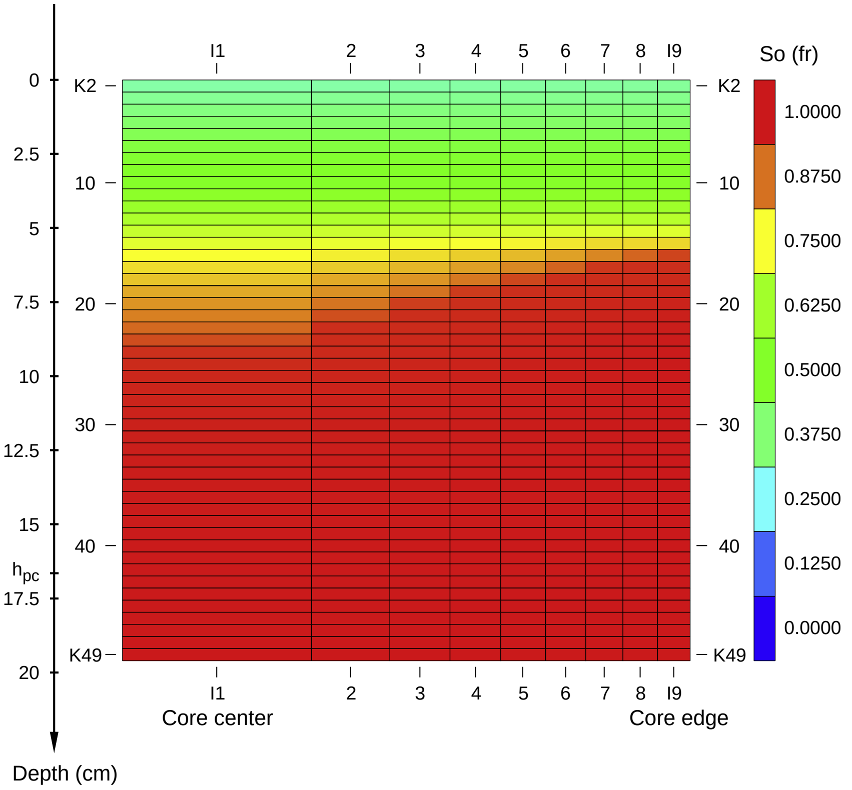

Fig. 8. Oil saturation map of core after 2.4 h for matched model with linear core relative permeability (at about 18% oil recovery).

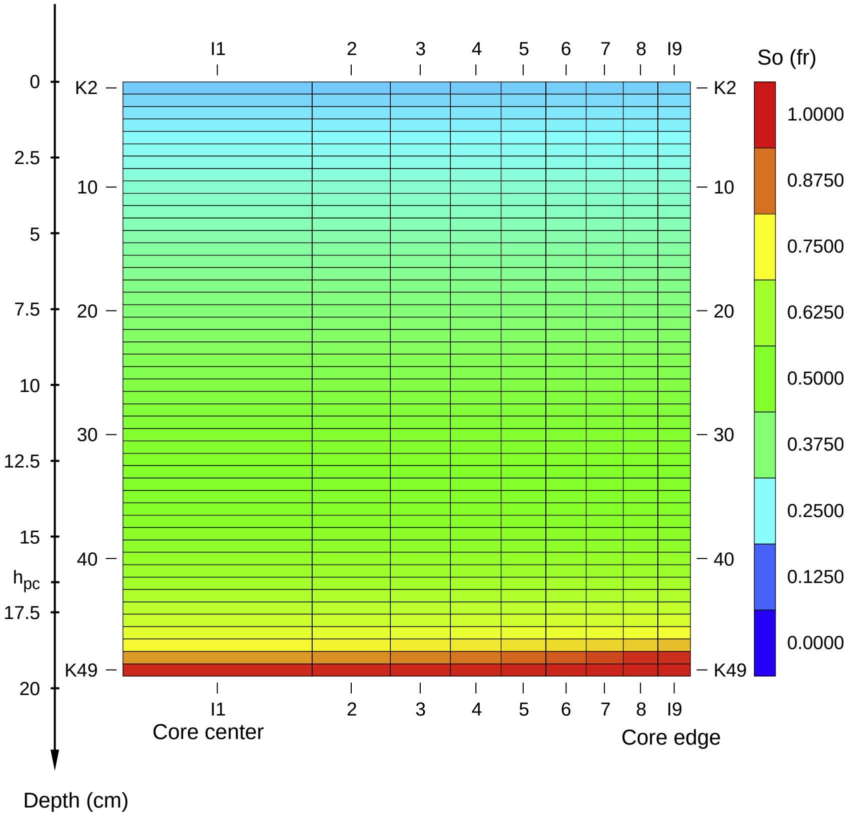

Fig. 9. Oil saturation map of core after 1 day for matched model with linear core relative permeability (at about 54% oil recovery).

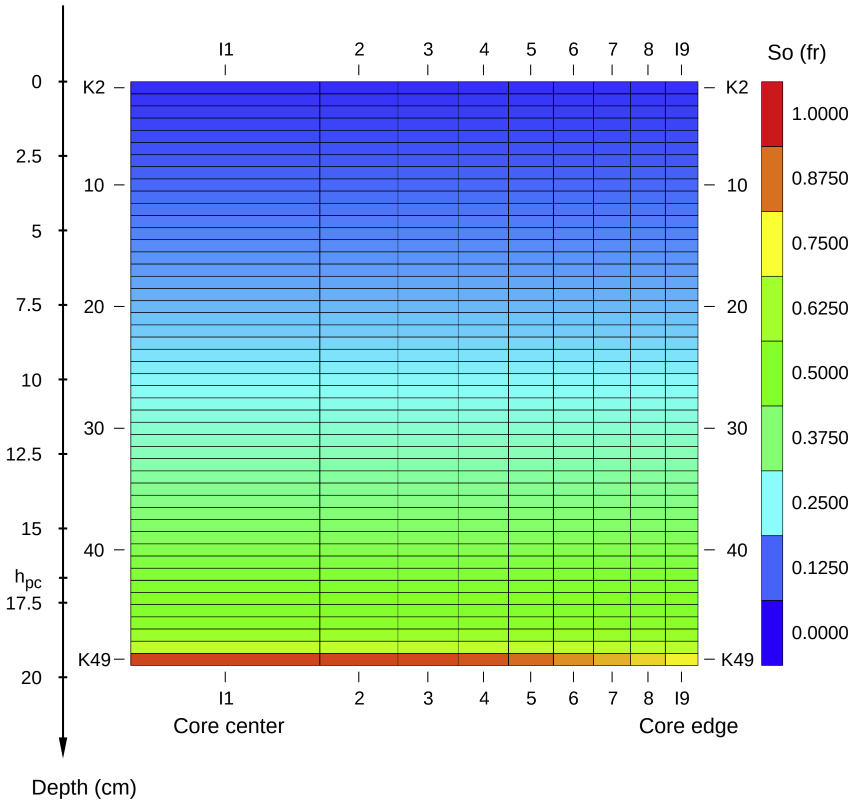

Fig. 10. Oil saturation map of core after 4.20 days for matched model with linear core relative permeability (at about 70% oil recovery).

6.3. CO_2 injection rates

Cumulative gas production was matched reasonably well during equilibrium gas injection, as illustrated in Fig. 3. There was a rapid increase in gas production when CO_2 injection started. This could be caused by: (a) increasing gas injection rate, (b) change in effective surface temperature and/or (c) decreasing gas formation volume factors. CO_2 was injected from the top, and gas produced from the bottom of core holder. It was expected that equilibrium gas would be produced early during CO_2 injection. On the other hand, Fig. 3 indicates that increasing temperature alone could not justify this change of gas production profile. Karimaie does not report an injection rate increase when CO_2 injection starts, but according to gas production behavior in Fig. 3 and and communication with Karimaie, the injection rate was in fact increased at about 4 days. By trial and error we found that CO_2 injection rate was increased from 0.1 cm^3/min to 0.364 cm^3/min at 4.2 days, and then reduced to 0.07 cm^3/min at 4.5 days, this CO_2 injection rate profile giving a consistent match to produced gas rate. The final injection rate profile during the entire experiment is shown in Fig. 4.

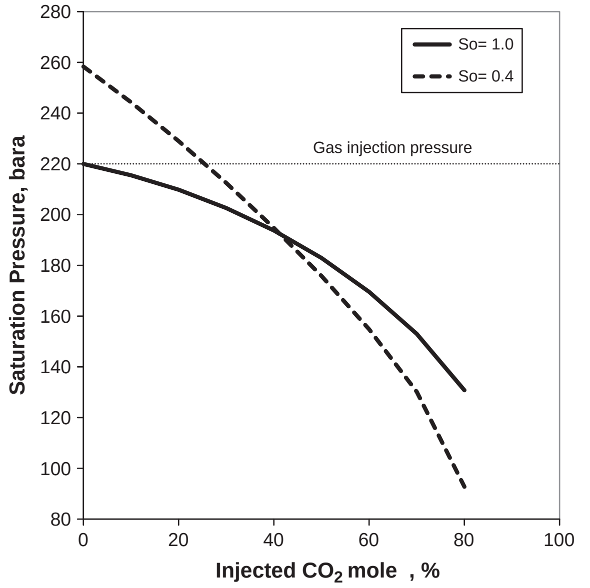

Fig. 11. Saturation pressure versus injected CO_2 mole percent calculated by swelling test for 1 and 0.4 oil saturation.

6.4. Surface SEPARATION

The produced mixture from the core holder was separated with a simple process, namely a flash to atmospheric pressure and temperature controlled by a pre-separation ice–water bath. The effective surface process temperature is assumed to vary with the injection rate, and particularly CO_2 injection because CO_2 has lower thermal conductivity than equilibrium gas. We found that the assumed separator temperature had a pronounced effect on volume produced, and the surface temperature model used for CO_2 injection was 30 °C (86 °F) in the period $0<t<0.086$ days, and 26.7 °C (80 °F) for $t>0.086$ days.

Table 6
Diffusion coefficients for oil and gas phase.

Component	D_o (cm^2/s)	Dg (cm^2/s)	Dg /Do
C_1	1.04E-05	3.43E-05	3.3
n-C_7	1.04E-05	3.43E-05	3.3
CO_2	1.27E-05	6.45E-05	5.1

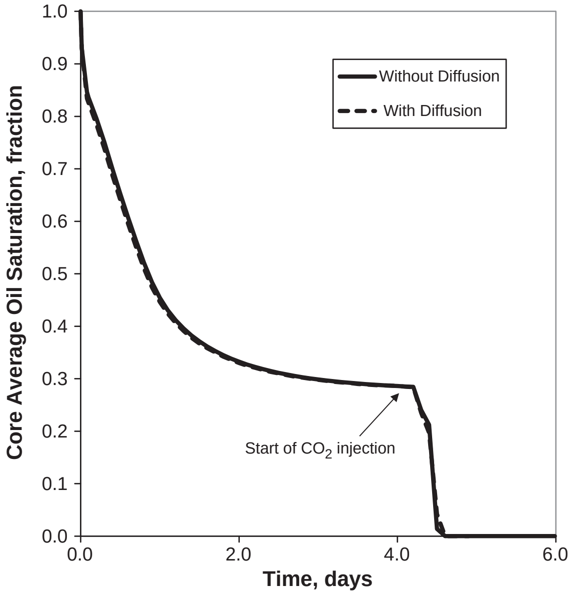

Fig. 12. Profile of oil saturation in the core during equilibrium gas and CO_2 injection period with and without diffusion.

6.5. Regression parameters

A number of laboratory parameters were considered as uncertain to the extent that their value could be adjusted as part of the history matching process. These include: (a) fracture permeability, (b) core residual oil saturation, (c) core porosity, (d) fracture porosity, and (e) separator temperature. Core relative permeability was also considered uncertain, but instead of using an IFT-dependent relative permeability model, we simply considered two cases — mild curvature with saturation exponent of n = 2, and low-IFT/near-miscible straight-line curves (n = 1). Automated regression was run to obtain a best fit of the measured cumulative oil produced by adjusting the five parameters above (a)–(e). Initial values, lower and upper limits of the regression parameters are given in Table 5. Because the experiment was conducted at a low IFT (0.15 mN/m) for equilibrium gas injection, and even lower for CO_2 injection, we used two sets of oil–gas relative permeabilities using saturation exponents of 2 and 1 both models giving a reasonable match of lab data (Fig. 5). Best-fit parameters for core and fracture porosities determined with straight-line relative permeabilities were more consistent with values reported by the lab. IFT decreased during CO_2 injection from 0.15 to 0.0001 mN/m at the displacement front, and therefore the n = 1 relative permeability model was considered the most appropriate to simulate the CO_2 injection period.

Fig. 6 shows measured cumulative oil production and simulation results.

7. Recovery mechanism

Reported oil recovery factor was not reliable because (a) it was based on the invalid assumption that only fracture oil, located in the space between the core and core holder, is produced at early times, and (b) initial oil in place used to calculate reported recovery factors was found to be erroneous. In this study, the model oil recovery factor is calculated from oil saturations and is used to study the oil recovery mechanism.

Viscous/gravity ($R_{v/g}$) dimensionless ratios were used to understand the importance of the various recovery mechanisms during the production (Wylie and Mohanty, 1999; Stalkup, 1983; Løvoll et al., 2005):

$$R_{v/g} = \frac{\Delta P_{visc}}{\Delta P_{grav}} = \frac{u\mu_o}{kg\Delta\rho_{og}}, \tag{3}$$

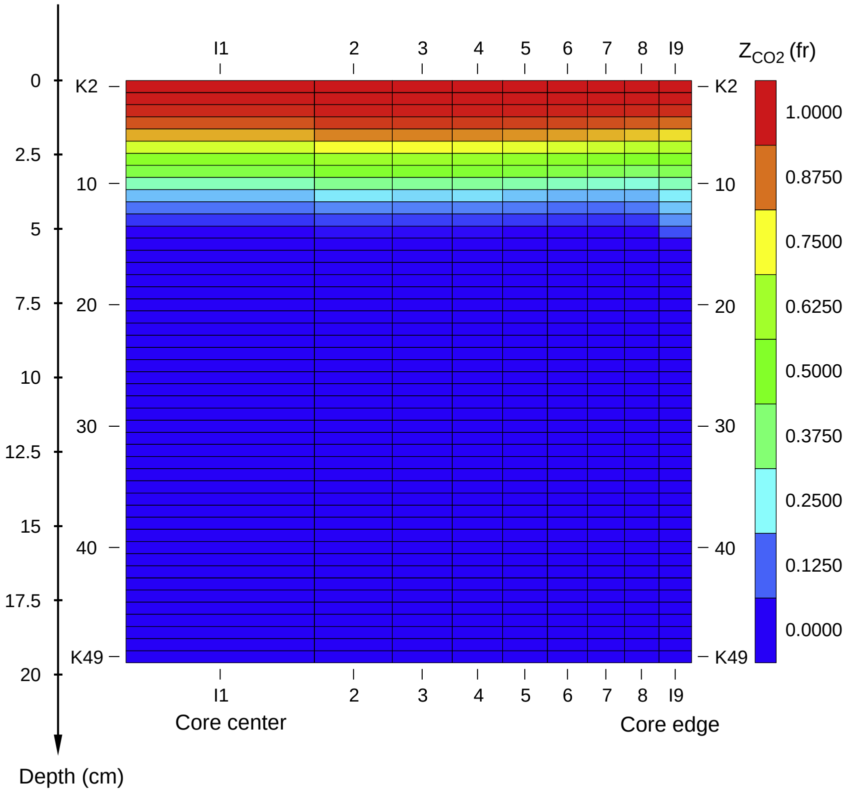

Fig. 13. CO_2 mole fraction map of core after 4.25 days for matched model without diffusion effect.

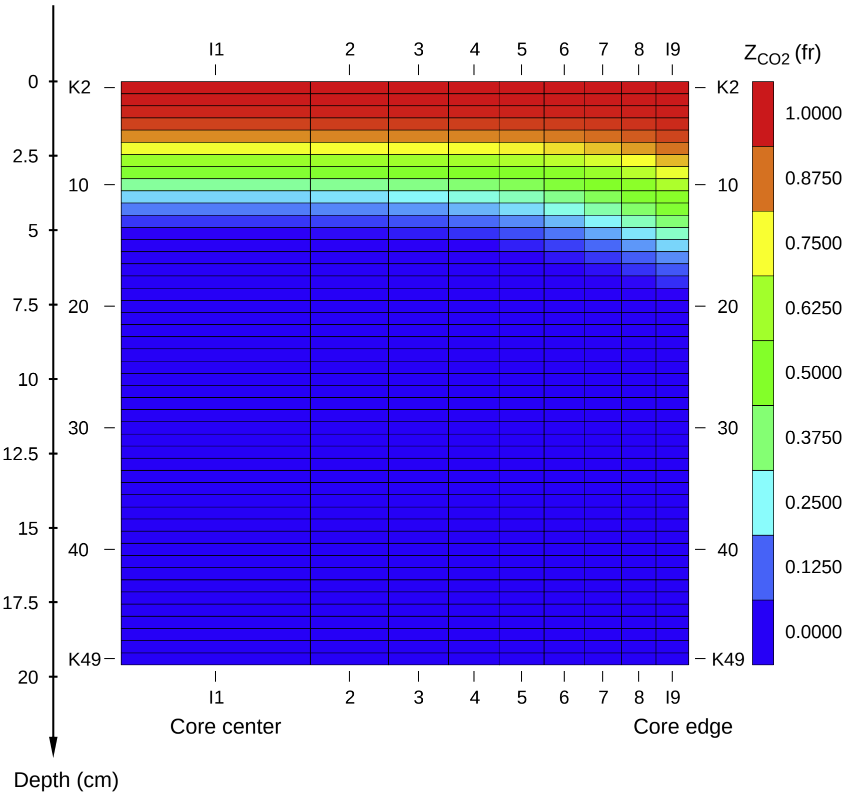

Fig. 14. CO_2 mole fraction map of core after 4.25 days for matched model with diffusion effect.

where u is linear Darcy velocity in z-direction, μ_o is oil viscosity, k is matrix-block permeability, $\Delta\rho_{og}$ is oil and gas density difference and g is gravity-acceleration constant.

This experiment was conducted to study low interfacial tension gravity drainage in fractured porous media. However, as mentioned above, fracture permeability was not sufficiently large to study fracture–matrix gravity drainage. One characteristic of gravity drainage with equilibrium-gas injection is that oil below the capillary threshold height is not recovered. As shown in Figs. 7–10 the displacement front from our history-matched model does not stop above the capillary threshold height (2.7 cm), and hence gravity drainage alone could not be the recovery mechanism. We found that viscous displacement was dominant during equilibrium-gas injection, as verified from a frontal viscous/gravity ratio $R_{v/g}$ of 5.5 calculated at the fifth hour of the experiment.

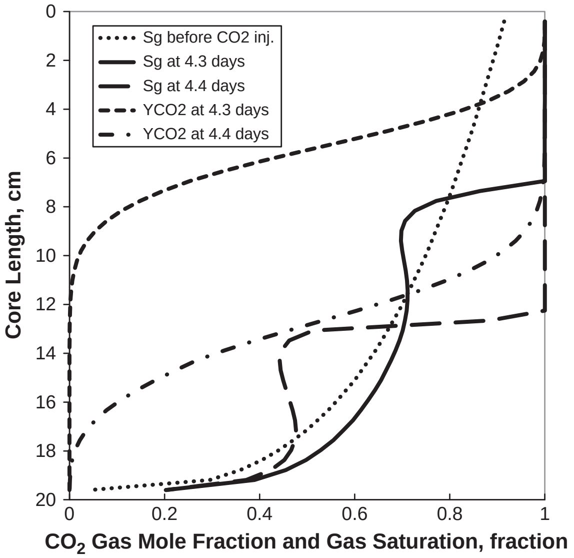

Fig. 15. Profile of CO_2 gas mole fraction and gas saturation in the core during CO_2 injection period.

More oil was produced after injecting CO_2, as shown in Fig. 6. At the end of the experiment no oil production was observed while still injecting CO_2. The model shows that 100% oil recovery was achieved after somewhat more than one PV CO_2 injected. As seen in Fig. 11, CO_2 is first-contact miscible with the equilibrium oil and first-contact miscible after reaching 30 mol% CO_2 content when contacting an equilibrium oil–gas mixture having approximately 60% gas saturation initially. A 100% recovery after about 1 PV CO_2 injected is expected given the thermodynamic miscibility conditions and an efficient top-down, gravity-stable core displacement.

Diffusion was another mechanism that could play a role in production during CO_2 injection period. We examined the effect of diffusion by running the model with and without diffusion transport. Diffusion coefficients were calculated from the extended Sigmund correlation (da Silva and Belery 1989), given in Table 6. As illustrated in Fig. 12 average oil saturation of the core was identical for runs with and without diffusion. Comparison of CO_2 map at 4.25 days (102 h) for diffusion and non-diffusion cases revealed small differences, as shown in Figs. 13 and 14. Our results agree with Hoteit and Firoozabadi (2006) who show that diffusion has minor effect in viscous-dominated displacements.

Near-miscible and viscous displacements were the main two production mechanisms during CO_2 injection. Pressure gradient caused CO_2 to enter into the core and the core oil was displaced miscibly by CO_2. Model oil saturation profile and gas mole fractions indicate that that an oil bank builds ahead of the miscible front (where $Sg \rightarrow 0$), as illustrated in Figs. 15 and 16. Note that the oil carrying capacity of gas ahead of and behind the front increases with time.

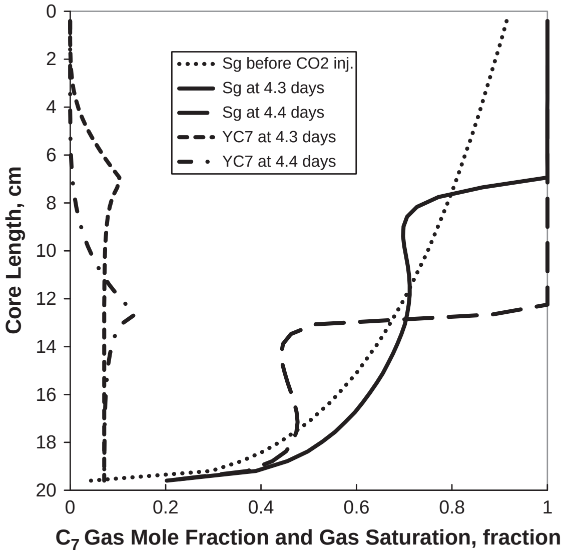

Fig. 16. Profile of n-C_7 gas mole fraction and gas saturation in the core during CO_2 injection period.

Because oil was produced from both the matrix and the fracture at early times, it is difficult to calculate matrix recovery factor based on produced oil. Therefore matrix oil recovery was calculated from total average oil saturation S_o in the core using the following relation:

$$RF = \left(1-\frac{S_o}{S_{oini}}\right) \tag{4}$$

For model results at a given time, the calculated oil recovery from Eq. (4) is slightly higher than oil recovery calculated based on production. The difference stems mainly from the oil carried in solution in the gas behind the displacement front, this oil being produced (by surface condensation) only after the enriched CO_2-rich gas reaches the end of the core and is produced. Calculated oil recovery is shown in Fig. 17. About 70% of the initial oil in place in the core was recovered by equilibrium gas injection and all residual oil was produced by CO_2 injection at the end of the experiment.

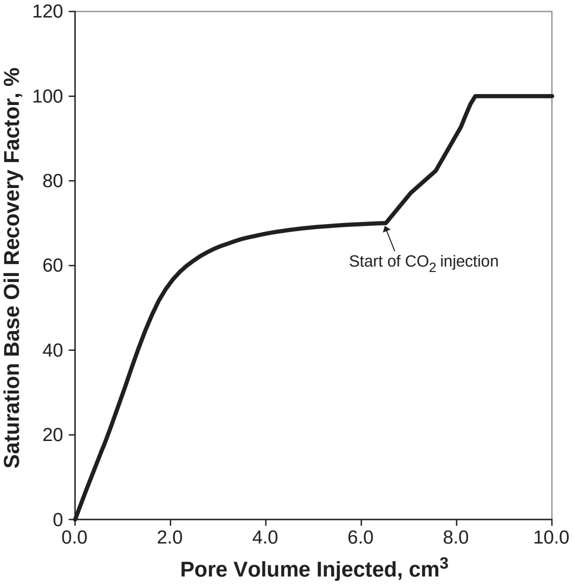

Fig. 17. Calculated oil recovery factor based on core oil saturation.

8. Designing fractured reservoir experiments using CO_2

We recommend the following experimental design procedures when performing CO_2 injection experiments for fractured reservoirs:

(1) Fracture (core-annulus) permeability should be measured after the core is initialized with oil. A rule-of-thumb for fracture conductivity is that total core + fracture pressure drop is small compared the pressure drop when flow occurs only through the core.
(2) Continuous measurement of separator temperature and pressure.
(3) Oil and gas produced mass and volume should be reported, together with periodic surface oil densities.
(4) Periodic measurement of produced surface gas and surface oil stream assumptions.
(5) Oil and gas compositions initially saturating the core should be determined experimentally.
(6) Additional PVT experiment like a swelling test that includes bubblepoint, near-critical, and dewpoint mixtures should be conducted for tuning the EOS model.
(7) Determine relevant (drainage and/or imbibition) capillary pressure and relative permeability of core used in the experiment.

9. Conclusions

Based on analysis of experimental results and a history-matched numerical model which describes accurately all key laboratory performance data; we make the following conclusion, which are specific to this particular experimental study:

(1) Viscous displacement is significant and gravity–capillary drainage is not significant in the Karimaie experiments due to low "fracture" (core-annulus) permeability.
(2) The laboratory data history matched include cumulative oil and gas produced during displacements with equilibrium gas and CO_2 injection.
(3) During the CO_2 injection period, near-first-contact miscible displacement is the dominant production mechanism.
(4) Separator conditions play an important role in measuring and modeling oil production for high-pressure, high-temperature CO_2 injection experiments — mainly because reservoir gas contains significant oil in solution which is produced by condensation at surface conditions.
(5) Diffusion has no impact on the CO_2 injection recovery mechanism because of the dominant viscous-force displacement.

Nomenclature

D_g	gas diffusion coefficient, L^2/t, cm^2/s
D_o	oil diffusion coefficient, L^2/t, cm^2/s
k	matrix-block permeability, L^2
M_g	gas molecular weight
M_o	oil molecular weight
N	number of grid cells
Nx	number of grid cells in x-direction
Nz	number of grid cells in z-direction
P_C	capillary pressure, m/Lt^2, bara
$P_{C,lab}$	measured capillary pressure, m/Lt^2, bara
P_{cgo}	drainage gas-oil capillary pressure, m/Lt^2, bara
Pi	parachor of component i
RF	oil recovery factor
S_o	oil saturation
S_{oini}	initial oil saturation
S_{org}	residual oil saturation to gas
u	linear Darcy velocity, L/t^2
x_i	oil mole fraction of component i
y_i	gas mole fraction of component i

$\Delta\rho_{og}$	oil and gas density difference, m/L^3
μ_o	oil viscousity, m/(t.L)
ρ_g	gas density, m/L^3, kg/m^3
ρ_o	oil density, m/L^3, kg/m^3
σ_{go}	gas-oil interfacial tension, m/t^2, mN/m
σ_{lab}	reference gas-oil interfacial tension, m/t^2, mN/m

Acknowledgment

We would like to thank Shell for financing this study, as part of Alavian's PhD research. This paper was presented at the SPE/EAGE Reservoir Characterization and Simulation Conference held in Abu Dhabi, October 2009 (SPE 125362).

References

Alavian, S.A., Whitson, C.H., 2005. CO_2 IOR potential in naturally-fractured Haft Kel Field, Iran. Paper IPTC 10641 Present at International Petroleum Technology Conference, Doha, Qatar, 21–23 November.

Asghari, K., Torabi, F., 2008. Effect of miscible and immiscible CO_2 flooding on gravity drainage: experiment and simulation results. Paper SPE 110587 Presented at the 2008 SPE/DOE Improved Oil Recovery Symposium, Tulsa, Oklahoma, U.S.A., 19–23 April.

Christoffersen, K., 1992. High-Pressure Experiments with Application to Naturally Fractured Chalk Reservoirs. PhD Dissertation, NTNU, Trondheim, Norway.

Coats, K.H., 2008. Sensor Manual. www.coatsengineering.com. 2008, 20 May.

Coats Enginering, 2010. *SENSOR*, www.coatsengineering.com.

da Silva, F.V., Belery, P., 1989. Molecular Diffusion in Naturally Featured Reservoirs: a Decisive Recovery Mechanism. Paper SPE 19672 presented at the 64th SPE Annual Technical Conference and Exhibition, San Antonio, Texas, U.S.A., 8–11 October.

Hoteit, H., Firoozabadi, A., 2006. Numerical modeling of diffusion in fractured media for gas injection and recycling schemes. Paper SPE 103292 Presented at the 2006 SPE Annual Technical Conference and Exhibition, San Antonio, Texas, U.S.A., 24–27 September.

Karimaie, H. 2007. Aspects of Water and Gas Injection in Fractured Reservoir. PhD Dissertation, NTNU, Trondheim, Norway.

Karimaie, H., Torsæter, O., 2010. Low IFT gas–oil gravity drainage in fractured carbonate porous media. J. Petrol. Sci. Eng. 70 (1–2), 67–73.

Li, H., Putra, E., Schechter, D.S., Grigg, R.B., 2000. Experimental investigation of CO_2 gravity drainage in a fractured system. Paper SPE 64510 Presented at the SPE Asia Pacific Oil and Gas Conference and Exhibition, Brisbane, Australia, 16–18October.

Løvoll, G., Meheust, Y., Måløy, K.L., Aker, E., Schmittbuhl, J., 2005. Competition of gravity, capillary and viscous forces during drainage in a two-dimensional porous medium, a pore scale study. Energy 30 (6), 861–872. doi:10.1016/j.energy.2004.03.100.

Petrostreamz AS, 2010. *Pipe-It/Streamz*, www.petrostreamz.com.

Stalkup Jr., F.I., 1983. Miscible displacement. In: Doherty, Henry L. (Ed.), Monograph Series, 8. SPE, Richardson, Texas, USA.

Talukdar, S. 2002. Ekofisk Chalk: core measurements, stochastic reconstruction, network modeling and simulation. PhD Dissertation, NTNU, Trondheim, Norway.

Wylie, P.L., Mohanty, K.K., 1999. Effect of wettability on oil recovery by near-miscible gas injection. SPE Res. Eval. Eng. 2 (6), 558–564. doi:10.2118/59476-PA SPE-59476-PA.

Zick Technologies, 2010. *PhazeComp*, www.zicktech.com.

Scale Dependence of Diffusion in Naturally Fractured Reservoirs for CO_2 Injection

Paper SPE 129666 presented at the 2010 SPE Improved Oil Recovery Symposium, Tulsa, Oklahoma, USA, 24–28 April

Paper III

SPE 129666

Scale Dependence of Diffusion in Naturally Fractured Reservoirs for CO_2 Injection

S.A Alavian, SPE, NTNU and C.H. Whitson, SPE, NTNU/PERA

This paper was prepared for presentation at the 2010 SPE Improved Oil Recovery Symposium held in Tulsa, Oklahoma, USA, 24–28 April 2010.

Abstract

Based on detailed compositional simulations of matrix/fracture systems, we present results of the impact of diffusion on oil recovery by CO_2 injection for small-scale laboratory experiments and field-scale systems. We consider reservoir conditions that lead to a range of recovery mechanisms from clearly immiscible to near-miscible.

Laboratory experimentation is a desirable approach to understanding the recovery mechanism of CO_2 injection in fractured oil reservoirs because an unusual combination of complex physical phenomena exists. A fundamental problem with this approach is scaling the results to field conditions, and particularly matrix block size which is often many (5-100) times larger than laboratory cores. Molecular diffusion is clearly affected by matrix block dimensions, and any affect of diffusion on the recovery mechanism would also be scale dependent. In this paper we provide guidelines and computational examples of laboratory tests to study CO_2 recovery processes, including diffusion. We also study the change in recovery processes as matrix/fracture dimensions approach field scale.

We recommend using reservoir core or outcrop samples similar to the actual reservoir rock, with dimensions (5-25 in^2 horizontal area and 10-30 in high). A synthetic model oil can be constructed to mimic PVT properties of the actual reservoir oil, and in particular the minimum miscibility pressure (MMP) as defined by a traditional 1D multi-contact displacement process – MMP_{1D}, reduced gas-oil interfacial tensions (IFT) and oil-gas density differences. The core should be placed in a container with annular space representing the fracture. CO_2 is injected at various rates into the annular space, at relevant reservoir pressures both above and below the MMP_{1D}.

In this work, the effect of several key parameters are studied – matrix permeability, matrix block size, CO_2 injection rate and reservoir pressure. One of the key results is the effect of diffusion on oil recovery, and how it varies with matrix block size and CO_2 injection rate. We show that diffusion has a dominant effect on recovery mechanism in experimental tests, except at very low CO_2 injection rates. For field-scale matrix/fracture systems, diffusion has a significant effect on the rate of recovery, the effect becoming noticeable for low reservoir pressures and/or high fracture densities.

Compared with earlier studies on the Iranian Haft-Kel reservoir considered in this paper, our current work shows that the rate of high recoveries by CO_2 injection reaches more than 90% 2-10 years with diffusion, versus >100 years in the absence of diffusion, for an 8x8-foot matrix grid.

Introduction

CO_2 injection has recently been shown to provide significant enhanced oil recovery from naturally fractured reservoirs. Alavian and Whitson (2005) study CO_2 injection in the naturally-fractured Haft Kel field, Iran, based on detailed compositional simulations of the matrix/fracture system. Significant recoveries >90% were reported at pressures close to initial and current reservoir conditions, but the studies showed recovery periods of >100 years. That work did not consider molecular diffusion which is the main topic of this study.

Few experiments are reported on CO_2 injection in fractured reservoirs. Li *et al* (2000) perform at 1750 psig CO_2 injection on artificially fractured cores after water flooding in a dead-oil system. Gravity drainage would appear to be the dominant recovery mechanism in these tests, with significant tertiary oil recovery after water flooding. They found that CO_2 gravity drainage declines as the rock permeability decreases and initial water saturation increases. Asghari and Torabi (2008) CO_2 gravity drainage experiments with a synthetic "dead" oil (n-C_{10}), above and below the CO_2 MMP. They were not able to match laboratory experiments with a simulation model. Hoteit and Firoozabadi (2006) have studied diffusion in fractured media for gas injection and recycling schemes by numerical modeling. They report that diffusion improves oil recovery and delays gas breakthrough. They neglect gas-oil capillary pressure in the matrix block in their modeling study.

This modeling study uses the Haft Kel reservoir fluid and field matrix/fracture system to study the mechanisms of CO_2 recovery including molecular diffusion. We also present a 3-component simple oil and laboratory-dimension matrix/fracture system that studies the CO_2 recovery mechanism including diffusion. This latter lab system could be used for laboratory testing and verification of our simulation results. Confirmation of those simulations of a lab system, or a similar lab system, using the modeling methods proposed in this paper would give more confidence to the field-scale simulation results we provide.

Description of Matrix/Fracture Models

Haft Kel Model. For the Haft Kel field-scale matrix/fracture system, a single matrix block surrounded by fractures was used to study the matrix/fracture fluid exchange and recovery mechanisms. Significant compositional variations develop within the matrix block, resulting in high recoveries.

Haft Kel petrophysical properties and initial fluid compositions are taken from Saidi (1987). The matrix is represented by a cube with 8-ft (2.44-m) dimension, 0.8 md isotropic permeability and default fracture width of 0.01 ft (0.30 cm) having 100 D permeability. Due to the matrix block symmetry, only half of the matrix block is modeled. A 2D Cartesian grid is used where the matrix block is surrounded by two horizontal fractures on the top and bottom and one vertical fracture on the right side of the matrix block.

The matrix block is initially filled with oil and the fractures are initialized with injection gas. Zero capillary pressure and high permeability of the fractures means that the viscous forces are negligible compared to gravity and capillary forces. Injection rate was investigated using production and gas injection wells at the bottom and top fracture, respectively. The production well is pressure controlled and injection well is rate controlled. Conceptually we are looking at a matrix block located at the no-flow boundary between an injector and a producer where lateral pressure gradients are negligible. All models use an 11x1x102 (N_x N_y N_z) grid where the 10x1x100 grid cells represent a half matrix block.

Eclipse 300 is used for all simulations. An 11-component tuned SRK (Soave-Redlich-Kwong) equation of state (EOS) describes phase and volumetric behavior; the Lorenz-Bray-Clark correlation, tuned to viscosity data, is used to calculate viscosities. EOS component properties and binary interaction parameters (BIPs) are given in **Tables 1** and **2** (Alavian and Whitson 2005).

PVT simulations needed to generate the EOS model from reported PVT data were made using *PhazeComp*. After tuning the EOS with black oil properties reported by Saidi (1987), the PVT simulator was also used to generate saturated oil compositions for initializing the matrix block at pressures higher than and lower than the current reservoir pressure. Saturation pressure of the original oil composition was 1400 psia. Constant composition expansion (CCE) experiments are simulated to determine oil compositions below 1400 psia.[1] Special "swelling" tests were made to calculate oil composition at higher pressures: incipient bubble point gas from a lower pressure was added to the bubble point oil to raise the bubble point pressure. This process was started at 1400 psia and repeated at 1500 psia. The 11-component compositions for the reservoir oils at different saturation pressure are given in **Tables 3**.

Laboratory Model. For the laboratory test simulations, a 2D Cartesian grid is used, where the core is surrounded by horizontal fractures on the top and bottom, and one vertical fracture on the right side of the matrix block. Fine gridding is needed for CO_2 gas injection (Alavian and Whitson 2005). The core has a square 0.2x0.2-ft top and bottom surface shape with a height of 2 ft (60.96 cm).

The binary mixtures of methane (C_1) and normal pentane (n-C_5) used have similar MMP_{1D} as the Haft Kel reservoir oil, about 1400 psia. EOS component properties and BIPs of the binary fluid system are given in **Tables 4** and **5**. The compositions of laboratory-test oils at different saturation pressures are given in **Tables 6**. Haft Kel fluid also used in laboratory-test models.

Oil recovery is calculated from total average oil saturation S_o in the matrix block using the relation

$$RF = (1 - \frac{S_o}{S_{oi}}) \quad \text{...}(1)$$

Capillary pressure and relative permeability are taken from Saidi (1987) and laboratory capillary pressures were scaled with IFT according to:

$$P_c = (\frac{\sigma}{\sigma_{lab}})P_{c,lab} \quad \text{...}(2)$$

where $P_{c,lab}$ is lab-reported capillary pressure, σ_{lab} is the gas-oil laboratory IFT, equal to 10 mN/m, and σ is reservoir gas-oil IFT calculated by simulator.

Diffusion coefficients were calculated from the extended Sigmund correlation (da Silva and Belery 1989) and are given in **Tables 3** and **6** for Haft Kel and lab models, respectively.

---

[1] Near-identical oil compositions result from CCE, differential liberation, constant-volume tests, or depletion that accounts for changing gas and oil motilities.

CO_2 Displacement Mechanism

In this section we will describe displacement mechanism for the laboratory system and the Haft Kel single matrix/fracture.

Lab Test Recovery Behavior. System pressure and CO_2 injection rate were set to 1000 psia (68.95 bara) and 0.5 cm^3/hr. Models were run with and without diffusion to understand the effect of diffusion on recovery. **Fig. 1** shows that all oil is recovered after 3 days when diffusion is used in the binary mixture model. Neglecting diffusion reduces recovery to only 7% after 10 days, and leads to a near-piston-like displacement from top to bottom, with final recovery controlled by the balance of capillary and gravity forces. As shown in **Fig. 2**, the displacement front is not uniform. The front develops from the fracture inwards, caused by CO_2 entry through gravity and molecular diffusion.

Fig. 3 shows that using Haft Kel fluid in the lab-test model[2] will give lower ultimate oil recovery and recovery rate. The oil saturation profile in **Fig. 4** shows that the displacement front is not uniform (like binary mixture laboratory model run). Gravity-drainage appears to be more pronounced, with less lateral displacement, for the reservoir oil system when compared with the binary mixture model results. The Haft Kel fluid system results also show more-gradual saturation changes at the near-horizontal displacement front. Behind the gravity-capillary front, CO_2 vaporizes the remaining oil's light and intermediate components which are then transported out of the matrix block by molecular diffusion as fresh CO_2 enters the fracture behind the displacement front.

Haft Kel Recovery Behavior. With the reservoir pressure set to 1000 psia (68.95 bara) and CO_2 injection rate of 3 Mscf/D, models run were made with and without diffusion. For the model run without diffusion, recovery was about 22%, achieved after only 5 years, as shown in **Fig. 5**. Oil recovery with molecular diffusion was about 78%, but requiring almost 10 years. The oil saturation profile shown in **Fig. 6**, for the run with diffusion, shows that the displacement front is not uniform. The front is more like the laboratory-test with reservoir oil model than binary mixture.

Reservoir Pressure Effect

In this section we study the effect of reservoir pressure on lab- and field-scale systems – at 1000, 1250 and 1500 psia. For each pressure the matrix block/core is initialized with saturated oil and the fracture is initialized with CO_2 gas. Matrix properties, injection rate, and gridding are the same as described above model for lab- and field-scale models.

For the simple C_1-C_5 fluid system, recoveries are 100% after short time (2-3 days) for all pressures (**Fig. 1**). The vaporization-gas-diffusion mechanism of recovery is very effective for this system. However the ultimate recovery and the rate of recovery increase with increasing pressure in the lab-test model with reservoir oil as shown in **Fig. 3**.

For the Haft Kel field system a similar ultimate recovery with and without diffusion is seen for 1250 and 1500 psia, though rate of recovery is much higher with diffusion. For 1000 psia reservoir pressure, ultimate recovery with diffusion is 78% vs. 22% without diffusion – mainly because CO_2 is able to penetrate the matrix below the threshold capillary height. For all simulations including diffusion, the total recovery and the rate of recovery increase with increasing pressure (**Fig. 5**).

Although cases with diffusion show that CO_2 recovers oil below capillary threshold height, with residual oil saturation decreasing for increasing reservoir pressure (**Fig. 7**). Higher pressures result in more vaporization, with vaporized oil components being transported by gas diffusion from the matrix block. Detail displacement mechanisms of models with no molecular diffusion are described in Alavian and Whitson (2005).

Matrix block Permeability Effect

We studied the effect of matrix block permeability for the field-scale Haft Kel system: system pressures of 1000, 1250 and 1500 psia with two matrix block permeabilities of 0.8 md and 5 md. For each pressure the matrix block/core is initialized with saturated oil and the fracture is initialized with CO_2 gas. All models are run with an 11x1x102 grid. Injection rate is set to 3 Mscf/D. Porosity is kept constant in all cases.

The rate of oil recovery increases with increasing matrix block permeability for all reservoir pressures, but ultimate oil recovery is not affected significantly, as shown in **Fig. 8**.

Matrix Block Dimension Effect

In this section we focus on field-scale matrix-size dimension. We consider cubic matrix blocks with 8, 16 and 35 ft dimension. Models were run with system pressure of 1000 and 1500 psia with 0.8 md matrix block permeability. For each pressure the matrix block is initialized with saturated oil and the fracture is initialized with CO_2 gas. All models used the 11x1x102 grid. Injection rate is set to 3 Mscf/D. Also cases are run with and without diffusion.

With diffusion, recovery is faster for smaller block size. Ultimate recovery appears to be similar for all block sizes (**Fig. 9**), about 80%, but requiring very long production times (10-50 years).

At 1500 psia all cases have the same ultimate oil recovery of about 90%, as illustrated in **Fig. 10**. The rate of recovery is dramatically higher for 1500 psia vs. 1000 psia, with ultimate recoveries taking 5-15 years. Molecular diffusion boosts mass

---

[2] All Haft Kel fluid in lab-test models were run with diffusion, because in the models without diffusion capillary threshold height is larger than the core height and CO_2 will not enter into the core.

transfer (CO_2 entering the matrix and hydrocarbons leaving the matrix), with oil recoveries accelerated approximately as the inverse of matrix block dimension.

Injection Rate Effect

Availability of fresh CO_2 in fractures surrounding the matrix block has a large impact on total fracture/matrix mass transfer, and consequently the rate of oil recovery. Injection rate is investigated for both lab-scale and field-scale systems.

For lab scale models, a 0.2x0.2x2 ft core dimension is used, with 0.8 and 5 md matrix block permeabilities considered. System pressure is set to 1000 psia. 0.5, 0.1 and 0.03 cm^3/min injection rates are used. All models are run with the 11x1x102 grid. Cases with and without diffusion studied.

For the Haft Kel field-scale simulations, we consider 8-ft cube matrix blocks with system pressure of 1000 and 1500 psia. Matrix block permeability is 0.8 md. For each pressure the matrix block is initialized with saturated oil and the fracture is initialized with CO_2 gas. For the case with 1000 psia reservoir pressure, three injection rates are used: 3, 0.3 and 0.03 Mscf/D, while for 1500 psia reservoir pressure, two injection rates are used: 3 and 0.3 Mscf/D.

As seen in **Fig. 11, 12** and **13** diffusion has a huge effect on rate of recovery for lab-scale simulations. Oil recoveries are delayed dramatically by decreasing injection rate. The lack of fresh CO_2 slows down the vaporization-gas-diffusion mass transfer mechanism.

For a single matrix block in the field-scale simulations, gas injection rate of 3 and 0.3 Mscf/D give similar results, though the rate of recovery is somewhat slower for 0.3 Mscf/D. A dramatic decrease in rate of recovery is seen for 0.03 Mscf/D at 1000 psia.[3] Results are shown in **Figs. 14** and **15**. We are aware that the actual distribution and movement of CO_2 in a naturally fractured reservoir will not be as simple as we are modeling here.

We consider the potential adverse effect of low CO_2 "injection rate" – i.e. conditions whereby the fracture is not replenished continuously with fresh CO_2 – to be a major obstacle in any field implementation of CO_2 injection in fractured reservoirs. The control of CO_2 concentration in the fracture system needs to be further studied, and may require optimization to determine the most efficient and practical means of maintaining CO_2 required to achieve maximum oil recovery and rate of recovery.

Conclusions

Conclusions from our numerical model studies include:

1. Molecular diffusion has a significant acceleration effect on oil recovery for all cases studied. The impact is related to accelerated CO_2 entry into the matrix block, subsequent effect on gravity-capillary drainage and capillary-induced displacement, and an efficient oil-vaporization/gas-diffusion recovery mechanism.
2. Ultimate oil recovery increases by CO_2 injection with increasing reservoir pressure in a single-matrix/fracture system.
3. Ultimate oil recovery is independent of pressure for the binary C_1-C_5 oil, lab-scale system in the range of 1000-1500 psia, where thermodynamic MMP was about 1400 psia.
4. Oil recovery rate is affected by CO_2 injection (replenishment) rate because of the importance of oil-vaporization/gas-diffusion mass transport.

Acknowledgement

We would like to thank Shell for financing this study, as part of Alavian's PhD research.

Nomenclature

D_g = gas diffusion coefficient, L^2/t, cm^2/s
D_o = oil diffusion coefficient, L^2/t, cm^2/s
N = number of grid cells
Nx = number of grid cells in x-direction
Ny = number of grid cells in y-direction
Nz = number of grid cells in z-direction
P_C = capillary pressure, m/Lt^2, bara
$P_{C,lab}$ = measured capillary pressure, m/Lt^2, bara
RF = oil recovery factor
S_o = oil saturation
S_{oini} = initial oil saturation
x_i = oil mole fraction of component i
σ = gas-oil interfacial tension, m/t^2, mN/m
σ_{lab} = reference gas-oil interfacial tension, m/t^2, mN/m

---

[3] Gas injection rate of 0.03 Mscf/D at 1500 psia resulted in unstable simulation results, and are therefore not presented here.

Reference

Alavian, S.A., and Whitson C.H. 2005. CO_2 IOR Potential in Naturally-Fractured Haft Kel Field, Iran. Paper IPTC 10641 present at International Petroleum Technology Conference, Doha, Qatar, 21-23 November.

Asghari, K and Torabi, F. 2008. Effect of Miscible and Immiscible CO_2 Flooding on Gravity Drainage: Experiment and Simulation Results., Paper SPE 110587 presented at the 2008 SPE/DOE Improved Oil Recovery Symposium, Tulsa, Oklahoma, U.S.A., 19-23April.

da Silva, F.V and Belery, P. 1989. Molecular Diffusion in Naturally Featured Reservoirs: a Decisive Recovery Mechanism., Paper SPE 19672 presented at the 64th SPE Annual Technical Conference and Exhibition, San Antonio, Texas, U.S.A., 8-11 October.

Eclipse Reservoir Engineering Software.E300. 2009. Schlumberger, http://www.slb.com.

Hoteit, H. and Firoozabadi, A. 2006. Numerical Modeling of Diffusion in Fractured Media for Gas Injection and Recycling Schemes. Paper SPE 103292 presented at the 2006 SPE Annual Technical Conference and Exhibition, San Antonio, Texas, U.S.A., 24-27 September.

Li, H., Putra, E., Schechter, D.S. and Grigg, R.B. 2000. Experimental Investigation of CO_2 Gravity Drainage in a Fractured System. Paper SPE 64510 presented at the SPE Asia Pacific Oil and Gas Conference and Exhibition, Brisbane, Australia, 16-18October.

Zick Technologies. PhazeComp. www.zicktech.com.

SI Metric Conversion Factors

bbl x 1.589 873 E – 01 = m^3
D x 9.869 23 E – 13 = m^2
dyne/cm x 1.000 000 E + 00 = mN/m
ft x 3.048* E – 01 = m
ft^3 x 2.831 685 E – 01 = m^3
^{o}F (oF+459.67)/1.8 E – 01 = K
in x 2.54* E – 02 = m
in^2 x 6. 4516* E – 04 = m
lbm/ft^3 x 2.831 685 E – 02 = m
psi x 6.894 757 E + 03 = Pa
^{o}R ^{o}R/1.8 E – 01 = K

*Conversion factor is exact.

Table 1 – Fluid Properties for The 11Component Soave-Redlich-Kwong Characterization

Component	MW	Tc, ^{o}R	Pc, psia	ω	Vshift	Zc	Parachor	Ωa	Ωb
N2	28.01	227.16	492.84	0.037	-0.001	0.29178	59.10	0.4275	0.0866
CO2	44.01	547.42	1069.51	0.225	0.217	0.27433	80.00	0.4275	0.0866
H2S	34.08	672.12	1299.97	0.090	0.102	0.28292	80.10	0.4275	0.0866
C1	16.04	343.01	667.03	0.011	-0.002	0.2862	71.00	0.4275	0.0866
C2	30.07	549.58	706.62	0.099	0.059	0.27924	111.00	0.4275	0.0866
C3	44.10	665.69	616.12	0.152	0.091	0.2763	151.00	0.4275	0.0866
C4-C6	70.43	840.66	527.88	0.214	0.098	0.27403	216.05	0.4275	0.0866
C7-C14	136.82	1147.73	411.95	0.353	0.099	0.29826	384.35	0.4275	0.0866
C15-C21	239.68	1395.61	283.74	0.605	0.131	0.29826	657.60	0.4275	0.0866
C22-C29	341.31	1546.43	225.55	0.818	0.130	0.29826	855.51	0.4275	0.0866
C30+	487.10	1692.33	184.60	1.06576	0.09103	0.29826	1062.75	0.4275	0.0866

Table 2 – Binary Interaction Coefficients for The 11Component Soave-Redlich-Kwong Characterization

	N2	CO2	H2S	C1	C2	C3	C4-C6	C7-C14	C15-C21	C22-C29	C30+
N2	-										
CO2	0.0000	-									
H2S	0.0000	0.1200	-								
C1	0.0250	0.1050	0.0800	-							
C2	0.0100	0.1300	0.0700	0.0000	-						
C3	0.0900	0.1250	0.0700	0.0000	0.0000	-					
C4-C6	0.1040	0.1154	0.0544	0.0000	0.0000	0.0000	-				
C7-C14	0.1100	0.1150	0.0500	0.0000	0.0000	0.0000	0.0000	-			
C15-C21	0.1100	0.1150	0.0500	0.0000	0.0000	0.0000	0.0000	0.0000	-		
C22-C29	0.1100	0.1150	0.0500	0.0000	0.0000	0.0000	0.0000	0.0000	0.0000	-	
C30+	0.1100	0.1150	0.0500	0.0000	0.0000	0.0000	0.0000	0.0000	0.0000	0.0000	-

Table 3 – Oil Composition for The 11 Component EOS at Different Saturation Pressures and Diffusion Coefficients

Component	1000 psia			1250 psia			1500 psia		
	X_i mole fr.	D_{ig} cm^2/s	D_{io} cm^2/s	X_i mole fr.	D_{ig} cm^2/s	D_{io} cm^2/s	X_i mole fr.	D_{ig} cm^2/s	D_{io} cm^2/s
N2	0.0004	2.34E-03	3.63E-05	0.0009	1.84E-03	3.42E-05	0.0011	1.49E-03	3.26E-05
CO2	0.0039	1.72E-03	2.44E-05	0.0043	1.35E-03	2.31E-05	0.0043	1.09E-03	2.20E-05
H2S	0.0133	1.70E-03	2.49E-05	0.0130	1.33E-03	2.36E-05	0.0128	1.08E-03	2.25E-05
C1	0.2211	1.57E-03	3.42E-05	0.2957	1.22E-03	3.10E-05	0.3113	9.90E-04	2.83E-05
C2	0.0494	1.62E-03	2.46E-05	0.0497	1.27E-03	2.32E-05	0.0496	1.03E-03	2.21E-05
C3	0.0542	1.28E-03	1.87E-05	0.0506	1.00E-03	1.77E-05	0.0499	8.14E-04	1.69E-05
C4-C6	0.1428	9.77E-04	1.34E-05	0.1282	7.65E-04	1.28E-05	0.1251	6.23E-04	1.23E-05
C7-C14	0.3761	6.57E-04	1.07E-05	0.3343	5.15E-04	1.04E-05	0.3257	4.20E-04	1.01E-05
C15-C21	0.0998	4.60E-04	6.82E-06	0.0887	3.60E-04	6.48E-06	0.0864	2.93E-04	6.20E-06
C22-C29	0.0299	3.69E-04	5.17E-06	0.0266	2.89E-04	4.90E-06	0.0259	2.35E-04	4.68E-06
C30+	0.0092	3.00E-04	4.13E-06	0.0082	2.35E-04	3.91E-06	0.0079	1.92E-04	3.74E-06
Tres= 110 ^OF									

Table 4 – Fluid Properties for The 3 Component Soave-Redlich-Kwong Characterization

Component	MW	Tc, ^oR	Pc, psia	ω	Vshift	Zc	Parachor	Ωa	Ωb
CO2	44.01	547.42	1069.51	0.225	0.217	0.27433	80.00	0.4275	0.0866
C1	16.04	343.01	667.03	0.011	-0.002	0.2862	71.00	0.4275	0.0866
n-C5	70.91	846.25	503.20	0.229	0.119	0.27119	205.17	0.4275	0.0866

Table 5 – Binary Interaction Coefficients for The 3 Component Soave-Redlich-Kwong Characterization

	CO2	C1	n-C5
CO2	-		
C1	0.1200	-	
n-C5	0.1500	0.0000	-

Table 6 – Oil Composition for The 3 Component EOS at Different Saturation Pressures and Diffusion Coefficients

Component	1000 psia			1250 psia			1500 psia		
	X_i mole fr.	D_{io} cm^2/s	D_{ig} cm^2/s	X_i mole fr.	D_{io} cm^2/s	D_{ig} cm^2/s	X_i mole fr.	D_{io} cm^2/s	D_{ig} cm^2/s
CO2	0.0000	1.54E-05	2.25E-04	0.0000	1.65E-05	1.75E-04	0.0000	1.81E-05	1.39E-04
C1	0.2735	1.99E-05	2.92E-04	0.3419	2.01E-05	1.13E-04	0.4099	2.07E-05	9.03E-05
n-C5	0.7265	1.99E-05	2.92E-04	0.6581	2.01E-05	1.13E-04	0.5901	2.07E-05	9.03E-05
Texp= 185 ^{O}F									

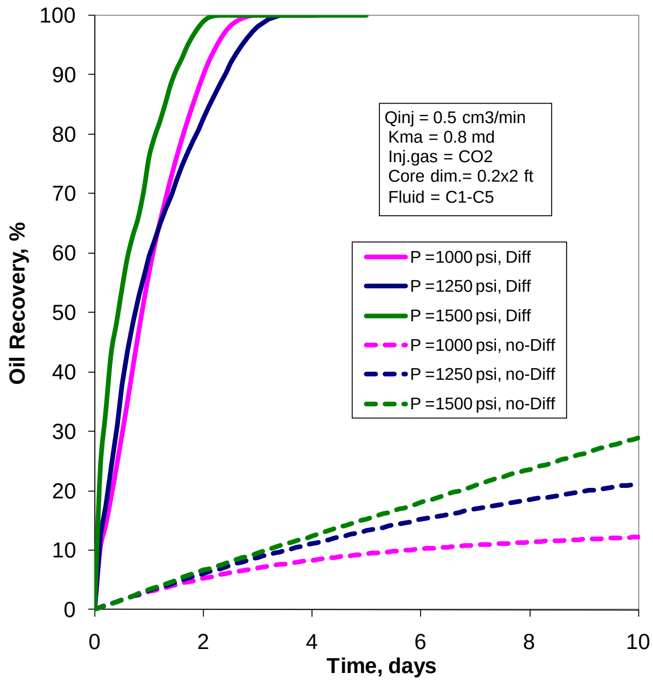

Figure 1 – Effect of reservoir pressure on oil recovery vs. time for C_1-C_5 lab system using CO_2 injection with (solid lines) and without diffusion (dash lines).

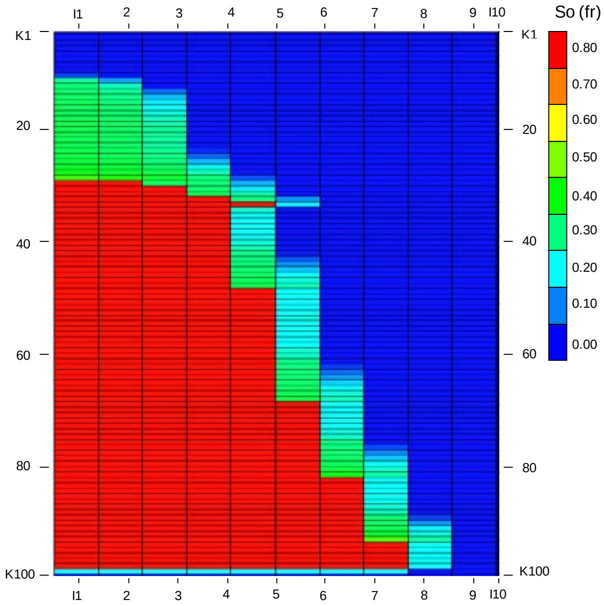

Figure 2 – CO_2 gas displacement, core oil saturation profile after 1 day for C_1-C_5 lab system at 1000 psia (at about 60% oil recovery).

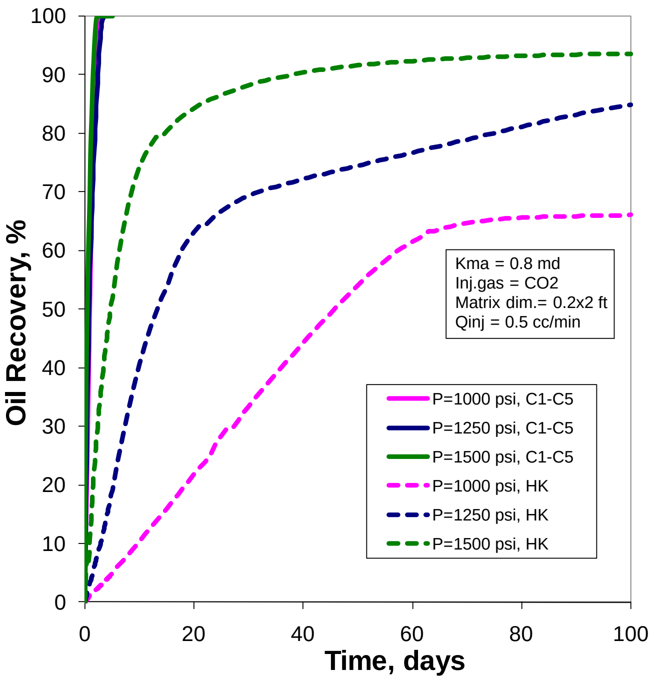

Figure 3 – Comparison of reservoir pressure effect on oil recovery vs. time for C_1-C_5 (solid lines) and Haft Kel (dash lines) lab system using CO_2 injection with diffusion.

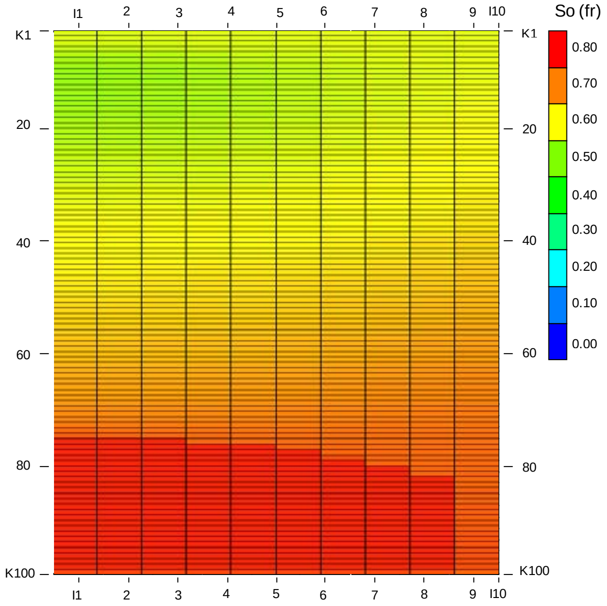

Figure 4 – CO_2 gas displacement, oil saturation profile inside core after 16 days for Haft Kel lab system at 1000 psia (at about 17% oil recovery).

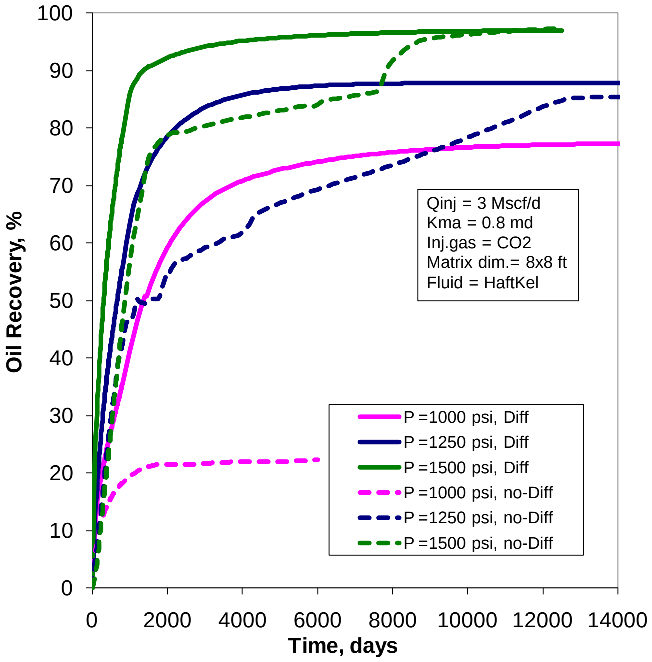

Figure 5 – Effect of reservoir pressure on oil recovery vs. time for 8-ft cube Haft Kel single matrix block system using CO_2 injection with (solid lines) and without diffusion (dash lines).

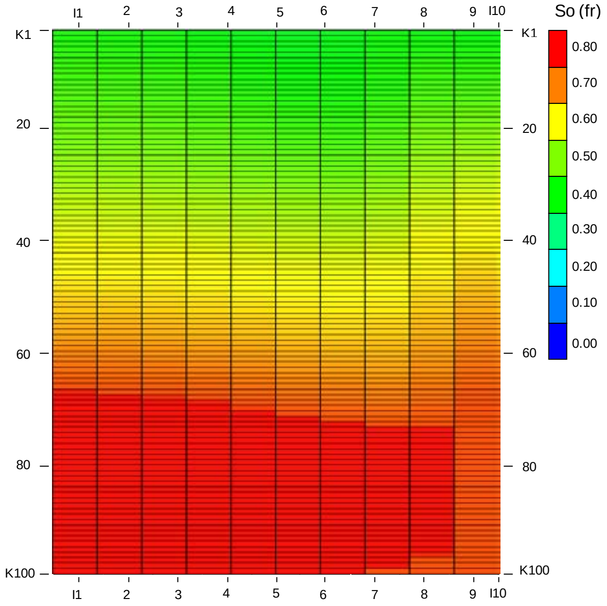

Figure 6 – CO_2 gas displacement, matrix block oil saturation profile after 300 days for 8-ft cube Haft Kel single matrix block system at 1000 psia (at about 21.5 % oil recovery).

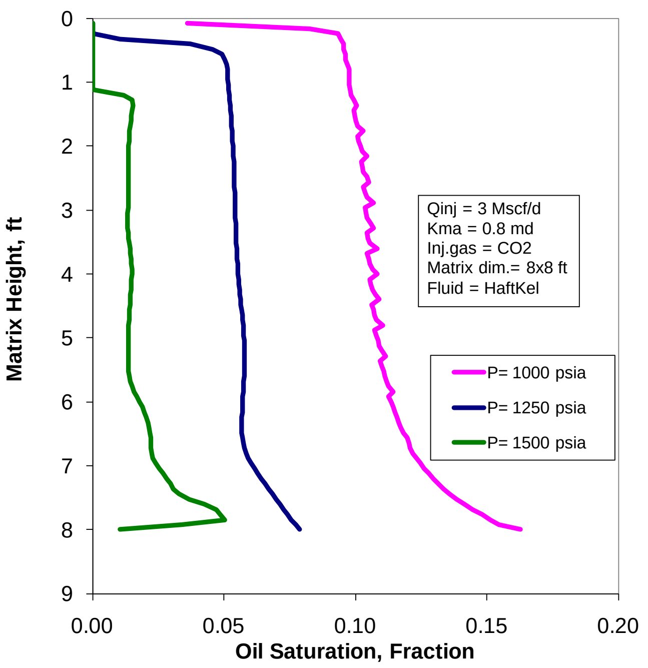

Figure 7 – Oil saturation profile for 8-ft cube Haft Kel single matrix block using CO_2 injection gas at 10000 days.

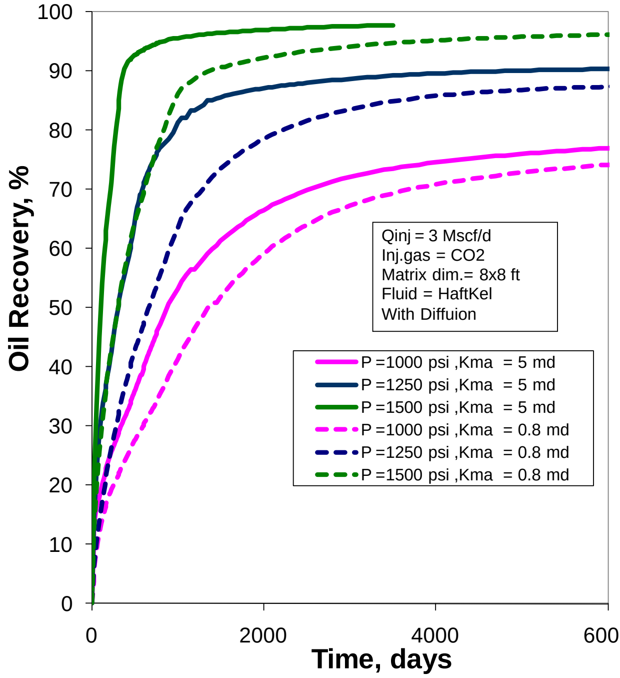

Figure 8 – Effect of matrix block permeability on oil recovery vs. time for 8-ft cube Haft Kel single matrix block using CO_2 injection gas at various system pressure.

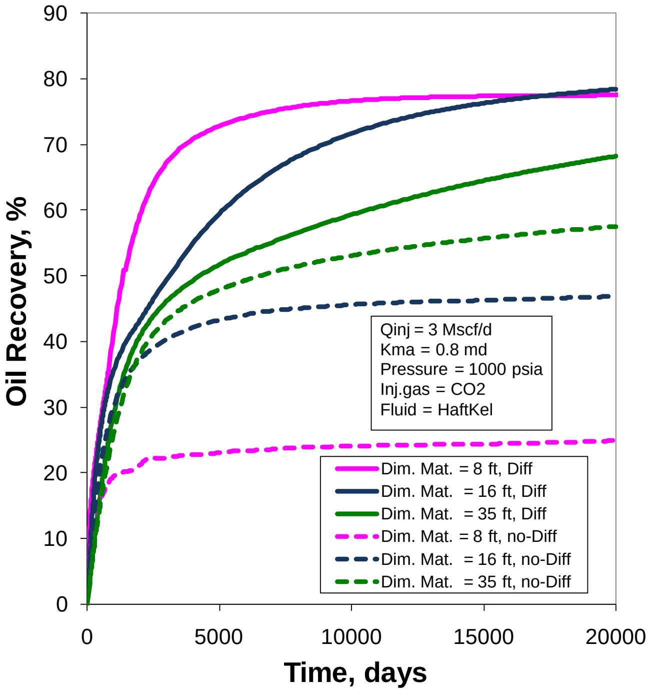

Figure 9 – Effect of matrix block dimension on oil recovery vs. time for Haft Kel single matrix block using CO_2 injection gas at system pressure of 1000 psia.

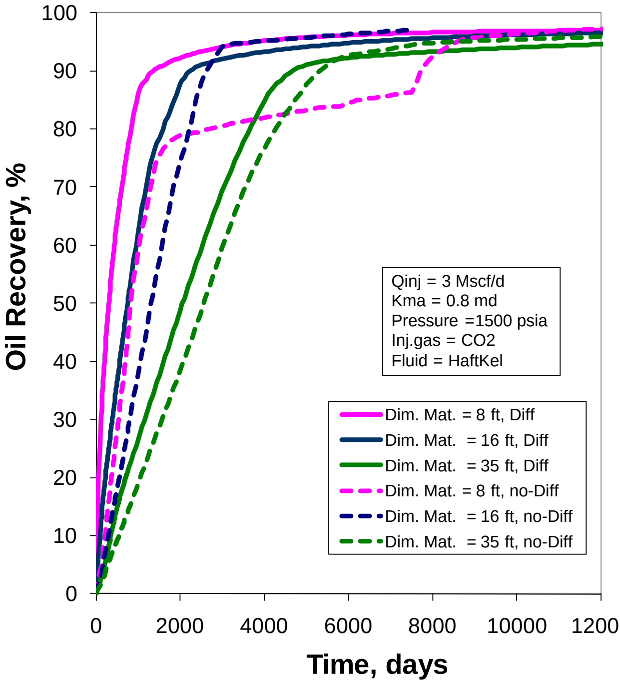

Figure 10 – Effect of matrix block dimension on oil recovery vs. time for Haft Kel single matrix block using CO_2 injection gas at system pressure of 1500 psia.

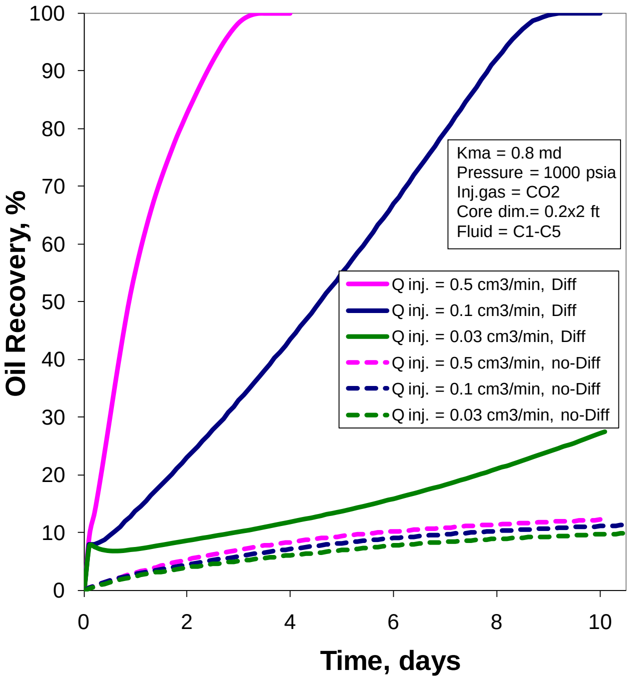

Figure 11 – Effect of injection rate on 0.8 md core during CO$_2$ gas injection for C$_1$-C$_5$ lab system at 1000 psia.

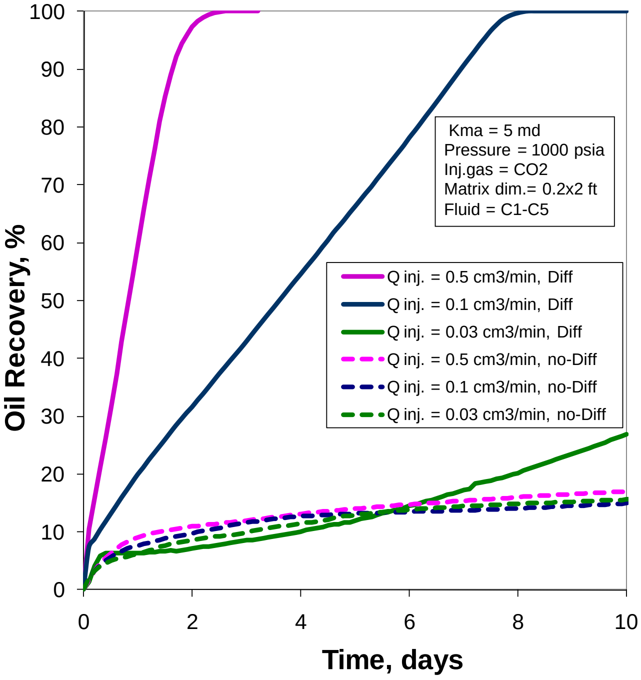

Figure 12 – Effect of injection rate on 5 md core during CO$_2$ gas injection for C$_1$-C$_5$ lab system at 1000 psia.

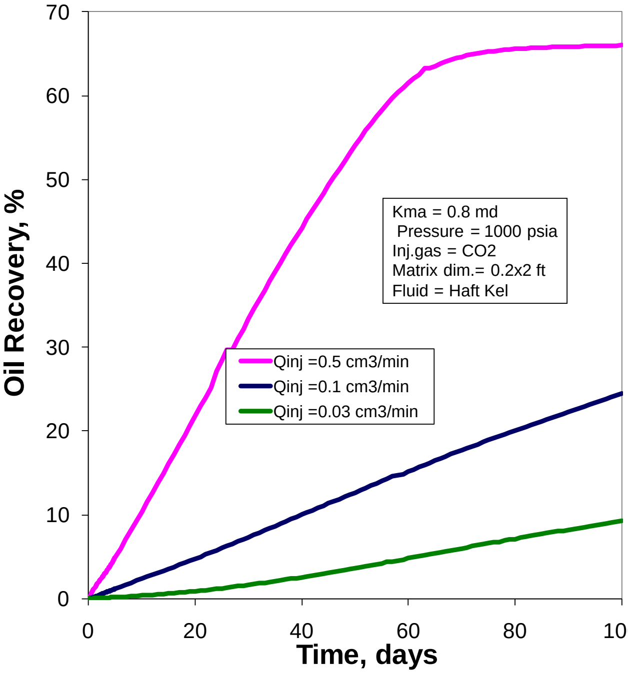

Figure 13 – Effect of injection rate on 0.8 md core during CO$_2$ gas injection for Haft Kel lab system at 1000 psia.

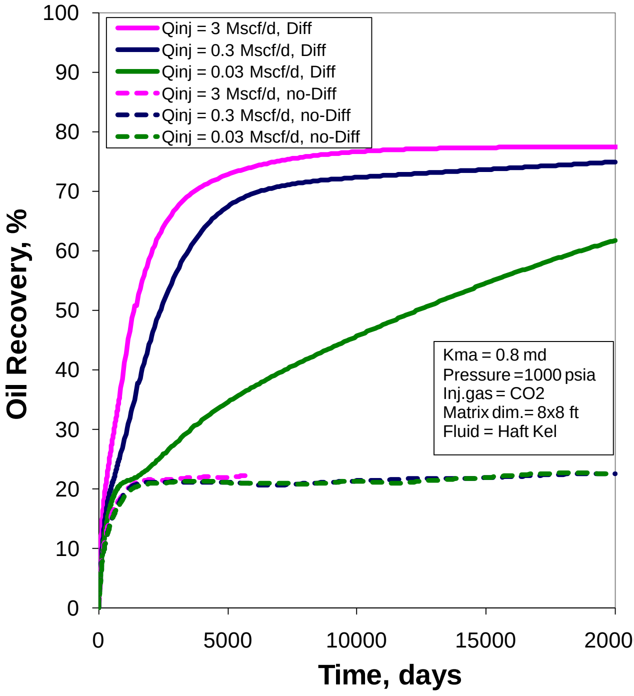

Figure 14 – Effect of injection rate on 0.8 md single matrix block during CO$_2$ gas injection for 8-ft cube Haft Kel system at 1000 psia.

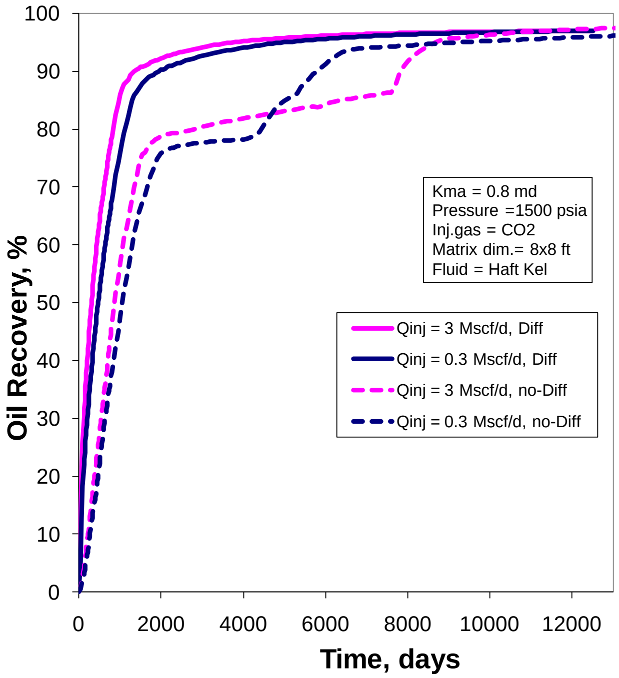

Figure 15 – Effect of injection rate on 0.8 md single matrix block during CO_2 gas injection for 8-ft cube Haft Kel system at 1500 psia.

Modeling CO_2 Injection Including Diffusion in a Fractured-Chalk Experiment

Paper SPE 135339 presented at the 2010 Annual Technical Conference and Exhibition, Florence, Italy, 19–22 September

Paper IV

SPE 135339

Modeling CO_2 Injection Including Diffusion in a Fractured-Chalk Experiment

S.A. Alavian, SPE, NTNU, and C.H. Whitson, SPE, NTNU/PERA

This paper was prepared for presentation at the SPE Annual Technical Conference and Exhibition held in Florence, Italy, 19–22 September 2010.

Abstract

This paper presents a modeling study of CO_2 injection in chalk core based on laboratory data reported by Darvish et al. (2006). The experiment consisted of a vertically-oriented 60-cm long chalk outcrop core initially saturated with live reservoir oil at 130 ^oC and 300 bar. After saturating the core with the oil mixture by displacement a small fracture volume surrounding the core was created by heating the solid Wood's metal that originally filled the volume between the core and core holder. Then CO_2 was injected for 22 days. The experiment was performed at a pressure above the minimum miscibility pressure (MMP) as defined by a traditional 1D multi-contact displacement process (MMP_{1D}).

Our modeling study was conducted with a compositional reservoir simulator. The 2D r-z model used fine grid for the core matrix and surrounding fracture. The match of reported production data gave a high degree of confidence in the model. Also, produced mass fractions of components measured periodically during the experiment were matched. The compositional data fit was sensitive to the modeling of diffusion and the EOS model fit to depletion and swelling test data which included oil and gas mixtures with a clear definition of a critical transition.

Our study indicates that gravitational drainage affected the recovery process for CO_2 injection in the Darvish experiment, but also mass transfer by vaporization, condensation, and molecular diffusion.

The injection of CO_2 in North Sea fractured chalk reservoirs is of keen interest, as a secondary and tertiary recovery process (e.g. in Ekofisk and Valhall). Proper modeling of experimentals such as the Darvish tests is not only a step to understand local (microscopic and matrix-fracture interaction) recovery phenomena, but also as an important step in model upscaling for pilot and full-field projects.

Introduction

CO_2 injection has been considered as potentially enhancing oil recovery from naturally fractured reservoirs. Alavian and Whitson (2005) study the IOR potential for CO_2 injection in the naturally-fractured Haft Kel field, Iran, based on detailed compositional simulations of the matrix-fracture system. Obviously, it would be useful to experimentally investigate the efficiency of gas injection in naturally fractured reservoirs, followed by CO_2 injection, before this procedure is applied to a reservoir.

Few experiments are reported in the literature to studying gravity drainage in CO_2 injection in fractured reservoirs. Li et al. (2000) perform CO_2 injection after water flooding in a dead oil system. They studied water imbibition followed by CO_2 injection on artificially fractured cores. They report that CO_2 gravity drainage could significantly increase oil recovery after water flooding. They found that CO_2 gravity drainage declines as the rock permeability decreases and initial water saturation increases. Asghari and Torabi (2008) conduct miscible and immiscible CO_2 gravity drainage experiments with dead oil (n-C_{10}). They show miscible CO_2 injection improves oil recovery, but they could not match laboratory experiment with a simulation model. Karimaie (Karimaie 2007, Karimaie and Torsæter 2008) performed equilibrium gas injection followed by CO_2 experiments on chalk and carbonate cores at reservoir conditions where cores were saturated with live synthetic oil. The experiments were designed to illustrate CO_2 injection in a fractured reservoir, but fracture permeability so low that it affected the production performance (Alavian and Whitson 2009).

Morel et al. (1990) and Le Romancer et al. (1994) studied effect of diffusion on C_1-C_5 mixture by injecting methane (C_1), nitrogen (N_2) and CO_2 in outcrop core. Hua, Whitson and Yuanchang (1991) simulated Morel's experiments with a model combining an analytical calculation in the fracture and a numerical model in the core.

Hoteit and Firoozabadi (2006) studied diffusion in fracture media for gas injection and recycling schemes by numerical modeling. They report that diffusion improves oil recovery and delays gas break through. They neglect gas-oil capillary pressure in matrix block in their study.

Darvish (2007) perform CO_2 injection experiment on outcrop chalk core at reservoir condition where core was saturated with live oil. Darvish et al. (2006) could not match experiment data by numerical compositional model that may be because of using improper equation of state (EOS) or incorrect input data in their models. Moortgat, Firoozabadi and Farshi (2009) are modeled the experiment by higher-order algorithm based on the combined discontinuous Galerkin, mixed hybrid finite element and discrete fracture techniques. In this paper, we use a commercial compositional simulator to model the experiment. The EOS is tuned to measured data.

Rock and Fluid Properties

Chalk core from Faxe area outcrop in Denmark is used in this experiment, which has similar rock properties to North Sea chalk. The core had a cylindrical shape with a length of 59.6 cm and 4.6 cm in diameter. Core porosity and permeability are reported as 44.4% and 4md respectively (Darvish et al. 2006; Darvish 2007).

Relative permeabilities and capillary pressure are not measured for the core. We use C_1- n-C_5 capillary pressure of Faxe outcrop chalk core measured by Christoffersen (1992). Linear and Corey-type relative permeabilities are used for modeling the experiment. Gas and oil exponents for Corey-type relative permeabilities are 2.4 and 3.8 respectively with unit end point.

Reservoir fluid was flashed to standard condition (T= 15.5 ^oC, P= 1 bar) and flashed oil and gas compositions are measured by Darvish 2007. These fluids are used to determine reservoir fluid composition with bubble point pressure 242 bar at 130 ^oC by combining it to measured gas oil ratio (GOR) 133.2 Sm^3/Sm^3. The EOS model has 39 components, including non-hydrocarbons N_2, CO_2, and hydrocarbon components C_1, C_2, C_3, i-C_4, n-C_4, i-C_5, n-C_5, and C_6; and single-carbon number (SCN) components C_7, C_8, … and C_{34} with a C_{35+} residue. The EOS reduced to 13 components with five heavy pseudo components. Lumped components are chosen same as pseudo components reported in Darvish 2007 because reported oil produced mass fractions will be compared with numerical model results. The Peng-Robinson (1979) equation of state (PR-EOS) with volume shift is used. PR-EOS is tuned to match measured constant composition expansion (CCE) and differential liberation expansion (DLE) and CO_2 swelling test experiments. Comparisons of measured and calculated properties are shown in **Fig. 1 – 5**.

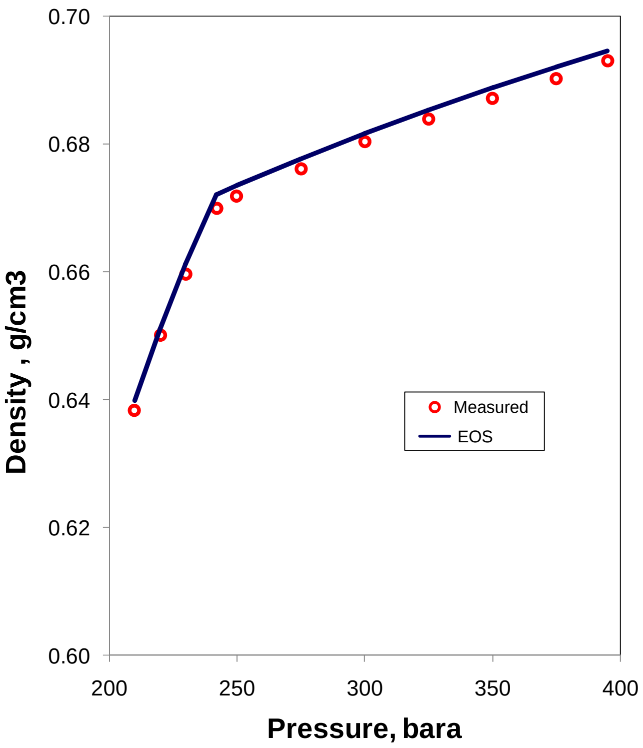

Figure 1 – Measured and calculated total (gas + oil) density at 130 ^oC.

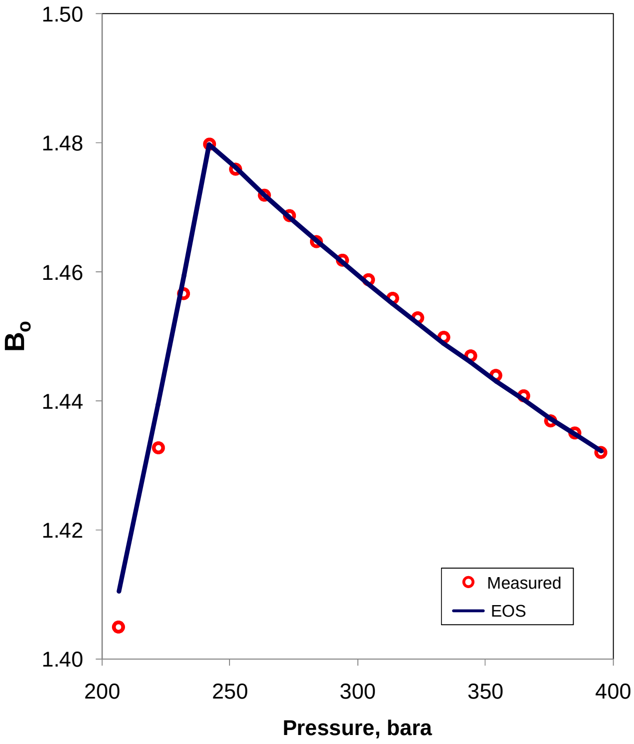

Figure 2 – Measured and calculated differential oil volume factor at 130 ^oC.

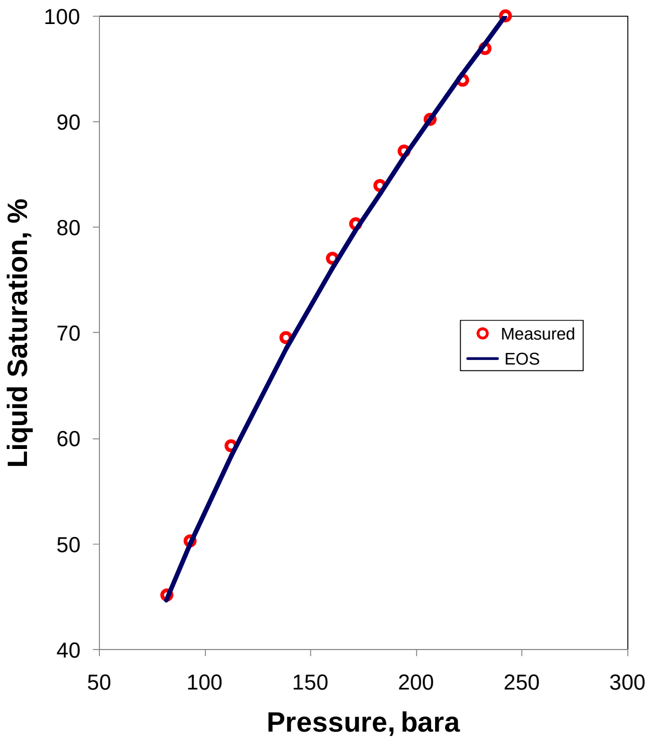

Figure 3 – Measured and calculated liquid saturation at 130 ^{o}C.

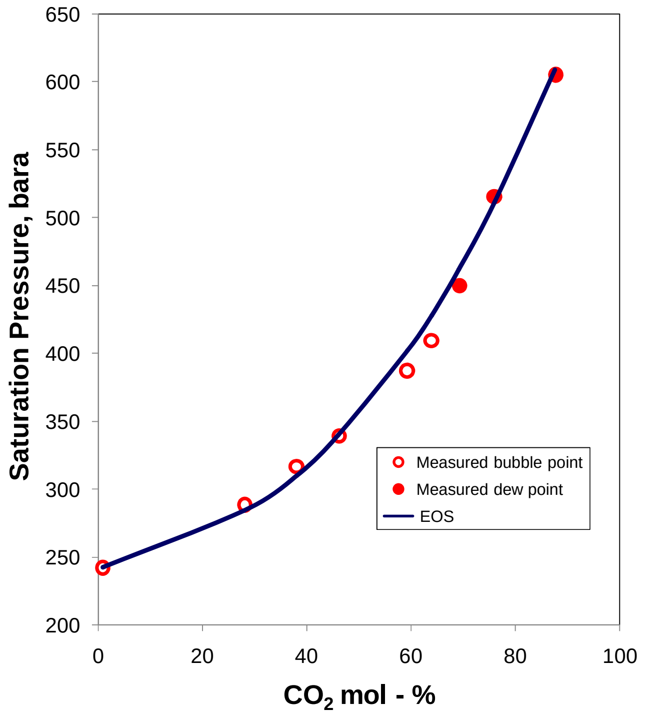

Figure 4 – Measured and calculated saturation pressure versus CO_2 mole injected at 130 ^{o}C from CO_2 swelling test.

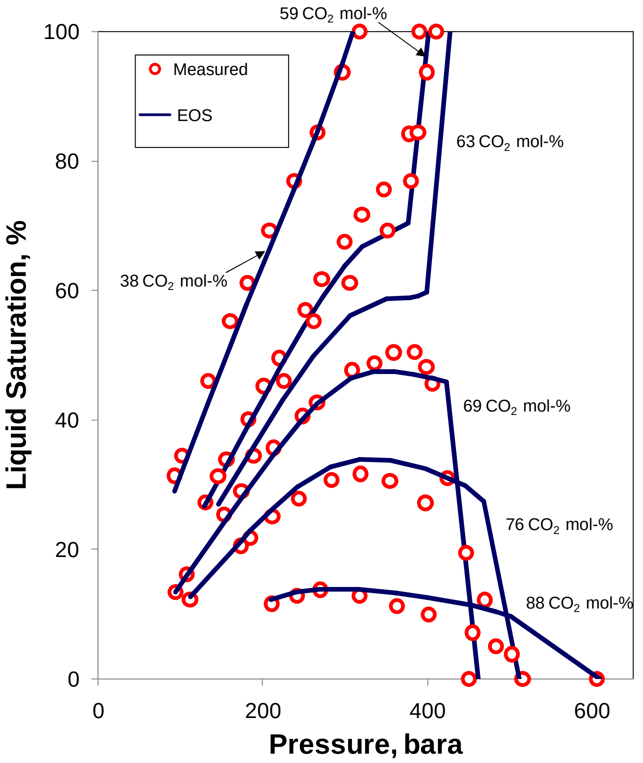

Figure 5 – Measured and calculated liquid saturation for different CO_2 mol-% mixtures from CO_2 swelling test.

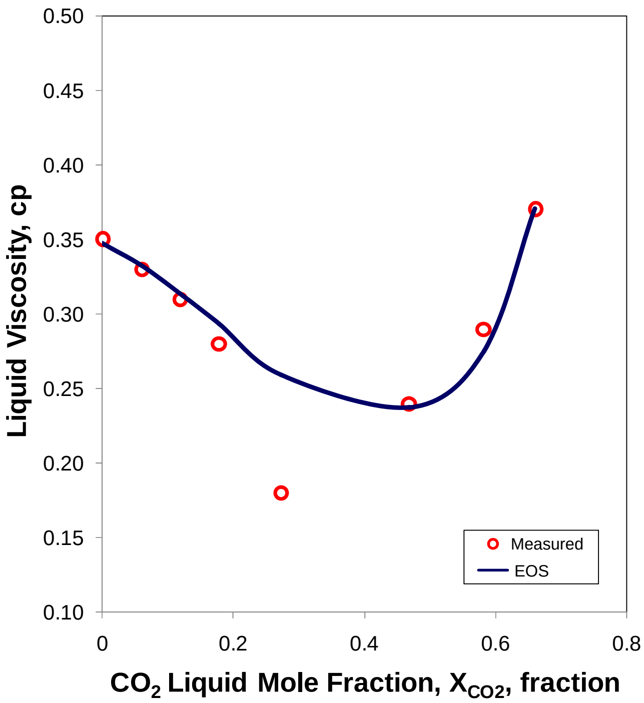

Figure 6 – Measured and calculated saturated oil viscosity versus CO_2 liquid mole fraction at 130 ^{o}C.

The Lohrenz-Bray-Clark (LBC) compositional viscosity correlation is usually adequate for gas viscosity predictions, but is not usually predictive for oil viscosity. The critical Z_c's of for C_6 and heavier components are modified to force fit the LBC correlation to measured oil viscosities with different CO_2 mole fraction (**Fig. 6**). The 13 components PR-EOS/LBC parameters used in this study are given in **Tables 1** and **2**.

Table 1 – Fluid Properties for the 13-Component Peng-Robinson Characterization

Component	MW	Tc, K	Pc, bar	ω	s	Tb, K	Zc	Parachor
N2	28.01	126.20	33.98	0.0370	-0.1676	77.25	0.2918	59.1
CO2	44.01	304.12	73.74	0.2250	-0.0057	184.88	0.2928	80.0
C1	16.04	190.56	45.99	0.0110	-0.1500	111.56	0.2862	71.0
C2	30.07	305.32	48.72	0.0990	-0.0628	184.43	0.2792	111.0
C3	44.10	369.83	42.48	0.1520	-0.0638	230.93	0.2763	151.0
C4	58.12	416.49	37.18	0.1930	-0.0580	267.06	0.2779	189.9
C5	72.15	465.10	33.76	0.2405	-0.0427	305.28	0.2703	229.2
C6	84.14	511.14	32.20	0.2598	-0.0027	338.81	0.2995	236.9
C7-C9	110.40	577.75	27.91	0.3262	0.0269	394.65	0.2797	300.0
C10-C15	167.32	682.95	20.72	0.4918	0.0909	495.49	0.2567	436.6
C16-C22	244.90	782.17	15.27	0.7082	0.1494	601.17	0.2402	622.8
C23-C34	347.73	874.10	11.56	0.9713	0.1890	705.51	0.2327	869.6
C35+	578.83	1024.78	10.21	1.4054	0.0726	859.68	0.2216	1424.2

Table 2 – Binary Interaction Coefficients for the 13-Component Peng-Robinson Characterization

	N2	CO2	C1	C2	C3	C4	C5	C6	C7-C9	C10-C15	C16-C22	C23-C34	C35+
N2	-												
CO2	0.0000	-											
C1	0.0250	0.2100	-										
C2	0.0100	0.2600	0.0000	-									
C3	0.0900	0.2500	0.0000	0.0000	-								
C4	0.0950	0.2349	0.0000	0.0000	0.0000	-							
C5	0.1051	0.2300	0.0000	0.0000	0.0000	0.0000	-						
C6	0.1100	0.2300	0.0000	0.0000	0.0000	0.0000	0.0000	-					
C7-C9	0.1100	0.1056	-0.0446	0.0000	0.0000	0.0000	0.0000	0.0000	-				
C10-C15	0.1100	0.0965	-0.0676	0.0000	0.0000	0.0000	0.0000	0.0000	0.0000	-			
C16-C22	0.1100	0.0870	-0.0896	0.0000	0.0000	0.0000	0.0000	0.0000	0.0000	0.0000	-		
C23-C34	0.1100	0.0784	-0.1079	0.0000	0.0000	0.0000	0.0000	0.0000	0.0000	0.0000	0.0000	-	
C35+	0.1100	0.0685	0.1949	0.0000	0.0000	0.0000	0.0000	0.0000	0.0000	0.0000	0.0000	0.0000	-

Experimental Procedure

This section describes an experiment done to study CO_2 injection in fractured reservoir. The experimental procedure is described based on Darvish (2007), Darvish et al. (2006) and personal communication with Darvish.

Dried cylindrical chalk core was placed in a steel core holder. The core holder inner diameter is 5.0 cm. The core diameter is 4.6 cm and has 59.6 cm length. The fracture is represented by a 2 mm space between the core and the core holder. Core porosity and absolute permeability are reported as 44.4% and 4 md respectively (Darvish 2007; Darvish et al. 2006).

Due to large permeability contrast between core and surrounding space (artificial fracture), it is complicated to initially saturate the core with live oil. Oil would flow through the high permeable space leaving core partially saturated with live oil. Therefore space between core and core holder wall was initially filled with Wood's metal. The metal melting point is 70^{o}C and experiment done at 130^{o}C. The metal was melted and poured into space between core and core holder. Fracture sealed with the metal and has zero permeability after cooling the system.

The core was evacuated and pressurized to 300 bar with 85% toluene and 15 % exxsol. Toluene-exxsol mixture has higher density than experimental fluid, and therefore it was injected from the top of the core with stable gravity displacement. Two pore volumes of live oil was injected at constant pressure (300 bar) and temperature (40 ^{o}C). The system was heated to 130^{o}C at a constant pressure (300 bar) and Wood's metal was removed from the annular space by injecting oil. Oil was injected from the top and metal drained from the bottom of the core holder. Fracture porosity and permeability were not measured after metal was removed from the system but pressure difference was measured between top and bottom of core holder, which could be used to determine fracture permeability in a model.

Oil in the fracture was replaced by CO_2. Injection rate during the first 30 min of the experiment was 5.6 cm^3/min and then reduced to 0.1cm^3/min. the experiment continued with CO_2 gas injection for 22 days. Produced fluid was diverted to a separator at ambient conditions. The mass of separated oil was measured continually and component mass fraction measured periodically.

Model Description

The matrix block (core) is initially filled with oil and fractures are initially filled with CO_2. The fractures are assumed to have negligible capillary pressure. The matrix and the fractures dimensions are the same as core and fracture in the experiment. A two dimension radial grid is used where the matrix block is surrounded by two horizontal fractures at the top and bottom and one vertical fracture. Fine grid is needed for CO_2 gas injection to reduce numerical dispersion (Alavian and Whitson 2005). Respectively, 10 and 51 grid cells are used in radial and vertical direction to simulate the experiment.

The *ECLIPSE 300* simulator with implicit solution method is used for all simulations. A 13 components PR-EOS is used. The EOS properties of the components are summarized in Table 1 and the binary interaction parameters are given in Table 2.

Table 3 – Gas and Oil Diffusion Coefficients and Initial Oil Composition

Component	z_i mole fr.	D_{ig} cm^2/s	D_{io} cm^2/s
N2	0.0012	5.15E-05	2.92E-06
CO2	0.0084	3.20E-04	7.26E-06
C1	0.4473	2.70E-04	7.72E-06
C2	0.0766	2.62E-04	7.09E-06
C3	0.0426	2.46E-04	5.84E-06
C4	0.0318	2.09E-04	4.91E-06
C5	0.0220	1.81E-04	4.25E-06
C6	0.0211	1.64E-04	3.83E-06
C7-C9	0.0799	1.42E-04	3.25E-06
C10-C15	0.0988	1.05E-04	2.55E-06
C16-C22	0.0654	7.66E-05	2.01E-06
C23-C34	0.0540	5.72E-05	1.52E-06
C35+	0.0510	4.30E-05	1.33E-06

Linear and Corey-type relative permeabilities are used for modeling the experiment. Gas and oil exponents for Corey-type relative permeabilities are 2.4 and 3.8 respectively with unit end point. C_1- n-C_5 capillary pressure measured by Christoffersen (1992) at similar core is taken as core capillary pressure in the model. This capillary pressure is scaled with IFT according to:

$$P_c = (\frac{\sigma}{\sigma_{ref}})P_{c,lab} \quad \text{..........} \quad (1)$$

Where $P_{c,lab}$ is original capillary pressure input in the model, σ_{ref} is reference interfacial tension (IFT) which is equal to 1.5 mN/m and σ is IFT calculated from:

$$\sigma_{go} = \left[\sum P_i (x_i \frac{\rho_o}{M_o} - y_i \frac{\rho_g}{M_g})\right]^4 \quad \text{..........} \quad (2)$$

There is no capillary pressure in the fracture.

The *Streamz* software is used to calculate cumulative mass of produced oil from reservoir simulation result. One separator is defined to simulate produced stream in the experiment. Separator pressures is atmospheric, the same as in the experiment. As mentioned above separator temperature was not measured during the experiment.

Gas and oil diffusion coefficients were calculated from the extended Sigmund correlation (da Silva and Belery 1989), as given in **Table 3**. Gas diffusion coefficients were determined from equilibrium gas of experimental fluid at bubble point pressure (240 bar) and 130 ^{o}C.

Matching Experimental Data

In this section, we try to match measured experimental data. As mentioned above cumulative mass of separator oil was measured and matched. Oil recovery reported in Darvish (2007) and Darvish et al. (2006) was based on produced mass and not mentioned in the references. Moortgat, Firoozabadi and Farshi (2009) consider that as volumetric oil recovery in their study. Fractured permeability was set to 80 md to get pressure difference measured in the experiment. As shown in **Fig. 7** measured pressure difference is slightly higher than calculated pressure difference because we account for pressure drop in inlet and outlet tube where measurement instrument was set in the experiment. There was no condenser or cooler in the outlet stream, consequently separator temperature was set to 30 °C which is slightly higher than ambient temperature accounting for high temperature (130 °C) of the outlet fluid.

Other parameters in the numerical model are taken from the reported values in the experiment. Two models are performed with two set of core relative permeability as described in the above section. Results of the models, as illustrated in **Fig. 8,** are similar. Mass transfer mechanism is more pronounce than viscous displacement in this experiment, as will discussed in next section. We select the model with linear core relative permeability thereafter in this study.

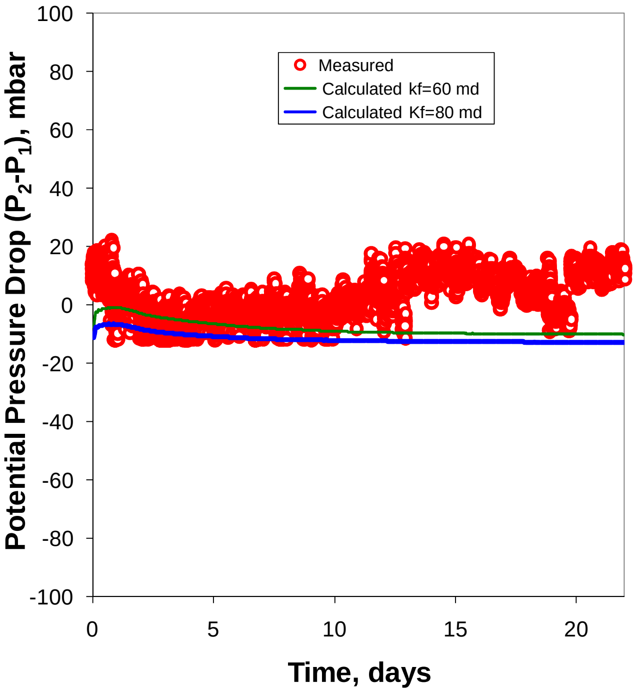

Figure 7 – Measured and Calculated pressure drop between top and bottom of the core holder.

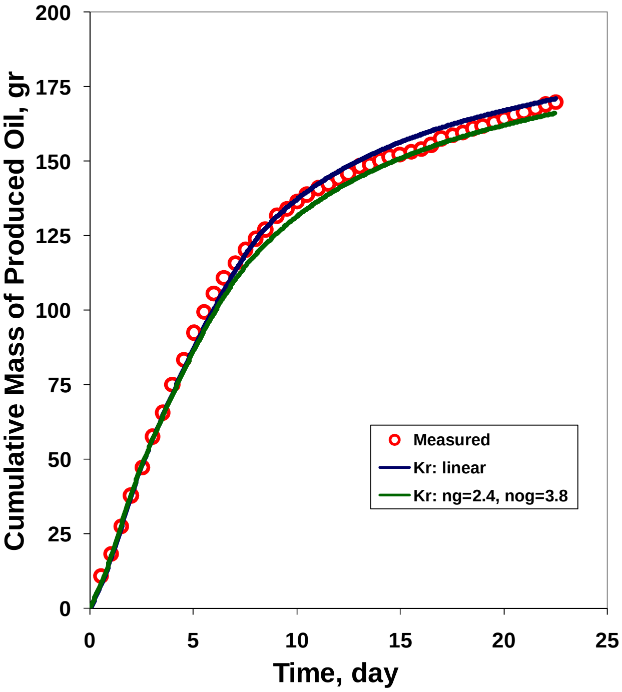

Figure 8 – Measured produced oil mass with matched simulation results for two set of core relative permeability with 80 md fracture permeability at 30 °C separator temperature.

Reported heavy component mass fractions from the experiment are compared with the numerical model result. All calculated mass fractions from the model follow the same trend as measured values as seen in **Fig. 9**. If C_{10} and heaver components are lumped together then numerical model results and experimental data are even closer, as shown in Fig. 9. That is probably means that the grouping of the C_{10+} components are done slightly different in laboratory than in EOS calculation. Calculated molecular weight of produced oil in laboratory has same trend as molecular weight of the numerical model (**Fig. 10**).

Recovery Mechanism

Darvish (2007) converts initial volume (V_{oi}) in the core to equivalent mass in laboratory separator condition ($m_{oi} = V_{oi}\rho_o/B_o$) and recovery is calculated from:

$$RF_{surf} = \frac{m_{op}}{m_{oi}} = \frac{m_{op}}{V_{oi}\left(\dfrac{\rho_o}{B_o}\right)} \qquad (3)$$

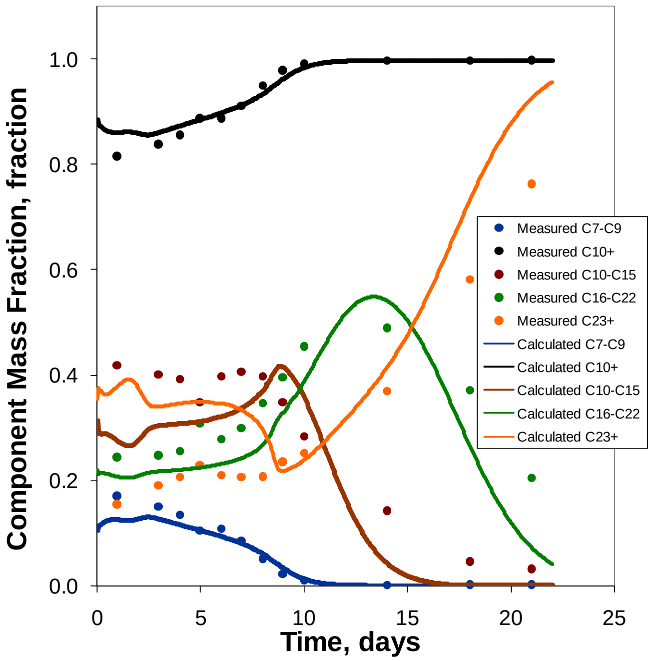

Figure 9 – Measured and calculated heavy components mass fraction of produced oil at separator condition.

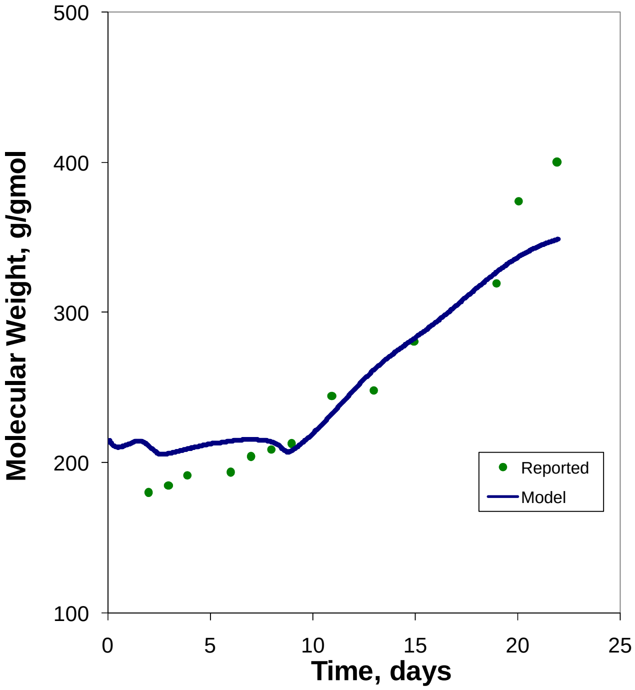

Figure 10 – Reported and calculated molecular weight of produced oil at separator condition.

Composition of produced oil varies during the experiment (Fig. 9), and as a result, the oil density (ρ_o) and oil formation volume factor (B_o) are not constant. Darvish (2007) used constant oil density and oil formation volume factor in their calculation. Therefore we did not use the recovery factor calculated by Darvish (2007).

Fig. 11 shows CO_2 condensation in the oil phase at experiment pressure and temperature. Consequently, oil saturation should be corrected as follow:

$$RF_{so} = 1 - \frac{S_o(1 - x_{CO2} + x_{CO2i})}{S_{oi}} \quad \text{.................................} \ (4)$$

Where S_{oi} and S_o are initial and current oil saturation in the core, respectively and x_{CO2i} and x_{CO2} are initial and current CO_2 mole fractions in liquid phase, respectively. Components and total oil recovery based on component moles is given by:

$$RF_{comp} = 1 - \frac{n_k}{n_{ki}} \quad \text{...} \ (5)$$

$$RF_{mole} = 1 - \frac{\sum_{k=N2}^{C35+} n_k}{\sum_{k=N2}^{C35+} n_{ki}} \quad \text{...} \ (6)$$

Where n_{ki} and n_k are initial and current mole of component *k*. Total oil recovery based on component mass calculated as below:

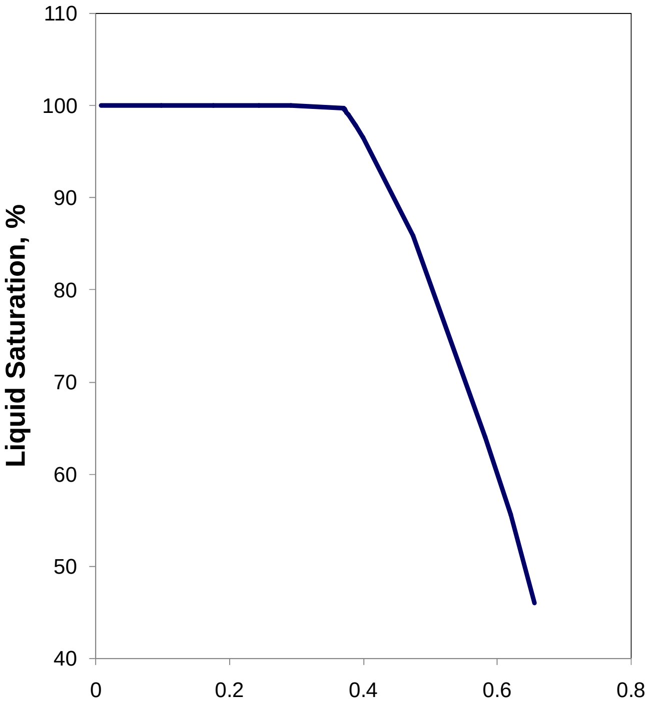

Figure 11 – Calculated liquid saturation versus CO_2liquid mole fraction from constant pressure (300 bara) and temperature (130 ^{o}C) swelling test.

$$RF_{mass} = 1 - \frac{\sum_{k=N2}^{C35+} m_k}{\sum_{k=N2}^{C35+} m_{ki}} \qquad \text{.........(7)}$$

Where m_{ki} and m_k are initial and current mass of component *k*.

Calculated oil recoveries from the above equations are given in **Fig. 12**. Oil saturation and mole base recovery are similar and give close ultimate recovery (at 22 days) of about 95 %. Mass-based recovery shows lower recovery (76%) because heavy components are recovered slower than light and medium components, as seen in **Fig. 13** and **14**. For consistency, and from this point forward mole-based oil recovery is considered as “oil recovery factor”.

Numerical models are performed with two set of core relative permeabilities. Mole-based recovery factor for these two models are similar and fall on top of each other (**Fig. 15**). A model is performed with 5 D fracture permeability to understand effect of actual permeability reduction on the experiment result. As seen in Fig. 15 oil recovery is very close with 80 md cases that mean viscous force has minor impact on the recovery mechanism. One more model is made where diffusion option is turned off to see effect of diffusion on this experiment. The result shows that oil recovery is slower and ultimate oil recovery (at 22 days) is reduced to 76 %.

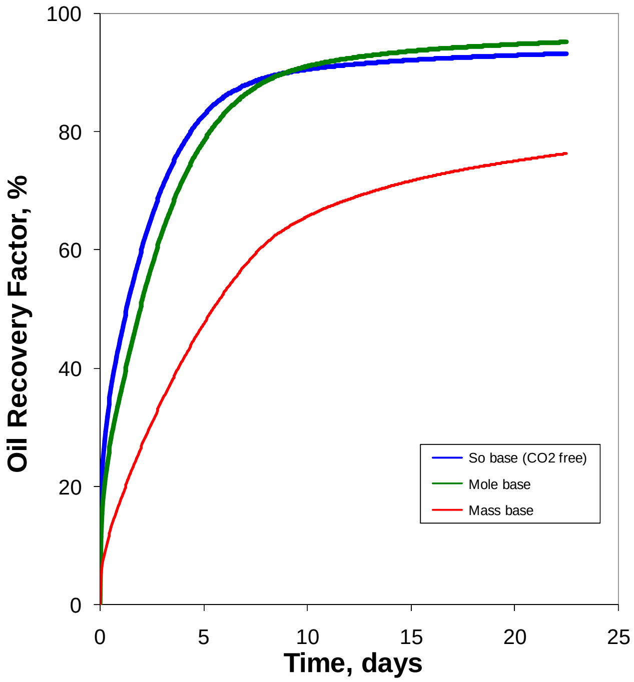

Figure 12 – Calculated oil recovery factor based on mole, mass and oil saturation from matched model with linear core relative permeability.

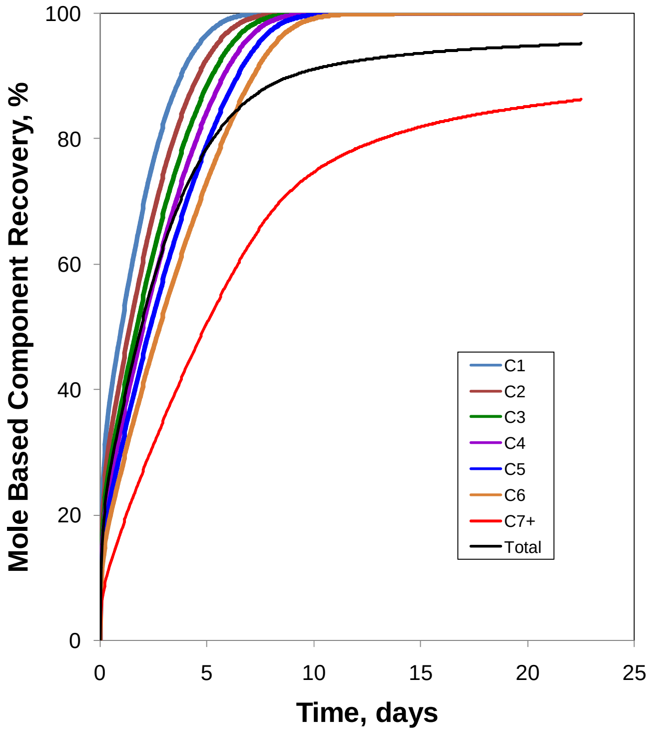

Figure 13 – Calculated mole based oil recovery of light and intermediate components from matched model with linear core relative permeability.

Fig. 13 and 14 show that lighter components produce first, meaning that CO_2 preferentially vaporizes light and intermediate components which are then transported out of the matrix block by molecular diffusion, as fresh CO_2 enters the fracture (annular space) and behind the front of displacement. In the early period of production, a front develops from the fracture inwards caused by CO_2 entry through gravity and mass transfer as shown in **Fig. 16**. After light components are vaporized (5 days), gravity-drainage appears to be more pronounced, with less lateral displacement compared with the early period of the experiment (**Fig. 17**).

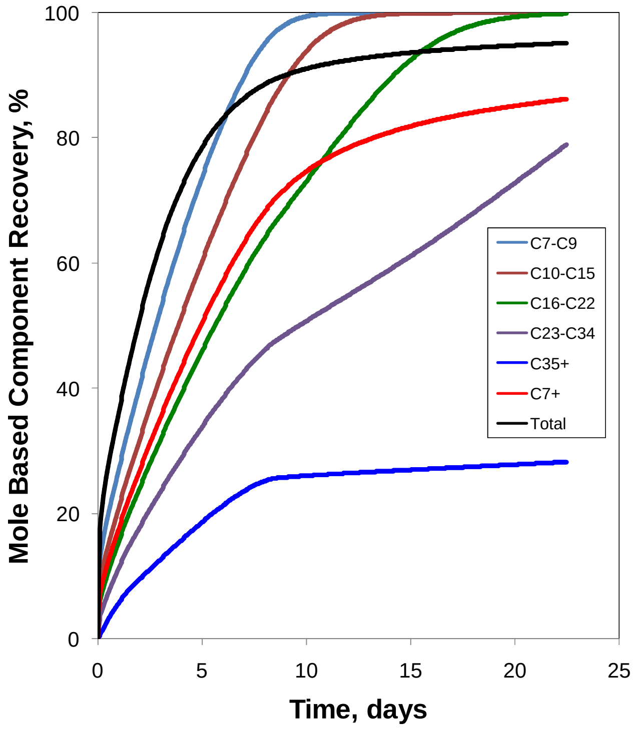

Figure 14 – Calculated mole based oil recovery of heavy components from matched model with linear core relative permeability.

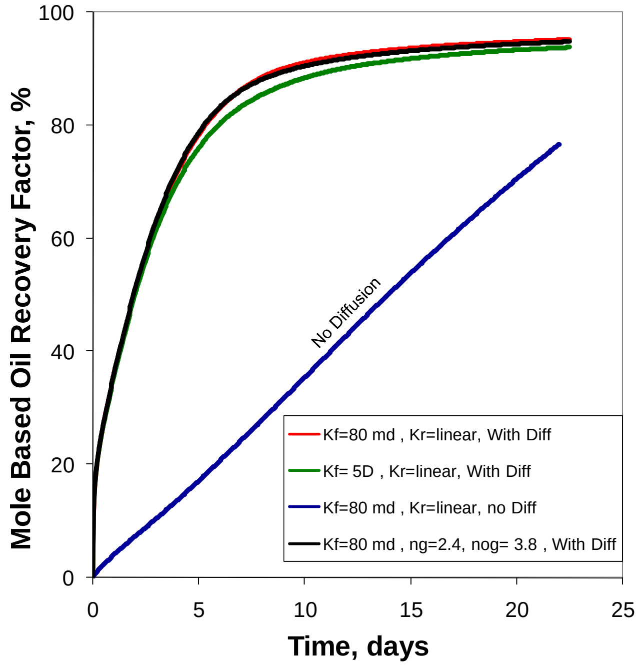

Figure 15 – Mole based oil recovery results from numerical sensitivity models at 30 °C separator temperature.

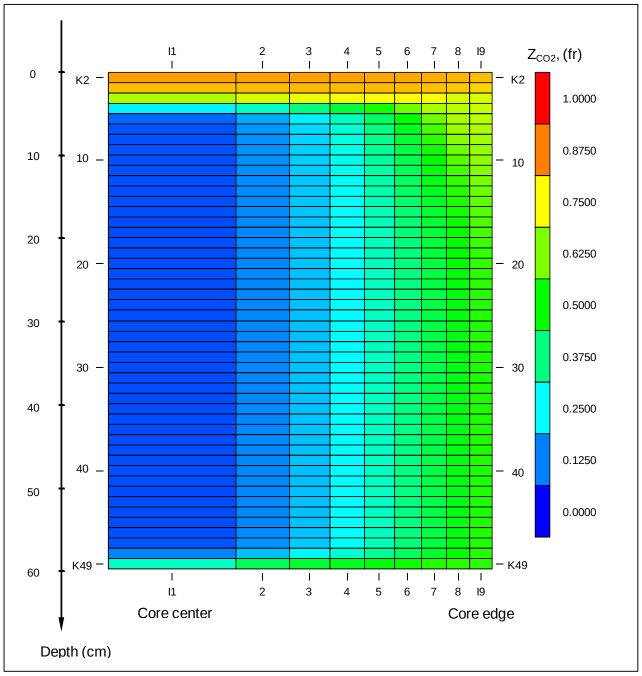

Figure 16 – CO_2 mole fraction profile of core after 12 hours for matched model with linear core relative permeability (at about 36% oil recovery).

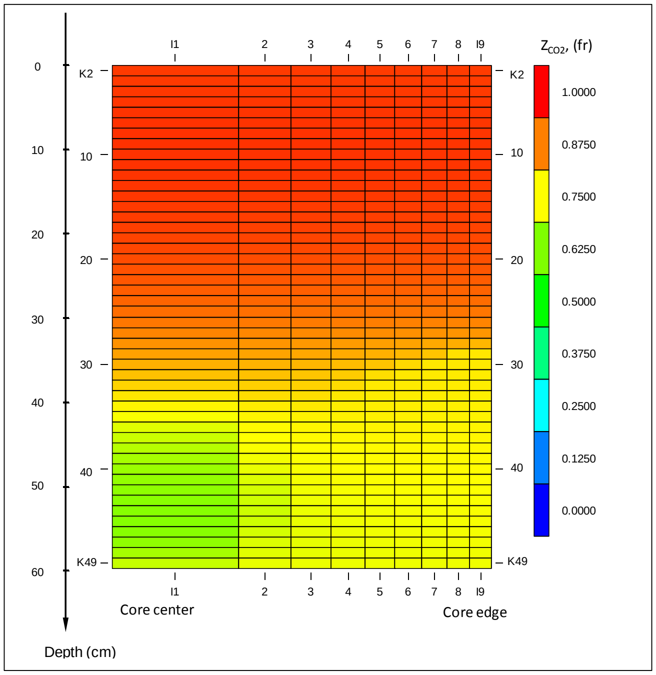

Figure 17 – CO_2 mole fraction profile of core after 5 days for matched model with linear core relative permeability (at about 79% oil recovery).

Conclusions

Some of the conclusion determined from analyzing the experiment and numerical studies are:

1. Measured production data from the experiment are matched with a commercial compositional finite-difference simulator model.
2. Mass transfer (vaporization, condensation and molecular diffusion) is the dominant production mechanism in the early stages of the experiment, where gravity drainage becomes more pronounced after light components are recovered.
3. Fractured permeability reduction as a result of remaining sealing material after core initialization does not affect the experiment results.
4. The high recoveries observed do not appear to be related with pressure exceeding the minimum miscibility pressure.

Acknowledgement

We would like to thank Shell for financing this study, as part of Alavian's PhD research.

Nomenclature

B_o = oil formation volume factor, L^3/L^3,
D_g = gas diffusion coefficient, L^2/t, cm^2/s
D_o = oil diffusion coefficient, L^2/t, cm^2/s
M_g = gas molecular weight
M_o = oil molecular weight
m_k = current mass of component *i* in place, m, kg
m_{ki} = initial mass of component *i* in place, m, kg
m_{op} = produced oil mass at surface condition, m, kg
m_{oi} = initial oil mass in place at experiment condition
N = number of grid cells
n_k = current moles of component *i* in place
n_{ki} = initial moles of component *i* in place
P_C = capillary pressure, m/Lt^2, bara
$P_{C,lab}$ = measured capillary pressure, m/Lt^2, bara
P_{cgo} = drainage gas-oil capillary pressure, m/Lt^2, bara
Pi = parachor of component i
RF = oil recovery factor
RF_{comp} = mole based component recovery factor
RF_{mole} = mole based oil recovery factor
RF_{mass} = mass based oil recovery factor
RF_{so} = saturation based oil recovery factor
RF_{surf} = oil recovery factor based on produced oil mass at surface condition
s = components volume shift
S_o = oil saturation
S_{oi} = initial oil saturation
S_{org} = residual oil saturation to gas
V_{oi} = initial oil volume in place, L^3, m^3
x_i = oil mole fraction of component i
y_i = gas mole fraction of component i
ρ_g = gas density, m/L^3, kg/m^3
ρ_o = oil density, m/L^3, kg/m^3
σ_{go} = gas-oil interfacial tension, m/t^2, mN/m
σ_{lab} = reference gas-oil interfacial tension, m/t^2, mN/m

Reference

Alavian, S.A., and Whitson C.H. 2005. CO_2 IOR Potential in Naturally-Fractured Haft Kel Field, Iran. Paper IPTC 10641 present at International Petroleum Technology Conference, Doha, Qatar, 21-23 November.

Asghari, K and Torabi, F. 2008. Effect of Miscible and Immiscible CO_2 Flooding on Gravity Drainage: Experiment and Simulation Results., Paper SPE 110587 presented at the 2008 SPE/DOE Improved Oil Recovery Symposium, Tulsa, Oklahoma, U.S.A., 19-23April.

Christoffersen, K. 1992. High-Pressure Experiments with Application to Naturally Fractured Chalk Reservoirs. PhD Dissertation, NTNU, Trondheim, Norway.

da Silva, F.V and Belery, P. 1989. Molecular Diffusion in Naturally Featured Reservoirs: a Decisive Recovery Mechanism., Paper SPE 19672 presented at the 64th SPE Annual Technical Conference and Exhibition, San Antonio, Texas, U.S.A., 8-11 October.

Darvish, G.R. 2007. Physical Effects Controlling Mass Transfer in Matrix Fracture system During CO2 Injection in to Chalk Fractured Reservoir. PhD Dissertation, NTNU, Trondheim, Norway.

Darvish, G.R., Lindeberg, E., Holt, T., Utne, S.A. and Kleppe, J. 2006. Reservoir Conditions Laboratory Experiments of CO_2 Injection into Fractured Cores. Paper SPE 99650 presented at the 2006 SPE Europec/EAEG Annual Technical Conference and Exhibition, Vienna, Austria, 12-15 June.

ECLIPSE 300 Reservoir Engineering Software. 2009. Schlumberger. www.slb.com.

Hoteit, H. and Firoozabadi, A. 2006. Numerical Modeling of Diffusion in Fractured Media for Gas Injection and Recycling Schemes. Paper SPE 103292 presented at the 2006 SPE Annual Technical Conference and Exhibition, San Antonio, Texas, U.S.A., 24-27 September.

Hua, H. Whitson, C.H., and Yuanchange, Q. 1991. A Study of Recovery Mechanisms in a Nitrogen Diffusion Experiment. Presented at the 9th European IOR Symposium, Stavanger, Norway, May.

Karimaie, H. 2007. Aspects of Water and Gas Injection in Fractured Reservoir. PhD Dissertation, NTNU, Trondheim, Norway.

Karimaie, H. and Torsæter, O. 2008. Low IFT Gas-Oil Gravity Drainage in Fractured Carbonate Porous Media. Paper SPE 113601 presented at the 2008 SPE Europec/EAEG Annual Technical Conference and Exhibition, Rome, Italy, 9-12 June.

La Romancer, J.F., Defives, D., Kalaydjian, F. and Fernandes, G. 1994. Influence of the Diffusion Gas on the Mechanism of Oil Recovery by Gas Diffusion in Fractured Reservoir. Presented at the IEA Collaborative Project on Enhanced Oil Recovery Workshop and Symposium, Bergen, Norway, August.

Li, H., Putra, E., Schechter, D.S. and Grigg, R.B. 2000. Experimental Investigation of CO_2 Gravity Drainage in a Fractured System. Paper SPE 64510 presented at the SPE Asia Pacific Oil and Gas Conference and Exhibition, Brisbane, Australia, 16-18October.

Moortgat, J., Firoozabadi, A. and Farshi M.M., 2009. A New Approach to Compositional Modeling of CO2 Injection in fractured Media Compared to Experimental Data. Paper SPE 124918 presented at the 2009 SPE Annual Technical Conference and Exhibition, New Orleans, Louisiana, U.S.A., 4-7 October.

Morel, D.D., Bourbiaux B., Latil, M., and Thiebot B. 1990. Diffusion Effect in Gas Flooded Light Oil Fractured Reservoir. Paper SPE 20516 presented at the 65th SPE Annual Technical Conference and Exhibition, New Orleans, Louisiana, U.S.A., September.

PhazeComp. Zick Technologies. www.zicktech.com.

Streamz. PERA as . www.pera.no.